HAROKOPIO UNIVERSITY OF ATHENS

Faculty of Environment, Geography and Applied Economics

Department of Geography

Postgraduate Programme "Applied Geography and Spatial Planning"

Stream C: Geoinformatics

INVESTIGATION ON THE CORRELATION OF REMOTE SENSING SATELLITE DATA, ENVIRONMENTAL PARAMETERS AND MEASUREMENTS OF ^{137}CS ACTIVITY CONCENTRATIONS IN THE GREEK MARINE ENVIRONMENT THROUGH THE DEVELOPMENT OF A GEOGRAPHICAL INFORMATION SYSTEM (GIS): *A PRELIMINARY APPROACH*

By

Mavrokefalou Georgia 214308

BSc in Geography, Harokopio University of Athens, 2014

A THESIS
Submitted in partial fulfillment of the requirements for the degree
MASTER OF SCIENCE

Athens, June 2016

INVESTIGATION ON THE CORRELATION OF REMOTE SENSING SATELLITE DATA, ENVIRONMENTAL PARAMETERS AND MEASUREMENTS OF ^{137}Cs ACTIVITY CONCENTRATIONS IN THE GREEK MARINE ENVIRONMENT THROUGH THE DEVELOPMENT OF A GEOGRAPHICAL INFORMATION SYSTEM (GIS): *A PRELIMINARY APPROACH*

By

Mavrokefalou Georgia

214308

Supervisors:

Dr. Parharidis Issaak, Associate Professor, Department of Geography, Harokopio University

Dr. Florou Heleny, Director of Research, Head of Environmental Radioactivity Laboratory, Institute of Nuclear & Radiological Sciences & Technology, Energy & Safety, National Center for Scientific Research "Demokritos"

Dr. Sykioti Olga, Associate Researcher, Institute for Astronomy, Astrophysics, Space Applications & Remote Sensing, National Observatory of Athens

ΧΑΡΟΚΟΠΕΙΟ ΠΑΝΕΠΙΣΤΗΜΙΟ ΑΘΗΝΩΝ

Σχολή Περιβάλλοντος, Γεωγραφίας και Εφαρμοσμένων Οικονομικών

Τμήμα Γεωγραφίας

Πρόγραμμα μεταπτυχιακών σπουδών: «Εφαρμοσμένη Γεωγραφία και Διαχείριση Χώρου»

Κατεύθυνση Γ: «Γεωπληροφορική»

ΔΙΕΡΕΥΝΗΣΗ ΣΥΣΧΕΤΙΣΗΣ ΔΟΡΥΦΟΡΙΚΩΝ ΠΑΡΑΤΗΡΗΣΕΩΝ ΠΕΡΙΒΑΛΛΟΝΤΙΚΩΝ ΠΑΡΑΜΕΤΡΩΝ ΚΑΙ ΠΕΙΡΑΜΑΤΙΚΩΝ ΜΕΤΡΗΣΕΩΝ ^{137}Cs ΣΤΟ ΘΑΛΑΣΣΙΟ ΠΕΡΙΒΑΛΛΟΝ ΤΟΥ ΕΛΛΑΔΙΚΟΥ ΧΩΡΟΥ ΜΕΣΩ ΤΗΣ ΑΝΑΠΤΥΞΗΣ ΕΝΟΣ ΣΥΣΤΗΜΑΤΟΣ ΓΕΩΓΡΑΦΙΚΩΝ ΠΛΗΡΟΦΟΡΙΩΝ: *ΜΙΑ ΑΡΧΙΚΗ ΠΡΟΣΕΓΓΙΣΗ*

Της

Μαυροκεφάλου Γεωργίας

Α.Μ.:214308

Επιβλέποντες:

Δρ. Παρχαρίδης Ισσαάκ, Αναπληρωτής Καθηγητής, Τμήμα Γεωγραφίας, Χαροκόπειο Πανεπιστήμιο

Δρ. Φλώρου Ελένη, Διευθύντρια Ερευνών, Υπεύθυνη του Εργαστηρίου Ραδιενέργειας Περιβάλλοντος, Ινστιτούτο Πυρηνικών και Ραδιολογικών Επιστημών και Τεχνολογίας, Ενέργειας και Ασφάλειας, Εθνικό Κέντρο Έρευνας Φυσικών Επιστημών “Δημόκριτος”

Δρ. Συκιώτη Όλγα, Εντεταλμένη Ερευνήτρια, Ινστιτούτο Αστρονομίας, Αστροφυσικής Διαστημικών Εφαρμογών και Τηλεπισκόπησης, Εθνικό Αστεροσκοπείο Αθηνών

PREFACE

This thesis is submitted as partial fulfilment for the degree master of science (MSc.) of the postgraduate degree program “Applied Geography and Spatial planning, stream C: Geoinformatics” in the Department of Geography in Harokopio University of Athens. The following work was completed in partnership with the Environmental Radioactivity Laboratory of National Centre for Scientific Research “Demokritos” ,the Institute of Astronomy, Astrophysics, Space Application and Remote Sensing of National Observatory of Athens and the Department of Geography of Harokopio University of Athens.

Firstly I would like to thank Dr. Heleny Florou, Head Director of Research, Environmental Radioactivity Laboratory, Institute of Nuclear & Radiological Sciences & Technology, Energy & Safety, National Center for Scientific Research “Demokritos” (NCSR “D”), and all the personnel in the Environmental Radioactivity Laboratory (ERL) for their help in understanding the subject area of environmental radioactivity and providing the ^{137}Cs measurement data that was necessary to complete the following work. I would also like to personally thank Dr. Heleny Florou, for being my co-supervisor and for the support she provided for completing the present thesis.

Secondly I would like to thank Dr. Sykioti Olga, Associate Researcher, Institute for Astronomy, Astrophysics, Space Applications & Remote Sensing (IAASARS), National Observatory of Athens (NOA) for also being my co-supervisor and for the support she provided for completing the present thesis.

I would also especially like to thank Dr. Parharidis Isaac, Associate Professor, Department of Geography, Harokopio University, my supervising professor, for transmitting his knowledge of satellite remote sensing.

Finally I would like to thank all the professors in the Postgraduate Programme “Applied Geography and Spatial Planning”, Stream C: Geoinformatics, for their valuable lessons they provided during the postgraduate program.

ACKNOWLEDGEMENTS

I would like to express my special thanks to European Space Agency (ESA) that provided the necessary SMOS images, for the ongoing study that is being carried out in NOA and NCSR”D” in the frame of the coordinated Cat-1 Project SMOS.4681.

I would also like to express my special thanks to NASA Goddard Space Flight Center, Ocean Biology Distributed Active Archive Center that provided level 2 and level 3 Ocean Data products.

Finally I would like to express my special thanks to the European Space Agency for the funding of an EC Student Grant, in order to attend and present part of this thesis at the Living Planet Symposium 2016 in Prague, Czech Republic from 9 to 13 May 2016.

CONTENTS

List of Figures

LIST OF TABLES

List of Equations

Appendices

ABSTRACT

Earth Observation satellites have proven through the years capable of recording changes on ecological parameters in the marine environment as well as pollution detection and tracking on cases. On the other hand radionuclide dispersion cannot be directly detected using remote sensing systems. However the levels of radionuclides in the marine environment, especially the levels for the soluble ones, are associated with other physical, chemical, biological and geological parameters of the natural environment. Considering this attribute, a program concept has been developed to utilize sea parameters like sea surface salinity (SSS), sea surface temperature (SST) and ocean color. The challenge of the study is the establishment of potential relations between satellite and in situ measurements of the marine environment and field radiological measurements. Such potential relations are expected to lead to an innovative tool based on remote sensing data and in situ ^{137}Cs measurements for the remote radioactivity detection of the Greek marine ecosystem both for routine control and emergency recordings.

The purpose of this study is to investigate the relations between ^{137}Cs activity concentrations, satellite data and in situ measurements. Satellite data series are acquired from SMOS, TERRA and AQUA satellites and in particular, measurements from MIRAS and MODIS instruments correspondingly (SMOS images were provided by ESA in the frame of the joint ESA, NOA, NCSR"D" project entitled SMOS.4681). These measurements include: sea surface temperature (SST), chlorophyll A (Chlor_a), particulate organic carbon (POC), particulate inorganic carbon (PIC), Cdom index (CDOM), instantaneous photosynthetically available radiation (iPAR) and daily photosynthetically available radiation (PAR) (Sykioti et al., 2014). Furthermore, salinity and sea surface temperature in situ measurements were acquired from the HCMR Poseidon system. The ^{137}Cs measurements were derived from sea water sample processing using an ammonium molybdophosphate (AMP) radioanalytical pre-concentration method (Folsom et al., 1970) and gamma spectrometry in the Environmental Radioactivity Laboratory (ERL) of the National Centre for Scientific Research "Demokritos" (NCSR "D") (Florou et al., 2010) (Florou et al., 2014). This study includes the creation of data timeseries and a spatial database in a GIS environment using all available measurements. Other steps include

the interpolation of the data and the study of the spatial and temporal variation of Aegean Sea and Souda bay respectively.

Here, the first findings on the spatial and temporal correlations of ^{137}Cs measurements with MODIS L2 and L3 ocean data, SMOS L2 ocean data and POSEIDON data are presented for Souda Bay area and Aegean Sea concerning the time period spanning December 2011 to June 2015 (for the timeseries) and March 2011 to February 2015 (for the analyses).

Keywords: Aegean sea, ^{137}Cs, Environmental Radioactivity, Geographic Information Systems, GIS, MODIS, Regression, Remote Sensing, SMOS, Souda Bay

ΠΕΡΙΛΗΨΗ

Έχει αποδειχθεί ότι τα δορυφορικά συστήματα Παρατήρησης της Γης, έχουν την ικανότητα να καταγράψουν και να αποτυπώσουν αλλαγές στο θαλάσσιο φυσικό περιβάλλον ενώ, επίσης είναι ικανά, σε ορισμένες περιπτώσεις, να παρακολουθήσουν την διασπορά και την εξέλιξη φαινομένων περιβαλλοντολογικής ρύπανσης. Αντίθετα, η διασπορά των ραδιονουκλίδιων στο περιβάλλον, δεν είναι δυνατόν να ανιχνευθεί άμεσα με τη χρήση δορυφορικών συστημάτων τηλεπισκόπησης. Ωστόσο, τα επίπεδα των ραδιονουκλιδίων στο θαλάσσιο περιβάλλον, ιδίως των διαλυτών, σχετίζονται με άλλες φυσικές, χημικές, βιολογικές και γεωλογικές παραμέτρους του φυσικού περιβάλλοντος. Λαμβάνοντας υπόψη αυτή την ιδιότητα, αναπτύχθηκε το σχέδιο για ένα πρόγραμμα, το οποίο κάνει χρήση θαλασσίων παραμέτρων από δορυφορικά δεδομένα, όπως η θαλάσσια επιφανειακή αλατότητα (SSS), η θαλάσσια επιφανειακή θερμοκρασία (SST) και το ωκεάνιο χρώμα καθώς επίσης και επίγειων μετρήσεων. Η κύρια πρόκληση στην παρούσα μελέτη, είναι η αναγνώριση των πιθανών σχέσεων μεταξύ δορυφορικών και επιτόπιων θαλάσσιων παραμέτρων με τις επιτόπιες ραδιολογικές μετρήσεις. Τέτοιες πιθανές σχέσεις αναμένεται να οδηγήσουν στη δημιουργία ενός καινοτόμου εργαλείου που θα βασίζεται σε δεδομένα δορυφορικής τηλεπισκόπησης και επιτόπιες μετρήσεις ^{137}Cs για την εξ αποστάσεως ανίχνευση της ραδιενέργειας στον Ελλαδικό θαλάσσιο χώρο, για την τακτική παρακολούθηση του φαινομένου καθώς και την παρακολούθηση έκτακτων περιστατικών.

Ο σκοπός της παρούσας μελέτης είναι η διερεύνηση των σχέσεων μεταξύ των συγκεντρώσεων ^{137}Cs, δορυφορικών παρατηρήσεων και των επιτόπιων μετρήσεων. Τα δορυφορικά δεδομένα προήλθαν από τους δορυφόρους SMOS, TERRA και AQUA, και ειδικότερα από τα αντίστοιχα όργανα καταγραφής MIRAS και MODIS. Ειδικότερα, οι εικόνες από το δορυφόρο SMOS παραχωρήθηκαν από τον Ευρωπαϊκό Οργανισμό Διαστήματος (ESA) στο πλαίσιο ενός κοινού προγράμματος της ESA, του Εθνικού Αστεροσκοπείου Αθηνών και του ΕΚΕΦΕ «Δημόκριτος» με τίτλο "Correlation of salinity variations from SMOS data in the Aegean Sea (Greece) to integrated time series measurements of ^{137}Cs activity concentrations: Mathematical modeling of pollution behavior and dispersion" (Cat-1 SMOS. 4681). Οι δορυφορικές μετρήσεις περιλαμβάνουν: την θαλάσσια επιφανειακή θερμοκρασία (SST), τη συγκέντρωση της χλωροφύλλης Α (Chlor_a), τη συγκέντρωση σωματιδίων οργανικού

και ανόργανου άνθρακα (POC, PIC) και τη στιγμιαία και ημερήσια φωτοσυνθετικά διαθέσιμη ακτινοβολία (iPAR, PAR) (Sykioti et al., 2014). Επιπλέον, επιτόπιες μετρήσεις θαλάσσιας επιφανειακής αλατότητας και θερμοκρασίας αποκτήθηκαν από το σύστημα ΠΟΣΕΙΔΩΝ του ΕΛΚΕΘΕ. Οι μετρήσεις των συγκεντρώσεων ^{137}Cs προήλθαν από δειγματοληψίες θαλασσινού νερού, την επεξεργασία τους με τη ραδιοαναλυτική μέθοδο προ-συγκέντρωσης ammonium molybdophosphate (AMP) (Folsom et al., 1970) και τη μέτρησή τους με γάμμα φασματοσκοπία στο Εργαστήριο Ραδιενέργειας Περιβάλλοντος (ΕΡΠ) του Εθνικού Κέντρου Έρευνας Φυσικών Επιστημών «Δημόκριτος» (ΕΚΕΦΕ «Δ») (Florou et al., 2010) (Florou et al., 2014). Η εν λόγω μελέτη περιλαμβάνει τη δημιουργία χρονοσειρών και μιας χωρικής βάσης δεδομένων σε ένα σύστημα γεωγραφικών πληροφοριών χρησιμοποιώντας όλες τις διαθέσιμες μετρήσεις. Άλλα στάδια της μελέτης περιλαμβάνουν τη χωρική παρεμβολή των δεδομένων και τη μελέτη των χωρικών και χρονικών σχέσεων των δεδομένων στην περιοχή του Αιγαίου Πελάγους και στον κόλπο της Σούδας αντίστοιχα.

Στην παρούσα εργασία, παρουσιάζονται τα πρώτα ευρήματα σχετικά με τις χωρικές και χρονικές συσχετίσεις των συγκεντρώσεων ^{137}Cs με τα θαλάσσια δεδομένα L2 και L3 του οργάνου MODIS, με τα θαλάσσια δεδομένα L2 του δορυφόρου SMOS και με τις μετρήσεις από το σύστημα ΠΟΣΕΙΔΩΝ. Τα ευρήματα αυτά αφορούν την περιοχή του Αιγαίου πελάγους και την περιοχή του κόλπου της Σούδας για τη χρονική περίοδο που εκτείνεται από το Δεκέμβριο 2011 έως τον Ιούνιο 2015 (για τις χρονοσειρές) και από το Μάρτιο 2012 έως τον Φεβρουάριο 2015 (για τις αναλύσεις).

Λέξεις κλειδιά: Αιγαίο Πέλαγος, ^{137}Cs, Δορυφορική Τηλεπισκόπηση, Κόλπος Σούδας, MODIS, Παλινδρόμηση, Ραδιενέργεια Περιβάλλοντος, Συστήματα Γεωγραφικών Πληροφοριών, ΣΓΠ, SMOS

1. INTRODUCTION

The use of satellite remote sensing systems for earth observation is quite common nowadays. Satellite systems have a wide range of applications such as the study of the environment. They are able to regularly record environmental parameters with high accuracy. These parameters can be either for the atmosphere, terrestrial or marine ecosystems. In particular in the marine environment, some satellite systems are able to detect insoluble hydrocarbon contaminants such as oil spills. However, the dispersion of radionuclides cannot be directly detected and recorded by satellite systems, due to their high solubility in sea water. Nevertheless, the levels of radionuclides in the marine environment can be associated with parameters such as salinity and temperature (Sykioti O. , 2015).

The present thesis concerns the investigation of potential relations between satellite and in situ measurements of the marine environment and field radiological measurements. Such potential relations are expected to lead to an innovative tool based on remote sensing data and in situ ^{137}Cs measurements for the remote radioactivity detection of the Greek marine ecosystem both for routine control and emergency recordings.

First an introduction on the dispersion and distribution of radionuclides in the marine environment will be presented; with main focus on ^{137}Cs and its dispersion in the Aegean Sea. Caesium-137 (^{137}Cs) measurements were acquired from the Environmental Radioactivity Laboratory of NCSR”D” database, where new measurements through seawater sampling and processing in the laboratory using an ammonium molybdophosphate (AMP) radioanalytical pre-concentration method (Folsom et al., 1970) and gamma spectrometry. At the same time remote sensing data will be collected and processed in order to extract information for marine environmental parameters like sea surface temperature (SST), sea surface salinity (SSS), chlorophyll-A concentration (Chlor_a), particulate organic carbon concentration (POC), particulate inorganic carbon concentration (PIC), Colored dissolved organic matter index (CDOM) and instant and daily photosynthetically available radiation (iPAR, PAR). Remote sensing data include SMOS, TERRA and AQUA images. SMOS images are recorded using the MIRAS instrument, whereas TERRA and AQUA images are recorded using the MODIS instrument. Additional data include in situ marine measurements from the POSEIDON buoy database system of the HCMR. POSEIDON data include sea surface temperature and salinity.

The analysis comprises of the creation of data timeseries and a spatial database in a GIS environment using all available measurements in order to observe the temporal and spatial relations between the satellite, insitu and radiological measurements. The first findings on the spatial and temporal correlations of ^{137}Cs measurements with MODIS L2 and L3 ocean data, SMOS L2 ocean data and POSEIDON data are presented in the form of plots and maps, for Souda Bay area and Aegean Sea concerning the time period spanning December 2011 to June 2015 (for the timeseries) and March 2011 to February 2015 (for the analyses). Finally in the conclusion section the main findings and future development of this work will be addressed.

2. Environmental Radioactivity

This chapter will analyze basic terms of radiation, radionuclides and radioactivity in order to continue with the analysis of Caesium-137 on the next chapter. Apart from of the analysis of the terms, an analysis of the sources, the dispersion, the transportation and the consequences of radionuclides in the environment will also be provided.

2.1. Introduction to Radioactivity

2.1.1. Basic Terms

Radiation is a natural phenomenon where energy is transferred in the form of particles and waves. The types according to wavelength are going to be presented in the chapter of satellite remote sensing. The types according to energy are ionizing and non-ionizing radiation. The Greek Atomic Energy Commission (GAEC) defines ionizing radiation, as radiation that carries enough energy to penetrate matter, cause ionization of its atoms, violently break chemical bonds and cause biological damage in living organisms. Ionization of the atom is a natural phenomenon that follows the interaction of high energy radiation with matter. It is the violent expulsion of an electron from the atom that creates a pair of opposite charged ions. Ionizing radiation that comes from the decay of radioactive nuclides is called radioactivity.

Nuclides are the nuclei of atoms who are composed of protons and neutrons. There are stable nuclides and unstable – radioactive nuclides. Stable nuclides for every number of protons have a specific number of neutrons. Generally in order for nuclei to be stable the number of neutrons has to be greater than the number of protons. Unstable nuclei emit ionizing radiation through their decay in three forms. These are alpha particles, beta particles and gamma radiation (Van Der Stricht et al., 2001) (Choppin et al., 1978). Alpha particles (α) are positively charged and are made up of two protons and two neutrons. Basically they are helium nuclei. They are very energetic, but they are so heavy that they use up their energy over short distances. Also they do not have penetration energy so they are not as harmful. Beta particles (β) are small, fast moving particles with an electrical charge. The charge can be negative or positive. They are electrons or positrons. They are similar to alpha particles in that their principal mechanism of interaction with matter is by making collisions with atomic orbital electrons. Even though they have more penetrating power than alpha particles, they are less damaging to living tissue because the ionizations they produce are more widely spaced. Gamma rays (γ) are packets of energy called photons. Unlike alpha and beta particles, which have both energy and mass, gamma rays are pure energy. They are often emitted along with alpha or beta particles during radioactive decay. They are the biggest radiation hazard because they can penetrate the whole body and cause ionization. Their penetrating power is so high that several centimeters of a dense material like lead or even few meters of concrete may be required to stop them. All three forms of ionizing radiation are hazardous, but alpha and beta particles can cause damage only if inhaled or ingested because they cannot penetrate clothes and skin. What makes gamma radiation extremely hazardous is the penetration power. The creation of α, β particles, γ-radiation and their penetration ability can be seen in figures 1, 2. According to the particles or rays emitted there are three forms of radioactive decay processes. The first process is Alpha-decay where alpha particles are emitted from an energy state in the source nucleus, taking kinetic energy with them, which leaves the nucleus in a different energy state. The second radioactive decay process is Beta-decay, which is the creation and emission of either electrons or positrons, or the process of electron capture. The third process is Gamma-decay, which is the emission of electromagnetic radiation where the transition occurs between energy levels of the same nucleus. An additional mode of radioactive decay is that of internal conversion in which a nucleus loses its energy by interaction of the nuclear field with that of the orbital electrons, causing ionization of an electron instead of γ-ray emission (Choppin et al., 1978) (Friedlander et al., 1981) (Van Der Stricht et al., 2001).

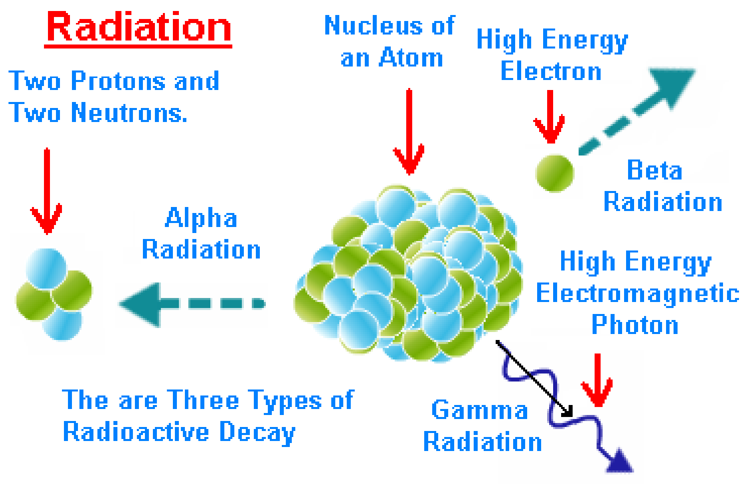

Figure 1. Creation of α,β particles and γ-radiation.

Source: *http://images.tutorvista.com/cms/images/38/gamma-emission.PNG*

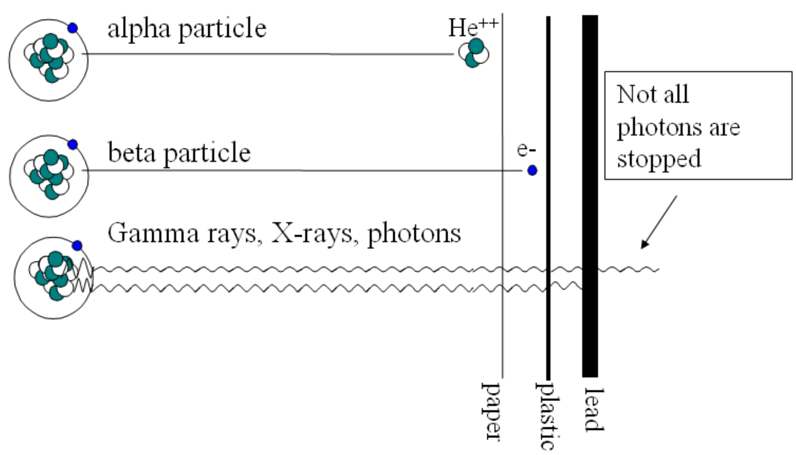

Figure 2. Penetration ability of α, β particles and γ-radiation.

Source: *https://ehs.mit.edu/site/book/export/html/54*

As it was mentioned before radioactivity is the emission of ionizing radiation from the decaying radionuclides. Radionuclides or unstable nuclei decay in order to achieve a more stable state. In order to study radionuclides and radioactivity is of utmost importance to study the terms of half-life, activity, absorbed dose, dose equivalent, effective dose equivalent and exposure.

Half- life is the time where the half quantity of a radionuclide needs to decay. Activity of a radionuclide is the rate at which the isotope decays.

The absorbed dose is the energy transportation rate per mass of absorption matter. The dose equivalent was established by the ICRP (International Commission on Radiological Protection) and ICRU (International Commission on Radiological Units). It combines the absorbed dose with a qualitative agent QF or Q.

The effective dose equivalent is the sum of the products of the dose equivalent to the organ or tissue and the weighting factors applicable to each of the body organs or tissues that are irradiated.

Exposure to radiation is the total amount of absorption of ionizing radiation or ingestion of a radioisotope. It is distinguished in internal and external exposure. External exposure happens from skin absorption through external sources of radiation and internal exposure is due to inhalation or ingestion of radionuclides (Florou H.).

An equally important term is the measurement units that are used in order to study radioactivity. The activity of a radioactive substance is measured in Bequerel (Bq) and Curie (Ci).Where 1 Bq is 1 decay per second and 1 Ci is 3.7 * 10^10 decays per second. Next measurement is the dose, absorbed dose is measured in Gray (Gy) or radiation absorbed dose (rad). Gray is the absorption of 1 joule of energy per kilo of matter. 1 rad is equivalent to 0.01 Gy. The dose equivalent is measured in roentgen equivalent in man (rem). Rem is equal to 0.01 Sv. The effective dose equivalent is measured in Sievert (Sv), where 1 Sv is equal to the effect of 1 joule of radioactivity in 1 kg of human tissue. Finally the exposure is measured in Roentgen where 1 R is equal to 2.58 x 10-4Cb/ kg (Florou H.). In figure 3 below, the radiation doses and effects on humans are available to be seen.

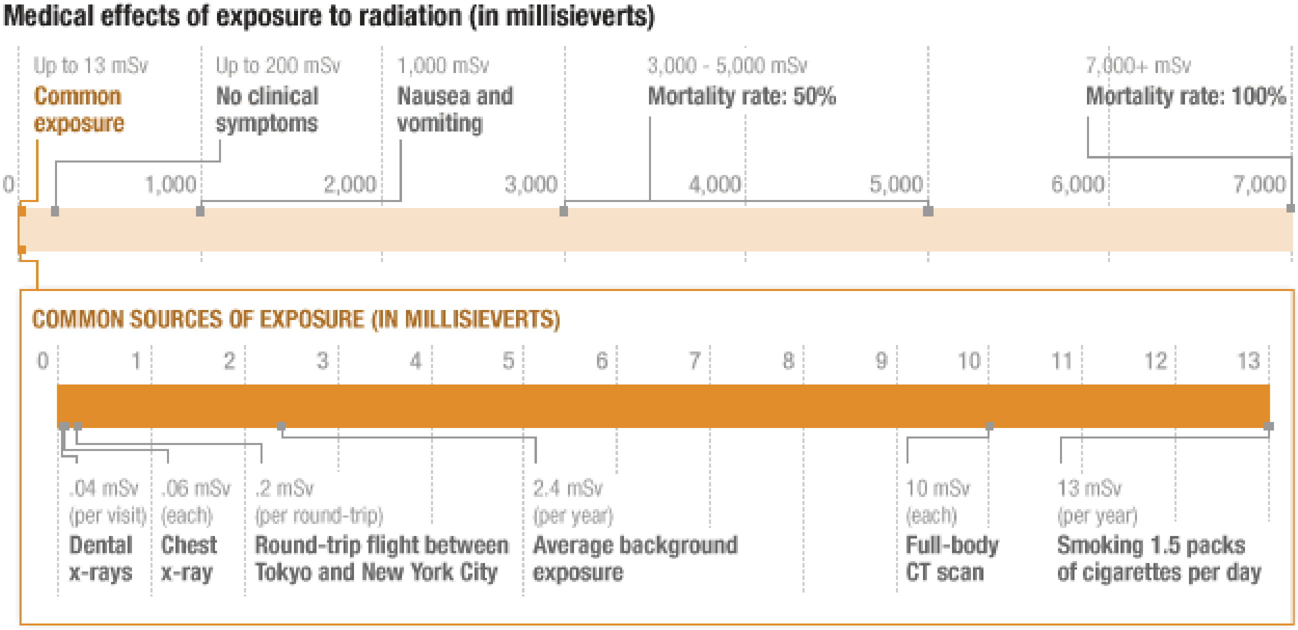

Figure 3. Radiation doses and effects on humans.

Source: http://www.npr.org/news/graphics/2011/03/gr-radiation-624.gif

2.1.2. SOURCES

Radionuclides are categorized according to their source. There are natural radionuclides, cosmogenic radionuclides and man-made radionuclides. Before analyzing the types of radionuclides, it is crucial to mention that life on earth was developed in condition of low level ionizing radiation. So radioactivity is not something invented by man but it was always in the natural environment.

Natural radioactivity comes from earth materials; these radionuclides are else called terrigenous. The terrigenous radionuclides are then divided into two sub categories. The first subcategory is the primordial radionuclides that exist since the formation of the earth and they are characterized by a very long half-life. Most known radionuclides from this category are Potassium-40 (^{40}K) and Rubidium-87 (^{87}Rb). The other subcategory is the radioactive series of actinides. This subcategory contains radionuclides like Uranium-235 (^{235}U), Uranium-238 (^{238}U) and Thorium-232 (^{232}Th) and their subsidiary radionuclides.

Cosmic radioactivity refers to the flow of extraterrestrial particles, of very high energy, that is observed on the upper layers of the atmosphere. This category has also

2 subcategories. The first subcategory is the primordial cosmic radiation of extraterrestrial source and the second subcategory is the secondary cosmic radiation resulting from the reaction of the primordial cosmic radiation with the particles of the atmosphere.

Finally the artificial nuclides began spreading in the environment with the invention of atomic bombs and atomic energy. These are nuclides with a relative small half live that decayed during the early years of earth. Some of the most known man made nuclides are Caesium-137 and Strontium-90 (Choppin et al., 1978) (Friedlander et al., 1981) (Florou H.).

Radionuclide sources in the environment are going to be presented in this part. Natural radionuclides exist naturally on earth, present in small amounts in virtually every biotic and abiotic environment. Cosmic nuclides come from cosmic radiation and its reaction with the earthen atmosphere. The most important sources of radiation in the environment are the artificial radioactivity sources. These are fallout, nuclear energy plants, nuclear accidents and nuclear powered vessels. Artificial radiation was introduced to the environment in the beginning of 1940’s with the use of nuclear energy in military and civil applications. Global fallout began in the early 1940s with the beginning of military nuclear tests. Even though the tests have stopped from the 1960s, there are still radionuclides due to testing in the environment. Most tests were executed by the United States of America in the Nevada dessert test site and in the Pacific and Atlantic Ocean. Fallout also exists from detonated nuclear weapons in Nagasaki and Hiroshima (Van Der Stricht et al., 2001).

Next source is the civil use of nuclear energy in nuclear power plants. There the fallout and the contamination are bigger than the nuclear weapons, when the guidelines are not followed. Nuclear power plants use the heat produced from the nuclear fission in order to produce steam and via turbines to produce electrical power. The production of the heat is done in a nuclear reactor, which is a device to initiate and control a sustained nuclear chain reaction. Contamination from the operation of a nuclear plant may occur from atmospheric release, water release and nuclear waste.

When regulations are not being followed or there are lesions in manufacturing or major natural disasters take place like earthquakes and tsunamis, then nuclear accidents happen like the ones in Three mile island, Chernobyl and Fukushima Daiichi plants. All nuclear accidents are rated in the International Nuclear and Radiological Event Scale (INES). INES is a tool for promptly and consistently communicating to the public the safety significance of events associated with sources of ionizing radiation. It classifies nuclear and radiological accidents and incidents. The events are rated at seven levels in this scale. The first level is Anomaly, the second level is Incident, the third level is Serious Incident, the fourth level is Accident with Local Consequences, the fifth level is Accident with Wider Consequences, the sixth level is Serious Accident and the final level is Major Accident (IAEA, International Atomic Energy Agency, 2016).

The Three Mile Island (TMI) accident happened on March 28 1979, in the Three Mile Island nuclear generating station in Dauphin County Pennsylvania, United States (Figure 4). The station has two reactors, TMI-1 and TMI-2, where there was a partial core meltdown in reactor TMI-2 (Figure 5). The core meltdown began at 4:37 am EST. According to IAEA the total atmospheric release was 10^{12} Bq. But due to proper containment no particulate material was released. The TMI-2 was shut down and never reopened, the TMI-1 is still operational and had its license renewed in 2009 in order to continue to be operational until 2034. The TMI-2 accident was rated level 5 in the international nuclear event scale (Kemeny, 1979) (Walker, 2004).

Figure 4. The Three Mile Island nuclear plant.

Source: http://media-2.web.britannica.com/eb-media/06/117706-004-CCA0764D.jpg

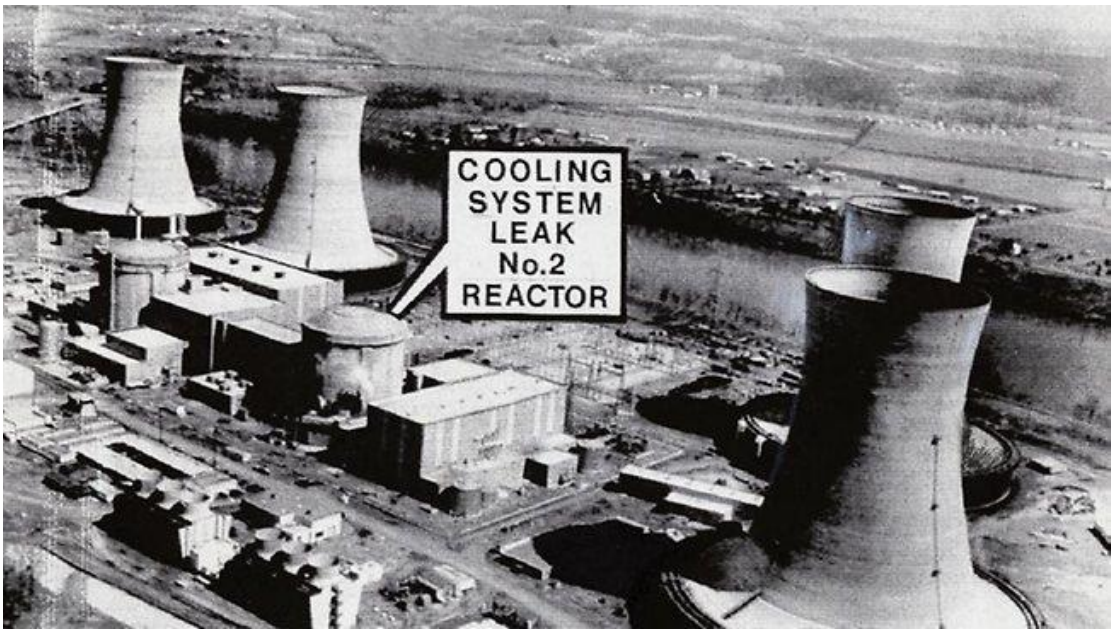

Figure 5. TMI accident on reactor 2.

Source:http://hcrusanthreemileislandaccident.weebly.com/uploads/5/4/1/3/54131419/6952234_orig.jpg

The next major accident happened in Chernobyl Nuclear Power Plant on 26 April 1986, in Ukraine. The Chernobyl disaster was one of the worst nuclear power plant accidents in history and was rated as level 7 in the international nuclear event scale. The accident began from a low power engineering experiment that was being conducted at the 4th reactor unit of the plant. This experiment led to the reactor becoming unstable which resulted in a nuclear excursion, thermal explosions and fires (Figure 6). The graphite started to burn and the fire listed for 10 days before the release of activity from the reactor could be stopped. The accident released about 11 EBq of radioactive material in the environment (NEA Committee on Radiation Protection and Public Health, 1995). Contamination was spread over large areas and was measurable in most parts in the Northern Hemisphere. The most contaminated countries were Russia, Ukraine and Belarus. The effects from the contamination were tremendous, apart from livestock and plants there were effects on people like radiation sickness for the workers and the firefighters (Figure 7) that tried to control the situation, cancer on adults and genetic deformation on embryos. The measures taken were the permanent evacuation of Pripyat and the creation of the exclusion zone of 30 kilometers, a concrete sarcophagus that sealed unit 4 and a new concrete structure that will be placed on the sarcophagus. The power plant continued to provide power with the remaining reactors until 2000 where the Chernobyl nuclear power plant was officially closed (Smith et al., 2005) (Saenko, 2011).

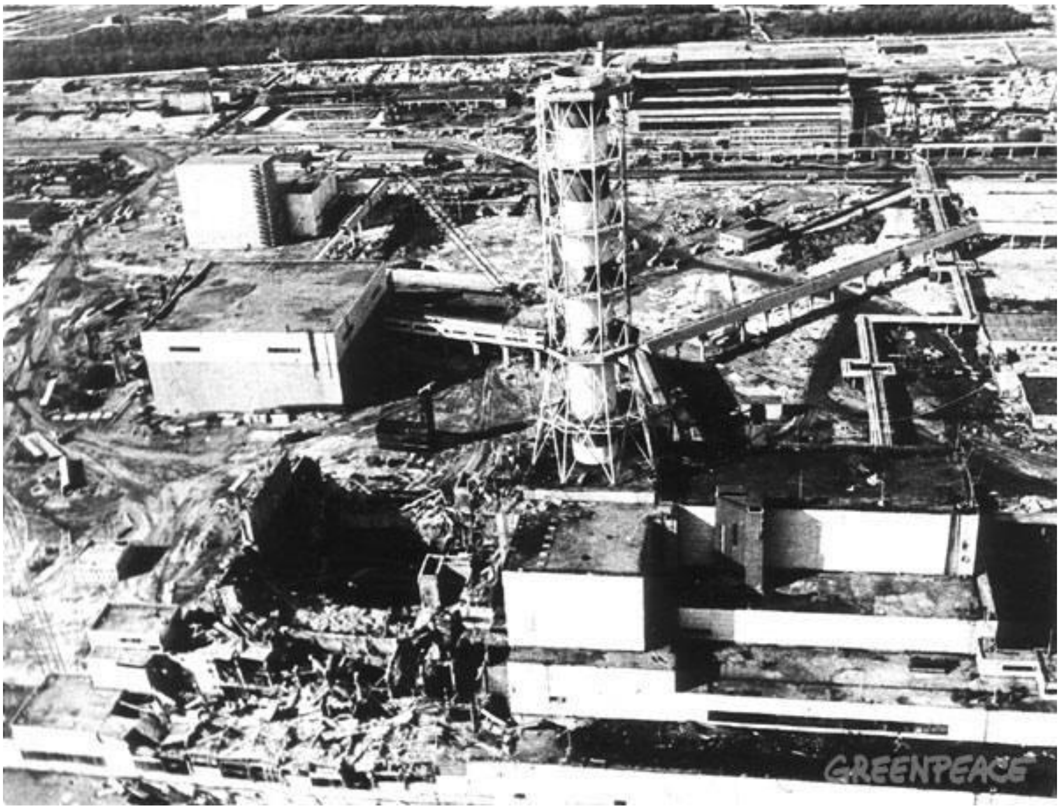

Figure 6. Chernobyl nuclear power plant reactor 4 after the explosion.

Source:http://www.greenpeace.org/international/Global/international/planet-2/image/2006/3/chernobylnuclearexpolsion.jpg

Figure 7. Firefighters on the roof of reactor 4 in Chernobyl.

Source:http://chernobylfoundation.org/wp-content/uploads/2012/12/chernobyl-reactor-roof.jpg

The most recent nuclear plant accident happened in Okuma, Fukushima Japan at the Fukushima Dai-ichi nuclear power plant on 11 March 2011. The problems in the nuclear plant occurred when the plant was hit by a tsunami that was triggered by the 9.0 magnitude Tohoku earthquake. The accident was rated level 7 in the international nuclear event scale. It was the largest nuclear incident since the Chernobyl disaster. The damage occurred after the tsunami overwhelmed the safety seawall causing the cooling systems to stop and the reactors to overheat resulting in a nuclear core meltdown in reactor units 1,2 and 3 (Figures 8, 9). The nuclear core meltdown was avoided in reactor units 4, 5, 6. The accident released radionuclides both in the atmosphere and the ocean environment. It was estimated that the total amounts of iodine and Caesium were about 4.7 PBq (Bailly du Bois, et al., 2012) (Holt et al., 2012). According to the Tokyo Electric Power Company, the contamination in the ocean environment was so big due to the highly contaminated water, which was used for the stabilization of the reactors, discharged directly into the sea. The most often detected radionuclides from the accident were Caesium 134 and 137 and Iodine 131. The Japanese government evacuated the area and started to find ways in order to decontaminate the area and stop the radioactive waters coming from the plant to get into the ocean.

Figure 8. Fukushima Dai-ichi reactor units 1,2 and 3 after their explosion.

Source:Photos shown are half-size of the originals. The 11 originals full-size: http://cryptome.org/eyeball/daiichi-npp/daiichi-photos.zip (5MB) Dates of photos taken from the EXIF data of the originals, supported by captions and credits later obtained from the Web.

Figure 9. Fukushima Dai-ichi nuclear power plant as seen from above during the fire.

*Source:*http://i.telegraph.co.uk/multimedia/archive/01848/Fukushima-japan_1848652c.jpg

Other sources than nuclear plant accidents include the radiation coming from nuclear powered ships and vessels. The first nuclear vessel was the USS Nautilus in 1955. Nuclear power is best for vessels which need to be at the sea without refueling, because 1 kilogram of fissionable material has 10,000,000 times the energy of 1 kilogram of chemical fuel. Also nuclear power provides powerful submarine propulsion. Not only submarines use nuclear power, but there is a range from icebreakers to aircraft carriers. In figure 10, the scheme of a submarine nuclear reactor is presented. The nuclear power ships are not only military, there also civil nuclear powered ships. Cases of radioactivity contamination have occurred in submarine accidents and sinking. In normal operation there is little to no leakage. The leakage comes mainly from the coolant. But there are not only ships and vessels that use nuclear fission for propulsion; some satellites use nuclear power in combination with solar power. Like transit or navsat system which was the first satellite navigation system and used small nuclear reactors and a radioisotope thermo electric generator (Friedlander et al., 1981). This energy system was called Systems for Nuclear Auxiliary Power (SNAP). Even though the system was successful, there was the incident of Transit 5BN-3 which failed to reach orbit and burned up over Madagascar. This had as a result the scattering of plutonium fuel over the area.

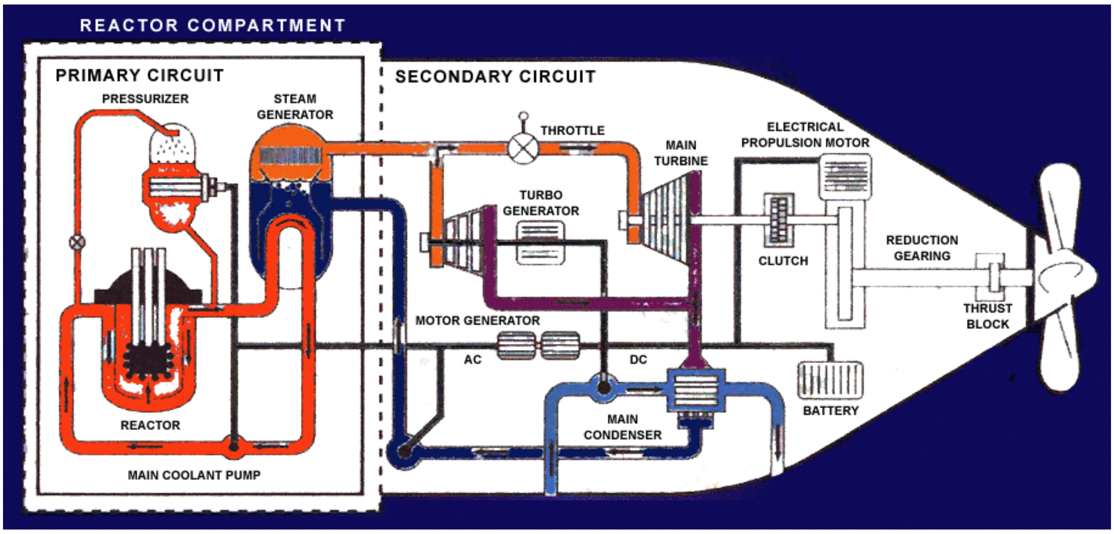

Figure 10. Example of a submarine nuclear reactor.

Source:http://www.world-nuclear.org/uploadedImages/org/info/Non-Power_Nuclear_Applications/Transport/UK_Nuclear_Submarine.gif

2.2. Radioactivity in the Marine Environment

In this part the behavior of radionuclides in the environment will be analyzed. The most important factor in the environmental transportation and dispersion is the type of the environment; because radionuclides behave differently in terrestrial and aquatic environment. The analysis according to the environment differs in difficulty due to different homogeneity. There is a greater difficulty in the terrestrial environment due to low homogeneity but there is a smaller difficulty in studying radionuclides in the aquatic environment due to high homogeneity. It is important to study the environmental behavior of radionuclides, because radionuclides are scattered into the air and water, settle on the soil and sediments, migrate into food chains and affect living organisms and man. But in order to study them, it is crucial to predict the movement and concentration of the radioactive material in the studied system and the radiation and toxicity of the radioactive material inside the organic components of the environment. The scientific field that studies the behavior of radionuclides in the environment is Radioecology. The purpose of radioecology is to detect the presence of radionuclides in the environment, to research their origins and to understand their process of transfer and their concentration in ecosystems (IPSN-Institut de protection et de surete nucleaire, 2001) (Van Der Stricht et al., 2001). In figures 11, 12 the transportation of radionuclides in the terrestrial and aquatic environment is displayed.

The aquatic environment is distinguished in two environments; the inland aquatic environment and the marine environment. Inland aquatic environment consists of fresh water distributed in lakes and rivers. Bodies of fresh water receive liquid radioactive waste from nuclear facilities and laboratories. Marine aquatic environment consists of the seas and oceans. It is important to study the oceans because they are an important source of human food supply and of raw materials, in addition to their role in transportation and the location of towns and cities along the coasts. The transportation is similar between the two environments; Radionuclides are spread by currents and the final stages are the sediments and living organisms. The marine environment exhibits the greatest stability from the other environments and it is easier to study radionuclides. As mentioned above, radionuclides are spread by currents; they fix themselves to particles suspended in water which gradually settle on the sea bed. Marine organisms can accumulate radionuclides by filtering the water that contains these radionuclides or consuming food that contains them. The final receptor of the marine radionuclides is the human that consumes the contaminated marine organisms (IPSN-Institut de protection et de surete nucleaire, 2001) (Van Der Stricht et al., 2001) (Polikarpov, 1966).

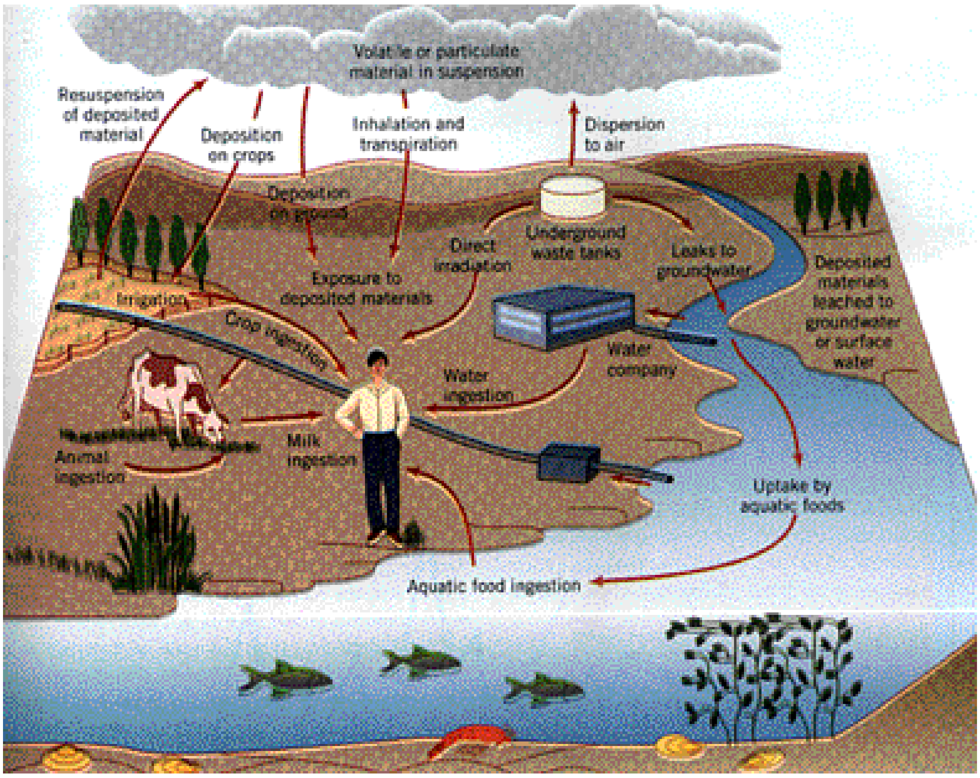

Figure 11. Transportation of radionuclides in terrestrial environments.

Source:http://www.umich.edu/~gs265/ROSEN5.gif

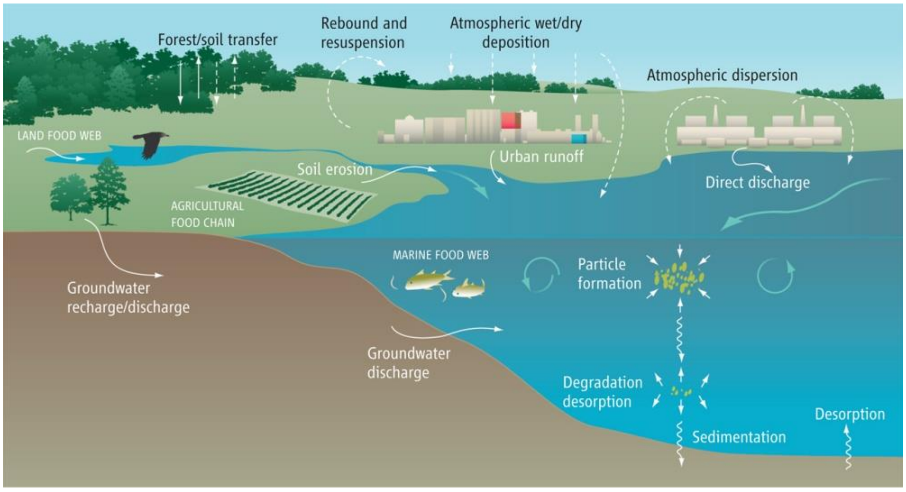

Figure 12. Transportation of radionuclides in aquatic and marine environments.

Source:http://www.sciencemag.org/content/336/6085/1115/F2.large.jpg

3. CAESIUM-137 (^{137}CS)

Caesium (Cs) is a soft, silvery white, ductile metal that is a member of the alkali metals. Its atomic number is 55 and its atomic weight is 132.91. Compared to other stable alkali metals, cesium has the lowest melting point of 28.4 ^{o}C, the lowest boiling point of 690 ^{o}C, the highest density of 1.90 g/cm^3 in near room temperature, the highest vapor pressure and the lowest ionization potential. These properties make it much more reactive than the other alkali metals. When it is exposed to air, it ignites, producing a reddish violet flame and forma a mixture of caesium oxides. Also caesium reacts violently with water to form cesium hydroxide (Finston et al., 1961) (ATSDR - Agency for Toxic Substances and Disease Registry, 2004) .

Caesium is widely distributed in nature, almost always associated with the other alkalis and usually in small amounts. The natural source yielding the greatest quantity of caesium is the mineral pollucite. It can also be obtained from carnallites (Finston et al., 1961). In nature it exists as caesium-133, which is caesium's only stable form. There are several radioactive isotopes of caesium ranging from ^{114}Cs to ^{145}Cs, with half-lives ranging from about 0.57 seconds to about 3 x 10^6 years. The most important isotopes of caesium are ^{134}Cs and ^{137}Cs. Caesium-134 has a half-life of 2.1 years and is produced as a fission product and via neutron capture from stable ^{133}Cs. It undergoes beta decay (β-), producing Barium-134 (ATSDR - Agency for Toxic Substances and Disease Registry, 2004).

Caesium-137 is the most known and important isotope of caesium and it was invented in 1930 by Glenn T.Seaborg and Margaret Melhase (Patton, 1999). It has a half-life of 30.2 years and it decays by beta (β-) decay to either Barium-137 (^{137}Ba) or to Barium-137m (^{137m}Ba). Then ^{137m}Ba, which has a half-life of 2 minutes, is converted to ^{137}Ba by gamma (γ-) decay producing gamma rays with an energy of 661.7 keV (Ashraf et al., 2014). It is a man-made radionuclide and it is produced from both Uranium (U-) and Plutonium reactors (Pu-); via the fission of Uranium-235 and Plutonium-239 with the fission yields of 6.2% and 5.2%, respectively (Devell et al., 1994). In figure 13 the fission chain of ^{235}U and the production of ^{137}Cs can be seen. In figure 14 the decay scheme of ^{137}Cs is presented.

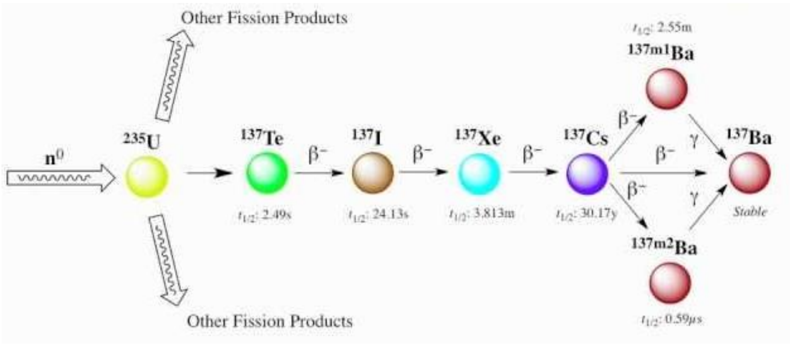

Figure 13. The creation of ^{137}Cs through ^{235}U fission.

Source:[*http://i.ytimg.com/vi/MPtBZig3fEw/sddefault.jpg*](http://i.ytimg.com/vi/MPtBZig3fEw/sddefault.jpg)

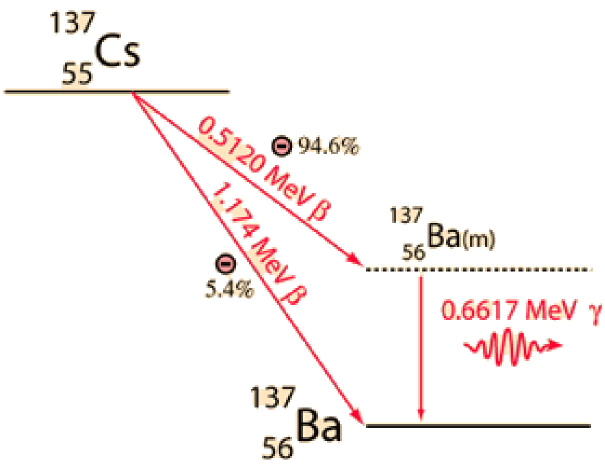

Figure 14. The decay scheme of ^{137}Cs.

Source:[*http://hyperphysics.phy-astr.gsu.edu/hbase/nucene/imgnuk/cs137decay.gif*](http://hyperphysics.phy-astr.gsu.edu/hbase/nucene/imgnuk/cs137decay.gif)

As a man-made radionuclide, ^{137}Cs can be released in the environment through a variety of ways. These can be global fallout from nuclear weapons tests, accidental releases from nuclear accidents, discharge from reprocessing plans and nuclear vessel accidents (Florou H. , 1992). In terrestrial ecosystems, ^{137}Cs is generally one of the less mobile radionuclide, because it adheres to soil. In the aquatic ecosystems ^{137}Cs is the most important indicator of radioactive pollution. Radioactive contamination of ^{137}Cs in the marine environment is caused by three main factors; these are global fallout, discharge from reprocessing plants and nuclear accidents. Its dispersion and transport is partially dependent on the physical, biological and chemical parameters of the marine environment. Its distribution in sea water is about 70% in ionic form, 23%

in a particle – reactive form and 7% in a colloidal phase (Polikarpov, 1966). In figure 15 the transportation and dispersion of ^{137}Cs in the marine environment is exhibited.

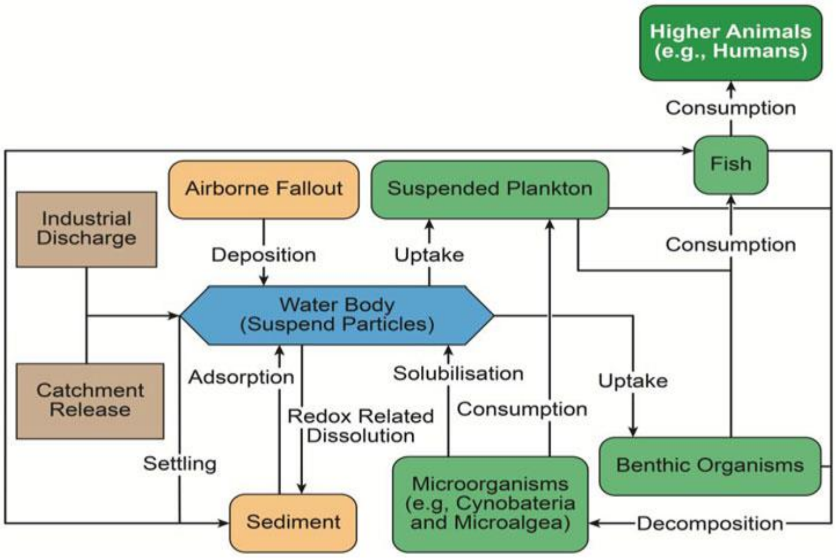

Figure 15. ^{137}Cs transportation and dispersion in the marine environment.

Source: (Ashraf, Akib, Maah, Yusoff, & Balkhair, 2014)

It was first introduced into the marine environment at the beginning of the atmospheric nuclear weapon testing in 1953 with a peak in 1959 and 1963, where it decreased until 1986 where the Chernobyl accident happened (Papucci & Delfanti, 1999). In the eastern Mediterranean region the most affected areas were the Black Sea, the Aegean Sea and the Ionian Sea. The Black Sea was the most contaminated of all, where the atmospheric fallout deposited about 1.7 – 2.4 PBq of ^{137}Cs in its surface (Florou, et al., 2002).

3.1. ^{137}Cs in the Aegean Sea

In the Aegean Sea area, ^{137}Cs was introduced from global fallout from atmospheric nuclear weapons testing and from releases from the Chernobyl nuclear power plant accident. Prior the Chernobyl accident the Aegean Sea was influenced by the global fallout; with ^{137}Cs levels being around 2.6±0.3 Bq/m^3 (Florou, et al., 2002). Since 1986, the impact of the contamination from the Chernobyl accident resulted in a great increase of ^{137}Cs to 820TBq due to atmospheric fallout and the discharge from the Black Sea (Evangeliou et al., 2009). The present radiological status in the Aegean, observed since 2000, is characterized by high values in the North Aegean and especially near the Dardanelles where the mean ^{137}Cs activity concentration is about 13.3 ± 1.3 Bq/m^3, presenting a decrease in the Southern Aegean with a mean value of 5 Bq/m^3 (Evangeliou et al., 2009). During 2010 a ^{137}Cs activity concentration of 82.7 Bq/m3 was observed in the mouth of the Dardanelles region that confirmed the annual outflow of 48TBq from the Black Sea. The rest of the Aegean Sea presented values than ranged from 1.1 to 16.5 Bq/m^3 (Florou et al., 2010). In figure 16, the ^{137}Cs activity concentration (Bq/m3) in the Aegean and Ionian Seas for 2014 corrected using the effective half-life of 7.2 years is presented.

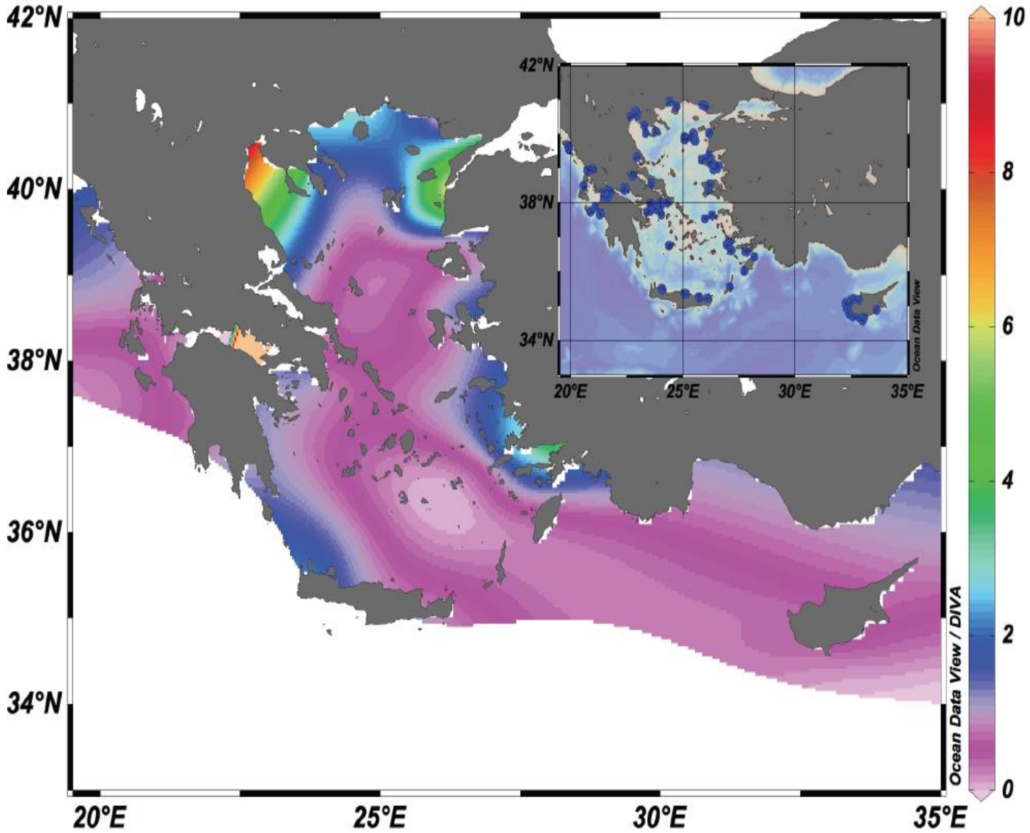

Figure 16.^{137}Cs activity concentration (Bq/m^3) in the Aegean and Ionian Seas for 2014 corrected using the effective half-life of 7.2 years.

Source: (Florou et al., 2014)

4. SATELLITE REMOTE SENSING

Remote sensing is the science of acquiring and analyzing data for an object without coming into contact with it. It is the science of studying an object from a distance (Kartalis et al., 2006). Remote sensing has three major components. The first component is the reaction of energy source with the target, the second component is the sensor and the third component is the sensing (ESA, European Space Agency, 2000-2014). Sensing is defined as acquiring knowledge about the object or the phenomenon after analysis of the signals received by a sensor. Satellite remote sensing is the principal form of remote sensing, where special sensors are placed in a satellite system in order to record and study the Earth's surface.

The sensors aboard the satellite systems are capable to detect and record the electromagnetic radiation that is emitted or reflected from a surface. They are capable to record electromagnetic radiation that belongs in the visible, infrared or microwave spectrum (Kartalis et al., 2006) (Mertikas, 2006). Using this attribute these systems can create images that contain information about the Earth's surface. Satellite remote sensing images have a lot of advantages like the coverage of large areas and continuous recording of phenomena. In order for a sensor to record an image the following process needs to be conducted. At first it is crucial that a source of energy or a source of electromagnetic radiation is present. In passive remote sensing this source is the sun, in thermal remote sensing the source is the heat that is emitted by the observed objects and in active remote sensing the source is the satellite system itself. The emitted radiation transits from the source, into the atmosphere in order to reach the target object where it reflects back to the satellite system. But before it returns to the satellite the radiation interacts with the target object. This interaction depends on both the wavelength of the radiation and by the target object properties. Then, the reflected energy is captured by the sensor and is transmitted to the recording and processing stations where an image is formed. The final stage is the interpretation and analysis of the images.

4.1. SATELLITE REMOTE SENSING SYSTEMS

There are two basic kinds of satellite remote sensing sensors. The first kind is the passive systems and the second kind is the active systems.

4.1.1. PASSIVE SYSTEMS

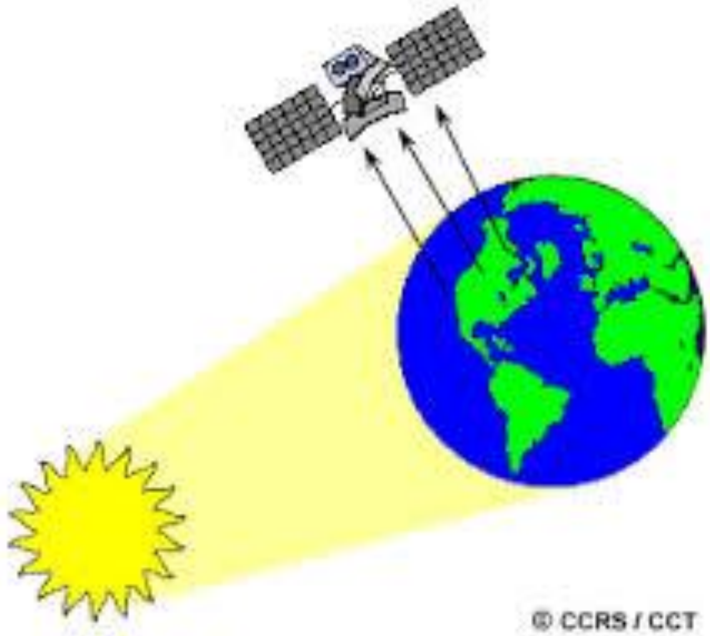

Figure 17. Passive remote sensing system.

Source:http://www.nrcan.gc.ca/sites/www.nrcan.gc.ca/files/earthsciences/images/resource/tutor/fundam/images/passiv.gif

The remote sensing systems that detect and record the reflected radiation from the Earth's surface are called passive. They are called passive because the radiation that they record comes from the sun and it is not generated by the satellite system (Figure 17) (Kartalis et al., 2006) (Mertikas, 2006). Therefore a sun synchronous orbit is necessary because they can record information only when the target area is illuminated by the sun. Another attribute of these systems is that they can record the naturally emitted thermal energy from the Earth’s surface. The thermal energy can be recorded both day and night. The passive systems are able to use the visible and infrared portion of the electromagnetic spectrum (from 0.38 μm to 1000 μm). However these systems are dependent to cloud coverage because the visible and infrared radiation cannot penetrate clouds. Thus when the cloud coverage is high, these systems are not able to record information.

4.1.2. Active systems

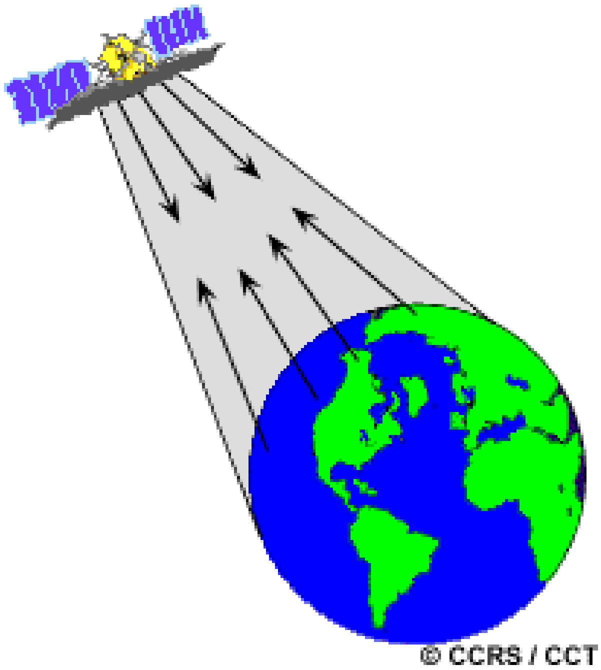

Figure 18. Active remote sensing system.

Source:http://www.nrcan.gc.ca/sites/www.nrcan.gc.ca/files/earthsciences/images/resource/tutor/fundam/images/sensors.gif

In contrast to passive systems, active systems do not record the radiation emitted from the sun, but they record the radiation that is transmitted from the system itself (Figure 18) (Kartalis et al., 2006) (Mertikas, 2006). These systems use long wave microwave radiation (3 cm to 25cm) in order to create an image. These systems have the advantage of recording regardless of whether the recording takes place day or night. Moreover they do not depend on weather conditions and cloud coverage because microwave radiation can penetrate clouds. Thus they are able to record information when the passive systems are unable to. The most known passive systems are radar (more specifically SAR Synthetic Aperture Radar) systems, sonar systems and LIDAR systems.

4.2. ATTRIBUTES OF SATELLITE REMOTE SENSING SENSORS

All the data that are recorded from a sensor system contain attributes that affect their quality. In addition the selection of the data used in research depends on these attributes. These attributes are spatial resolution, spectral resolution, radiometric resolution and temporal resolution.

4.2.1. SPATIAL RESOLUTION

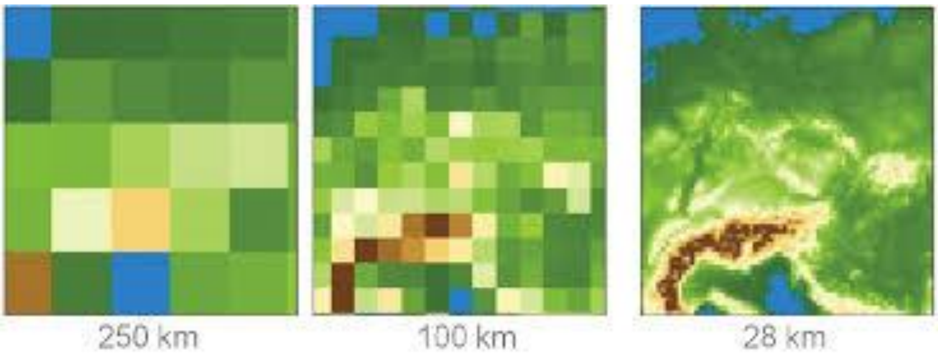

Figure 19. Example of spatial resolution.

Source:https://encrypted-tbn0.gstatic.com/images?q=tbn:ANd9GcTTaUeH1mUJQDUiC2DxX_CvalbXfzG407lChaOYvFWZsI6H5ADq

Spatial resolution is the minimum distance between two objects that a sensor can record distinctly (Kartalis et al., 2006) (Mertikas, 2006). Spatial resolution is measured in meters or kilometers of a pixel area in the image (Figure 19).

4.2.2. Spectral resolution

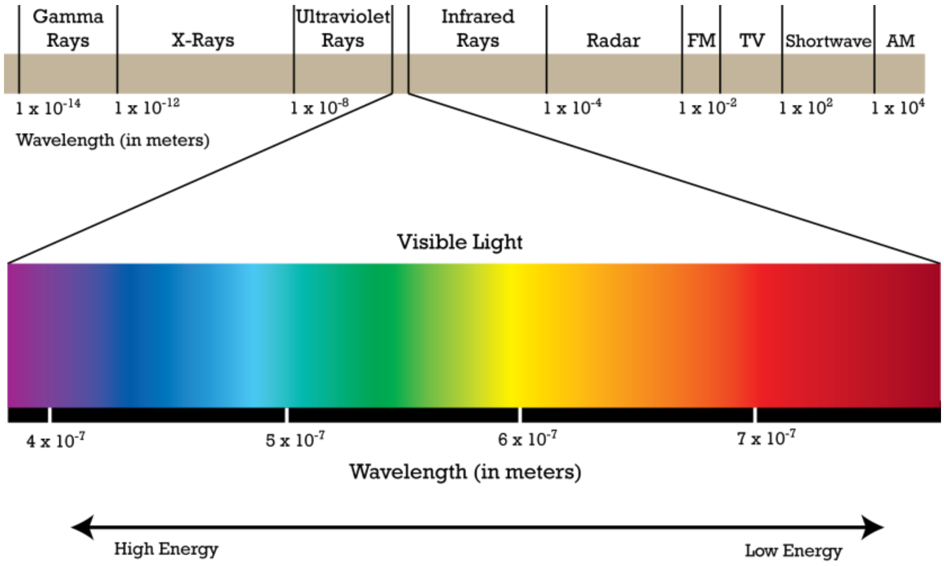

Figure 20. The electromagnetic spectrum.

Source:http://www.pion.cz/_sites/pion/upload/images/a14cf10a5583d19f7cfdebd63cf64382_electromagnetic-spectrum.png

Spectral resolution is defined as the range of the areas in the electromagnetic spectrum where a detector can record information (Figure 20) (Kartalis et al., 2006) (Mertikas, 2006). These areas are called bandwidths. A bandwidth defines a spectral band. Multispectral detectors can record information from several bandwidths or bands. The higher the spectral resolution of a sensor is for a spectral band, the smaller the range of the bandwidth. Hence more channels are recorded.

4.2.3. RADIOMETRIC RESOLUTION

Figure 21. Example of radiometric resolution.

Source:https://encrypted-tbn3.gstatic.com/images?q=tbn:ANd9GcT-7hrBvaVuZ9YZmgcev0y-9cBjRf2pZvhorK6GaQ4UcpLayvm6

Radiometric resolution is the ability of the sensor to detect differences in the intensity of the reflected or emitted radiation. Basically is the sensitivity of the sensor (Kartalis et al., 2006) (Mertikas, 2006). The radiometric resolution of the sensor is important because the information contained in the satellite data is determined by the radiometric values recorded by the sensor. The radiometric values recorded by the sensor are converted into digital values ranging from 0 to a value that is a power of 2. These values correspond to pixels of the digital images, and typically range from 0 to 255, with 0 values corresponding to black color and 255 values to white color in the image (Figure 21).

4.2.4. TEMPORAL RESOLUTION

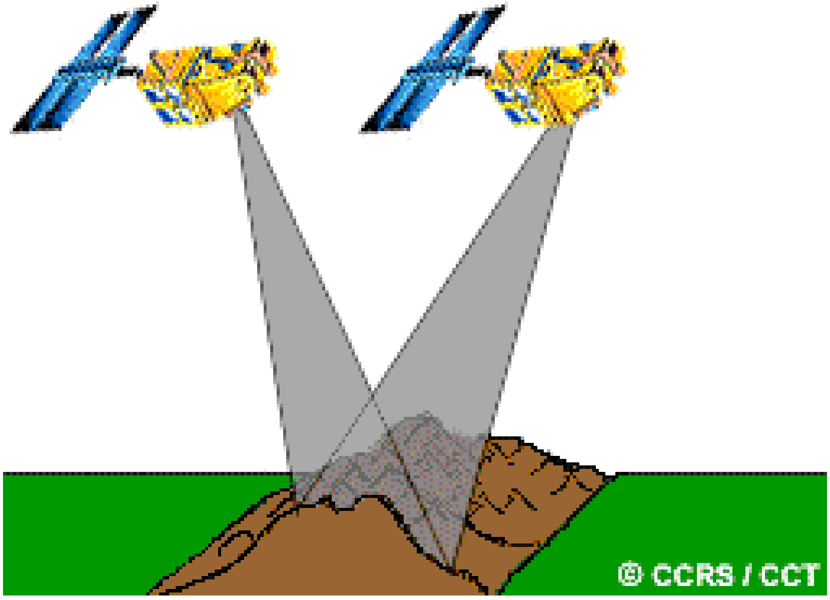

Figure 22. Example of temporal resolution.

Source:http://www.nrcan.gc.ca/sites/www.nrcan.gc.ca/files/earthsciences/images/resource/tutor/fundam/images/spotpoint.gif

The temporal resolution is related to the time interval between two successive visits of an area by a remote sensing satellite system (Figure 22) (Kartalis et al., 2006) (Mertikas, 2006). It is dependent from the satellite orbit and ranges from a few minutes for geostationary satellites to a few weeks for polar orbit satellites. Smaller the revisit time the better is the temporal resolution, but it depends on the studied phenomenon.

5. AREA OF INTEREST

The areas of interest in this thesis are the Aegean Sea and the area of Souda Bay in northern Crete (Figure 23). These two areas are located in Greece and they are a part of the Eastern Mediterranean region. The Aegean Sea constitutes the northeastern segment of the Mediterranean Sea and Souda Bay is located north in the island of Crete.

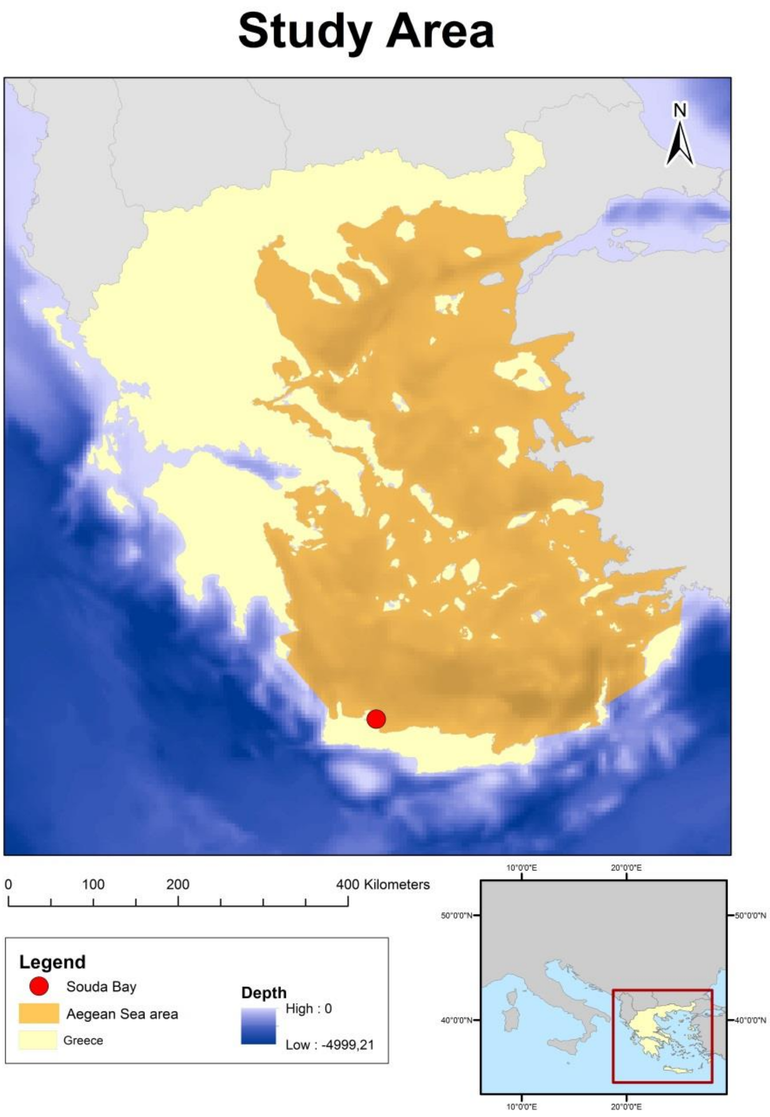

Figure 23. Study area.

5.1. AEGEAN SEA

The Aegean Sea is located in the Eastern Mediterranean Sea, and is defined as the marine area between the Greek mainland and Turkey. It is the third largest sea in the Eastern Mediterranean, with the fourth being Adriatic Sea. The main feature of the Aegean Sea is its really long and irregular coastline and a plethora of islands and islets and characterized by a complex bathymetry. It is bounded to the north and west by the Greek mainland, to the southwest by Cythera Island, to the south by Crete Island, to the east by Turkey and to the northeast by Dardanelles strait. It is the biggest marine water mass in Greece with an area of 240,000 square meters and a volume of 74,000 cubic meters (Hopkins, 1978). As the largest Sea in Greece, the Aegean Sea includes the Myrtoan Sea, the Thracian Sea, the Icarian Sea, the Cretan Sea, the Carpathian Sea and the Dodecanese Sea. It is also characterized by an abundance of Gulfs and Ports. The most known Bays in the Aegean are the Argolis gulf, the Saronic Gulf, the Gulf of Evia, the Pagasetic Gulf, the Thermaic or Thermaikos Gulf, the Gulf of Saros, the Edremit Gulf, the Gulf of Izmir and the Gulf of Kos. The biggest Ports in the Aegean Sea are Piraeus Port, Thessaloniki Port and Izmir Port. The Aegean Sea is also Region of Greece with a population of 503,697 inhabitants. It is divided in two sub divisional regions, the North Aegean Region and the South Aegean Region.

The Aegean Sea was created by the subsidence of Aegiis and the simultaneous intrusion of sea water during the Miocene Epoch. The current form of the Aegean Sea was created by tectonic changes that occurred during the Quaternary Period. These changes created the peculiar morphology of complex coastlines, numerous islands and irregular sea floor. The most important water masses in the Aegean Sea are the brackish and cold Black Sea Water (BSW), the very saline and warm waters of Levantine origin and the very dense deep waters that fill the bottom of the various sub-basins (Zervakis et al., 2001). The water circulation in the Aegean is rather complex and variable. This is due to many factors such as the distribution of the various island chains and straits, the irregular bottom topography, the seasonal variability of the atmospheric forcing, the presence of strong meteorological events that may alter the local circulation patterns and the presence of many different water masses (Sofianos, et al., 2002).

The Aegean Sea is characterized by a typical Mediterranean type of climate, where the annual climatic variability has two main periods. The first period is from November to March and is a cool and rainy period. The second period is from May to September and is a hot and dry period. The months of October and April are intermediate periods between the two main periods (Poulos et al., 1997). The mean annual air temperature over the Aegean varies between 16 ^{o}C and 19.5 ^{o}C, while annual precipitation varies between 400 and 700 mm. Sea Surface Temperature values vary from a minimum of 15 ^{o}C in February to a maximum of 26 ^{o}C in August (Skliris et al., 2010).Sea surface salinity values vary from 32 to 39 psu (Valaoras, et al., 2013). It presents an increasing pattern from North to South Aegean. Bigger salinity fluctuations are present during the summer, while during the winter salinity is mostly stable. Chlorophyll-A values vary from 0.03 mg/m3 to 0.70 mg/m3 with the higher values present in North Aegean due to incoming water from Black Sea (Melin et al., 2007).

5.2. SOUDA

Souda Bay is located in the Southern Aegean Sea, in the island of Crete. The bay is a natural harbour about 15 km long and 2 to 4 km wide. It is an area of intense human activities as it is one of the largest natural embayments in the Mediterranean, being an important post for freight, ferries and the location of three major military bases, the Hellenic Navy’s Crete Naval station, which also NATO Missile Firing Station. Shipping, coastal fisheries, aquaculture, tourism and agricultural and industrial activities are among the most common human activities on the area (Katsanevakis et al, 2009). The area of Souda Bay was chosen due to its most frequent 137Cs activity concentration measurements provided by the Environmental Radioactivity Laboratory (ERL, NCSR“Demokritos”) database.

6. DATA

The data used in the methodology contain satellite and in situ measurements. In this chapter the origin of the properties of data is presented. Satellite data were acquired from SMOS, TERRA and AQUA satellites. In situ data were acquired from the Environmental Radioactivity Laboratory of NCSR "D" (National Centre for Scientific Research "Demokritos") and from the POSEIDON buoy database system of the HCMR (Hellenic Centre for Marine Research).

The marine parameters issued from satellite data used in the analysis include sea surface temperature, sea surface salinity, chlorophyll-A, particulate organic carbon concentration, particulate inorganic carbon concentration, cdom index, instantaneous photosynthetically available radiation, daily photosynthetically available radiation and ^{137}Cs activity concentration.

Sea surface temperature is the temperature in sea depth from 1 mm to 20 m. It is a really important environmental parameter because it affects the atmosphere system and the hydrologic cycle by creating phenomena like cyclones, sea fog and sea breeze. Moreover sea surface temperature contributes significantly in water masses movement, because in conjunction with sea surface salinity they create ocean currents circulation. Sea surface temperature is measured in Celsius degrees (^{o}C).

Sea salinity is defined as the salt concentration in sea water. Sea surface salinity is the sea salinity in sea depth from 1 mm to 20 m. Sea salinity is equally important to sea temperature because it affects density and the thermal capacity of water bodies. It is measured in practical salinity units (PSU) which depends from water conductivity and is 1 PSU is equal to $1\frac{gr}{kg}$ (concentration of dissolved salt in water).

Chlorophyll concentration in the marine environment is measured using the chlorophyll-A concentration. In aquatic environments, chlorophyll-A is mainly found in phytoplankton. The phytoplankton concentration is greater in waters with a greenish tint. Chlorophyll-A is measured in mg in a cubic meter (mg/m^3).

Particulate organic carbon concentration is measured in mg in a cubic meter (mg/m^3) and is derived from the vegetation decomposition, the growth of microorganisms and the metabolic activity of living organisms.

Particulate inorganic carbon concentration is measured in mol in a cubic meter (mol/m^3) and consists of carbonate, bicarbonate and dissolved carbon dioxide.

CDOM index or else colored dissolved organic matter index quantifies the deviation in the relationship between CDOM and chlorophyll concentration. CDOM is defines as the optically measurable component of the dissolved organic matter in water. It occurs naturally and is a result of tannin-stained waters released from decaying detritus.

Photosynthetically Available radiation is defined as the quantum energy flux from the Sun in the spectral range 400-700 nm. It is expressed in Einstein/ (m^2*day). Einstein is defined as the energy of one mole of photons. Instantaneous Photosynthetically Available radiation is the instant measurement of PAR and it is measured in Einstein/ (m^2*sec).

Caesium-137 (^{137}Cs) is a manmade radionuclide with a half-life of 30.2 years and it is an atomic fission product of both uranium (U-) and plutonium (Pu-) reactors. It is an important indicator of radioactive pollution in aquatic environments (Ashraf, 2014). In the aquatic environment ^{137}Cs is measured in Bq/m^3.

6.1. Satellite measurements.

6.1.1. SMOS/MIRAS

SMOS Satellite or Soil Moisture Ocean Salinity (Figure 24) is a European Space Agency (ESA) Satellite designed to monitor the moisture of the land areas and the salinity of the oceans. It was launched on November 2, 2009 from the Plasetsk cosmodrome in Northern Russia. It has is an innovative recording instrument that uses the microwave portion of the electromagnetic spectrum called MIRAS or Microwave Imaging Radiometer using Aperture Synthesis (ESA, European Space Agency, 2011). General information about SMOS satellite can be seen in Table 1.

Figure 24. SMOS satellite.

Source:http://due.esrin.esa.int/news/LogoImages/20130403145033.pjpeg

Mission	SMOS
Launched	2 November 2009
Duration	Minimum 3 years
Instrument	Microwave Imaging Radiometer using Aperture Synthesis - MIRAS
Instrument concept	Passive microwave 2D-interferometer
Frequency	L-band (21 cm-1.4 GHz)
Number of receivers	69
Receiver spacing	0.875 lambda = 18.37 cm
Polarisation	H & V (polarimetric mode optional)
Spatial resolution	35 km at centre of field of view
Tilt angle	32.5 degrees
Radiometric resolution	0.8 - 2.2 K
Angular range	0-55 degrees
Temporal resolution	3 days revisit at Equator
Instrument data rate	89 kbps H & V pol.
Mass	Total 658 kg launch mass comprising: platform 275 kg, payload 355 kg, fuel 28 kg
Orbit	Sun-synchronous, dawn/dusk, quasi-circular orbit at altitude 758 km. 06.00 hrs local solar time at ascending node.
Launcher	Rockot, KM-Breeze upper stage
Bus	Proteus (1 m cube)
Power	Up to 1065 W (511 W available for payload; 78 AH Li-ion battery.
Spacecraft Operations Control Centre	CNES,Toulouse, France
S-Band TTC link	4 kbps uplink, 722 kbps downlink
Payload Mission and Data Centre	ESAC, Villafranca, Spain
X-Band data downlink	16.8 Mbps

Table 1. Information about SMOS satellite.

Source:http://www.esa.int/Our_Activities/Observing_the_Earth/The_Living_Planet_Programme/Earth_Explorers/SMOS/Overview3

6.1.1.1. MIRAS SENSOR

SMOS satellite uses the MIRAS (Microwave Imaging Radiometer using Aperture Synthesis) instrument (Figure 25), which is a passive two dimensional interferometer capable to record faint microwave emissions from the Earth's Surface in the L band (1.4 GHz and wavelength of 21 cm), in order to monitor the levels of soil moisture and ocean salinity. MIRAS interferometer uses the interferometry principle of measuring the phase difference between electromagnetic waves emitted from two sensors in a defined distance. On the MIRAS instrument 69 small sensors measure the phase difference of the recorded radiation. These sensors are placed at a distance 18.37 cm from each other in a Y shaped antenna. From an altitude of 758 km, the antenna has a view field of 3000 km in diameter. But due to the interferometric principle and the Y-shaped antenna, the field of view is restricted to an approximately hexagonal shape with a diameter of 1,000 km. It has a spatial resolution of 35 km in the center of view field and a temporal resolution of 3 days (ESA, European Space Agency, 2011).

Figure 25. The MIRAS recording instrument.

Source:http://sciences.blogs.liberation.fr/.a/6a00e5500b4a6488330120a64ac053970b-pi

6.1.1.2. SMOS DATA

SMOS satellite data were provided by ESA using the Eolisa software (Figures 26, 27). Eolisa provided level 0 data to level 2. From 2016 Eolisa software no longer provides SMOS images. The images are currently available only via FTP using an ESA Earth Online account. In this study the data used were Level 2 ocean salinity products. These products - images contain information about Sea Surface Salinity (SSS) and Sea Surface Temperature (SST) for the period December 2011 to June 2015. The images have a spatial resolution of 50 kilometers. A special limitation is applied in SMOS data due to RFI (Radio Frequency Interference) contamination from radio waves that affect the natural microwave emission in the band L. Radiofrequency contamination results in less accurate microwave measurements. These radiofrequencies are anthropogenic in nature and come from ground emitters and aircrafts. Therefore to avoid errors in sea surface parameters calculation, this spatial limitation was adopted. The limitation requires that pixels must refrain 100 kilometers from the nearest coastline (Mecklenburg, et al., 2011). Applying this limitation in the Aegean Sea area, which has a unique geomorphology with a lot of islands and islets, there are only 39 pixels resolved. Timeseries of SMOS SST and SSS for the Aegean Sea and Souda Bay can be seen in the appendix (pages 204 and 207 respectively).

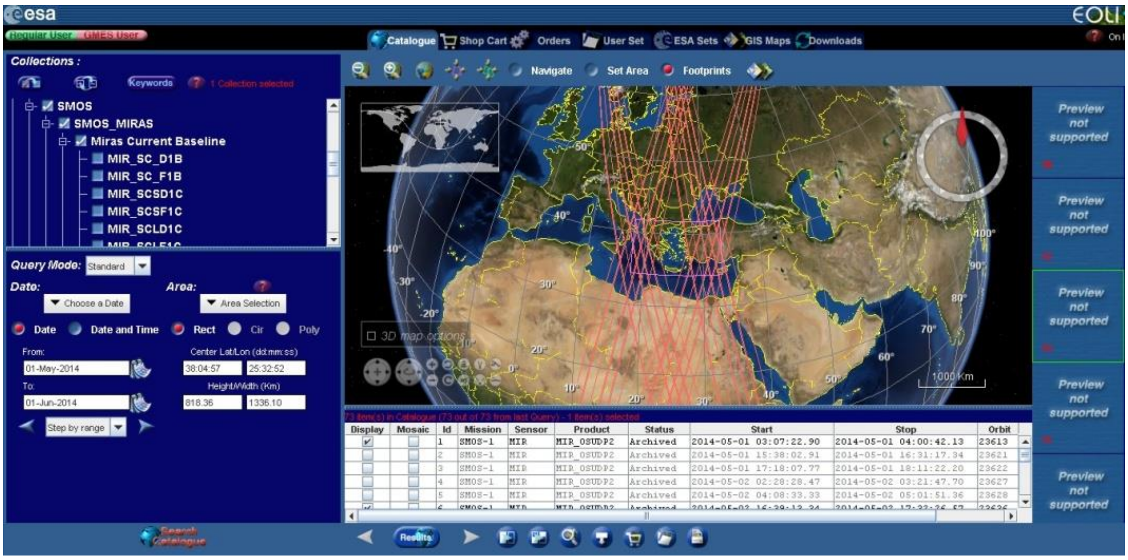

Figure 26. EOLi-SA software.

Source: https://earth.esa.int/web/guest/eoli

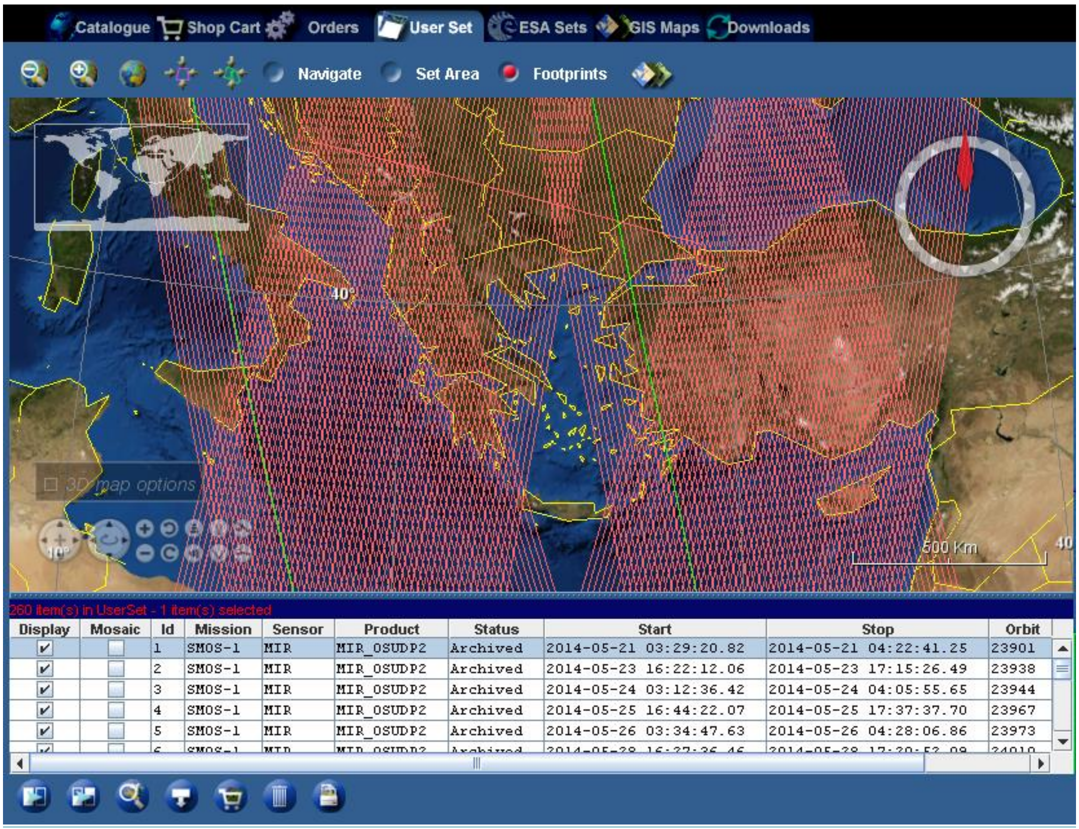

Figure 27. Image selection procedure in EOLi-SA.

As it was mentioned above, in this analysis the level 2 ocean salinity product will be used. Level 2 ocean salinity products contain Sea Surface Salinity (SSS) and Sea Surface Temperature (SST) information. The MIRAS instrument calculates SST and SSS by measuring the polarized radiometric brightness temperature Tb which is calculated by the Earth's emitted microwave radiation. The brightness temperature Tb is calculated using the equation:

$$Tb = e * Ts$$

Eq 1. Brightness Temperature (Tb).

Where *Ts* is the real sea surface temperature and *e* is the emissivity of the sea surface. In this calculation SMOS takes into consideration the ocean surface roughness and the Faraday rotation. Once the brightness temperature is calculated, the salinity algorithm is used to calculate Sea surface Salinity (Thomson et al., 2014).The salinity algorithm is the L2SPP (Level 2 Salinity Prototype Processor), which produces 3 salinity models SSS1, SSS2 and SSS3. The SSS1 model is retrieved using a two scale model that utilizes surface roughness and sea foam. The SSS2 model is retrieved using an empirical method that utilizes sea surface slope and the SSS3 model is retrieved using an empirical method that utilizes field measurements (Font, et al., 2013) (Mecklenburg, et al., 2011) (Spurgeon, et al., 2010). The received L2 images contain SST in Celsius degrees and SSS1, SSS2, SSS3 in psu.

6.1.2. TERRA AND AQUA/MODIS

TERRA (EOS AM) and AQUA (EOS PM) satellites are part of NASA’s Earth Science program and they both contain the MODIS (Moderate Resolution Imaging Spectrometer) instrument. They are twin satellites despite of containing different sensors and having different equator passing time. Together they have a temporal resolution of 1-2 days.

6.1.2.1. TERRA SATELLITE

TERRA satellite (Figure 28) was launched on 18 December 1999 by NASA thus marking the beginning of the Earth Observing System mission for understanding global changes and their impact. Apart from the MODIS instrument, it contains the CERES (Clouds and Earth’s Radiant Energy System), the MISR (Multi-angle Imaging Spectroradiometer), the MOPITT (Measurements of Pollution in the Troposphere and ASTER (Advanced Spaceborne Thermal Emission and Relfection) sensors. TERRA’s observations provide researchers with important data for natural disasters such as forest fires, volcanic eruptions and floods. The satellite has a sun synchronous polar orbit with a height of 705 km above the Earth and it passes over the Equator at 10:30 AM (NASA Goddard Flight Center, last update 2016).

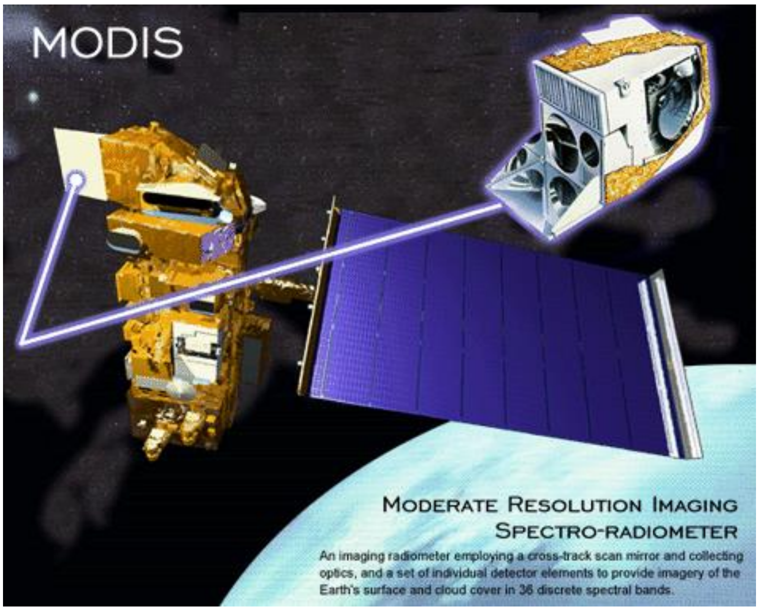

Figure 28. NASA's TERRA satellite.

Source: *http://modis-sr.ltdri.org/rationale/sc2-modis.gif*

6.1.2.2. AQUA SATELLITE

AQUA Satellite (Figure 29) was launched on 4 May 2002 and is also a part of NASA's Earth Observing System mission. The collected data contain information for ocean evaporation, water vapors in the atmosphere, precipitation, sea ice and snow coverage. The satellite includes the AIRS (Atmospheric Infrared Sounder), the AMSU-A (Advances Microwave Sounding Unit), the HSB (Humidity Sounder for Brazil), the AMSR-E (Advanced Microwave Scanning Radiometer for EOS), the CERES (Clouds and Earth's Radiant Energy System) and the MODIS instrument. It has the same orbit and height with TERRA satellite and it passes over the Equator at 1:30 PM (NASA Goddard Space Flight Center, last updated 2016).

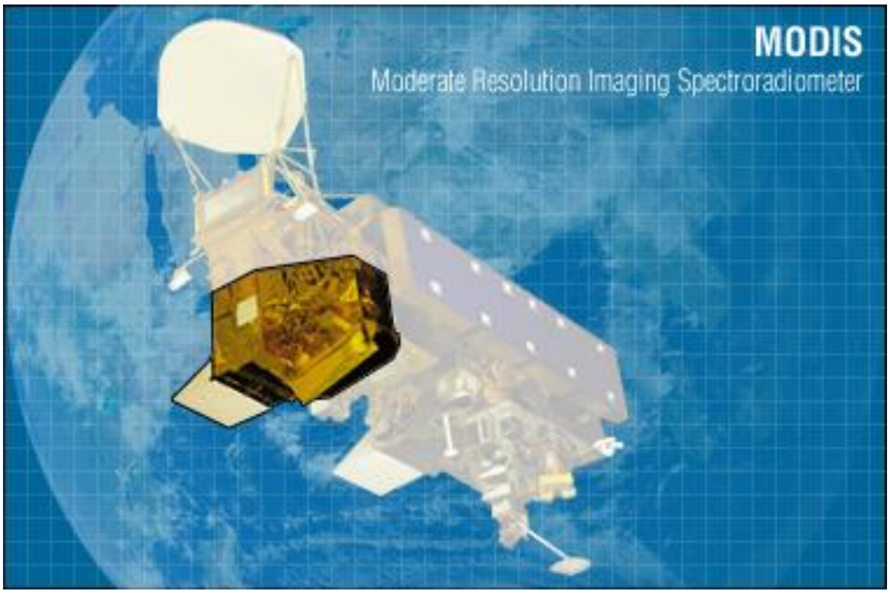

Figure 29. NASA's AQUA satellite.

Source: *http://aqua.nasa.gov/about/images/modis.jpg*

6.1.2.3. MODIS INSTRUMENT

MODIS or Moderate Resolution Imaging Spectrometer (Figure 30) is a spectral radiometer with 36 spectral bands that records visible and infrared radiation. As mentioned above there are two MODIS sensors. The first one named Proto Flight Model was launched in December 1999 on Terra satellite. The second one named Flight Model 1 was launched in May 2002 on Aqua Satellite. MODIS instrument has an adequate spectral resolution with 36 spectral bands ranging from 0.4 μm to 14.4 μm wavelength. The first 21 spectral bands range from 0.4-3μm and the rest 15 range from 3-14.4 μm (Table 2). It has three categories of spatial resolution where in the 2 first bands the spatial resolution is 250 meters, in the next 5 bands the resolution is 500 meters and in the rest of the spectral bands the spatial resolution is 1000 meters. In addition the MODIS instrument has an incline of 98 degrees and is at a height of 705 kilometers from the Earth’s surface. It also has a view field of 2330 kilometers and a temporal resolution of 1 to 2 days (NASA Goddard Space Flight Center, last updated 2016).

It collects environmental data about the atmosphere, land and aquatic environments. These data include cloud coverage information, sea surface temperature, ocean color, land coverage, land temperature and vegetation properties.

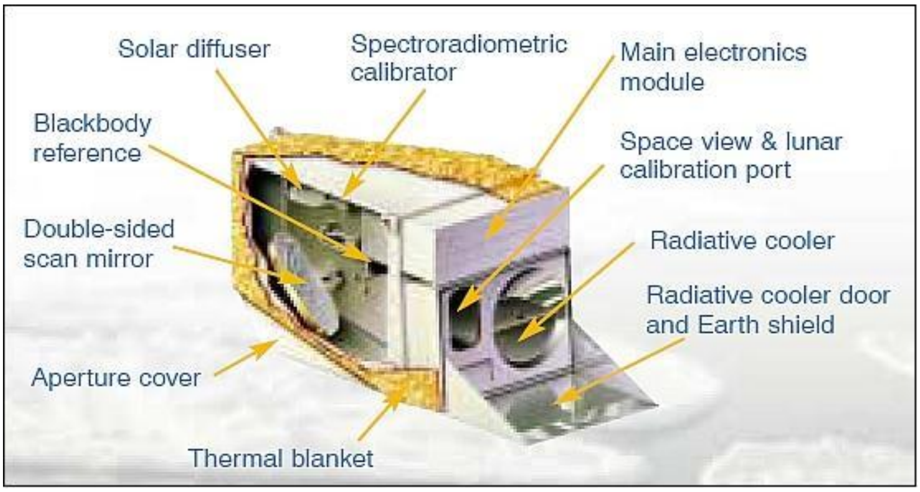

Figure 30. MODIS recording instrument.

Source: https://directory.eoportal.org/web/eoportal/satellite-missions/t/terra

Primary Use	Band	Bandwidth[1]	Spectral Radiance[2]	Required SNR[3]
Land/Cloud/Aerosols Boundaries	1	620 - 670	21.8	128
	2	841 - 876	24.7	201
Land/Cloud/Aerosols Properties	3	459 - 479	35.3	243
	4	545 - 565	29.0	228
	5	1230 - 1250	5.4	74
	6	1628 - 1652	7.3	275
	7	2105 - 2155	1.0	110
Ocean Color/ Phytoplankton/ Biogeochemistry	8	405 - 420	44.9	880
	9	438 - 448	41.9	838
	10	483 - 493	32.1	802
	11	526 - 536	27.9	754
	12	546 - 556	21.0	750
	13	662 - 672	9.5	910
	14	673 - 683	8.7	1087
	15	743 - 753	10.2	586
	16	862 - 877	6.2	516
Atmospheric Water Vapor	17	890 - 920	10.0	167
	18	931 - 941	3.6	57
	19	915 - 965	15.0	250
Surface/Cloud Temperature	20	3.660 - 3.840	0.45(300K)	0.05
	21	3.929 - 3.989	2.38(335K)	2.00
	22	3.929 - 3.989	0.67(300K)	0.07
	23	4.020 - 4.080	0.79(300K)	0.07
Atmospheric Temperature	24	4.433 - 4.498	0.17(250K)	0.25
	25	4.482 - 4.549	0.59(275K)	0.25
Cirrus Clouds Water Vapor	26	1.360 - 1.390	6.00	150(SNR)
	27	6.535 - 6.895	1.16(240K)	0.25
	28	7.175 - 7.475	2.18(250K)	0.25
Cloud Properties	29	8.400 - 8.700	9.58(300K)	0.05
Ozone	30	9.580 - 9.880	3.69(250K)	0.25
Surface/Cloud Temperature	31	10.780 - 11.280	9.55(300K)	0.05
	32	11.770 - 12.270	8.94(300K)	0.05
Cloud Top Altitude	33	13.185 - 13.485	4.52(260K)	0.25
	34	13.485 - 13.785	3.76(250K)	0.25
	35	13.785 - 14.085	3.11(240K)	0.25
	36	14.085 - 14.385	2.08(220K)	0.35

[1] Bands 1 to 19 are in nm; Bands 20 to 36 are in µm
[2] Spectral Radiance values are (W/m^2 -µm-sr)
[3] SNR = Signal-to-noise ratio
[4] NE(delta)T = Noise-equivalent temperature difference

Note: Performance goal is 30-40% better than required

Table 2. MODIS' spectral bands.

Source: http://modis.gsfc.nasa.gov/about/specifications.php

6.1.2.4. MODIS DATA

In this analysis MODIS Level 2 (L2) and Level 3 (L3) Sea Surface Temperature and Ocean Color data were used. Level 2 data consist of derived geophysical variables at the same resolution as the source Level 1 data (NASA Goddard Space Flight Center, Ocean Biology Processing Group, 2014). These variables are grouped into a few product suites. On the other hand, Level 3 data are derived geophysical variables that have been aggregated/projected onto a well-defined spatial grid over a well-defined time period. Level 3 data are produced in two distinctive types, L3 Binned data and L3 Mapped Data. The L3 Binned data products consist of the accumulated data for all L2 products in a product suite, for the specified instrument and resolution, corresponding to a period of time (daily, 8 days, monthly) and stored in a global, nearly equal-area, integerized sinusoidal grid. The L3 Standard Mapped Image (SMI) products are created from the corresponding Level 3 binned products. Each SMI file contains a Plate Carrée, pixel-registered grid of floating-point values (or scaled integer representations of the values) for a single geophysical parameter (NASA Goddard Space Flight Center, Ocean Biology Processing Group, 2014). A color look-up table is also provided in each file that may be uses to generate an image from the data. In this study the L3 SMI data were preferred.

The images were obtained from NASA's Ocean Color Web Level 1&2 browser (Figure 31) and Ocean Color Web Level 3 Browser (Figure 32). These images were acquired for the time span March 2011 to June 2015 and had a spatial resolution of 1 km and 4 km accordingly. Sea Surface Temperature data contain Night Sea Surface Temperature (SSTnight), Night Sea Surface Temperature at 4μm (SST4night) and Morning Sea Surface Temperature (SSTmorning). Ocean Color data contain Chlorophyl–A (Chlor_a), Particulate Inorganic Carbon (PIC), Particulate Organic Carbon (POC), Colored dissolved organic matter Index (CDOM), Instantaneous Photosynthetically Available Radiation (iPAR) and Photosynthetically Available Radiation (PAR). Timeseries of MODIS measurements for the Aegean Sea and Souda Bay can be seen in the appendix (pages 205 and 208 respectively).

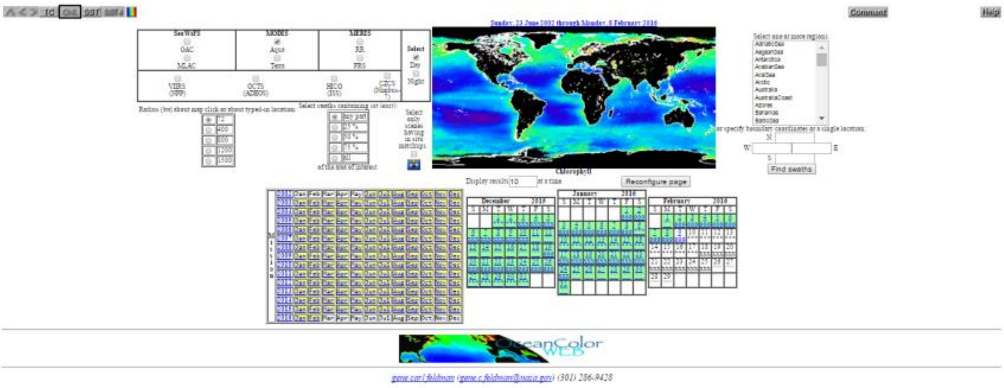

Figure 31. OceanColor web-browser for level 1 and level 2 images.

Source: *http://oceancolor.gsfc.nasa.gov/cgi/browse.pl?sen=am*

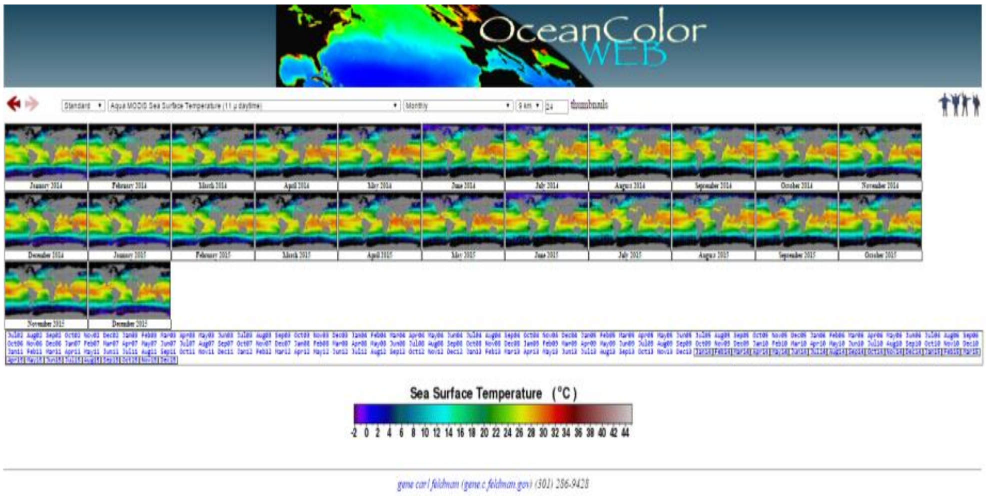

Figure 32. OceanColor web-browser for level 3 images.

Source: *http://oceancolor.gsfc.nasa.gov/cgi/l3*

Sea Surface Temperature is measured by MODIS instrument using two methods. The first method is the Long-Wave SST algorithm that produces Sea Surface Temperature at 11µm (SSTnight and SSTmorning). This algorithm makes use of MODIS bands 31 and 32 at 11 and 13 µm. The brightness temperatures are derived from the observed radiances by inversion (in linear space) of the radiance versus blackbody temperature relationship (Brown et al., 1999). The second method is the Short-Wave SST that produces Sea Surface Temperature at 4µm (SST4night). This algorithm makes use of MODIS bands 22 and 23 at 3.959 and 4.050 µm. The brightness temperatures are derived from the observed radiances by inversion (in log space) of the radiance versus blackbody temperature relationship (Brown et al., 1999).

Chlorophyll-A (Chlor_a) algorithm returns the near surface concentration of chlorophyll-a in mg/m^3, calculated using an empirical relationship derives from in situ measurements of chlorophyll-a and blue to green band ratios of in situ remote sensing reflectances (Rrs). Implementation is contingent on the availability of three or more sensor bands spanning the 440 – 570 nm spectral regime (Werdell et al., 2005).

Particulate Inorganic Carbon (PIC) algorithm derives the concentration of particulate inorganic carbon in mol/m^3, calculated using in situ relationships between water leaving radiances, spectral backscattering coefficients and concentrations of PIC (calcium carbonate, calcite). Algorithm implementation is contingent on the availability of sensor bands near 443 and 555 nm (Balch et al., 2005).

Particulate Organic Carbon (POC) algorithm returns the concentration of particulate organic carbon in mg/m^3, calculated using an empirical relationship derived from in situ measurements of POC and blue to green band ratios of remote sensing reflectances (Rrs). Support for this algorithm is contingent on the availability of bands centered at 443 nm in the blue region and between 547 and 565 nm in the green region (Stramski et al., 2008).

Color dissolved organic matter (CDOM) absorbs light in an exponentially decreasing manner as a function of wavelength. Pheopigments, detritus and bacteria similarly absorb more strongly at 412 nm than they do at 443 nm. Phytoplankton, on the other hand, absorb more strongly at 443 nm than at 412nm. Thus, by measuring the relative amounts of light leaving the sea surface at those two wavelengths, we can estimate the CDOM index (Carder et al., 2003).

Photosynthetically Available Radiation (PAR) algorithm estimates daily average photosynthetically available radiation at the ocean surface in Einstein/(m^2*d). Implementation of this algorithm is contingent on the availability of observed top of the atmosphere radiances in the visible spectral regime that do not saturate over clouds.

Instantaneous Photosynthetically Available Radiation (iPAR) algorithm returns the instantaneous photosynthetically available radiation in Einstein/(m^2*s). This product represents the total PAR incident on the ocean surface at the time of the satellite observation.

6.2. ^{137}Cs Measurements

The activity concentrations of ^{137}Cs used in this study were mainly retrieved from the ERL's database of ^{137}Cs. In addition, new sea water samplings and laboratory analyses were performed in order to retrieve new additional measurements. The sea water samples were analyzed for ^{137}Cs using an ammonium molybdophosphate (AMP) radioanalytical pre-concentration method and gamma spectrometry analysis that are described in the methodology below.

6.3. Poseidon system

Responding to the need of systematic marine observations the Hellenic Center of Marine Research (HCMR) has established a monitoring, forecasting and information system for the Greek Seas named POSEIDON (Figure 33) (HCMR, Hellenic Centre for Marine Research, 2012). Considering both the variability of the system and the need for high frequency information a mixture of platforms was chosen, ranging from coastal buoys with few basic met-ocean sensors to open sea stations with an extensive list of sensors targeted to both physical and biochemical processes and their coupling at various time scales.

These buoys consist of seven Seawatch buoys, three Seawatch-Wavescan buoys and one Seawatch Deep Sea Module platform (HCMR, Hellenic Centre for Marine Research, 2012). Seawatch buoys are placed in areas where the water depth does not exceed 300m and can monitor temperature, salinity, pressure and other bio-chemical and meteorological parameters in several depths. Seawatch-Wavescan buoys are placed in deep offshore locations and can provide measurements about temperature, salinity, pressure, oxygen, chlorophyll and meteorological parameters. The Seawatch Deep Sea Module platform is deployed at southern Ionian Sea and can record sea pressure, temperature and salinity, as well as detect anomalies on the sea surface altimetry.

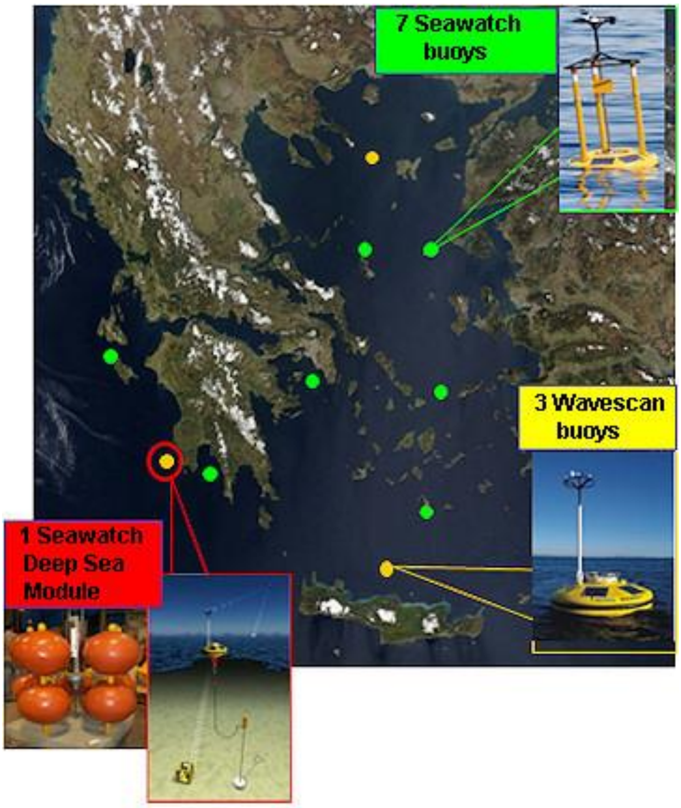

Figure 33. The POSEIDON system.

Source: [*http://www.poseidon.hcmr.gr/upload_files/Image/Picture7.jpg*](http://www.poseidon.hcmr.gr/upload_files/Image/Picture7.jpg)

Currently there are three active buoys placed in the Aegean Sea (Figure 34). These are the Athos buoy, the Petrokaravo buoy and the E1-M3A buoy. In this thesis only the E1-M3A buoy in Crete area was considered for the study of Souda Bay area. However time-series have been performed for all active buoys in the Aegean Sea. The E1-M3A buoy of the Cretan Sea is oriented towards air-sea interaction studies, biochemical processes in the euphotic zone and variability of intermediate and deep water mass characteristics. Its payload includes an extended set of meteorological sensors, a series of radiometers like multispectral sensors, optical and biochemical sensors and sensors for physical parameters (Petihakis et al., 2009). This buoy records parameters about temperature, salinity, chlorophyll, turbidity, meteorological parameters like humidity and precipitation, radiance, irradiance, wind speed and wind direction. Timeseries of POSEIDON measurements for the Aegean Sea and Souda Bay can be seen in the appendix (pages 206 and 209 respectively).

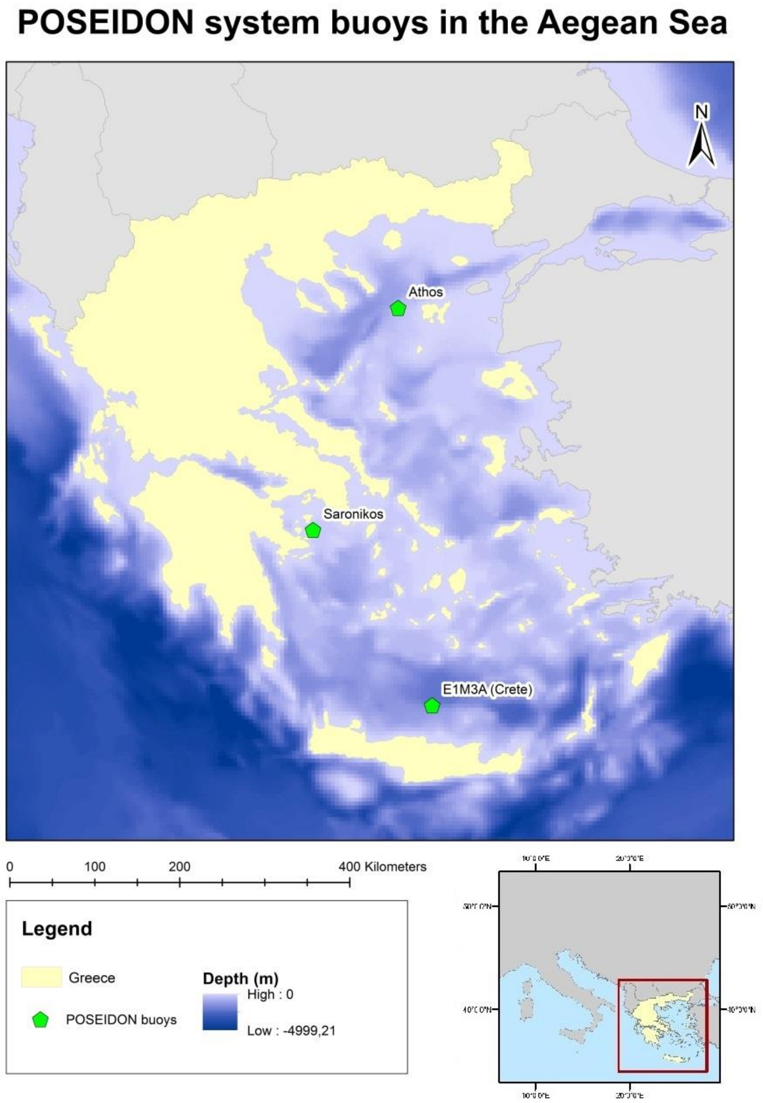

Figure 34. POSEIDON Buoys in the Aegean Sea.

7. METHODOLOGY

The methodology in this study is divided in two parts. The first part is the methodology followed in the Aegean Sea and the second part is the methodology followed in Souda Bay. These methods have some similar and some different stages. The stages that are similar are the laboratory analyses and the satellite data retrievals. The differences are in the relation analysis, where for the Aegean Sea is a map oriented relation analysis and in Souda Bay is a temporal statistical relation analysis. In this chapter the methodology followed is described. At first the satellite data retrievals method will be shown. Then the ^{137}Cs analysis follows that contains sea water sampling, laboratory analyses and gamma spectroscopy. Finally the statistical analysis and the map analysis for Souda bay and Aegean Sea respectively, are examined. The flowchart of the methodology is presented in figure 35.

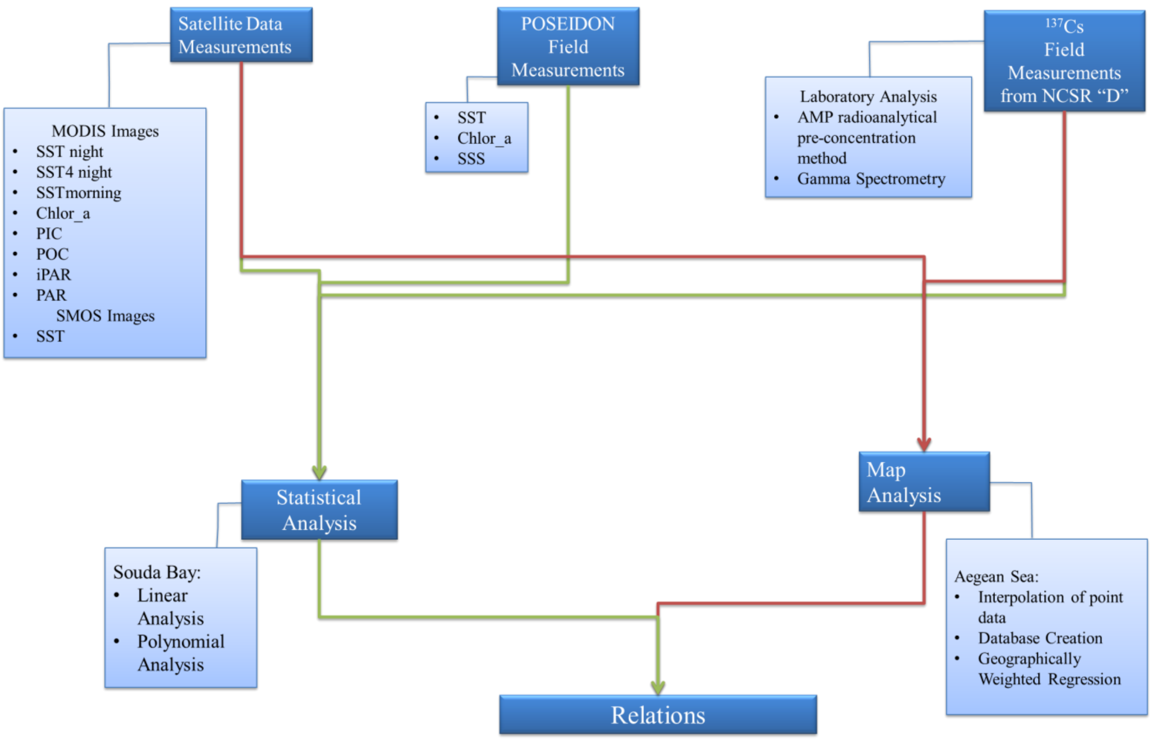

Figure 35. Flowchart of methodology: in green is the methodology followed in Souda Bay and in red is the methodology followed in Aegean Sea.

7.1. Data Collection

7.1.1. Satellite Data Collection

The SMOS and MODIS satellite images were downloaded and then were analyzed using the BEAM/VISAT (Figures 36, 37) and SeaDAS (Figures 38, 39) software respectively.

BEAM/VISAT is an open-source toolbox and development platform for viewing, analyzing and processing of remote sensing data. The special toolboxes can support, read, visualize and process specific data formats from various satellites (ESA, 2016). In this study the SMOS – Box was used for the SMOS data retrievals. SMOS data were retrieved for the dates December 2011 to June 2015 and contained measurements for SST and SSS. Due to RFI restrictions in the Aegean Sea only 39 points were resolved.

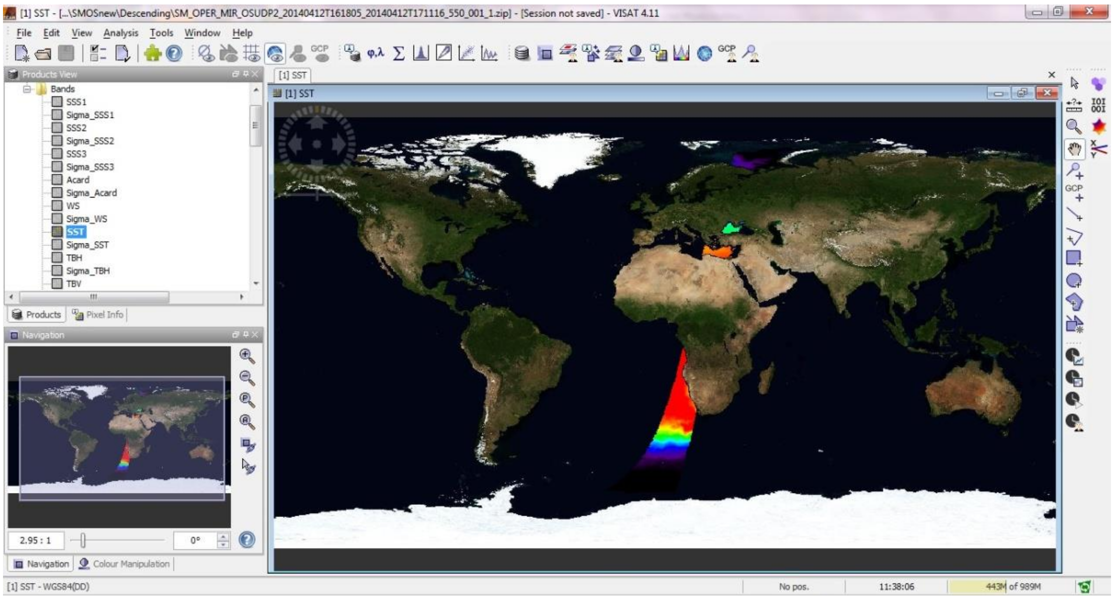

Figure 36. BEAM/VISAT software.

Source: http://www.brockmann-consult.de/cms/web/beam/

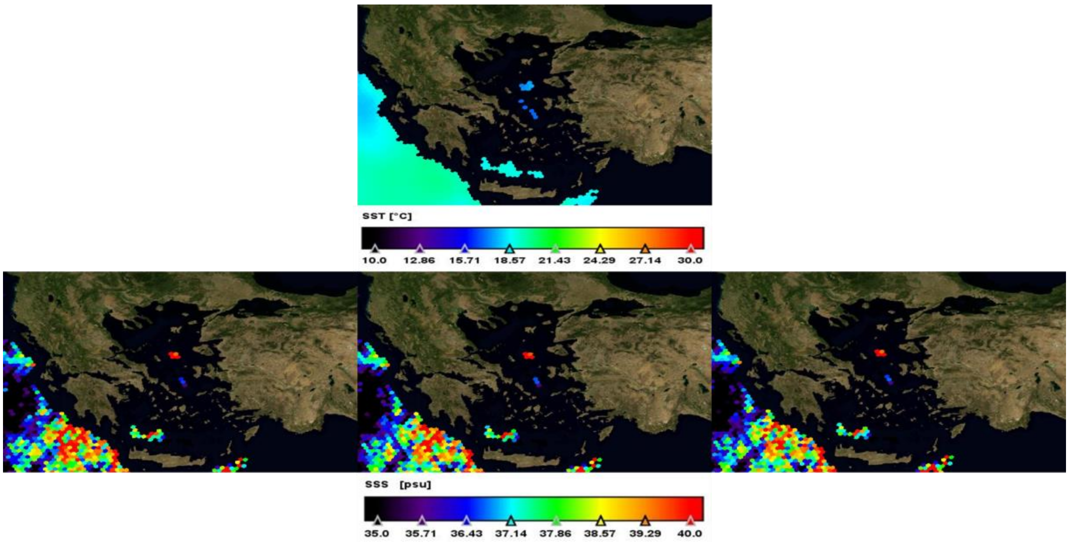

Figure 37. Indicative L2 SMOS Images of SST (above) and SSS (Below (where SSS1,SSS2,SSS3 from left to right)) for 15/12/2014.

SeaDAS is a comprehensive image analysis package for the processing, display, analysis and quality control of ocean color data. It is the result of the collaboration of the developers of ESA's BEAM/VISAT with NASA. It is based on the BEAM framework, but it supports NASA's Earth Science satellites (NASA, 2016). Using this software MODIS instrument L2 and L3 were analyzed in order to retrieve the needed measurements of SSTnight, SST4night, SSTmorning, Chlor_a, PIC, POC, CDOM, iPAR and PAR. The measurements were retrieved for the time period of December 2011 to June 2015 for the Aegean Sea timeseries and analysis, and for the time period of March 2011 to February 2015 for the Souda bay area analysis. For Souda Bay Level 2 daily images were used, while for the Aegean Sea Level 3 monthly standard mapped images were considered.

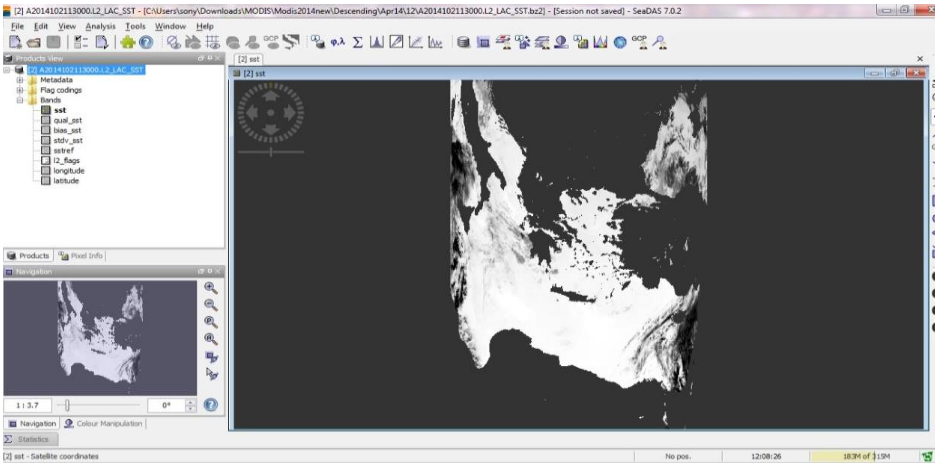

Figure 38. SeaDAS software.

Source: [*http://seadas.gsfc.nasa.gov/*](http://seadas.gsfc.nasa.gov/)

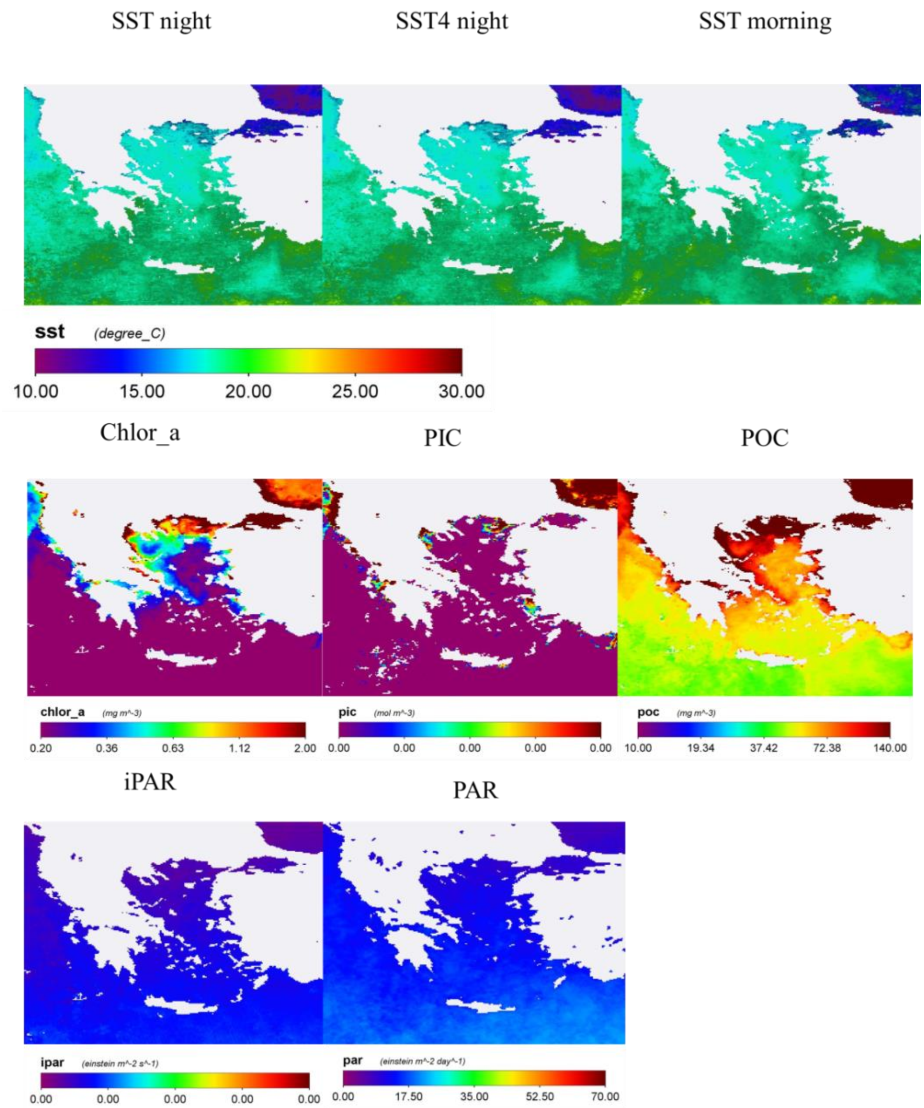

Figure 39. Indicative L3 MODIS ocean images of SSTnight, SST4night, SSTmorning, Chlor_a, PIC, POC, iPAR and PAR for the month of December 2012.

For the Souda Bay area, SMOS data were retrieved for the nearest to the bay points. Using the ArcMap geographic information system's tool of Euclidean Distance these points were point 26, point 27, point 32, point 36 and point 38 and are shown in a purple color figure 40.

Due to the higher spatial resolution, it was possible to retrieve MODIS data closer to the sampling station, with these points being pin 1, pin 2, pin 3, pin 4 and pin 5 (Figure 40). Using these points time series of the satellite parameters were created. An analysis of satellite data with POSEIDON buoy data followed, leading to the decision of not using SMOS sea surface salinity data due to high error risk in the values retrieved (Appendix page 210).

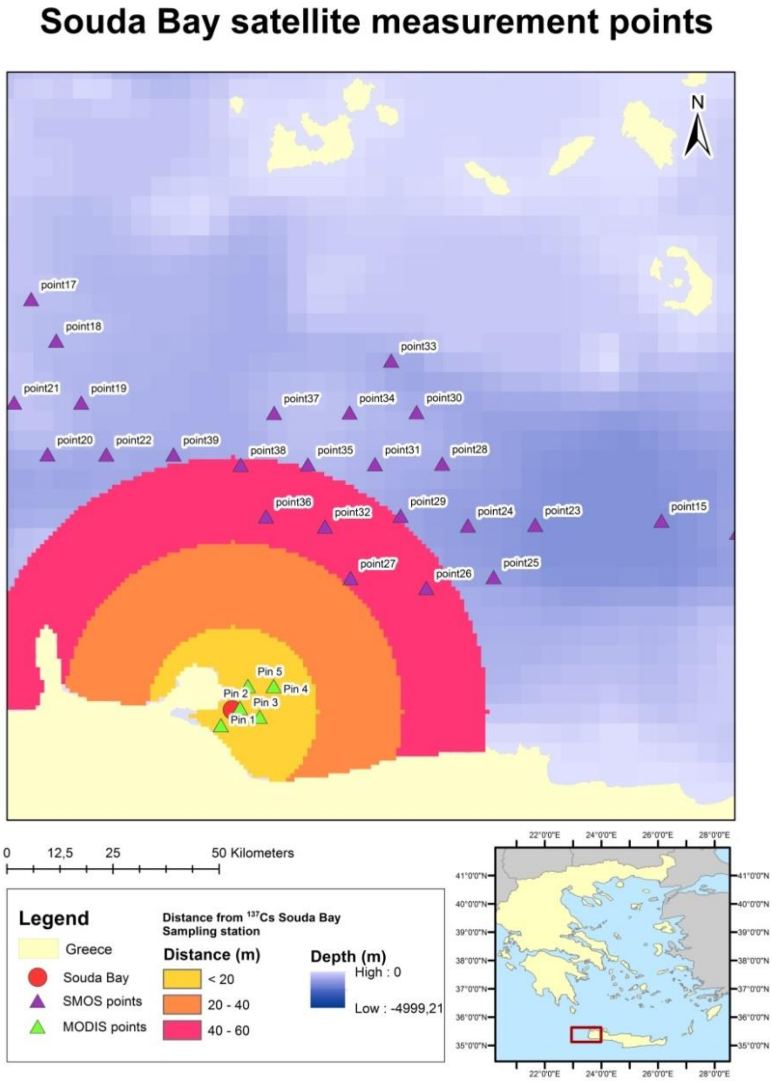

Figure 40. Souda Bay satellite measurement points.

For the Aegean Sea area SMOS data were retrieved for all the 39 points resolved in the Aegean (Figure 41). MODIS monthly L3 ocean images were cropped in order to keep the information only for the Aegean Sea area and were prepped for their insertion into the geographical information system. Time series were then created using SMOS and L2 MODIS ocean data. Using these timeseries in combination with POSEIDON data for the Aegean Sea buoys, it was decided not to use SMOS salinity data due to high error risk. However SST measurements from both satellites presented r^2 values higher than 0.8 when compared to POSEIDON buoy SST data (Appendix page 211).

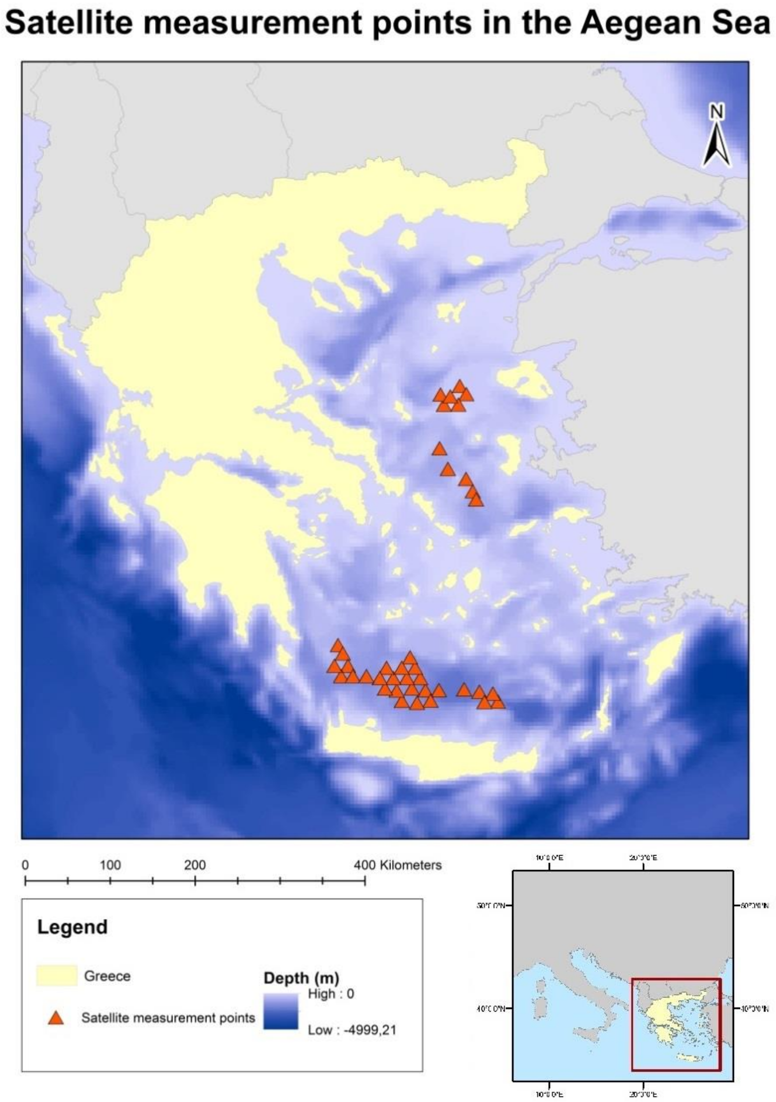

Figure 41. Satellite measurement points in the Aegean Sea

7.1.2. ^{137}Cs Activity Concentrations Data

Caesium-137 activity concentrations data mainly derived from the Environmental Radioactivity Laboratory's database that contains activity concentrations dating from 1984. In order to obtain new ^{137}Cs activity concentrations for this study, it was necessary to perform sea water sampling and laboratory analyses. The processes described below were executed in a specially formatted laboratory inside the Environmental Radioactivity Laboratory of NCSR "Demokritos".

7.1.2.1. Laboratory Analyses

For most samples, the concentrations of ^{137}Cs can be detected directly by using gamma spectrometry. However water samples require pre-concentration analysis before measuring them with gamma spectrometry. The sea water samples obtained from the sampling stations (Figure 42) are analyzed using an ammonium molybdophosphate (AMP) radio analytical pre-concentration method (Folsom et al., 1970) (Wong et al., 1994) (Wurl, 2009). This method is based in the ion exchange of dissolved ^{137}Cs with ammonium molybdophosphate $[(NH_4)_3P(Mo_3O_{10})_4]$ which is an insoluble yellow reagent (Figure 43). It is an effective ion exchanger of alkali metals and it has been known to form insoluble compound with Caesium. For this process a volume of at least 60 to 100 liters of sea water is necessary. Water samples can be obtained by using several methods. The most commonly used procedures to collect water samples are through seawater supply hose in the ship (only for the sea surface), submersible pump (only for the sea surface), rosette sampling (using Niskin or Go-Flo bottles at predetermined depths), large-volume containers (Gerard water sampling bottle) and in situ pumps (with special filters for radionuclide absorption). In this study the sea surface water samples have been pumped using a submersible pump. Every sample is pumped to high volume containers, previously rinsed with distilled water and 10% HNO_3. Acidification of the samples using 65% HNO_3 to pH 1.5, occurs after the transportation to the laboratory.

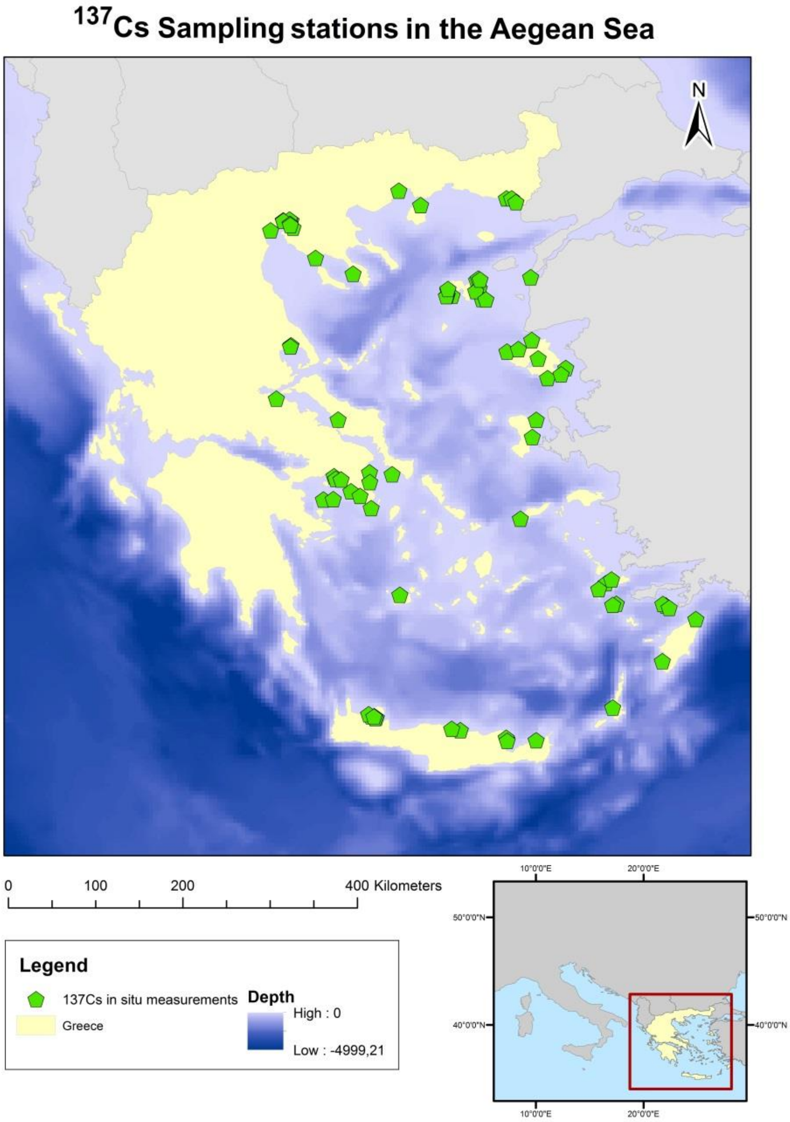

Figure 42. ^{137}**Cs Sampling Stations in the Aegean Sea.**

Figure 43. Ammonium Molybdophospate.

The laboratory analysis process continues by adding 400 mg of microcrystalline ammonium molybdophosphate per liter of sample for co-sinking via ion exchange with Caesium (Folsom et al., 1970) (Florou et al., 1994). Also 0.5Bq of 134Cs per liter of sample is added as a carrier and yield tracer. Afterwards the sample is continuously stirred for 15-30 minutes and then is allowed to precipitate for 48 hours. The supernatant is pumped away and the AMP slurry is transferred to a 2 liter beaker using 0.05N HNO_3 to rinse it and then it is again allowed to precipitate. This process includes several transfers to decreased volume beakers sequentially until the slurry reaches the desirable volume. When the desirable volume is reached, the slurry is transferred in a calibrated measurement pot that has a radius of 3.4 cm and height 2 cm. The slurry is then dried at 60 ^{o}C for 1h and is measured for ^{137}Cs using gamma spectroscopy (Florou et al., 2010). Parts of the AMP radioanalytical pre-concentration method in the laboratory are presented in figure 44.

Figure 44. The AMP radioanalytical pre-concentration method in the laboratory.

7.1.2.2. GAMMA SPECTROSCOPY

Gamma ray spectrometry (γ-spectrometry) is an analytical method that allows the identification and qualification of gamma emitting isotopes in a variety of matrices. In on single measurement and with little sample preparation, gamma ray spectrometry allows the user to detect several gamma emitting radionuclei in the sample (Reguigui, 2006). The equipment used in gamma spectroscopy includes an energy sensitive radiation detector, special electronics to process detector signals, amplifiers, data readout devices, rate meters and peak position stabilizers. The most common detectors are sodium iodide (NaI) scintillation counters and high purity germanium (HPGe) detectors. In this study an HPGe detector is used.

Germanium detectors are semiconductor diodes having a p-i-n structure (intrinsic semiconductor between a p-type semiconductor and an n-type semiconductor) in which the intrinsic (I) region is sensitive to ionizing radiation, particularly x-rays and γ-rays. When photons interact with the material within the depleted volume of a detector, charge carriers are produced and are swept by the electric field to the p and n electrodes. This charge, which is in proportion to the energy deposited in the detector by the incoming photon, is converted into a voltage pulse by an integral charge sensitive preamplifier. These detectors use liquid nitrogen as a cooling medium in order to reduce the thermal generation of charge carriers to an acceptable level. Otherwise, leakage current induced noise destroys the energy resolution of the detector (Canberra Industries, 2014).

In order to analyze the treated sea water samples for ^{137}Cs, gamma spectrometry was essential to be carried out; due to the subsequent gamma decay of the excited Barium-137 (^{137}Ba) that has energy of 661.7 keV. The gamma spectrometry was carried out using a Canberra system comprising of a High Purity Germanium detector system with an efficiency of 90% and resolution of 2.1 keV (Figure 45). The detector is connected to an 8k multi-channel analyzer operated with the Genie 2000 software. The energy calibration to the system has been performed using standard active sources of Sodium-22 (^{22}Na), Manganese-54 (^{54}Mn), Cobalt-57 (^{57}Co), Cobalt- 60 (^{60}Co), Cadmium-109 (^{109}Cd), Barium-133 (^{133}Ba), Caesium-137 (^{137}Cs) and Americium-241 (^{241}Am). These cover an energy range up to 2000keV. The efficiency of the detector was calculated using a standard active source of Radium-226 (^{226}Ra) under the same geometry with the pot used for the measurement of the samples. The samples were measured for 70,000 seconds or 19.444 hours (Florou, Nicolaou, & Evangeliou, 2010). The result of gamma spectroscopy is an interaction distribution in the detector depending on the energy, where the x axis is the energy deposited in the detector in keV and the y axis is the number of pulses received at a given energy (Figure 46). The activity of the sample (Bq/kg) is calculated by:

$$A = \frac{1000 \times \frac{N}{T}}{m\varepsilon P\gamma}$$

Eq 2. Activity of the sample.

Source: (Reguigui, 2006)

Where N is net counts of the photo peak, T is the live time of measurements in seconds, m is the mass of the sample used in grams, ε is the counting efficiency of the specific nuclide's energy and Pγ is the gamma transition probability through the specific energy (Reguigui, 2006) (Canberra Industries, 2010).

Then half-life corrections are made by multiplying the activity by an exponential factor. Half-life correction is done by using the following equation.

$$A = A_0 \times e^{-\lambda t}$$

Eq 3. Calculation of activity according to half-life.

Where A is the activity remaining in the radioactive material after time (t) from when the initial activity was measured, A_0 is the initial activity of the radioactive material, e is the base of the natural logarithm, λ is the decay constant (($\frac{ln2}{T_{1/2}}$), $T_{1/2}$= half-life) and t is the time in days since the initial activity was measured (Reguigui, September 2006) (Canberra Industries, 2010). However ^{137}Cs is not removed from sea water only due to physical decay, but also due to environmental processes. Some of these environmental processes are advection, diffusion, downwelling, horizontal and vertical migration and upwelling. For this reason, in this study the effective half-life was used for the activity correction instead of the half-life. The effective half-life is a function of half-life and ecological half-life. Ecological half-life (T_{eco}) is the time required for 50% decline of radionuclide in a population in a natural ecosystem. This combination of physical decay and ecological half-life, incorporates all processes that can reduce ^{137}Cs concentrations in the marine environment.

In the Aegean Sea, the effective half-life has been estimated to be 8.2 years in the Northeast and 6.2 ± 1.5 years in Central Aegean (Florou, et al., 2001) (Evangeliou et al., 2012). In this study the average value of 7.2 years has been used (Florou et al., 2014).This correction was necessary to be considered for the Aegean Sea area study; this correction using the above equation (Eq 3) was crucial to calculate the mean ^{137}Cs activity concentrations necessary for the analyses in GIS. The monthly mean value was the correction at the last day of each month; due to the effective half-life of 7.2 years there was no significant difference between the start, the middle or the end of the month. Aegean Sea activity concentrations were corrected for the months of March 2012, April 2012, June 2012, November 2012, December 2012, January 2013, February 2013, April 2013, May 2013, March 2014, August 2014, November 2014, December 2014 and February 2015. Caesium-137 samplings were not consistent in time; they were scattered through the years of study. Water samplings in the Aegean Sea performed by the ERL started in 1984 and they are ongoing. The months mentioned above for the Aegean Sea were chosen due to the most frequent and recent samplings. However in Souda Bay no corrections were necessary due to the simultaneous measurements of sea sampling and satellite passes (Appendix page 209) for the dates presented in table 3.

Figure 45. ERL's Gamma Spectrometry laboratory.

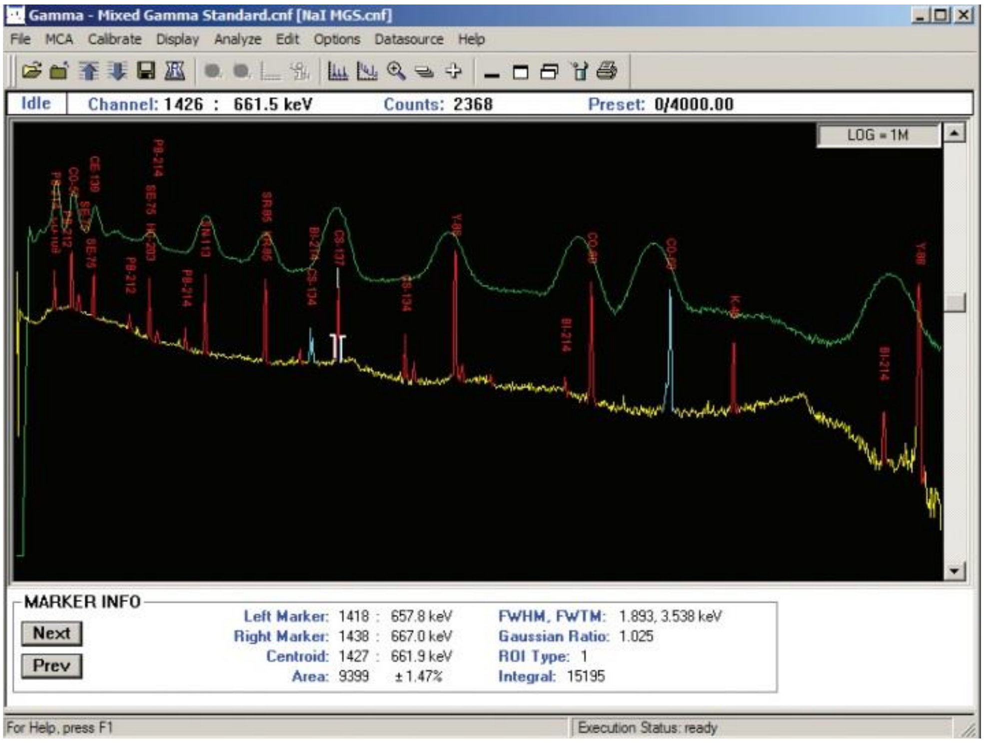

Figure 46. Genie 2000 software from Canberra Industries, comparing two spectrums.

Source: http://www.canberra.com/products/radiochemistry_lab/pdf/G2K-BasicSpect-SS-C40220.pdf

Souda Bay sea water sampling dates joint with satellite passes dates	
25/3/2011	2/2/2013
26/3/2011	5/2/2013
27/3/2011	11/2/2013
28/3/2011	12/2/2013
29/3/2011	20/4/2013
8/4/2011	22/4/2013
9/4/2011	23/4/2013
10/4/2011	25/4/2013
11/4/2011	20/5/2013
12/4/2011	21/5/2013
13/4/2011	24/5/2013
18/6/2012	25/5/2013
19/6/2012	10/8/2014
20/6/2012	11/8/2014
21/6/2012	12/8/2014
22/6/2012	13/8/2014
23/6/2012	14/8/2014
2/11/2012	15/8/2014
7/11/2012	6/11/2014
25/12/2012	10/11/2014
20/1/2013	24/12/2014
21/1/2013	25/12/2014
1/2/2013	25/2/2015

Table 3. Souda Bay sea water sampling dates joint with satellite passes dates.

7.2. Statistical Study for the Area of Souda Bay

The statistical study for the area of Souda Bay included the examination of potential linear or polynomial relations between satellite measurements and ^{137}Cs activity concentrations for the dates mentioned in table 3. The first step was to investigate the linear relations that would be expressed in the form of: $y = ax + b$. These relations were studied for the time period of March 2011 to February 2015 (presented in table 3). Relations were examined using all 5 of Souda Bay MODIS points, all 5 of SMOS points and POSEIDON buoy data from the E1-M3A buoy. Linear relations were examined in two ways; the first way was calculated taking into account the errors of ^{137}Cs activity concentrations and the second way was calculated ignoring the errors of ^{137}Cs activity concentrations. This was necessary in order to observe the activity error effects on the regression. The scatter plots presenting the linear relations are presented in the results.

The second step of investigating the relations, was to investigate the second degree polynomial relations of the measurements, that would be expressed in a form of: $y = ax^2 + bx + c$. The second degree polynomial relations were studied for the exact same time period as the linear relations. In the same manner as linear analysis the second degree polynomial analysis was performed in two ways; the first by taking into account the errors of ^{137}Cs activity concentrations and the second by ignoring them. This was necessary in order to observe the activity error effects on the regression. The scatter plots presenting the polynomial relations are presented in the results.

7.3. Geographic Information systems

A geographic information system (GIS), lets the user visualize, question, analyze, and interpret data to understand relationship, patterns and trends. It is designed to capture, store, manipulate, analyze, manage and present all types of spatial or geographical data. They are a special class of information systems that can keep track not only of events, activities and thing, but also where these events, activities and things happen or exist (Longley et al., 2011).

Acknowledging these properties, an effort is made to examine the spatial relations of satellite measurements and ^{137}Cs activity concentrations in the Aegean Sea area. At first, data were inserted into the GIS system. Point data were inserted as tables and then converted to points. Satellite images were inserted as raster layers. Data include SMOS measurements (SST_ascending and SST_descending), MODIS data (images of SSTnight, SST4night, SSTmorning, Chlor_a, PIC, POC, iPAR and PAR) and finally ^{137}Cs activity concentrations from the sampling stations that have been previously corrected for decay.

All the above measurements were analyzed for the months of March 2012, April 2012, June 2012, November 2012, December 2012, January 2013, February 2013, April 2013, May 2013, March 2014, August 2014, November 2014, December 2014 and February 2015. The measurements considered were monthly mean measurements, in order to reduce the data load and the analysis time from when using daily measurements. As aforementioned these months were chosen due to the most frequent and recent sea water samplings for ^{137}Cs activity concentrations performed by the ERL

7.3.1. MAP PRODUCTION

In the figures 47, 48 the steps followed for the examination of the spatial relations in ESRI's ArcMap are being shown. The first step was the projection transformation from WGS 1984 to the Greek Grid format. This was performed using the Raster Projection tool and the Project tool, from the data management tools – projections and transformations, on the data used in this study. The next step was to transform the unsinged integer values of all MODIS Sea Surface Temperature images into Celcius Degrees (^oC) using the raster calculator tool from Spatial Analyst and the following expression:

$$SST\ in\ Celcius\ Degrees = image\ in\ unsigned\ integer\ \times slope + intercept$$

Eq 4. Expression for transforming unsigned integer SST images to Celsius degrees

Source: (NASA-OceancolorBiology Processing Group, 2010)

Where the slope and the intercept factors are given in the metadata of MODIS images; Slope is 0.000717185 and Intercept is -2.0 for all SST data.

So the SST is calculated using the expression: $SST\ in\ Celcius\ Degrees = image\ in\ unsigned\ integer\ \times 0.000717185 - 2$

This transformation was used to create the MODIS SSTnight, SST4night and SST morning rasters for the months of study.

Following up is the interpolation of the point data using the Inverse Distance Weighted (IDW) tool. Interpolation is a procedure used to predict the values of cells at locations that lack sampled points. In this study the Spatial Analyst- IDW tool was used which determines cell values using a linear-weighted combination set of sample points. It estimated the cell values by averaging the values of sample data points in the neighborhood of each processing cell (Childs, 2004). Using this tool ^{137}Cs activity concentrations, SMOS SST_ascending and SMOS SST descending were interpolated with output cell size of 4 and 5 km respectively using a fixed radius of 100 km for both measurements. At this point a spatial database was created containing all measurements; Maps of each parameter can be seen in the appendix (page 212).

7.3.1.1. GEOGRAPHICALLY WEIGHTED REGRESSION (GWR)

The next step was to prepare the data with the purpose of performing Geographically Weighted Regression (GWR). Regression is the method of modelling the relationship between a dependent variable and a set of one or more independent variables. Geographically Weighted Regression is a local form of linear regression used to model spatially varying relationships (Brunsdon et al., 1998). The idea of GWR is that parameters may be estimated anywhere in the study area given a dependent variable and a set of one or more independent variables which have been measured at places whose location is known. It constructs a separate linear equation for every feature inserted, incorporating the dependent and explanatory variables. However the shape and the extent of the bandwidth are dependent on the user input and in particular on the spatial distribution of data (Charlton et al., 2009). Data used to perform GWR should be in a feature form. The parameters were simplified by dividing the values into categories first. However, when nominal or categorical data are used in a GWR model there is a strong risk of local multicollinearity issues, which render the results unstable. Even though categorizing the data can produce unstable results due to collinearity, this was a first approach of observing the general relation of satellite measurements and ^{137}Cs activity concentrations. The results were interpreted as valid by making the assumption that in every category polygon the values are the same and there are not variations in a category. The categories for the parameters are presented in Table 4.

Classification of the parameters values								
Classes	SSTnight (^oC)	SST4night (^oC)	SSTmorning (^oC)	PIC (mol/m^3)	POC	iPAR	PAR	^{137}Cs (Bq/m^3)
1	<15	<15	<15	<0.00010	<20	<0.0010	<10	<1
2	15-17	15-17	15-17	0.00010-0.00015	20-40	0.0010-0.0012	10-20	1-2
3	17-19	17-19	17-19	0.00015-0.00020	40-60	0.0012-0.0014	20-30	2-3
4	19-21	19-21	19-21	0.00020-0.00025	60-80	0.0014-0.0016	30-40	3-4
5	21-23	21-23	21-23	0.00025-0.00030	80-100	0.0016-0.0018	40-50	4-5
6	23-25	23-25	23-25	>0.00030	100-120	0.0018-0.0020	50-60	>5
7	>25	>25	>25		>120	>0.0020	>60	

Table 4. Classification of the parameters values.

After the classification, the data were transformed into polygon layers using the tool Raster to Polygon, which is located in the Conversion toolbox. When using this tool the simplify polygons option was not checked in order to perform a more detailed analysis. The parameters polygon layers were then unified in pairs with the ^{137}Cs activity concentrations using the Union tool, which is located in the Analysis- Overlay toolbox. The parameters were paired in the following way: SSTnight-^{137}Cs, SST4night- ^{137}Cs, SSTmorning- ^{137}Cs, PIC- ^{137}Cs, POC- ^{137}Cs, iPAR-^{137}Cs, PAR-^{137}Cs. SMOS SST data were not included in this step due to their invalid interpolation; the 39 resolved pixels in the Aegean Sea were not spatially dense enough to perform an interpolation with valid values. Then on the paired parameters GWR was performed, which is located in the Spatial statistics toolbox. In all analyses performed the dependent variable was the ^{137}Cs activity concentrations and the independent variable was the satellite parameter in study. The kernel type used was fixed and the bandwidth method chosen was AICc. AICc or the corrected Akaike Information Criterion provides a measure of the information distance between the model which has actually been fitted and the unknown “true” model. The model with the lower AICc value provides a better fit to the observed data. However it is not an absolute measure of goodness of fit, but is useful for comparing models. The result of the GWR tool is an output feature class table that includes fields for the observed and predicted values, the condition number, the local r^2, residuals and explanatory variable coefficients and standard errors. In this study the Aegean Sea results comprise of maps that depict the local r^2 values between ^{137}Cs and the satellite parameters and maps that depict the estimated ^{137}Cs by using the satellite parameters. All results are presented in the next chapter by parameter; at first there are maps of local r^2 and then are maps of the predicted ^{137}Cs activity concentrations.

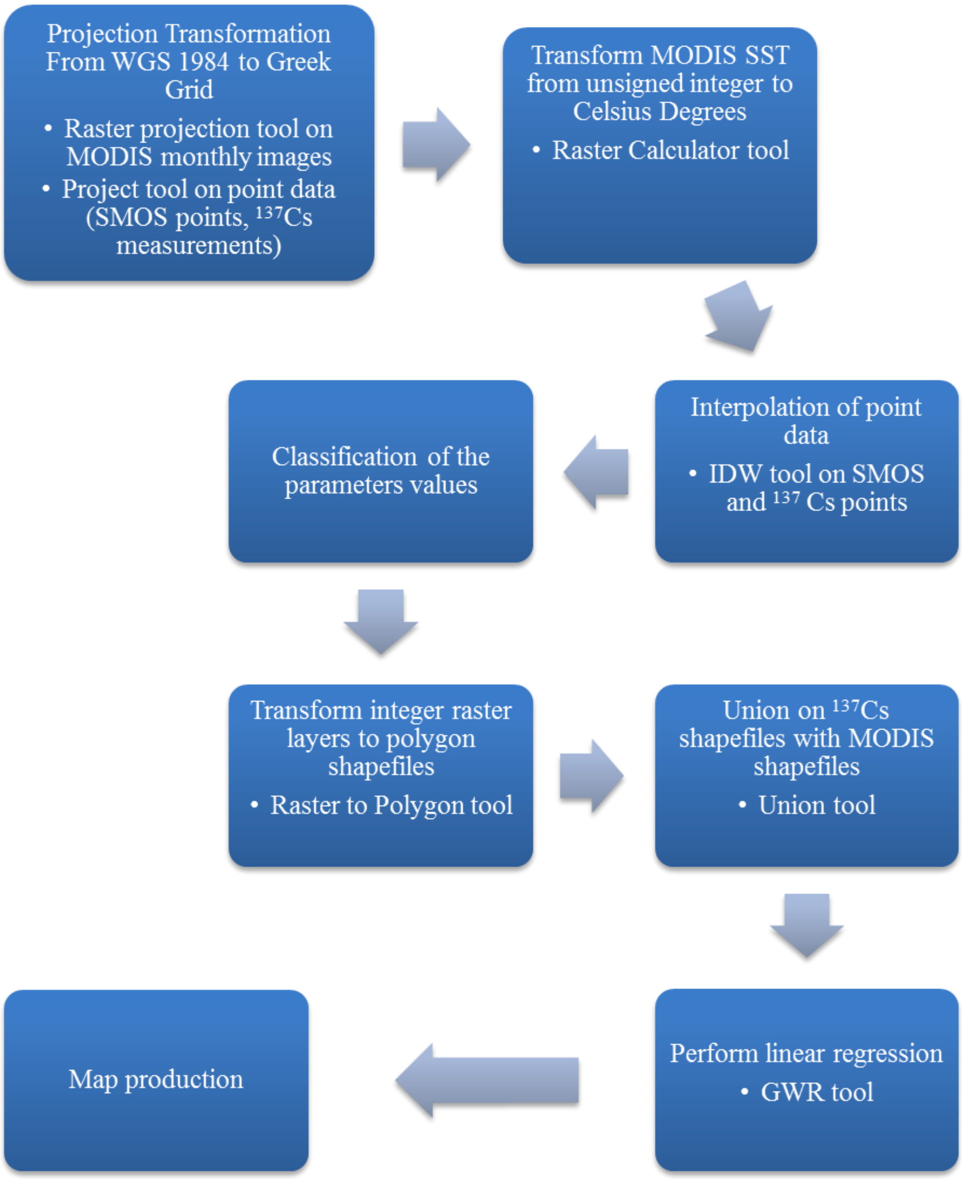

Figure 47. ArcMap methodology for the examination of spatial relations between satellite measurements and ^{137}Cs concentrations.

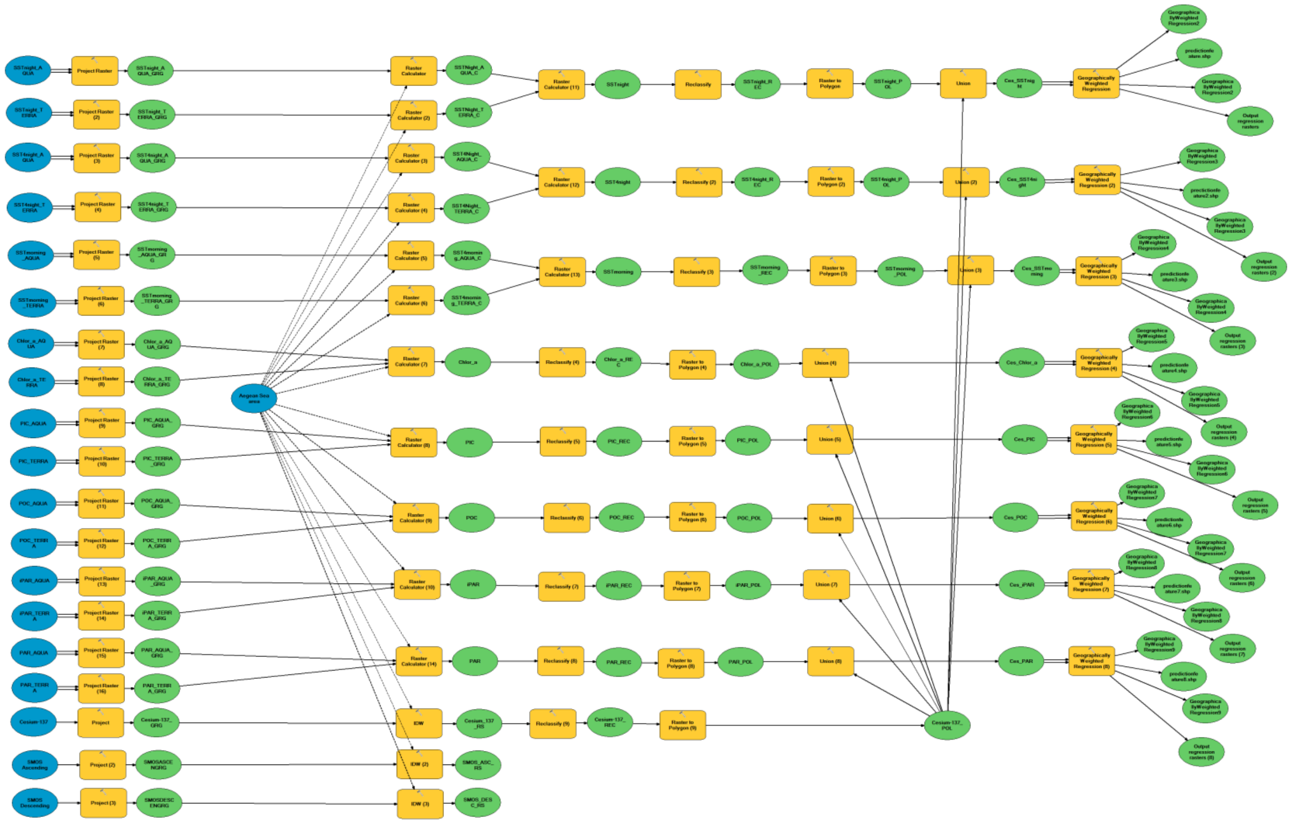

Figure 48. ArcMap model for the examination of spatial relations between satellite measurements and ^{137}Cs concentrations.

8. RESULTS

In this chapter, the results of the aforementioned methodology are presented and analyzed. The results correspond to graphs and maps revealing the relations between ^{137}Cs activity concentrations, MODIS and SMOS satellite measurements and POSEIDON buoy measurements. At first the results for Souda Bay area are presented, where the results are graphs that portray the linear and second degree polynomial relations between^{137}Cs activity concentrations, MODIS and SMOS satellite measurements and POSEIDON buoy measurements.

The Souda Bay results are categorized as follows: MODIS, SMOS, and POSEIDON. For the Aegean Sea area the results correspond to maps portraying the spatial linear relations between ^{137}Cs activity concentrations and MODIS measurements. Additional Aegean Sea results include the predicted ^{137}Cs activity concentrations using MODIS measurements. These results are categorized by parameter as follows: SSTnight, SST4night, SSTmorning, Chlor_a, PIC, POC, iPAR and PAR. The predictions of ^{137}Cs activity concentrations are compared to the original ^{137}Cs activity concentrations (Appendix page 212).

To be noted here some of the following results were presented at ESA's Living Planet Symposium 2016 under the title "Integration of Earth Observation satellite data and real time measurements in the Greek marine environment to GIS for advances in radiological remote control" (Mavrokefalou et al., 2016).

8.1. SOUDA

The relations between the ^{137}Cs activity concentrations and MODIS, SMOS and POSEIDON data are displayed. At first the relations between ^{137}Cs activity concentrations and MODIS parameters are presented; categorized by parameter for all the 5 points of MODIS measurement points in Souda Bay. Then the relations of ^{137}Cs and SMOS SST Ascending and Descending are shown, for the relative SMOS measurement points: point 26, point 27, point 32, point 36 and point 38. The final relations that will be exhibited for Souda Bay will be the relations between the ^{137}Cs activity concentrations and the POSEIDON system's SST, Chlor_a and SSS. The relations were examined temporally and concern the time period spanning March 2011 to February 2015.

8.1.1.1. MODIS

8.1.1.1.1. SSTNIGHT

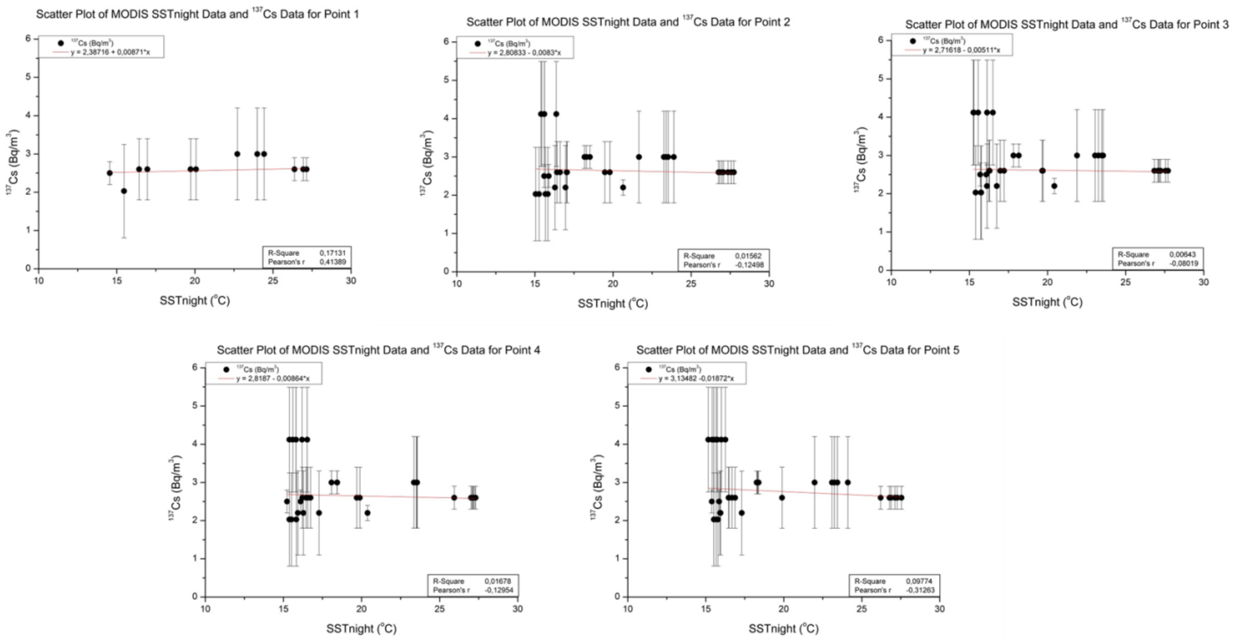

Figure 49. Scatter plots of MODIS SSTnight data and ^{137}Cs data depicting the linear relation (including errors).

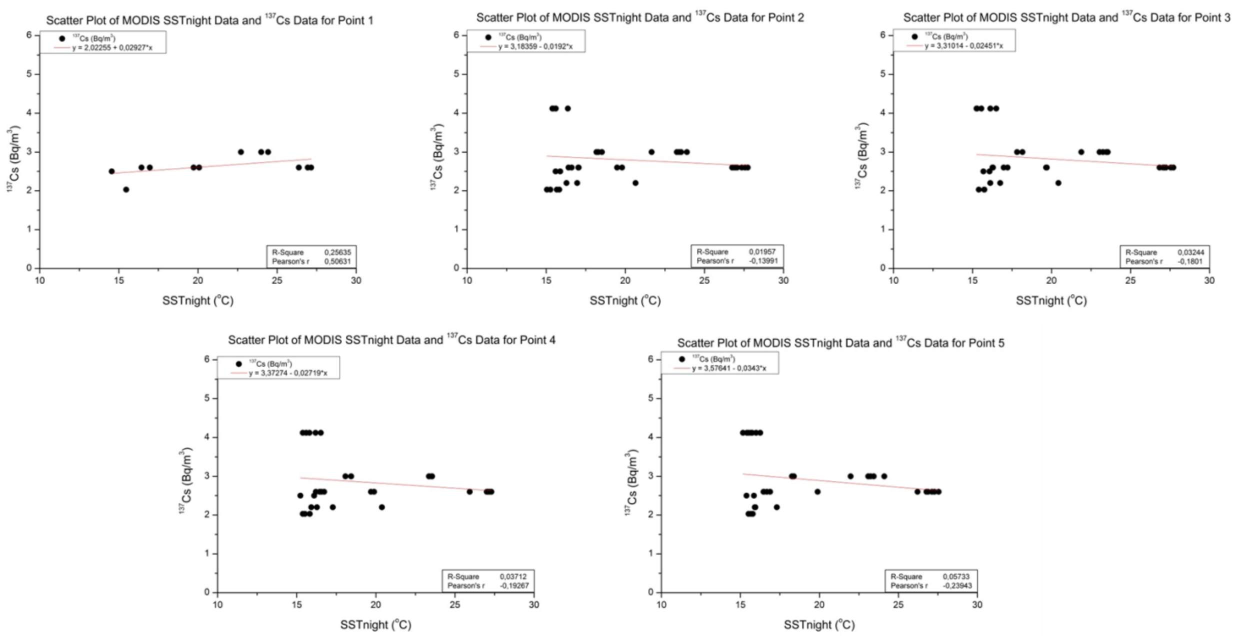

Figure 50. Scatter plots of MODIS SSTnight data and ^{137}Cs data depicting the linear relation.

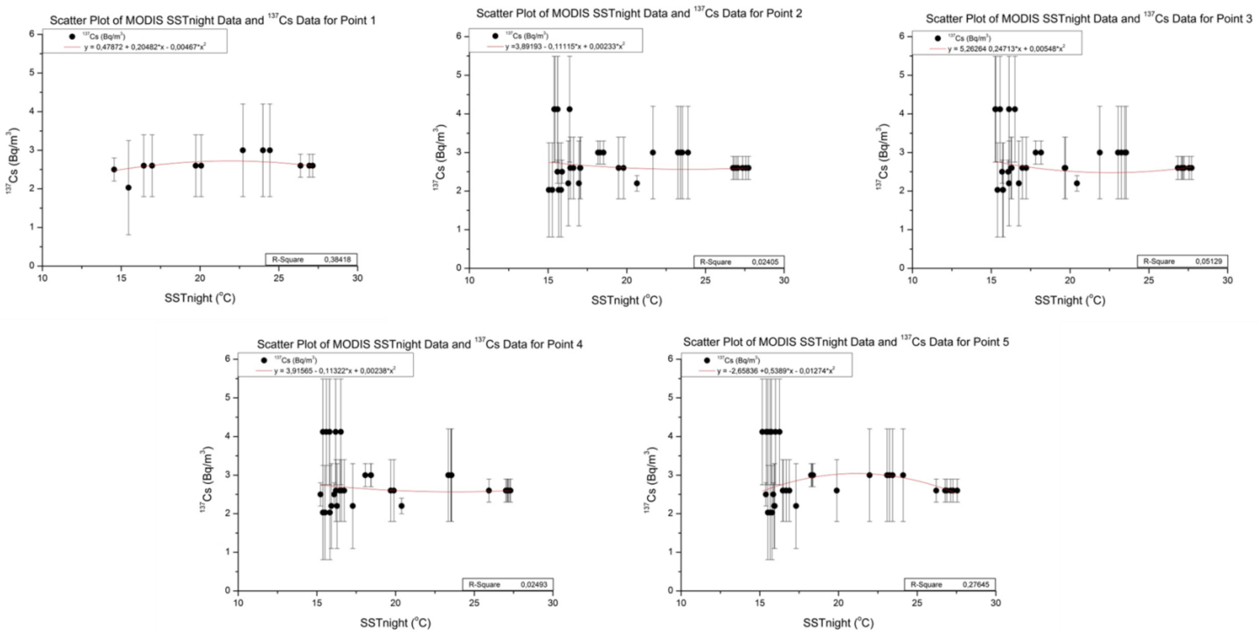

Figure 51. Scatter plots of MODIS SSTnight data and ^{137}Cs data depicting the 2nd degree polynomial relation (including errors).

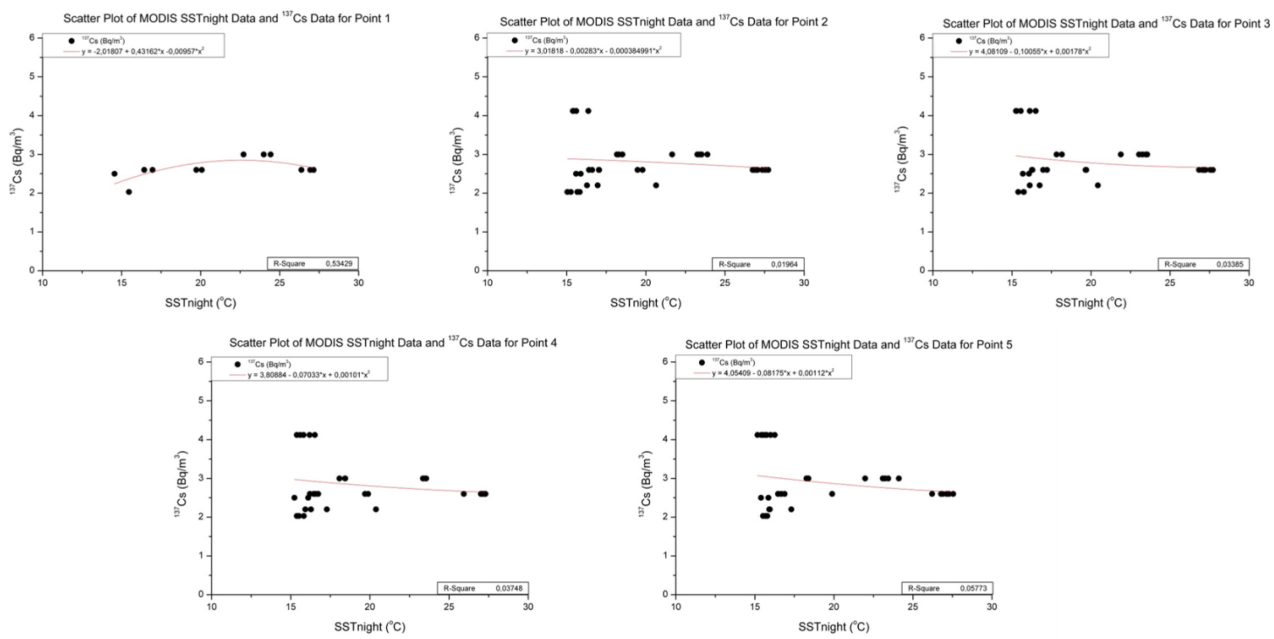

Figure 52. Scatter plots of MODIS SSTnight data and ^{137}Cs data depicting the 2nd degree polynomial relation.

The above results (Figures 49, 50, 51, 52) depict the linear and polynomial relations of ^{137}Cs activity concentrations and MODIS SSTnight measurements for the 5 MODIS measurement points in Souda Bay.

The relations are presented when including and excluding ^{137}Cs activity concentration errors. This is important in order to observe the impact of the errors in the values. Concerning the linear relation, at first the ^{137}Cs activity errors are included, and then is the linear relation where the errors are not included. Following is the second degree polynomial relation, where the errors are included and finally is the second degree polynomial relation where the errors are not included.

It seems that the polynomial correlations provide better results than the linear ones. Also for most of the points the results where the errors were not considered are better than the ones where the errors were considered. It is important to be noted that in the first point (Souda MODIS pin 1) the correlation result is better than the correlation in the other 4 points and it presents an r^2 of 0.38 when the errors are included and an r^2 of 0.53 when the errors are not included (Mavrokefalou et al. , 2016).

However these values are shown only in the second degree polynomial regression. The other points do not present any significant results in either linear or polynomial regression.

8.1.1.1.2. SST4night

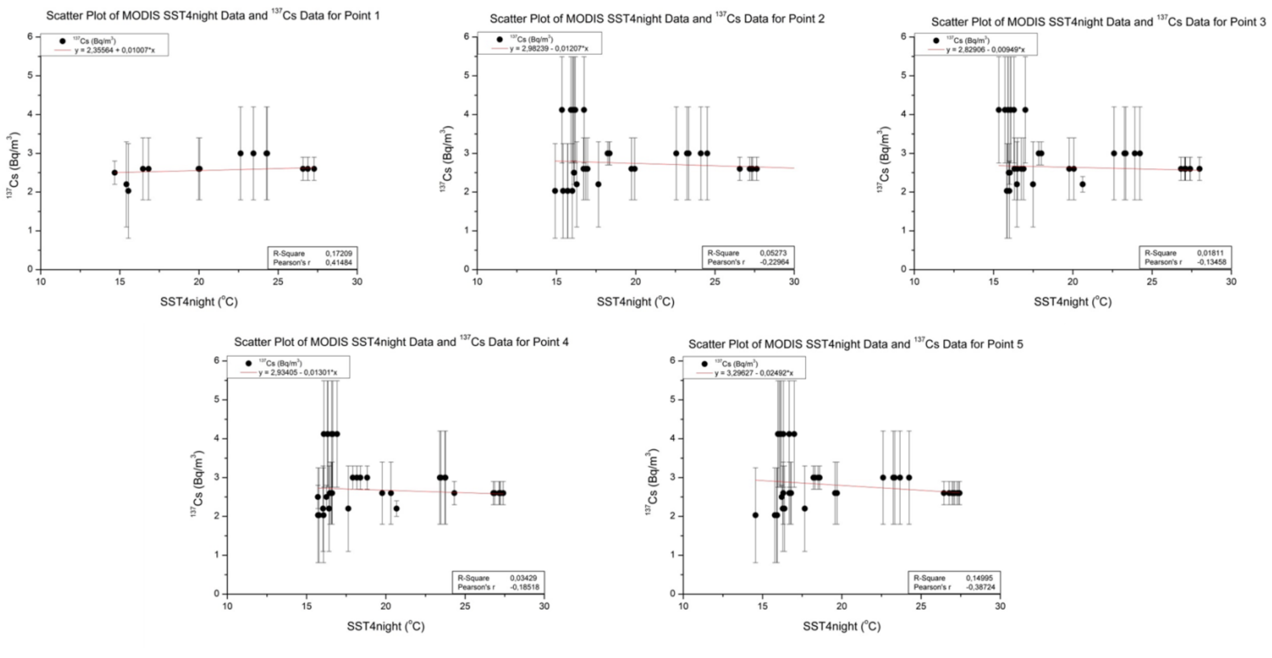

Figure 53. Scatter plots of MODIS SST4night data and ^{137}Cs data depicting the linear relation (including errors).

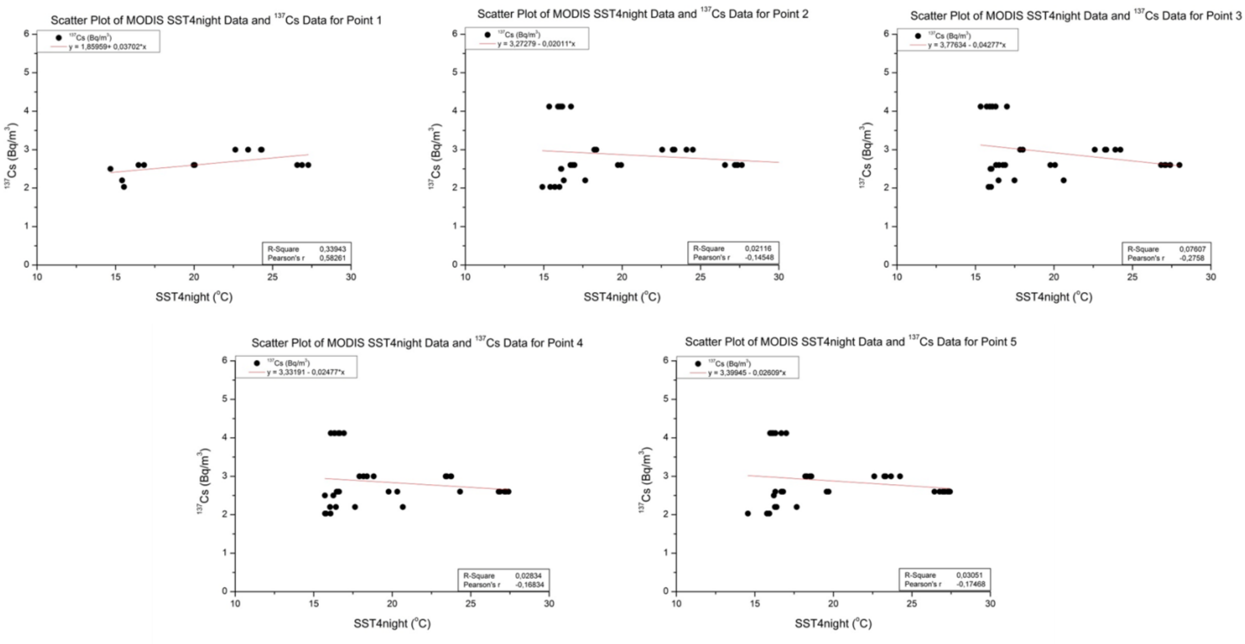

Figure 54. Scatter plots of MODIS SST4night data and ^{137}Cs data depicting the linear relation.

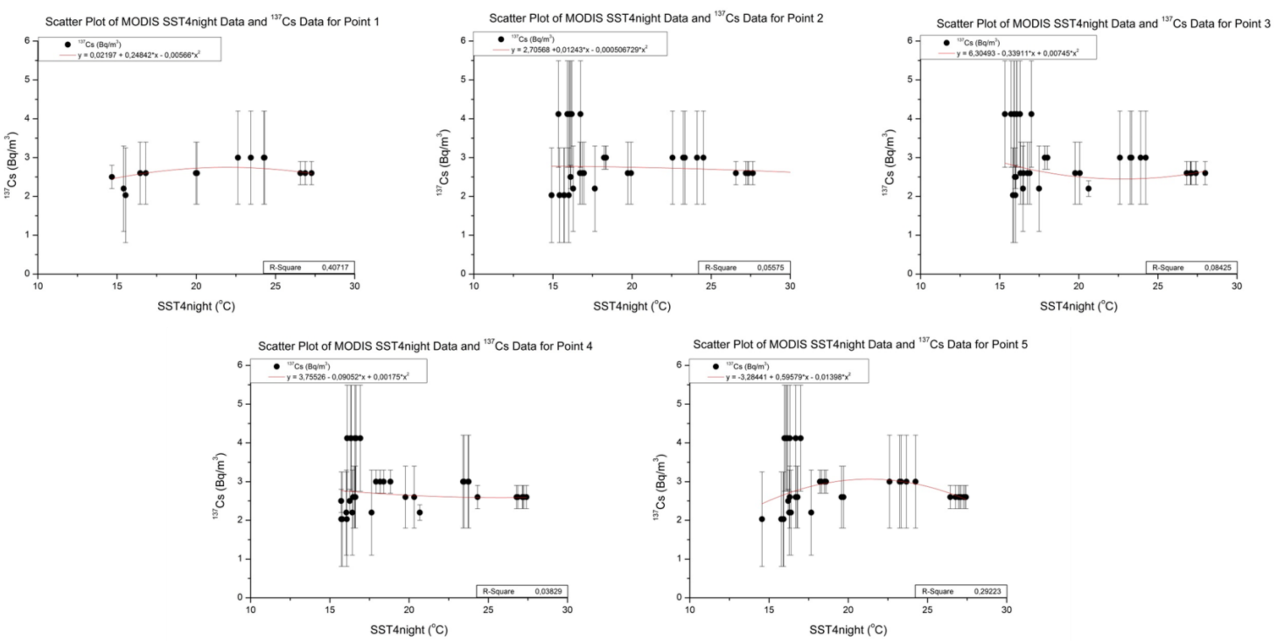

Figure 55. Scatter plots of MODIS SST4night data and ^{137}Cs data depicting the 2nd degree polynomial relation (including errors).

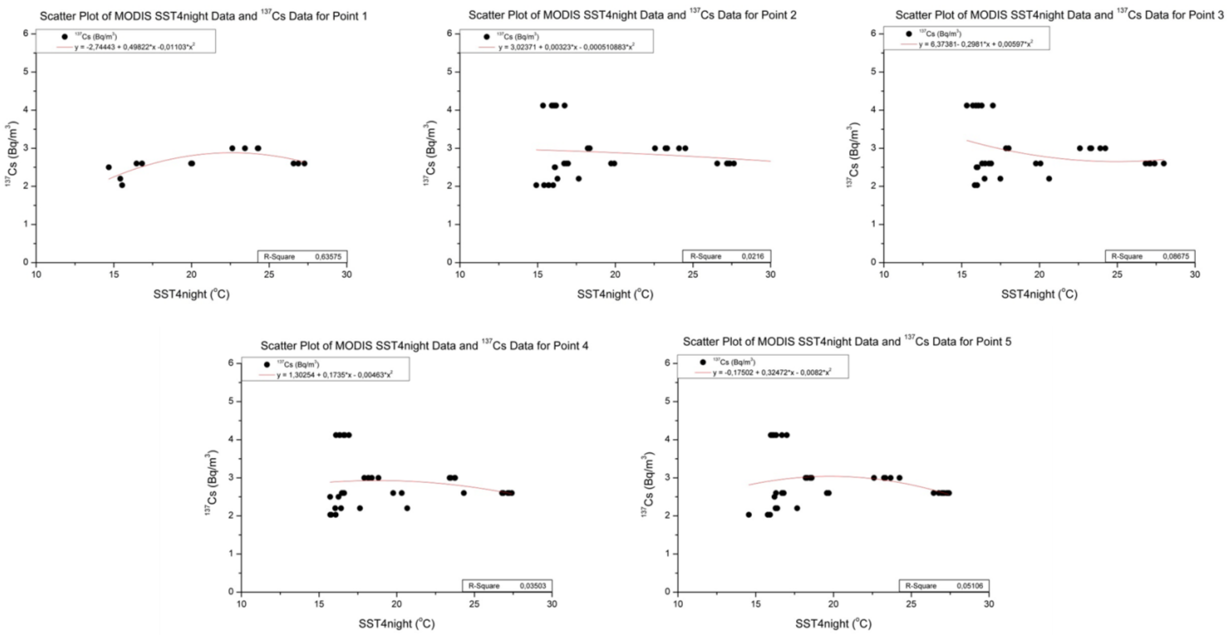

Figure 56. Scatter plots of MODIS SST4night data and ^{137}Cs data depicting the 2nd degree polynomial relation.

Following the results of the linear and second degree polynomial relations between ^{137}Cs activity concentrations and MODIS SST4night measurements are displayed for the 5 Souda Bay MODIS measurement points (Figures 53, 54, 55, 56). Like SSTnight the relations are presented when including and excluding ^{137}Cs activity concentration errors. The first point (Souda MODIS pin 1) here also presents the best results from the other 4 points, with an r^2 value of 0.34 in the linear regression excluding the errors, an r^2 value of 0.41 in the second degree polynomial regression including the activity errors and an r^2 value of 0.64 in the second degree polynomial regression excluding the activity errors (Mavrokefalou et al., 2016). In a similar manner like the results with MODIS SSTnight, the results of MODIS SST4night for the rest of the points do not present any significant results in either linear or polynomial regression.

8.1.1.1.3. SSTMORNING

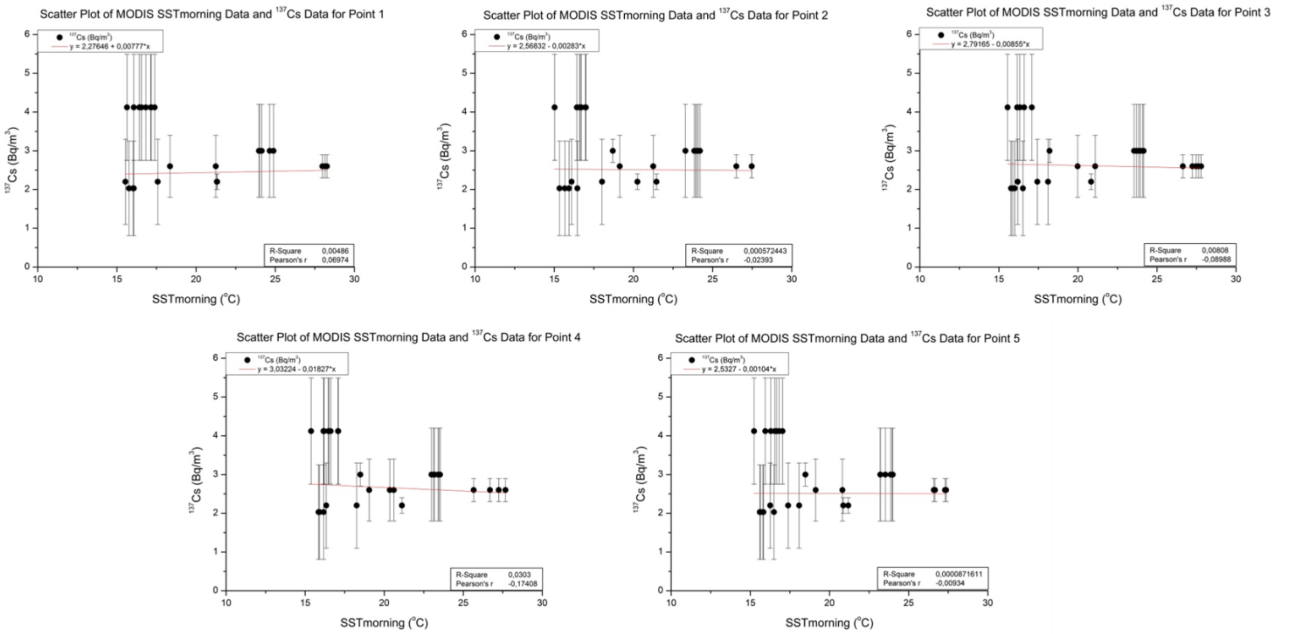

Figure 57. Scatter plots of MODIS SSTmorning data and ^{137}Cs data depicting the linear relation (including errors).

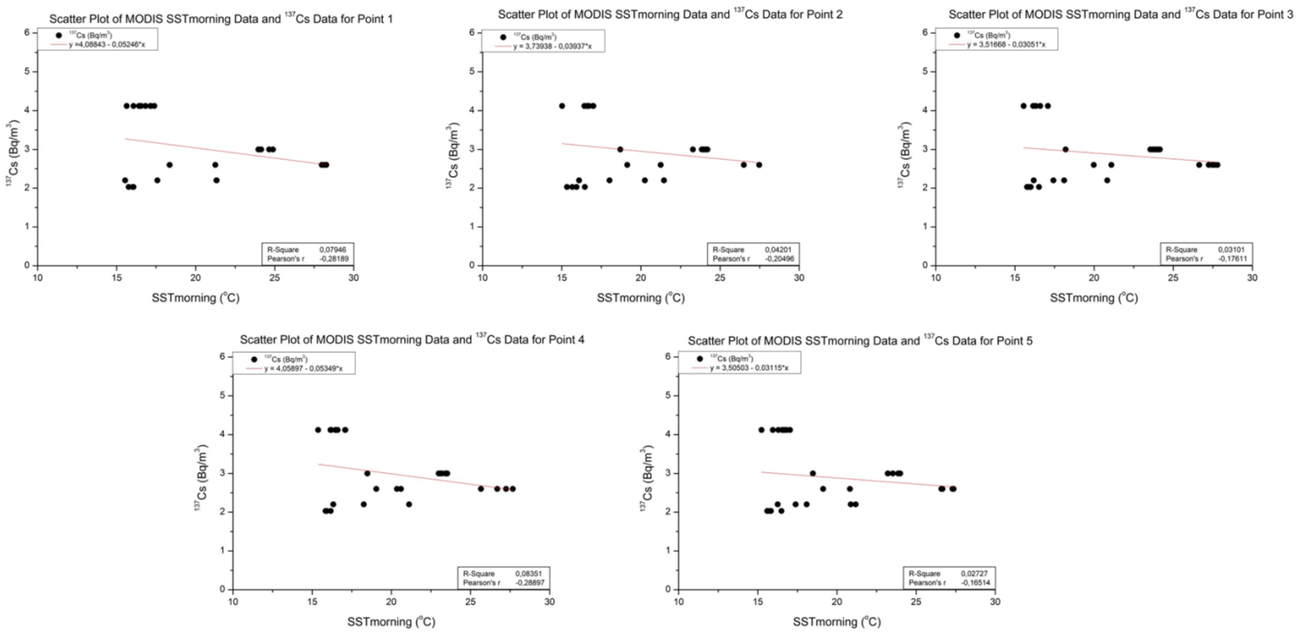

Figure 58. Scatter plots of MODIS SSTmorning data and ^{137}Cs data depicting the linear relation.

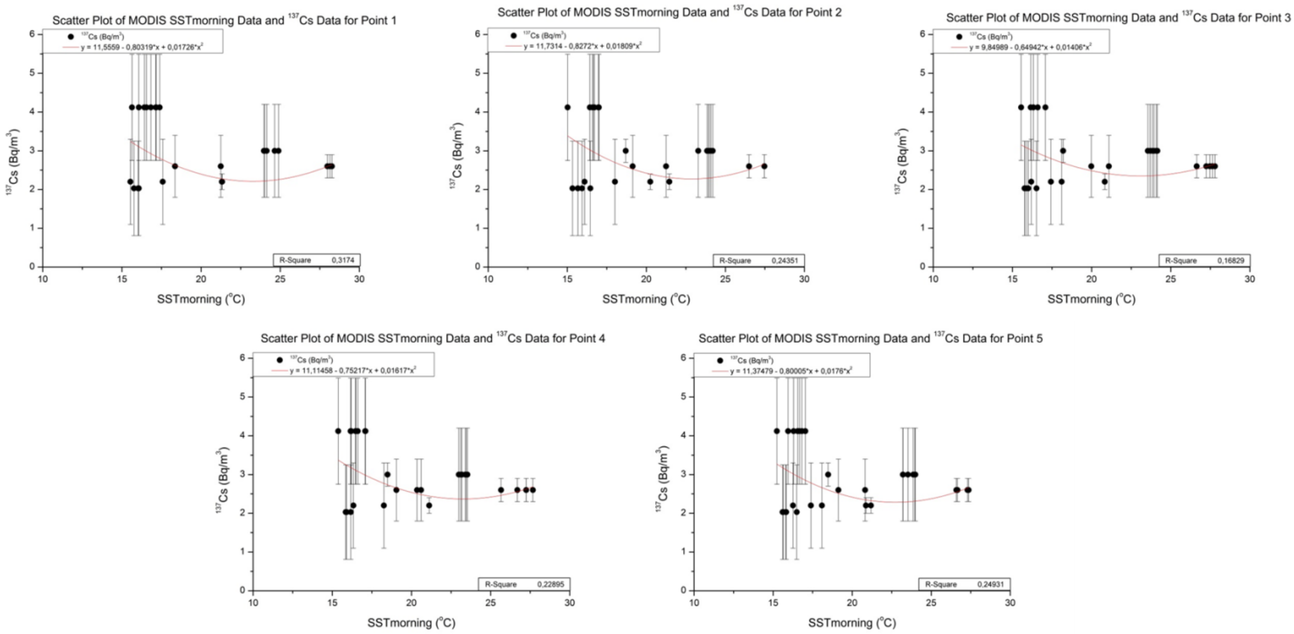

Figure 59. Scatter plots of MODIS SSTmorning data and ^{137}Cs data depicting the 2nd degree polynomial relation (including errors).

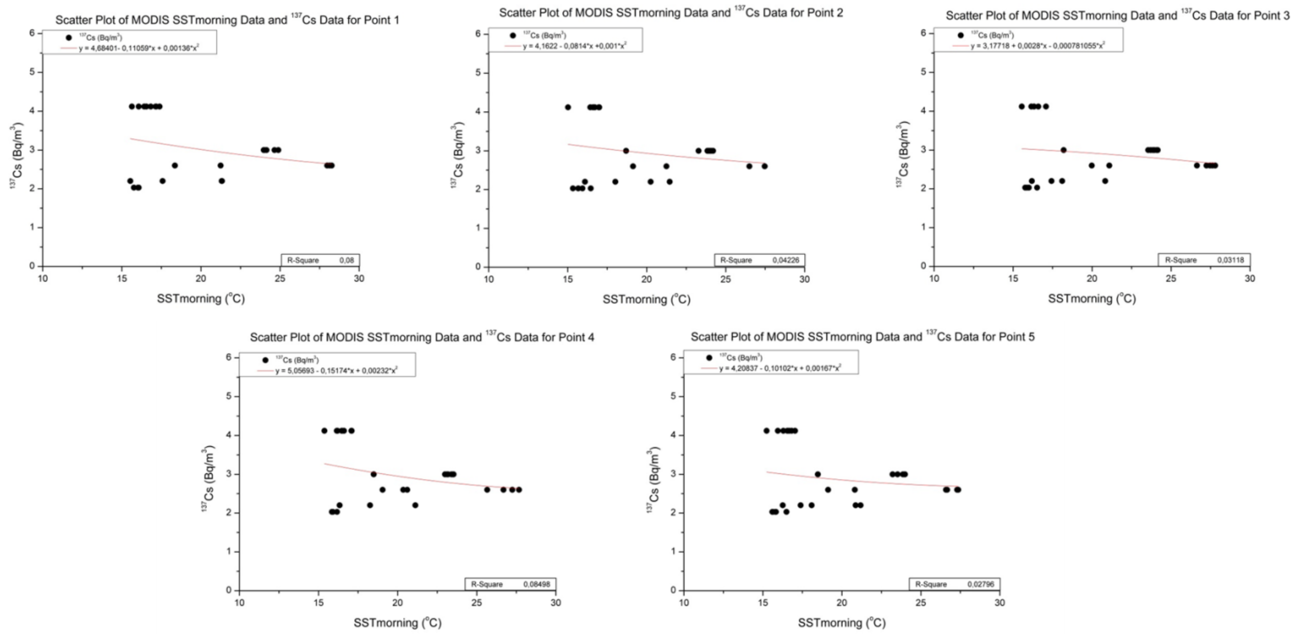

Figure 60. Scatter plots of MODIS SSTmorning data and ^{137}Cs data depicting the 2nd degree polynomial relation.

The results of the linear and second degree polynomial regression of ^{137}Cs activity concentrations and MODIS SSTmorning for all the 5 points of MODIS measurement points in Souda Bay are presented in this part (Figures 57, 58, 59, 60). Results show that the type of regression models used cannot sufficiently explain the ^{137}Cs activity concentrations in Souda Bay using MODIS SSTnight. The r^2 values for all the 5 points of measurement are below 0.35; thus rendering SSTmorning the least preferred result of all MODIS SST measurements and SST4night the most preferred.

8.1.1.1.4. CHLOR_A

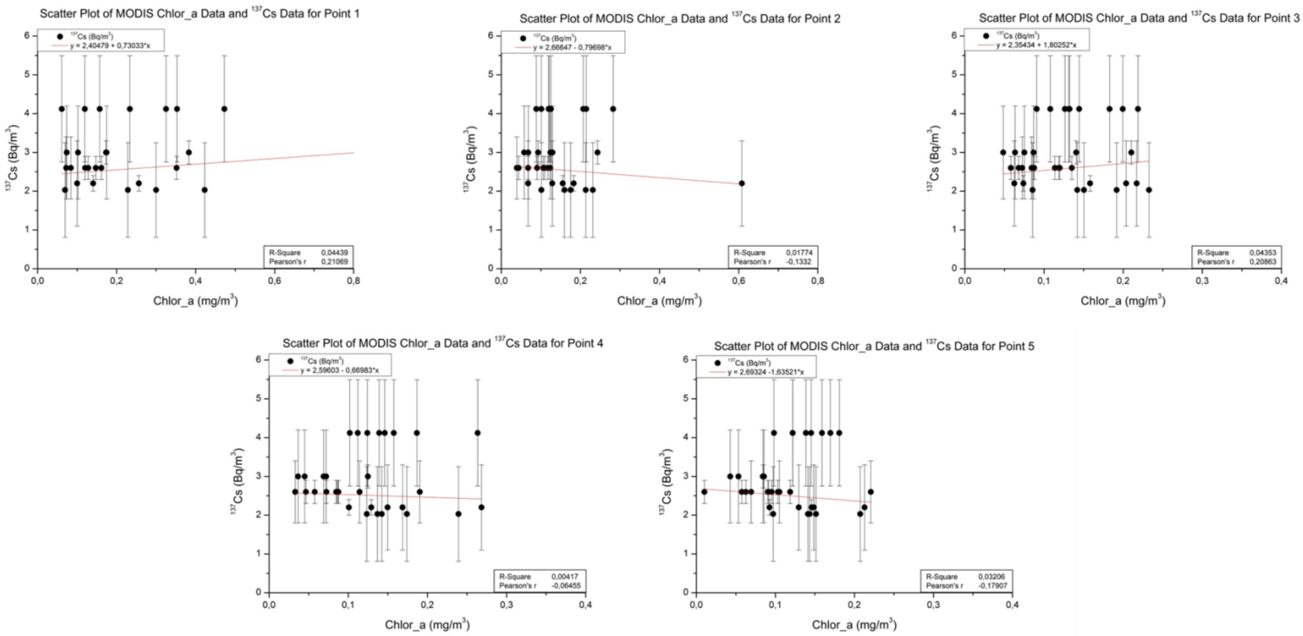

Figure 61. Scatter plots of MODIS Chlor_a data and ^{137}Cs data depicting the linear relation (including errors).

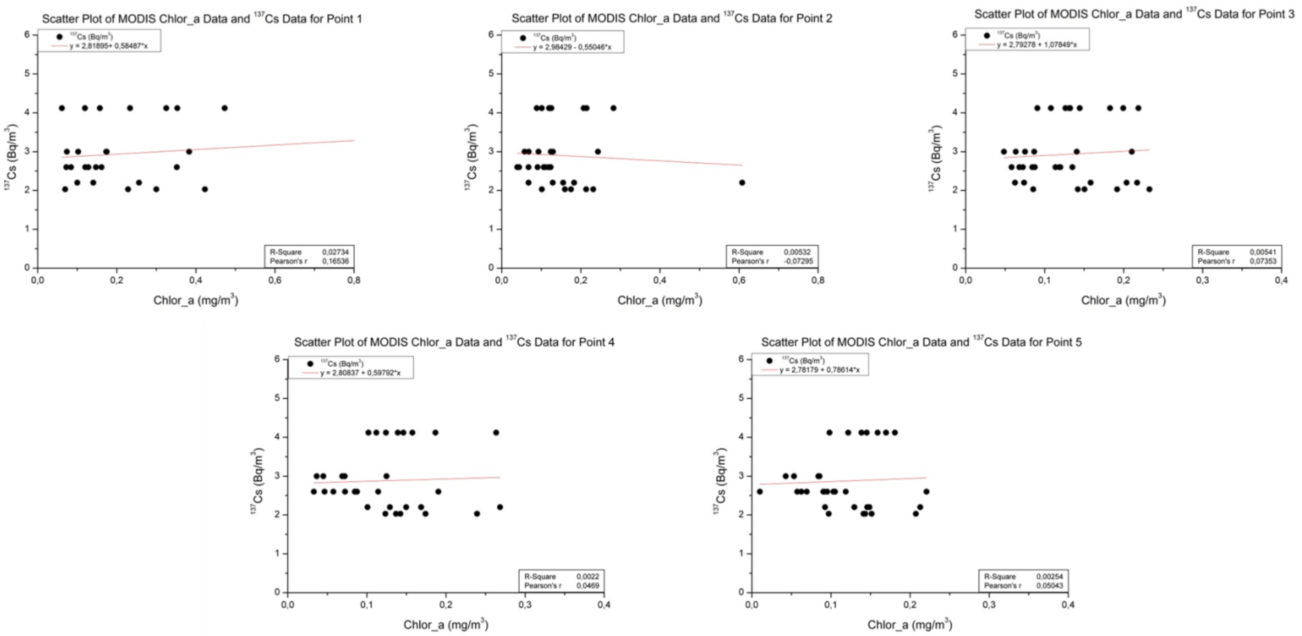

Figure 62. Scatter plots of MODIS Chlor_a data and ^{137}Cs data depicting the linear relation.

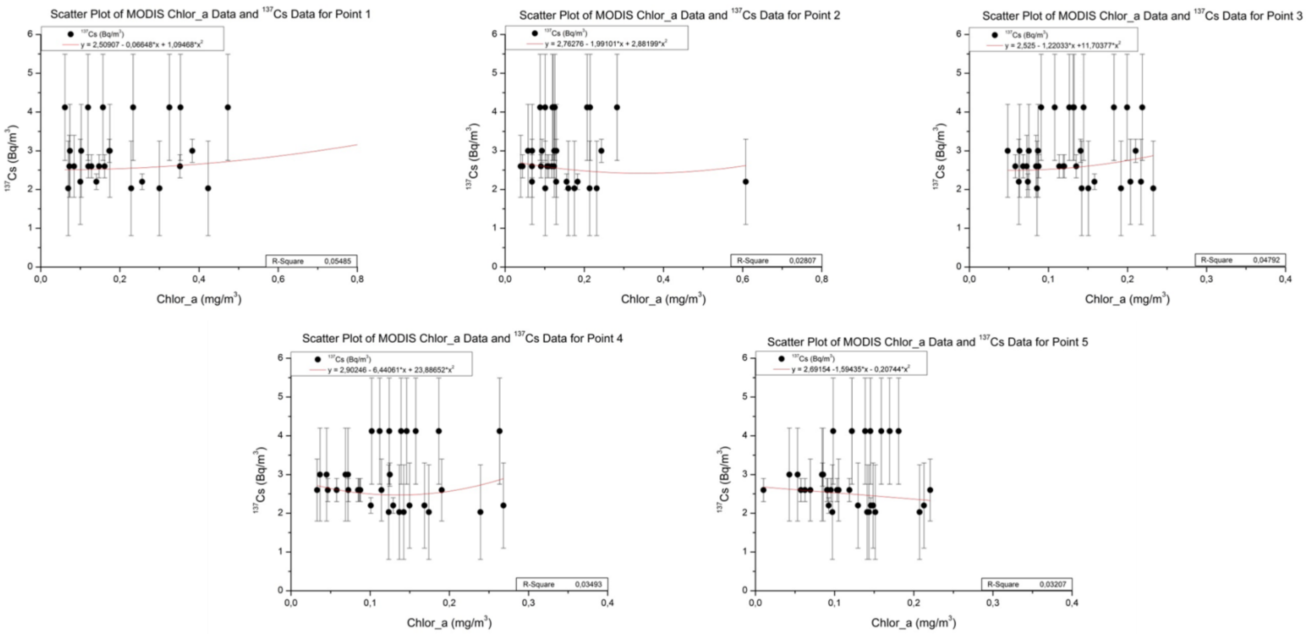

Figure 63. Scatter plots of MODIS Chlor_a data and ^{137}Cs data depicting the 2nd degree polynomial relation (including errors).

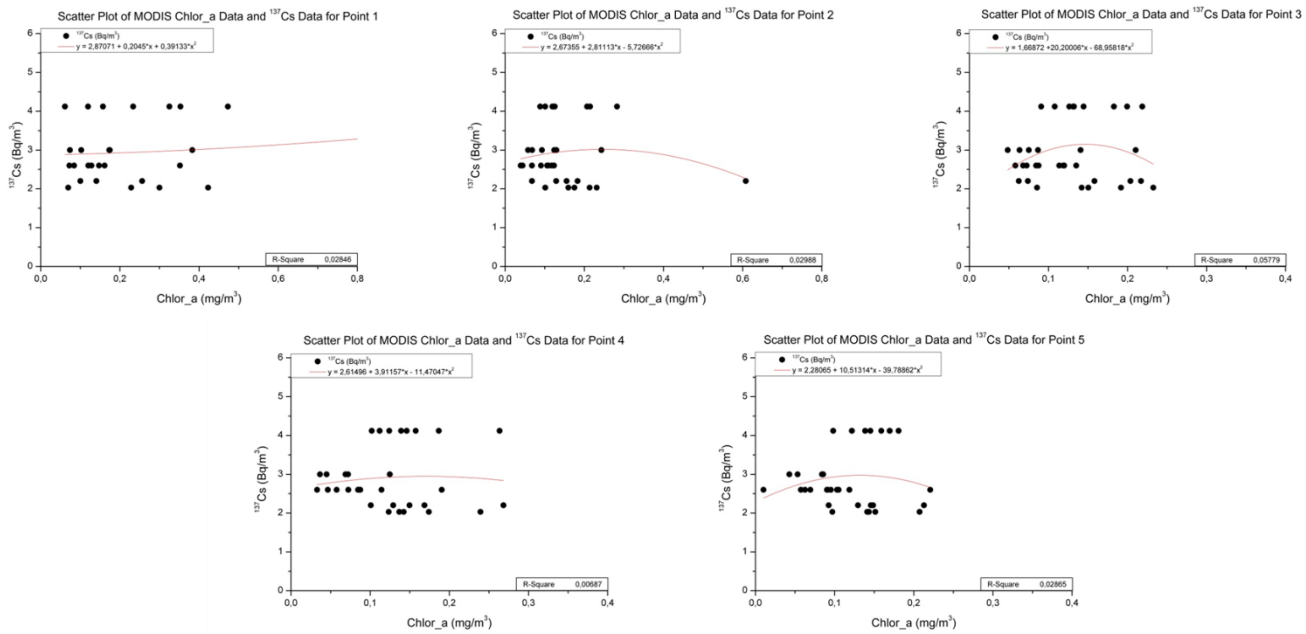

Figure 64. Scatter plots of MODIS Chlor_a data and ^{137}Cs data depicting the 2nd degree polynomial relation.

Here the results of linear and second degree polynomial regression of ^{137}Cs activity concentrations and MODIS Chlor_a concentration are presented (Figures 61, 62, 63, 64). By observing the results for all the 5 points of measurement, including and excluding ^{137}Cs activity errors, it is obvious that the linear and second degree regression models are not able to explain the ^{137}Cs activity concentrations using MODIS Chlor_a, with r^2 values being below 0.1.

8.1.1.1.5. PIC

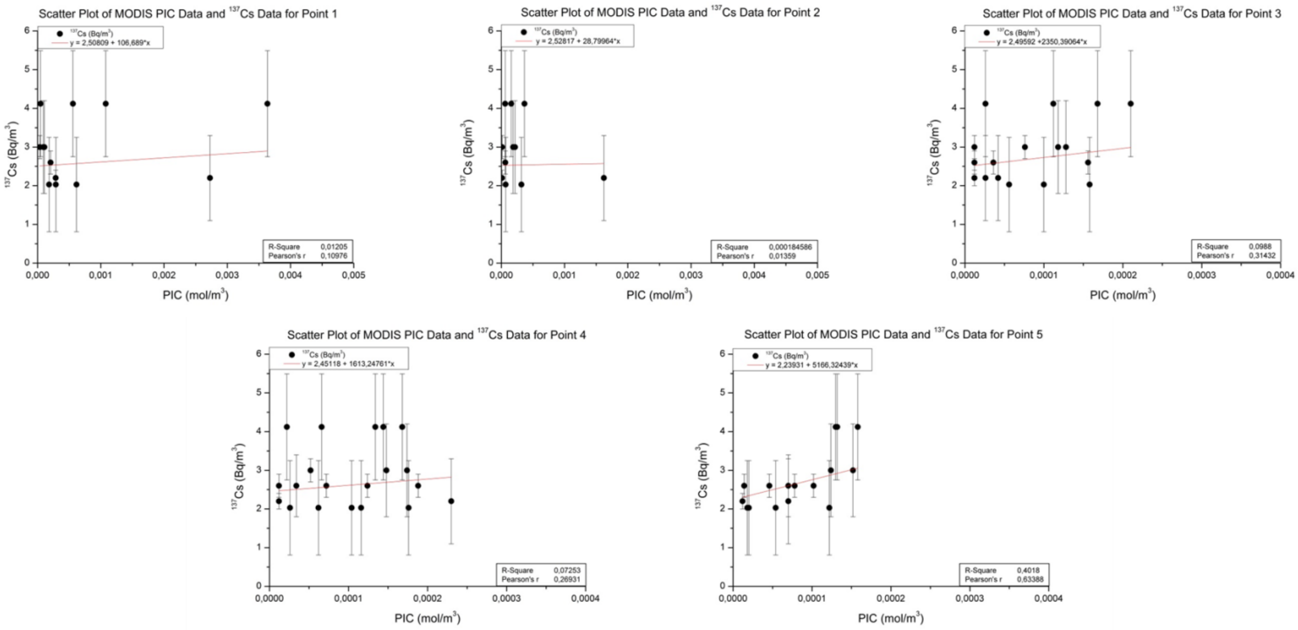

Figure 65. Scatter plots of MODIS PIC data and ^{137}Cs data depicting the linear relation (including errors).

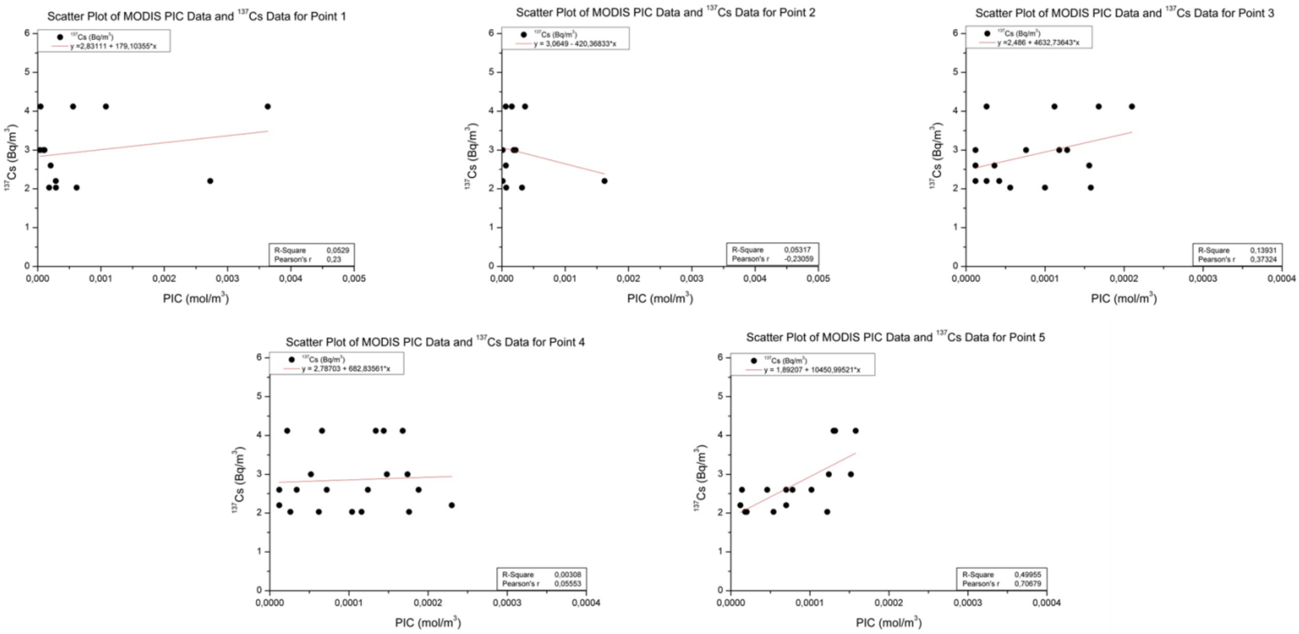

Figure 66. Scatter plots of MODIS PIC data and ^{137}Cs data depicting the linear relation.

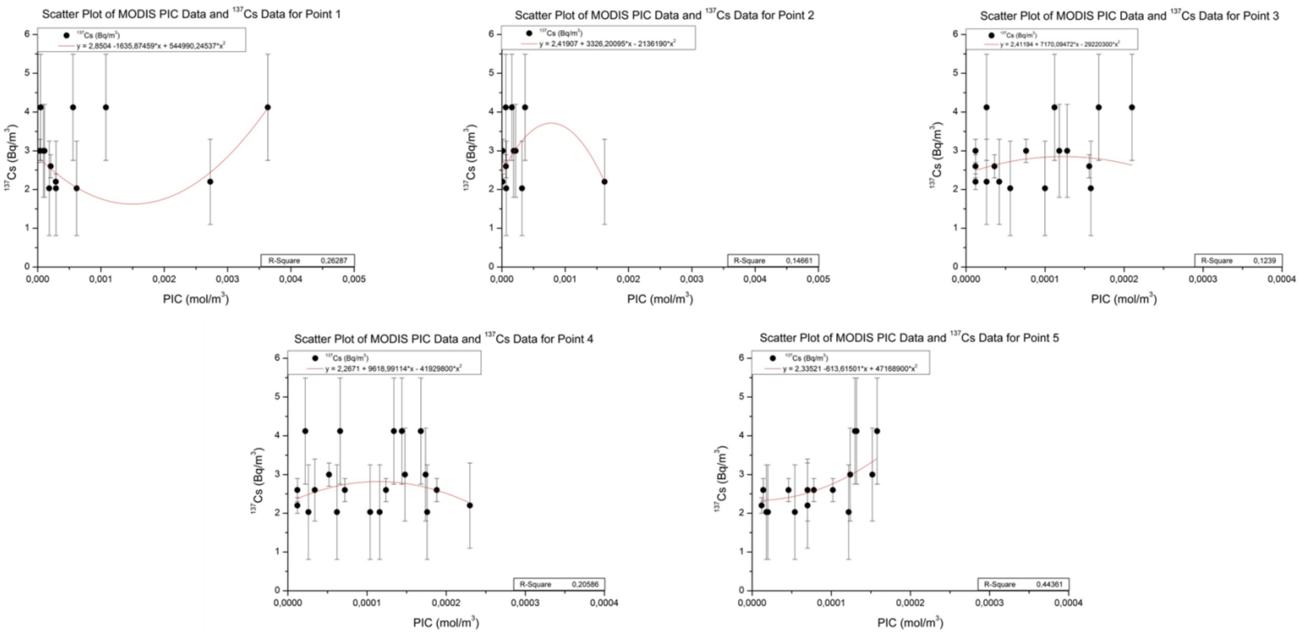

Figure 67. Scatter plots of MODIS PIC data and ^{137}Cs data depicting the 2nd degree polynomial relation (including errors).

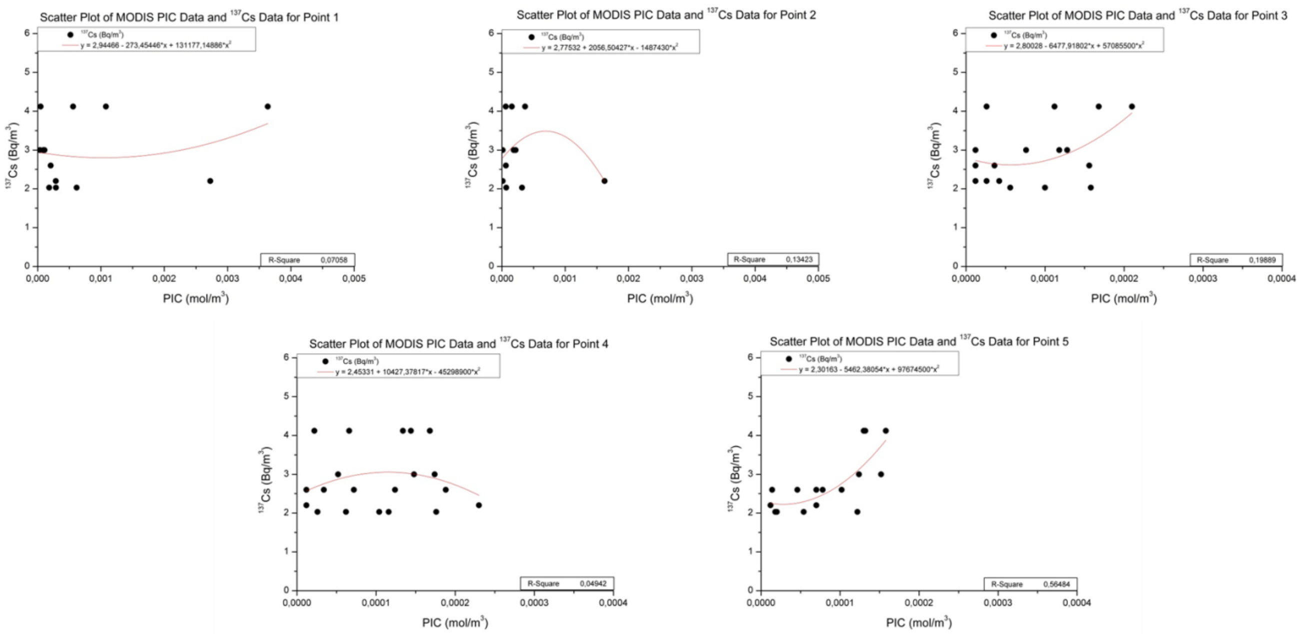

Figure 68. Scatter plots of MODIS PIC data and ^{137}Cs data depicting the 2nd degree polynomial relation.

The results of linear and second degree polynomial regression of ^{137}Cs activity concentrations and MODIS PIC are presented in this section (Figures 65, 66, 67, 68). Point 5 (Souda MODIS pin 5) presents the best results from all Souda Bay MODIS points of measurement, with an r^2 value of 0.4 on linear regression including the activity errors, an r^2 value of 0.5 in linear regression excluding the activity errors, an r^2 value of 0.44 on second degree polynomial regression including the activity errors and an r^2 value of 0.56 on second degree polynomial regression excluding the activity errors. These results show that the regression models using MODIS PIC in MODIS measurement point 5 can sufficiently explain the ^{137}Cs activity concentrations in Souda Bay.

8.1.1.1.6. POC

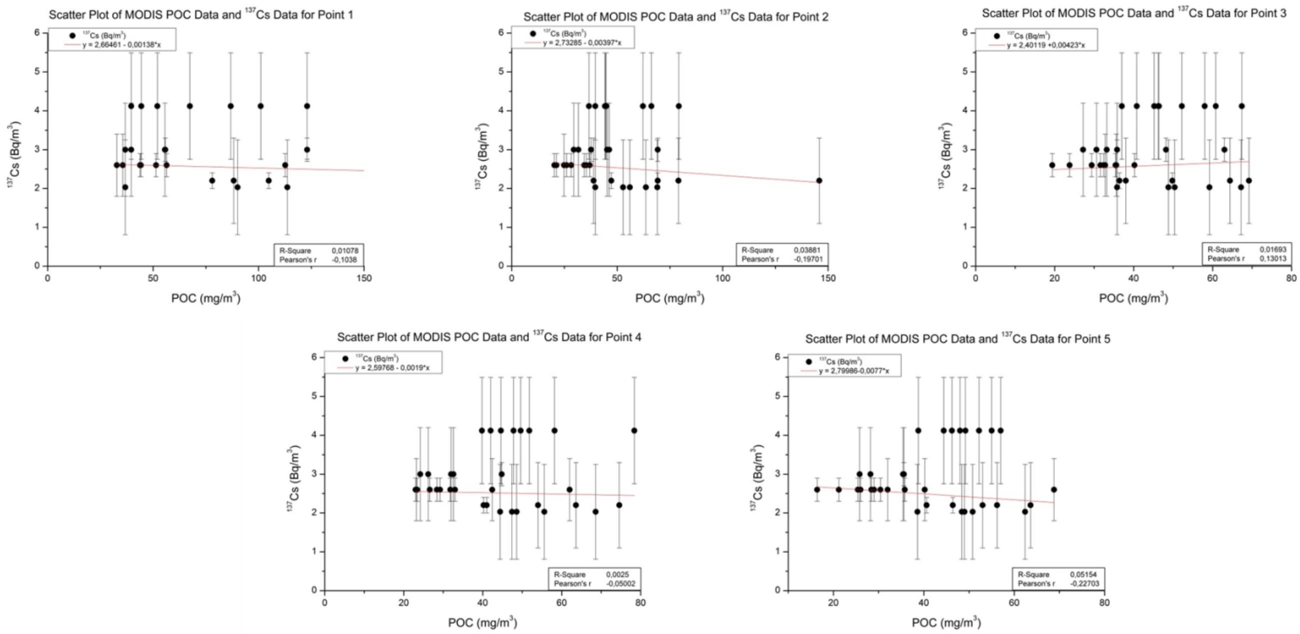

Figure 69. Scatter plots of MODIS POC data and ^{137}Cs data depicting the linear relation (including errors).

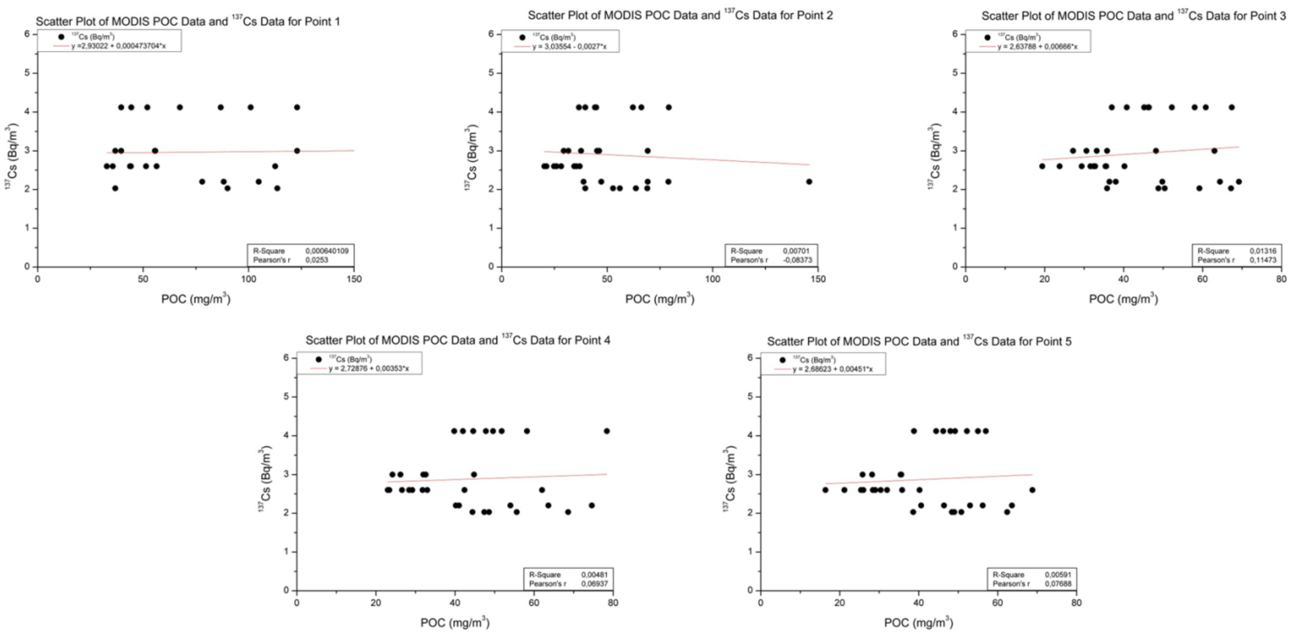

Figure 70. Scatter plots of MODIS POC data and ^{137}Cs data depicting the linear relation.

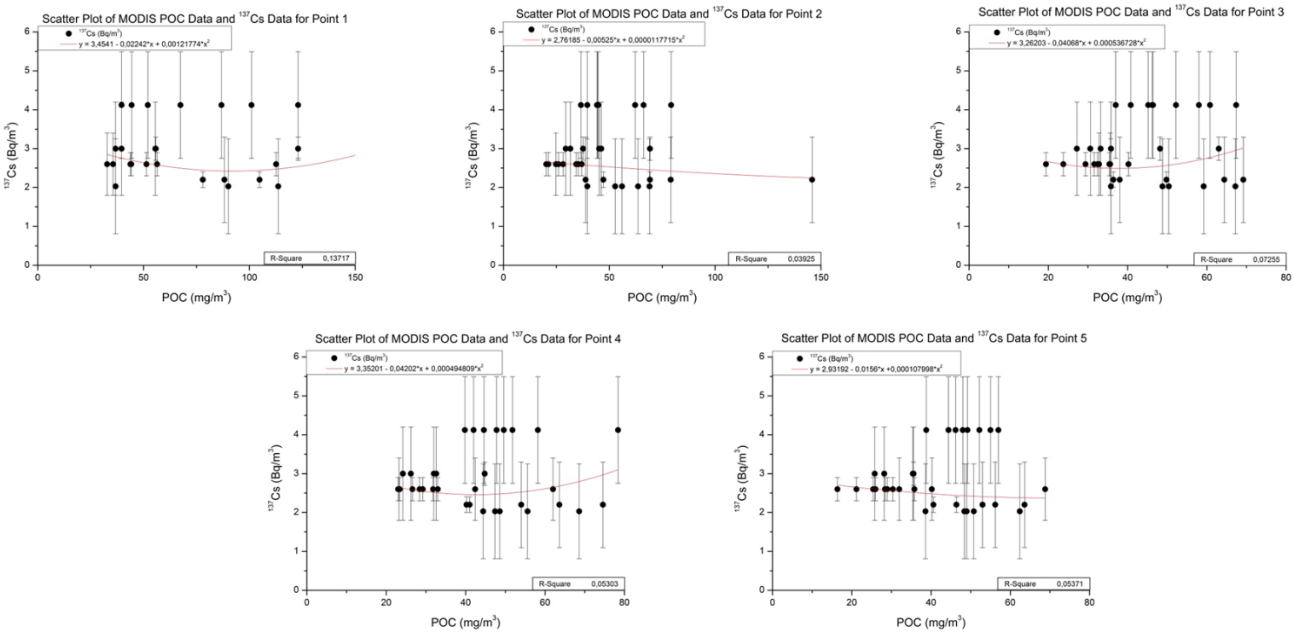

Figure 71. Scatter plots of MODIS POC data and ^{137}Cs data depicting the 2nd degree polynomial relation (including errors).

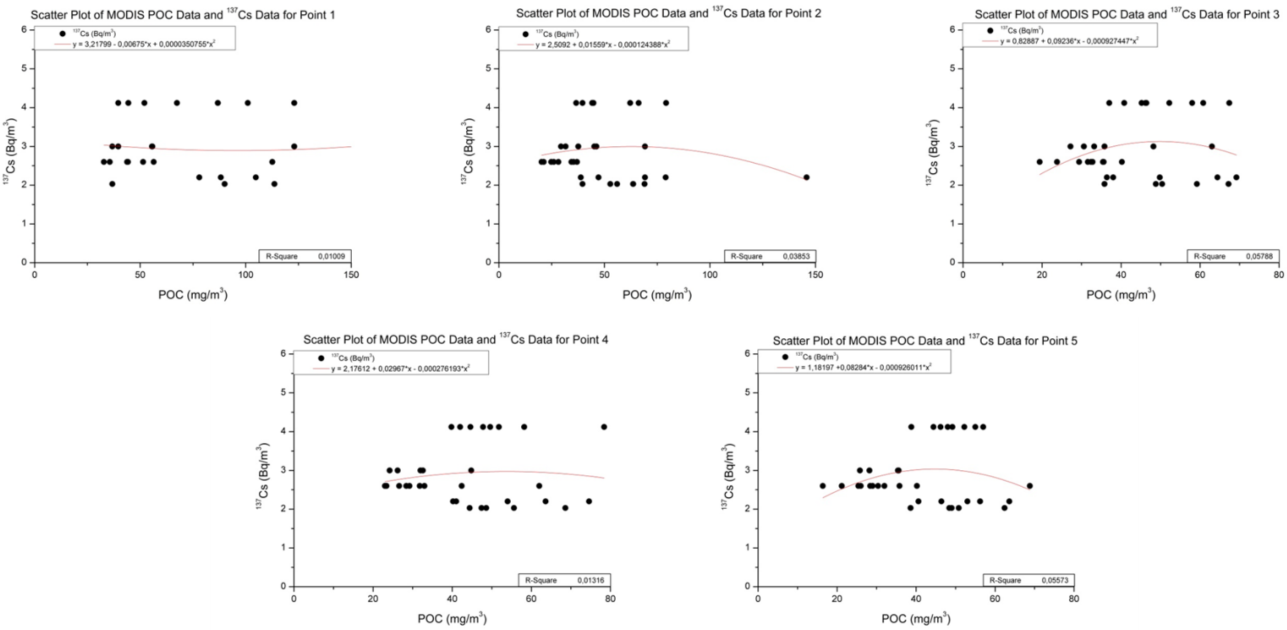

Figure 72. Scatter plots of MODIS POC data and ^{137}Cs data depicting the 2nddegree polynomial relation.

In this point the results of linear and second degree polynomial regression of ^{137}Cs activity concentrations and MODIS POC are exhibited (Figures 69, 70, 71, 72). The results show that in contrast to MODIS PIC, MODIS POC cannot sufficiently explain the ^{137}Cs activity concentrations in Souda Bay area. This was a phenomenon observed in all MODIS measurement points, with r^2 values being below 0.2.

8.1.1.1.7. CDOM

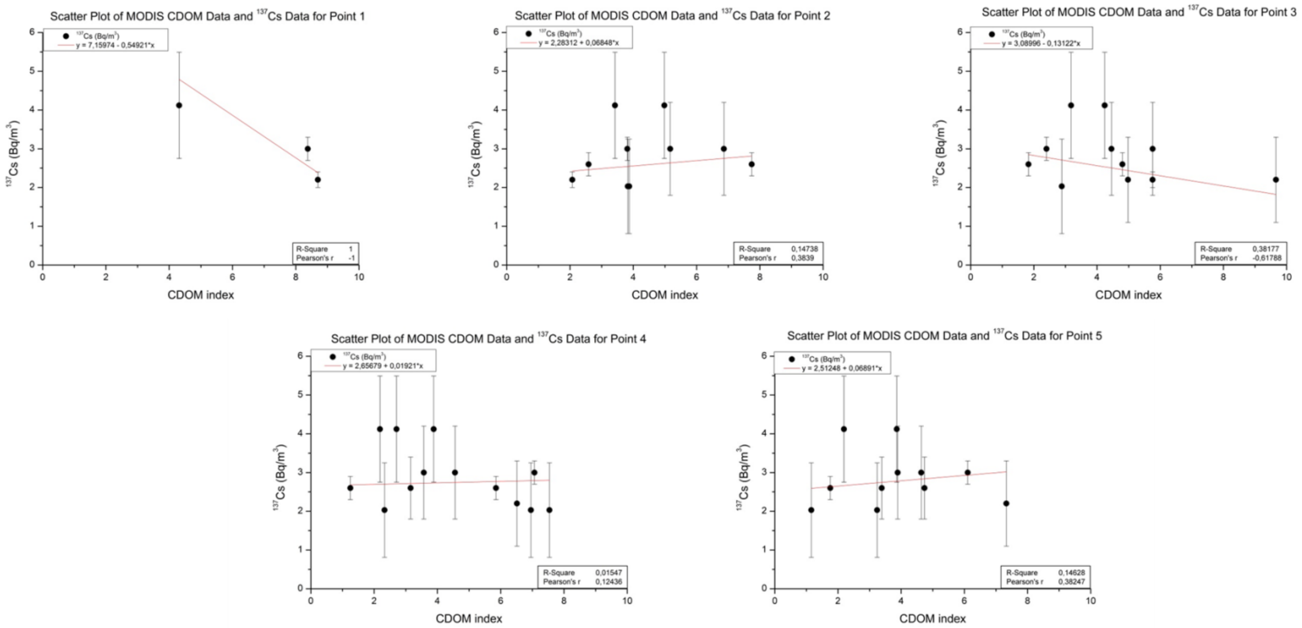

Figure 73. Scatter plots of MODIS CDOM data and ^{137}Cs data depicting the linear relation (including errors).

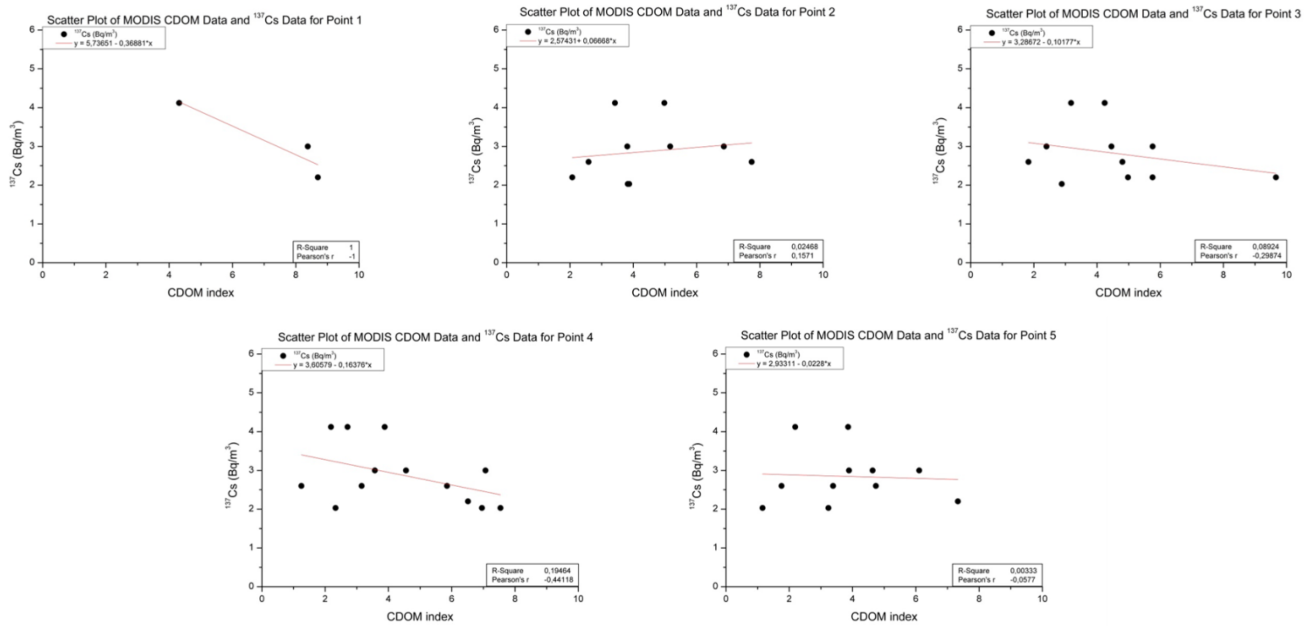

Figure 74. Scatter plots of MODIS CDOM data and ^{137}Cs data depicting the linear relation.

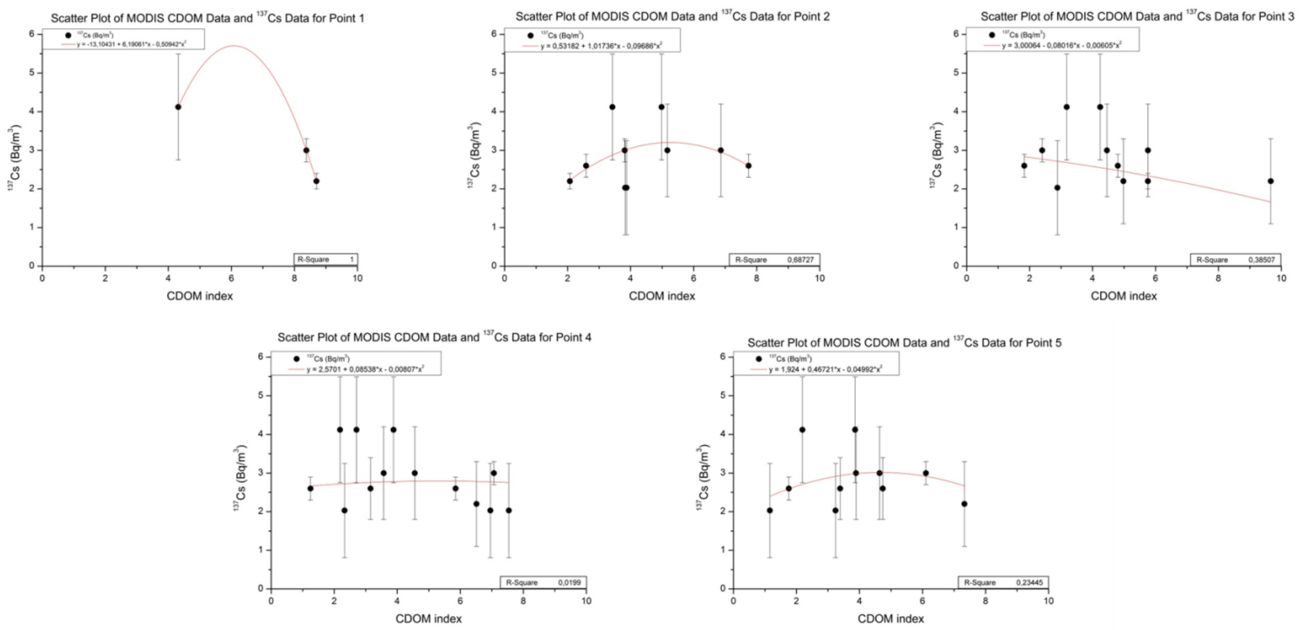

Figure 75. Scatter plots of MODIS CDOM data and ^{137}Cs data depicting the 2nd degree polynomial relation (including errors).

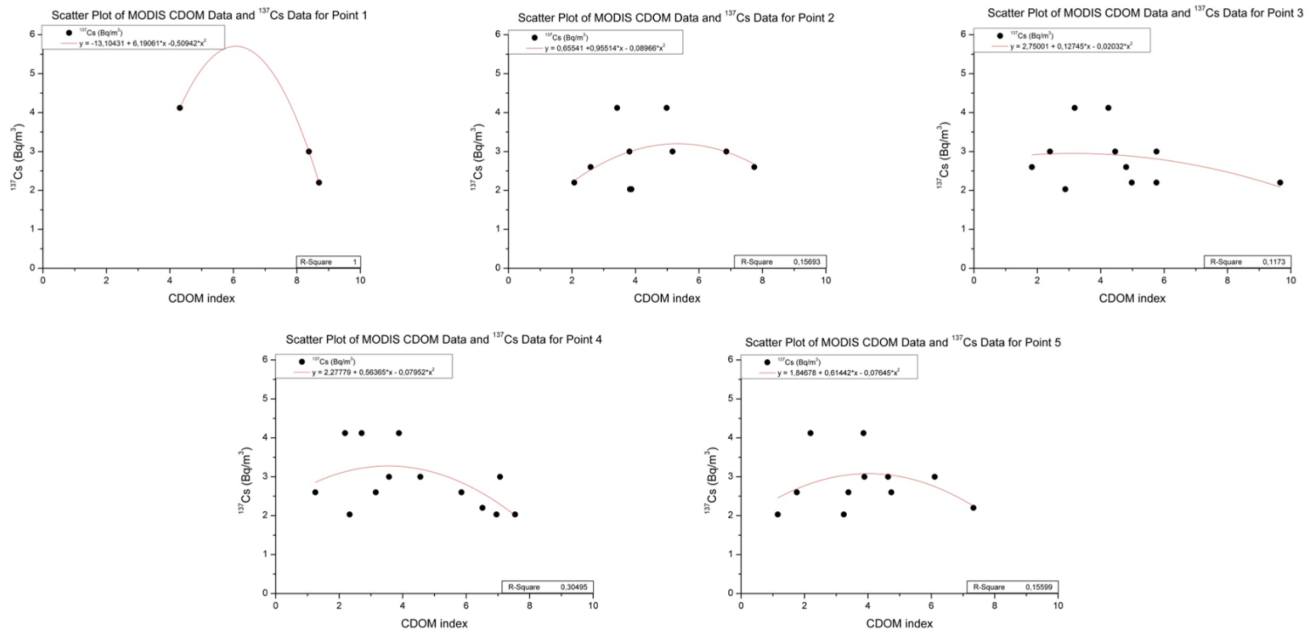

Figure 76. Scatter plots of MODIS CDOM data and ^{137}Cs data depicting the 2nd degree polynomial relation.

Similarly to the other MODIS parameters, in this part the linear and second degree polynomial relations of ^{137}Cs activity concentrations and MODIS CDOM are displayed (Figures 73, 74, 75, 76). By observing the results, it should be noted that the MODIS measurement point 1 (Souda MODIS pin 1) results should not be taken into consideration due to the lack of measurements, thus making it invalid. The point 2 and point 3 present quite sufficient results with point 2 presenting an r^2 of 0.69 on second degree polynomial regression including the errors, and point 3 presenting an r^2 of 0.38 in linear regression including the errors and an r^2 of 0.39 in second degree polynomial regression including the activity errors.

8.1.1.1.8. IPAR

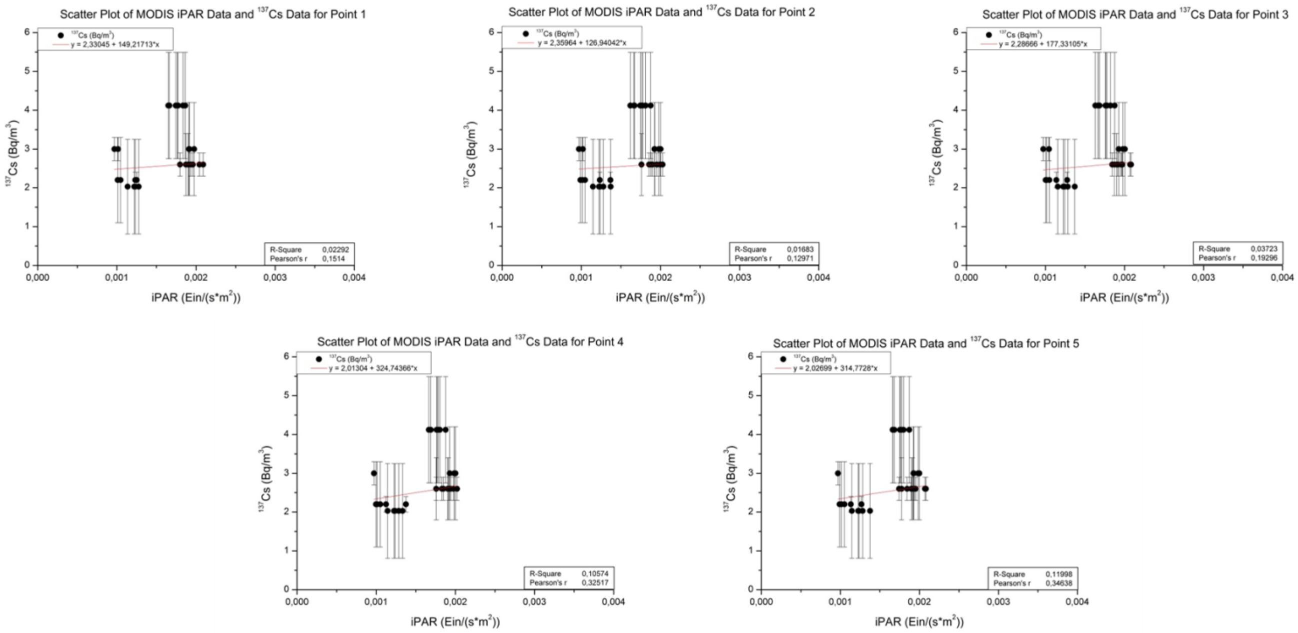

Figure 77. Scatter plots of MODIS iPAR data and ^{137}Cs data depicting the linear relation (including errors).

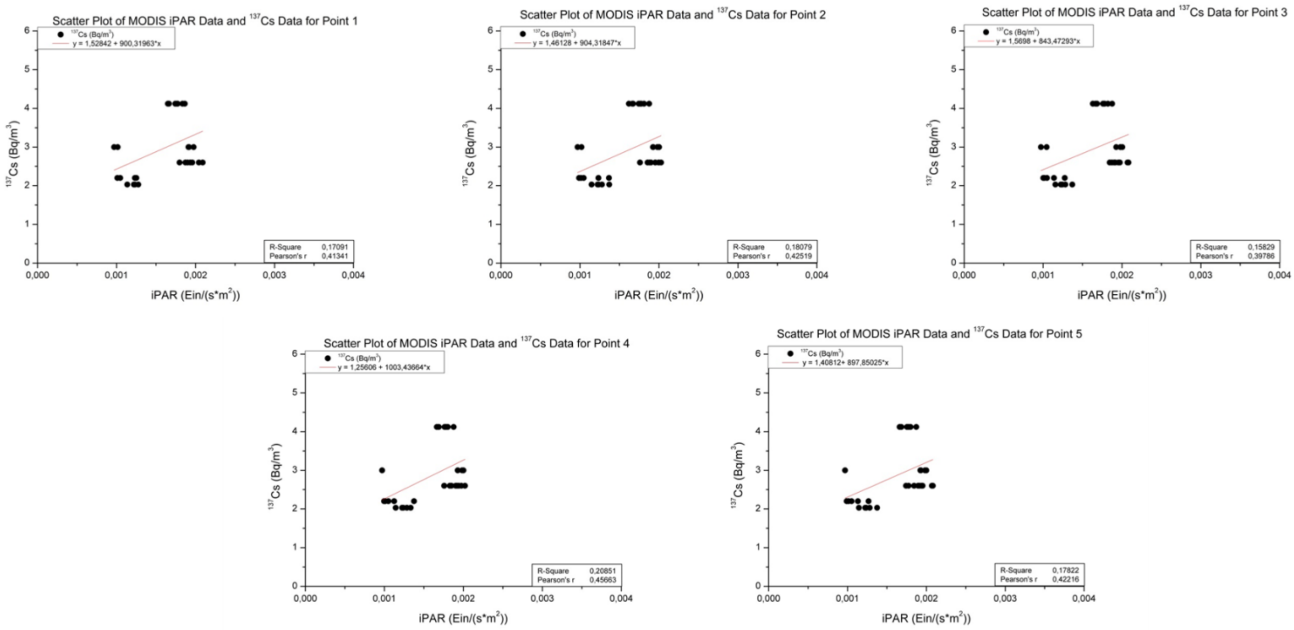

Figure 78. Scatter plots of MODIS iPAR data and ^{137}Cs data depicting the linear relation.

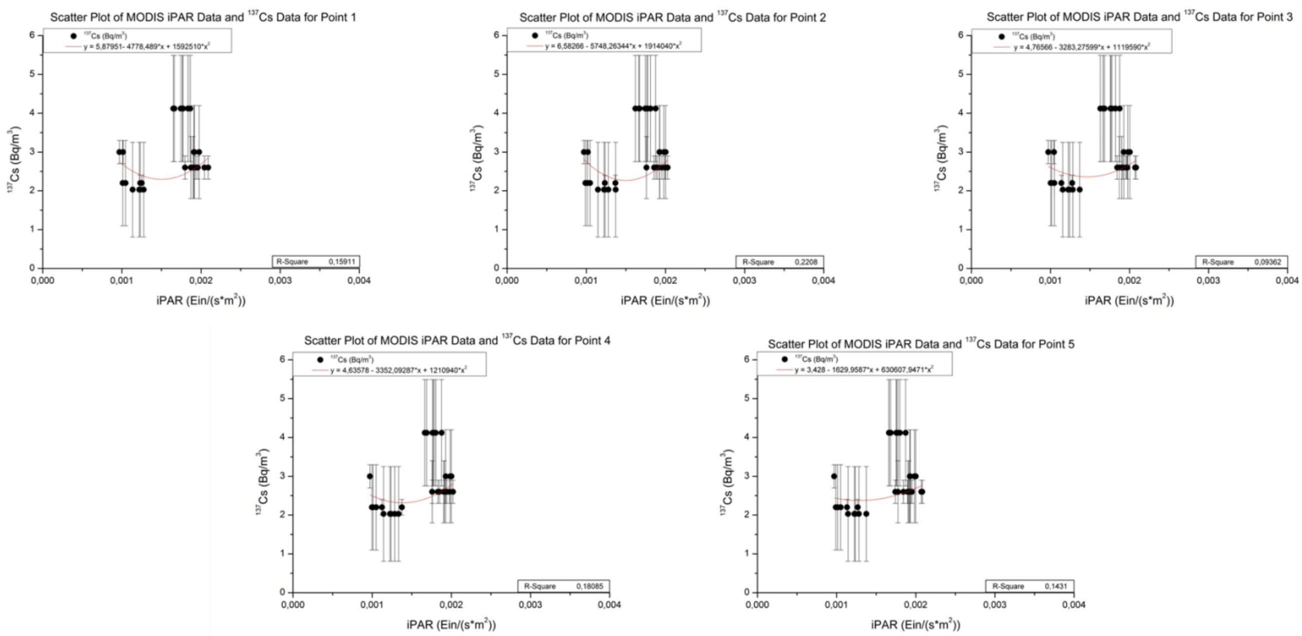

Figure 79. Scatter plots of MODIS iPAR data and ^{137}Cs data depicting the 2nd degree polynomial relation (including errors).

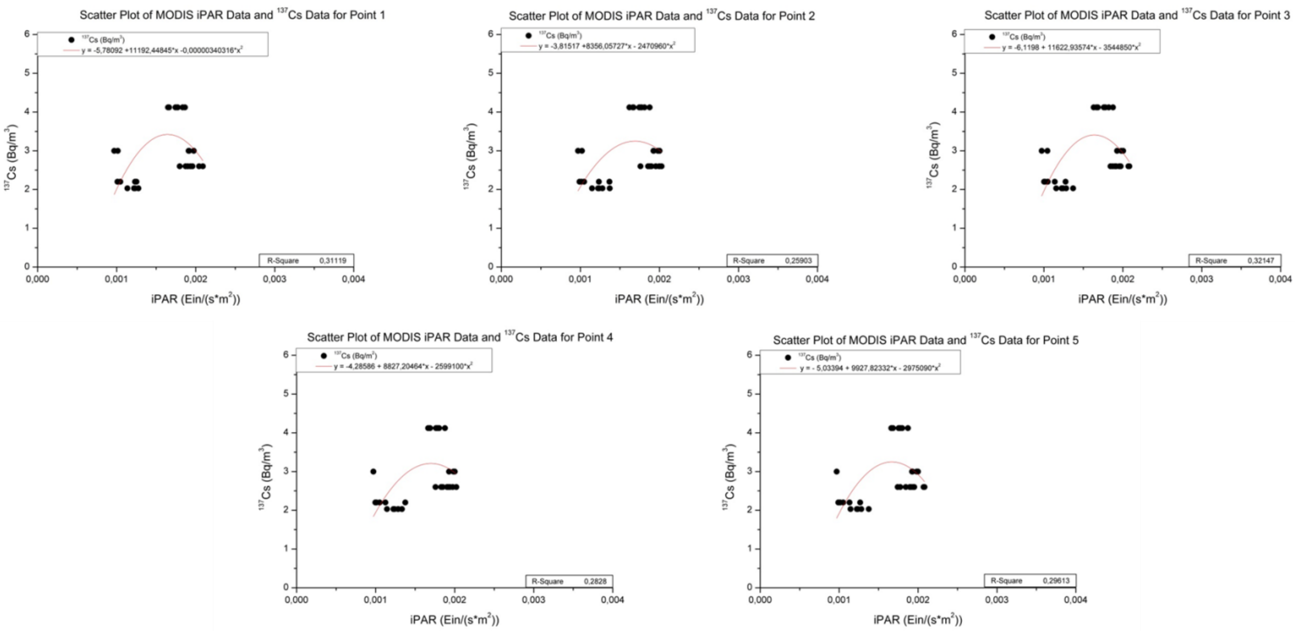

Figure 80. Scatter plots of MODIS iPAR data and ^{137}Cs data depicting the 2nd degree polynomial relation.

The linear and second degree polynomial relations of ^{137}Cs activity concentrations and MODIS iPAR are shown here (Figures 77, 78, 79, 80). The results show a similar line-curve in all 5 of the MODIS measurement points and an r^2 below 0.35 regardless the regression type and the inclusion of the activity errors. The regression models using MODIS iPAR do not sufficiently explain the ^{137}Cs activity concentrations in Souda Bay.

8.1.1.1.9. PAR

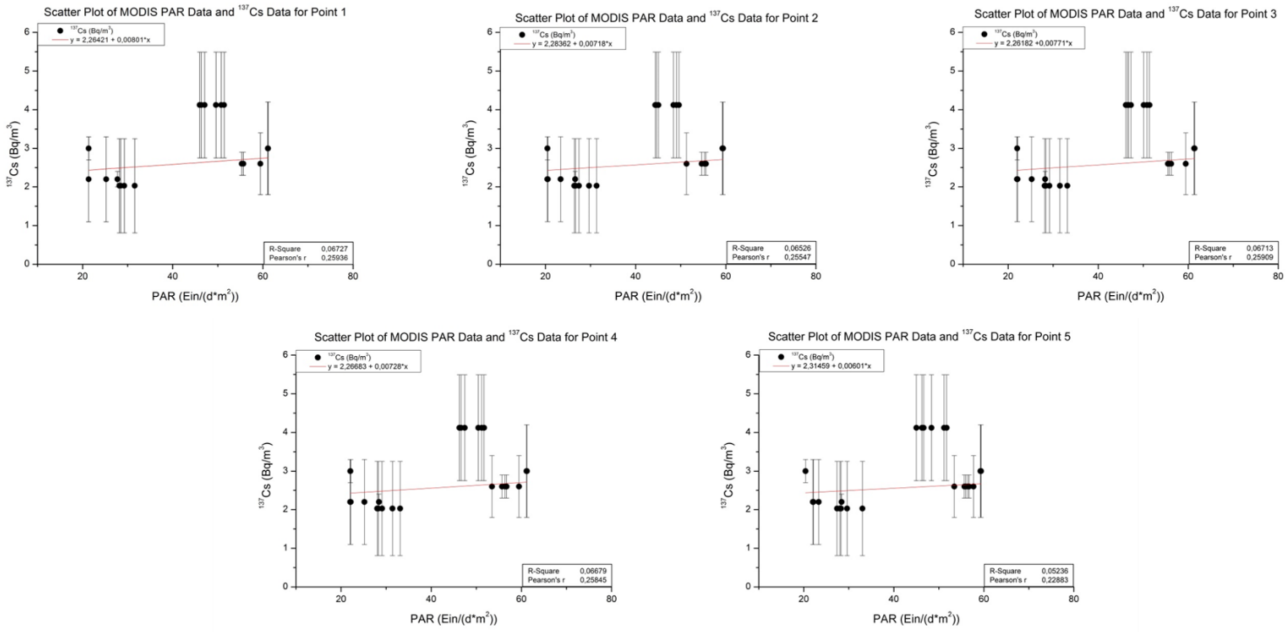

Figure 81. Scatter plots of MODIS PAR data and ^{137}Cs data depicting the linear relation (including errors).

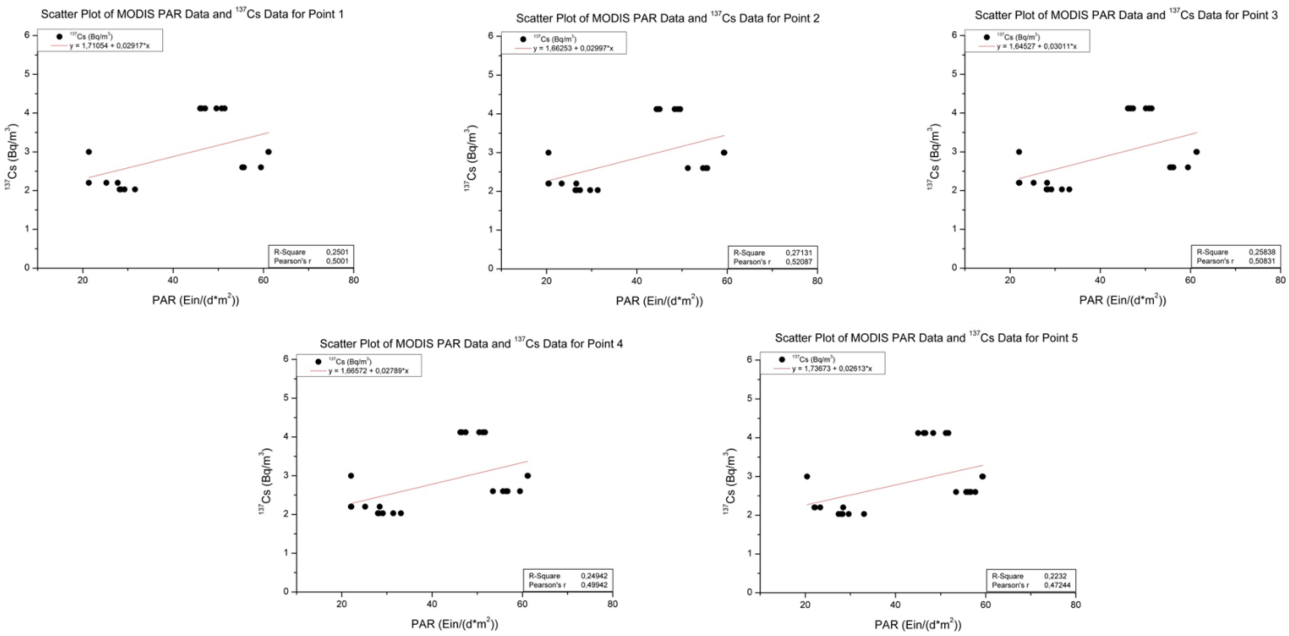

Figure 82. Scatter plots of MODIS PAR data and ^{137}Cs data depicting the linear relation.

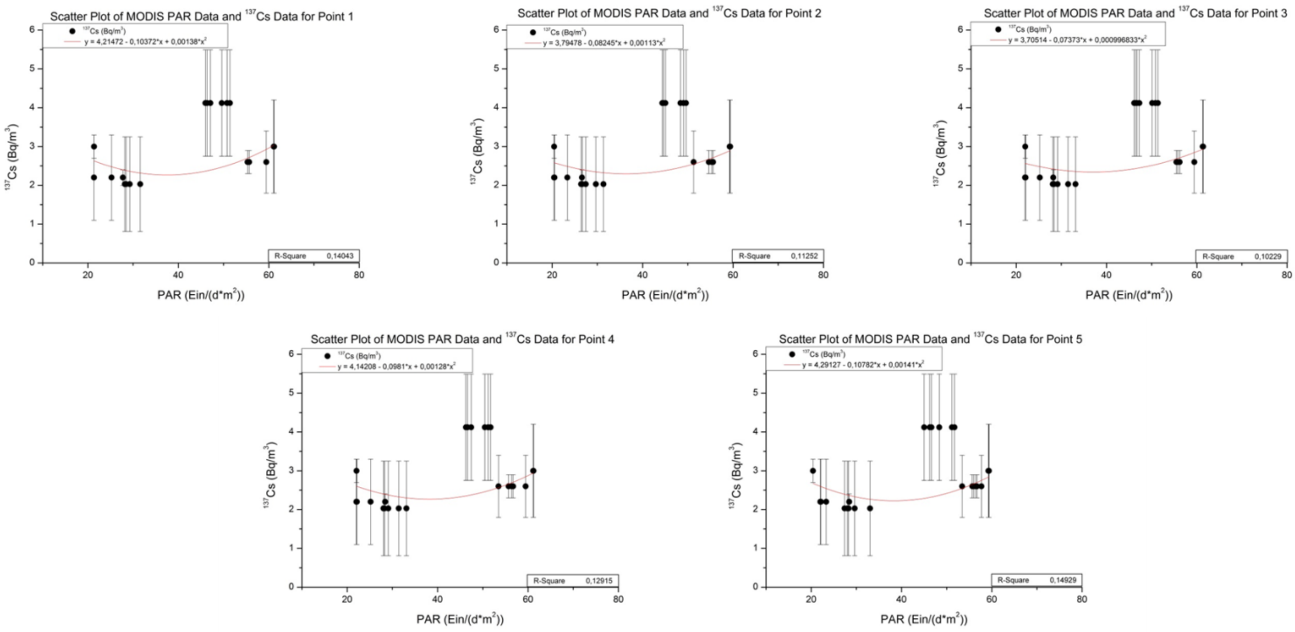

Figure 83. Scatter plots of MODIS PAR data and ^{137}Cs data depicting the 2nd degree polynomial relation (including errors).

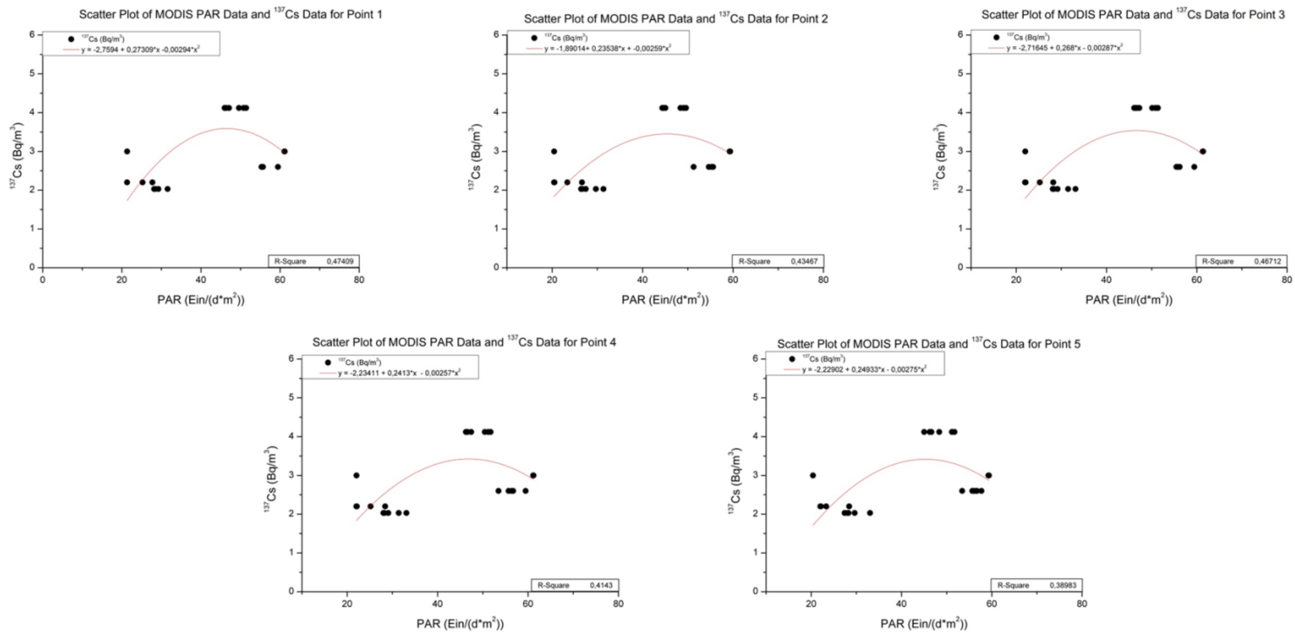

Figure 84. Scatter plots of MODIS PAR data and ^{137}Cs data depicting the 2nd degree polynomial relation.

The linear and second degree polynomial relations of ^{137}Cs activity concentrations and MODIS PAR are presented in this section (Figures 81, 82, 83, 84). In the same way as the MODIS iPAR, MODIS PAR presents the same lines-curves in all 5 MODIS measurement points. However the r^2 values are far better than the MODIS iPAR r^2 values; the first point presents an r^2 value of 0.47, the second point presents an r^2 value of 0.43, the third point presents an r^2 value of 0.47, the fourth point presents an r^2 value of 0.41 and the fifth point presents an r^2 value of 0.39. These r^2 values correspond to the second degree polynomial regression.

8.1.1.2. SMOS

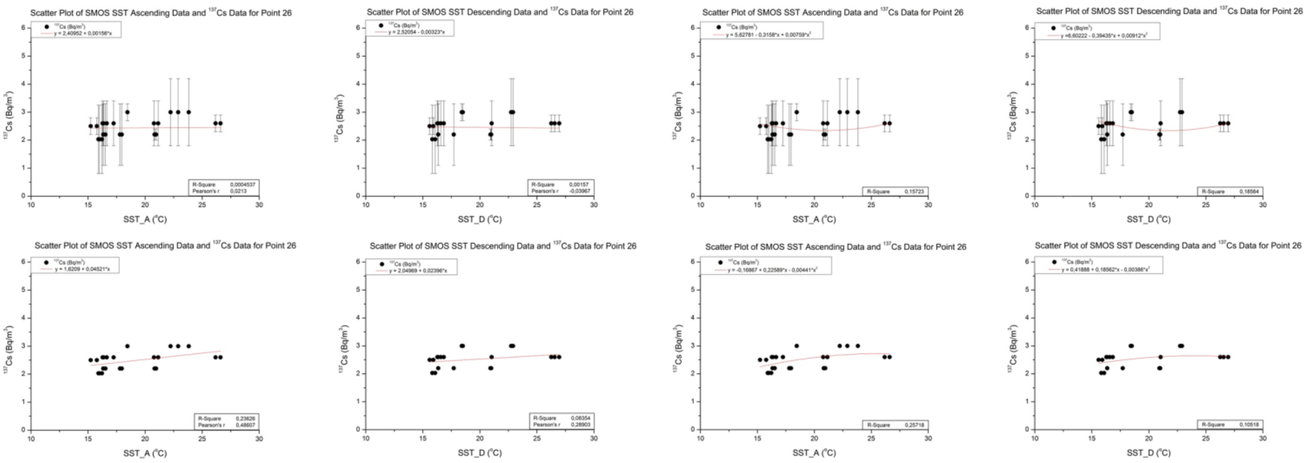

Figure 85. Scatterplots of SMOS SST Ascending, Descending and ^{137}Cs activity concentrations depicting linear and 2nd degree polynomial relations (including and excluding errors) for SMOS point 26.

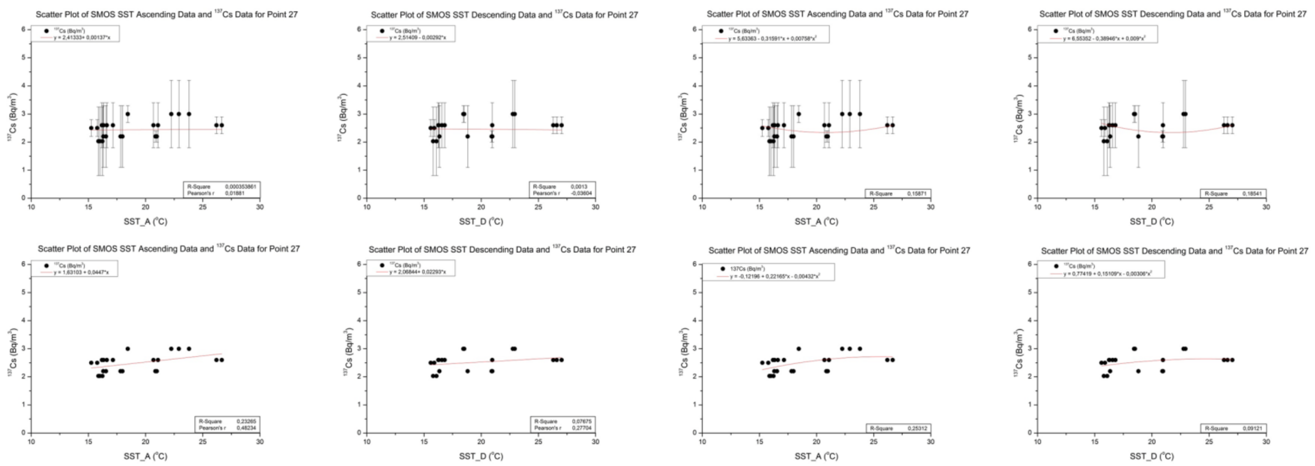

Figure 86.Scatterplots of SMOS SST Ascending, Descending and ^{137}Cs activity concentrations depicting linear and 2nd degree polynomial relations (including and excluding errors) for SMOS point 27.

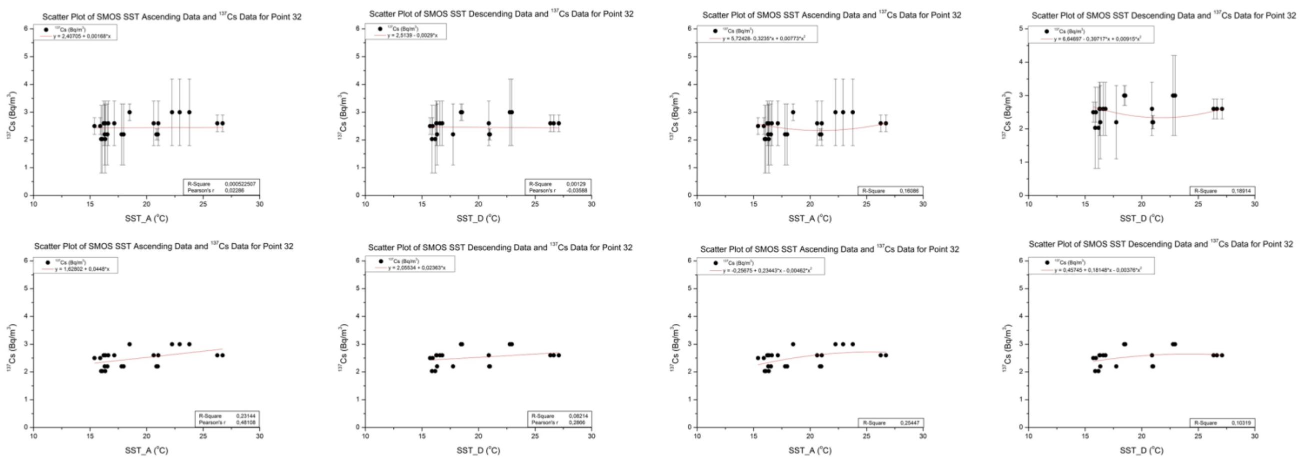

Figure 87. Scatterplots of SMOS SST Ascending, Descending and ^{137}Cs activity concentrations depicting linear and 2nd degree polynomial relations (including and excluding errors) for SMOS point 32.

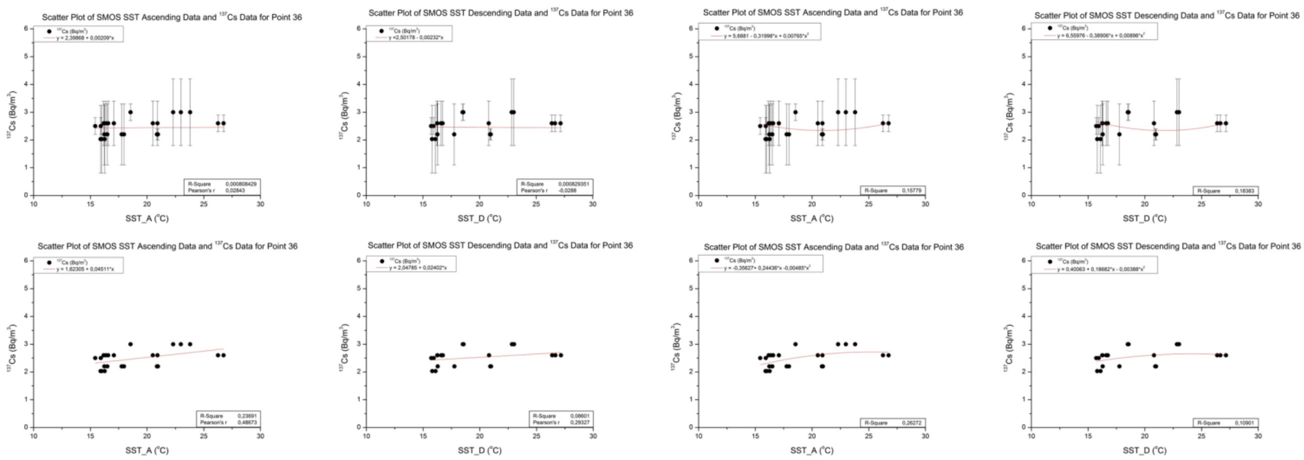

Figure 88. Scatterplots of SMOS SST Ascending, Descending and ^{137}Cs activity concentrations depicting linear and 2nd degree polynomial relations (including and excluding errors) for SMOS point 36.

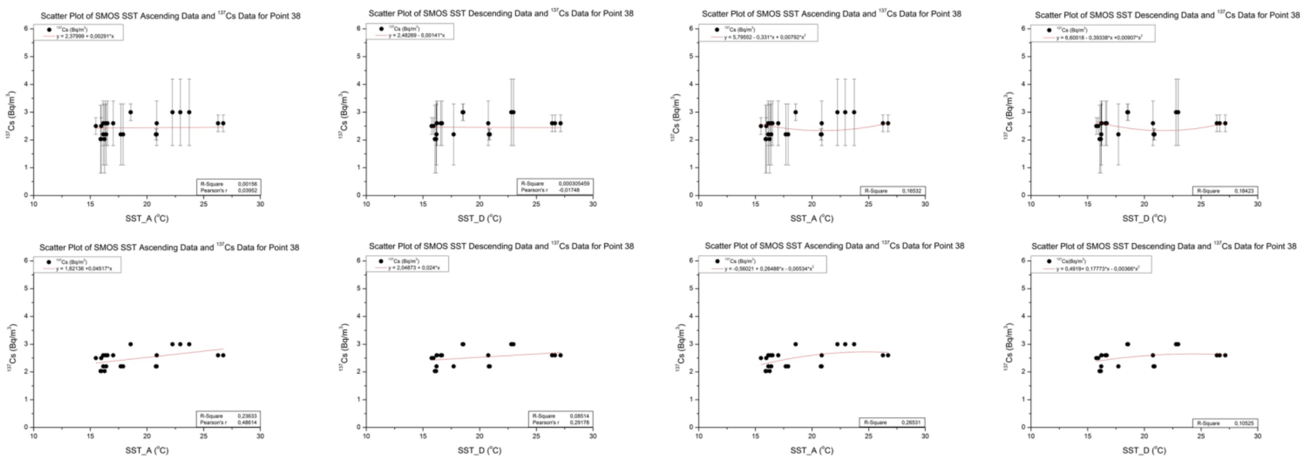

Figure 89. Scatterplots of SMOS SST Ascending, Descending and ^{137}Cs activity concentrations depicting linear and 2nd degree polynomial relations (including and excluding errors) for SMOS point 38.

In this section the linear and second degree polynomial relations of ^{137}Cs activity concentrations and SMOS SST Ascending and Descending are displayed (Figures 85, 86, 87, 88, 89). The relations were estimated for the SMOS measurement points 26, 27, 32, 36 and 38. The relations are presented in 2 formats. In the first format the relations include the ^{137}Cs activity errors and in the second format the relations exclude the activity errors. By observing the results, it is evident that the SMOS Ascending SST relations with ^{137}Cs are better than the SMOS Descending SST with ^{137}Cs activity concentrations. All the points display similar results; however the models using SMOS SST are not adequately describe the ^{137}Cs activity concentrations in Souda Bay and present an r^2 below 0.3.

8.1.1.3. POSEIDON

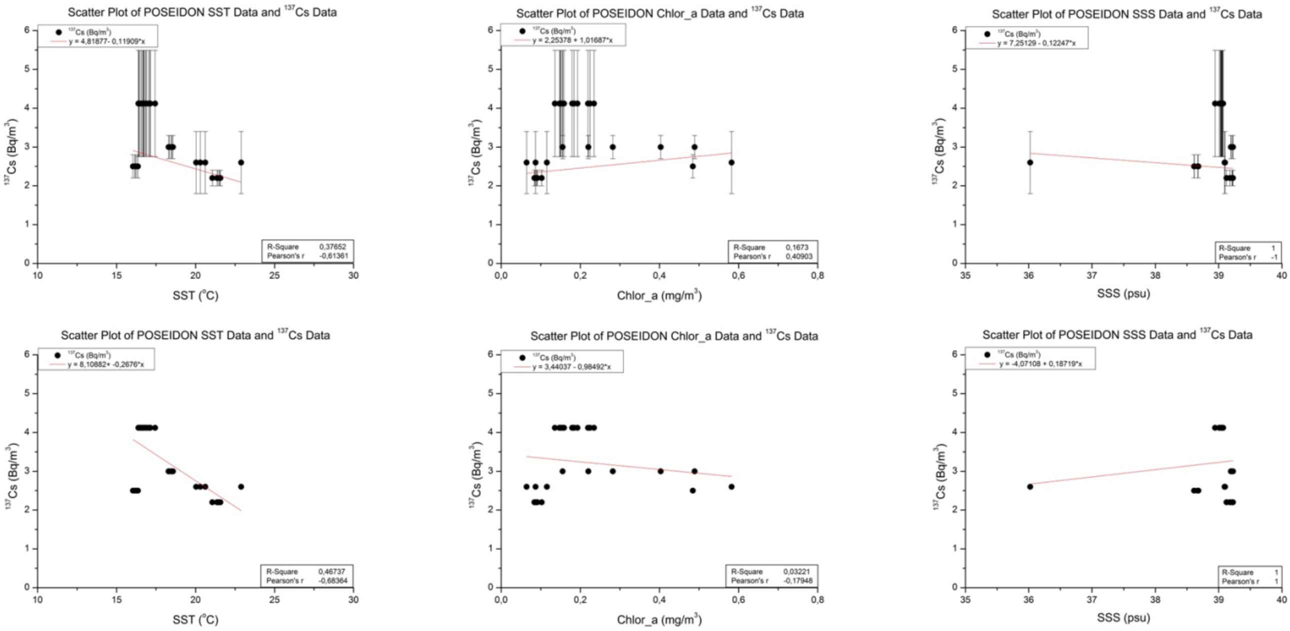

Figure 90. Scatterplots of POSEIDON SST, Chlor_a, SSS and ^{137}Cs activity concentrations depicting linear relations (including and excluding errors).

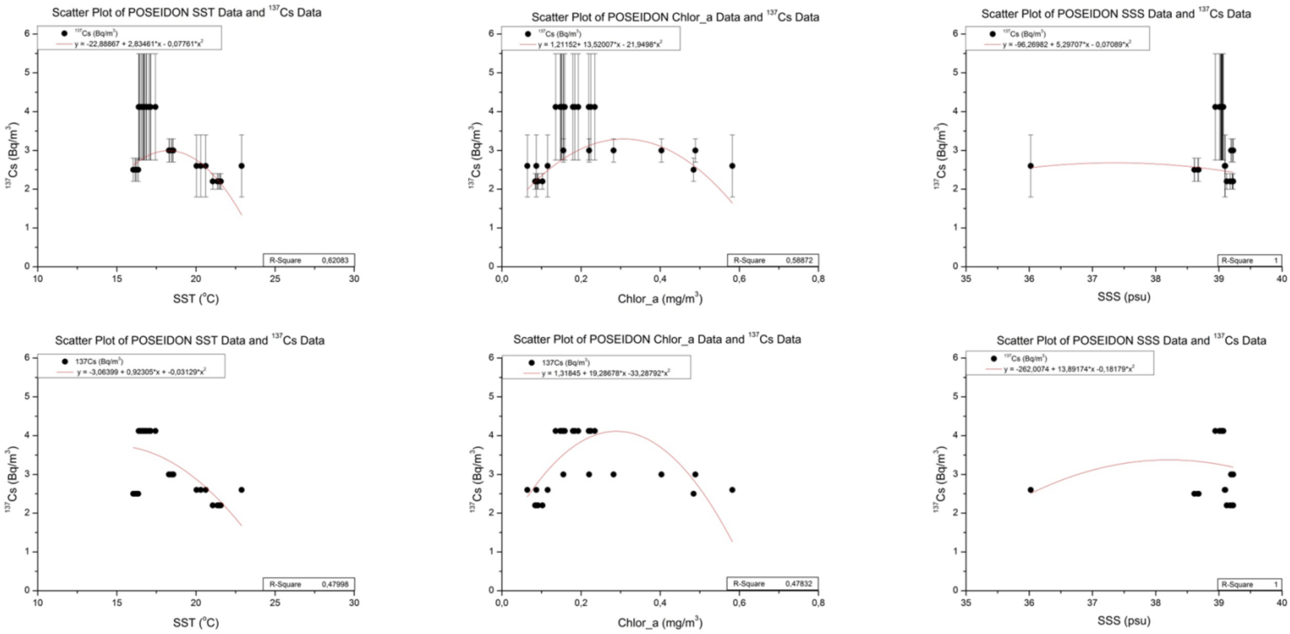

Figure 91. Scatterplots of POSEIDON SST, Chlor_a, SSS and ^{137}Cs activity concentrations depicting 2nd degree polynomial relations (including and excluding errors).

The final results presented for the Souda bay area are the linear and second degree polynomial relations of ^{137}Cs activity concentrations with POSEIDON system's SST, Chlor_a and SSS (Figures 90, 91). By observing the linear results, the relation is better when the activity errors are not included with an r^2 value when using the POSEIDON SST of 0.46. The second degree polynomial regression results are better than the linear ones; however in this case the results that include the activity concentrations errors are better than the ones that exclude the activity concentrations. Relations of POSEIDON SST present an r^2 value of 0.62 when the errors are included and an r^2 value of 0.48 when the errors are excluded (Mavrokefalou et al., 2016). Relations of POSEIDON Chlor_a present an r^2 value of 0.59 when the activity errors are included and an r^2 value of 0.47 when the activity errors are excluded. All the relations of POSEIDON SSS and ^{137}Cs activity concentration present an r^2 value of 1.

8.2. AEGEAN SEA

In this section the results of the relation analysis for the Aegean Sea are presented. The results contain the spatial relations of ^{137}Cs activity concentrations and MODIS parameters, derived from the GWR tool. The first segment of this section are the local r^2 results in the form of maps, when using the MODIS SSTnight, SST4night, SSTmorning, Chlor_a, PIC, POC, iPAR and PAR parameters. The second segment of this section contains the predicted ^{137}Cs activity concentrations, estimated by using the MODIS SSTnight, SST4night, SSTmorning, Chlor_a, PIC, POC, iPAR and PAR parameters. These predictions are then compared to the original ^{137}Cs activity concentrations (Appendix page 212). All the following results concern the months of: March 2012, April 2012, June 2012, November 2012, December 2012, January 2013, February 2013, April 2013, May 2013, March 2014, August 2014, November 2014, December 2014 and February 2015.

8.2.1. GWR Results

8.2.1.1. Local R^2

8.2.1.1.1. SSTnight

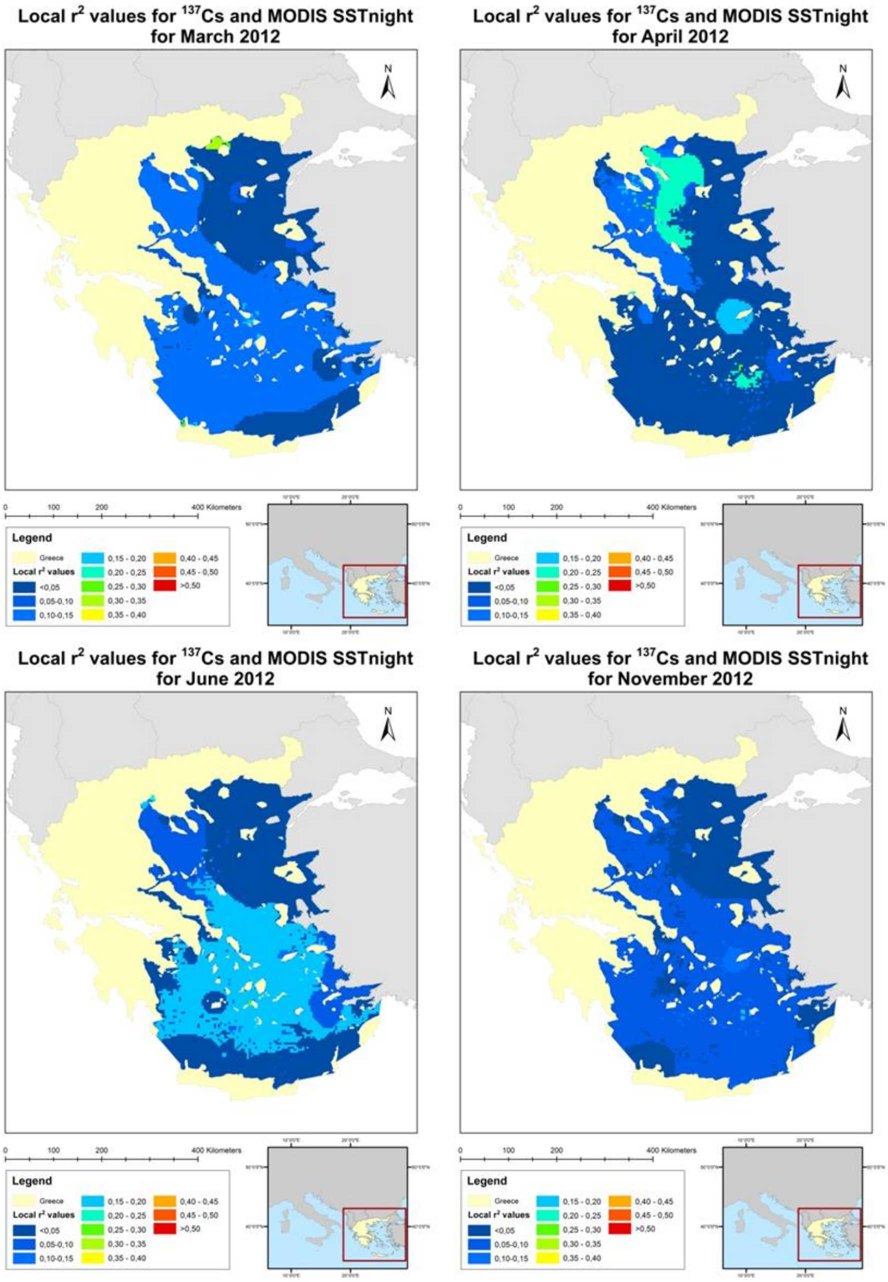

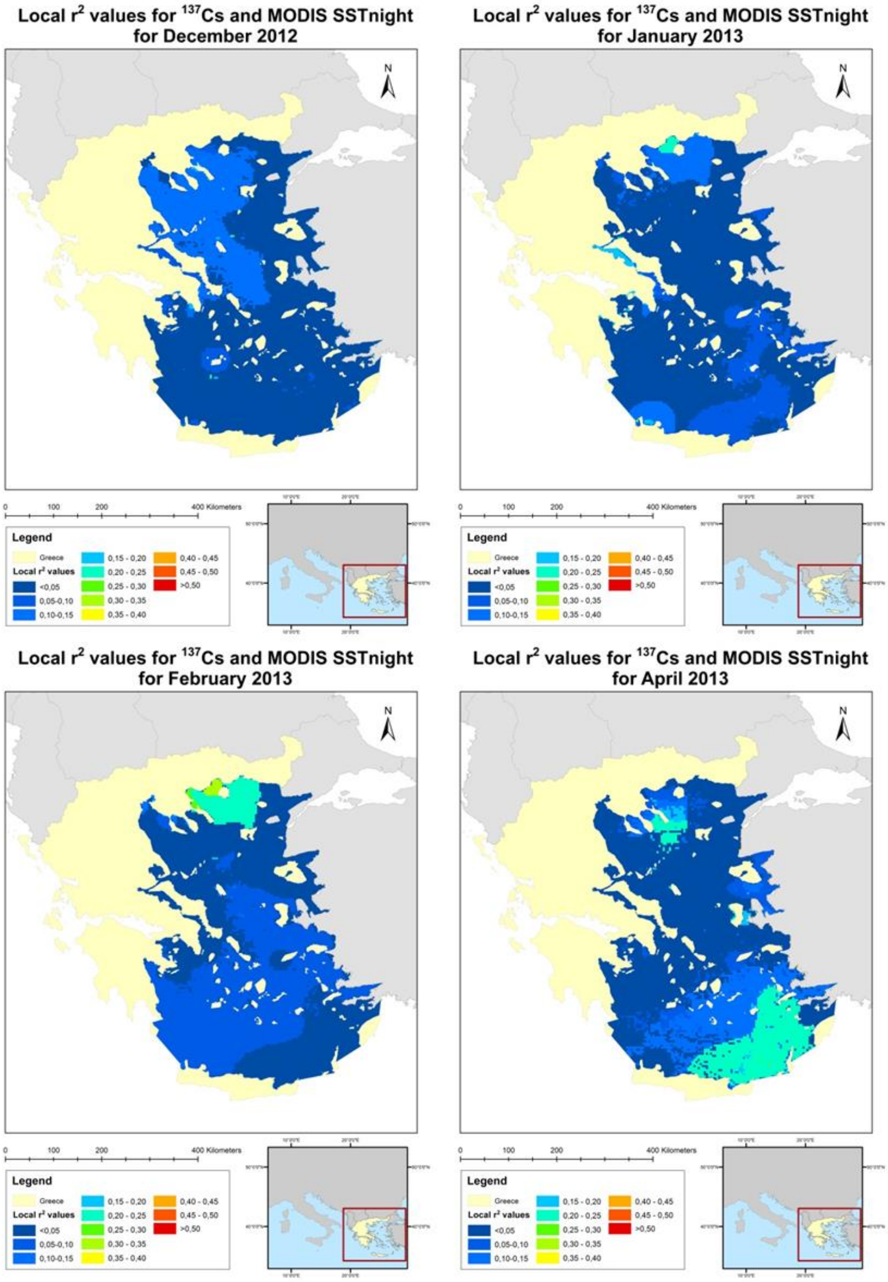

Local r2 values for 137Cs and MODIS SSTnight for December 2012
Local r2 values for 137Cs and MODIS SSTnight for January 2013
Local r2 values for 137Cs and MODIS SSTnight for February 2013
Local r2 values for 137Cs and MODIS SSTnight for April 2013
N
0 100 200 400 Kilometers
Legend
Greece
Local r2 values
<0,05
0,05-0,10
0,10-0,15
0,15 - 0,20
0,20 - 0,25
0,25 - 0,30
0,30 - 0,35
0,35 - 0,40
0,40 - 0,45
0,45 - 0,50
>0,50

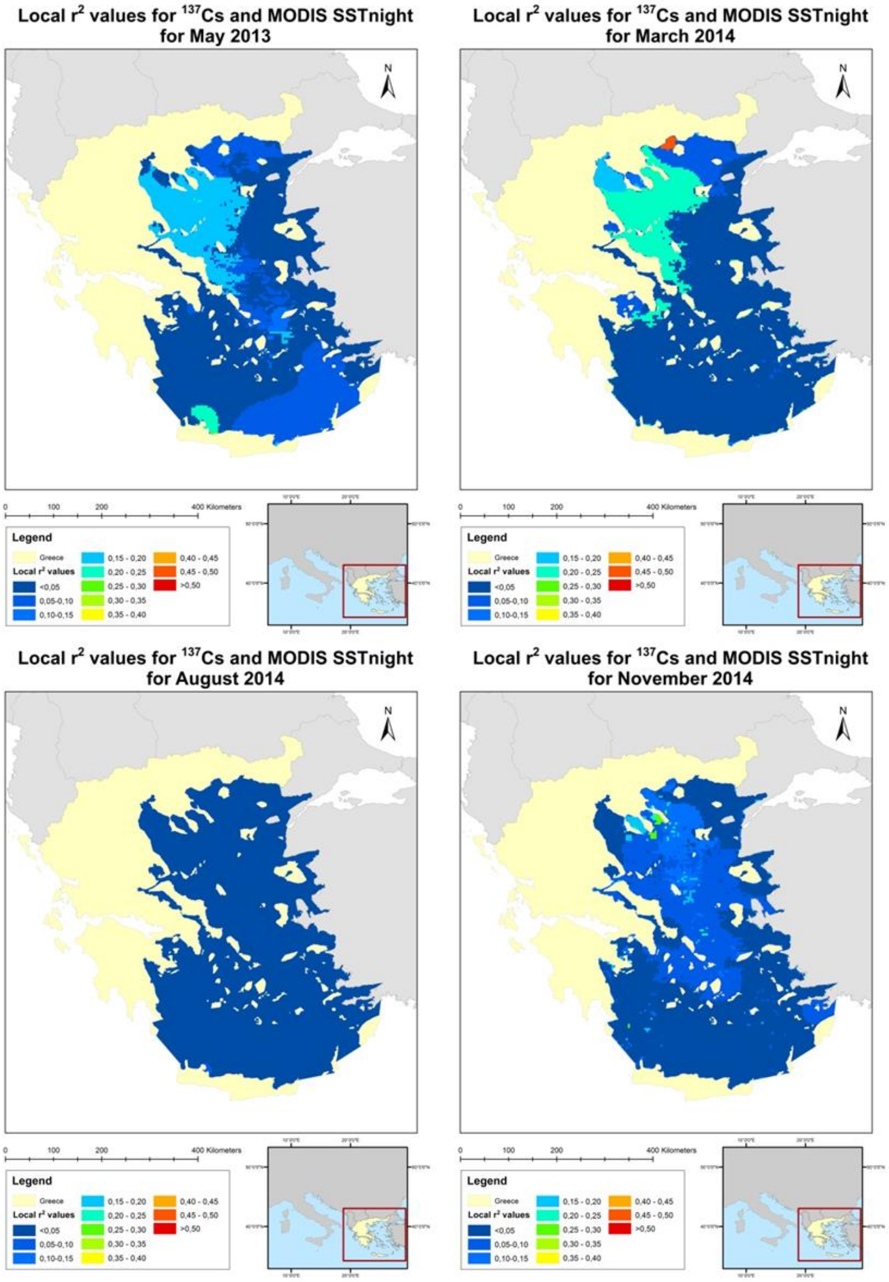

Local r2 values for 137Cs and MODIS SSTnight for May 2013
Local r2 values for 137Cs and MODIS SSTnight for March 2014
Local r2 values for 137Cs and MODIS SSTnight for August 2014
Local r2 values for 137Cs and MODIS SSTnight for November 2014
N
0 100 200 400 Kilometers
Legend
Greece
Local r2 values
<0,05
0,05-0,10
0,10-0,15
0,15 - 0,20
0,20 - 0,25
0,25 - 0,30
0,30 - 0,35
0,35 - 0,40
0,40 - 0,45
0,45 - 0,50
>0,50

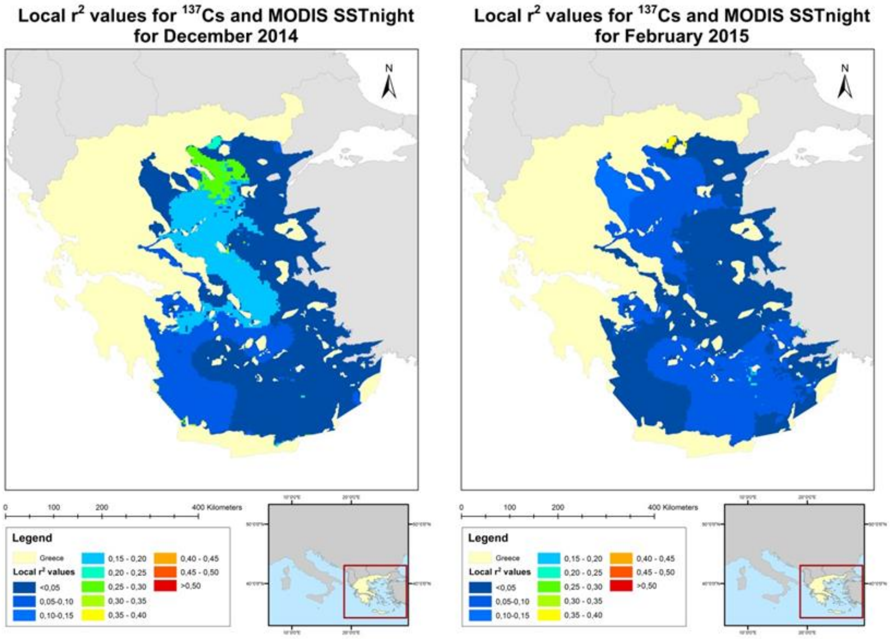

Figure 92. Local r^2 values for ^{137}Cs activity concentrations and MODIS SSTnight for the time period March 2012 to February 2015.

In this segment the GWR results concerning the local r^2 and the relation of ^{137}Cs activity concentrations and MODIS SSTnight are presented (Figure 92). Overall the maps present quite similar r^2 values with most of them being below 0.3, which indicates that the linear model using SSTnight does not sufficiently explain the ^{137}Cs activity concentrations. However there are some exceptions that have r^2 values over 0.3 that are mainly located in the North Aegean and some small parts in Crete, with the maximum r^2 value of 0.47 present in the month of March 2014.

8.2.1.1.2. SST4NIGHT

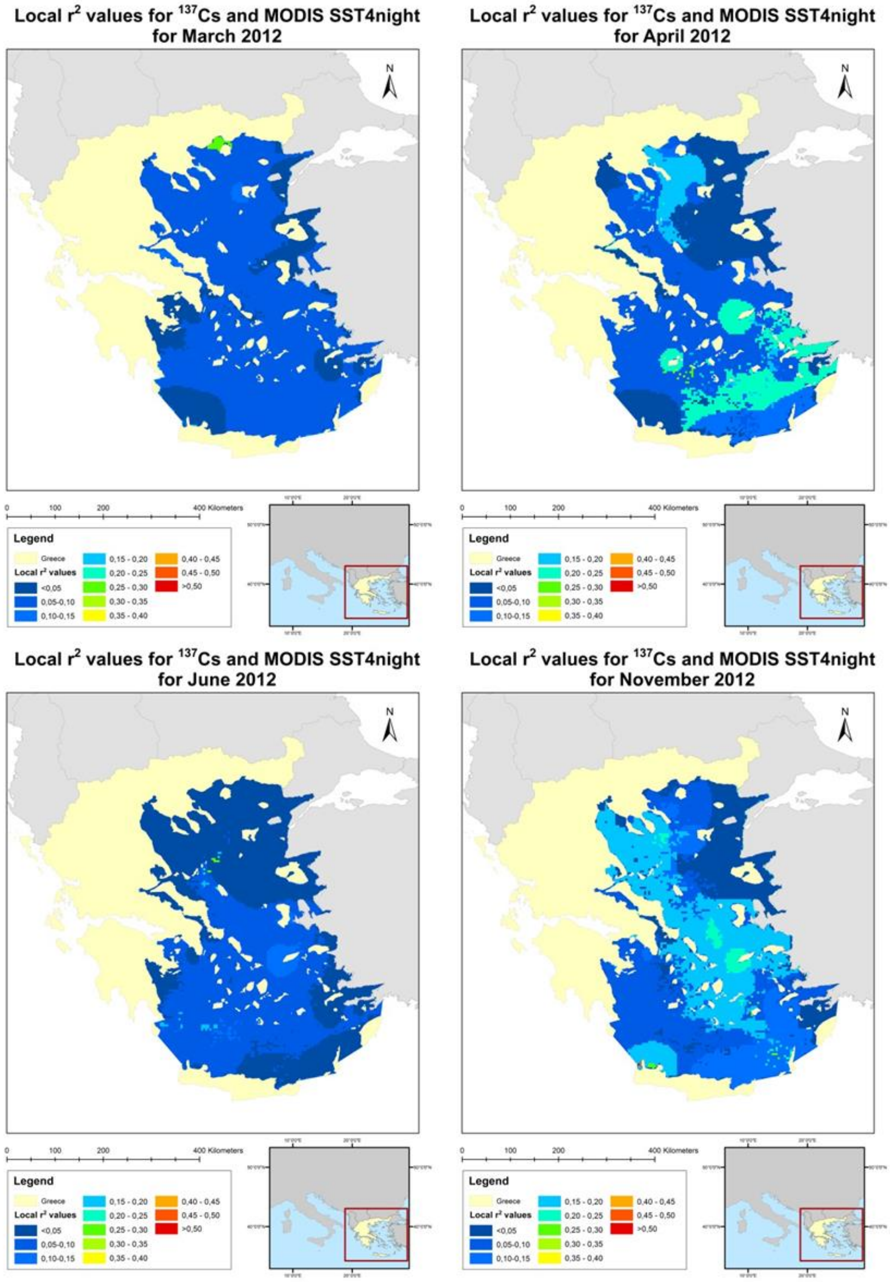

Local r^2 values for ^{137}Cs and MODIS SST4night for December 2012

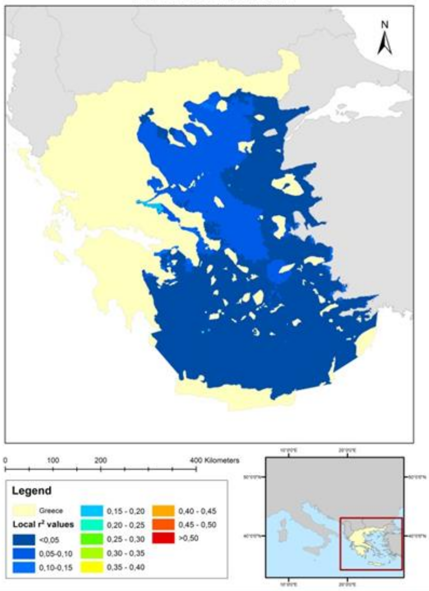

Local r^2 values for ^{137}Cs and MODIS SST4night for January 2013

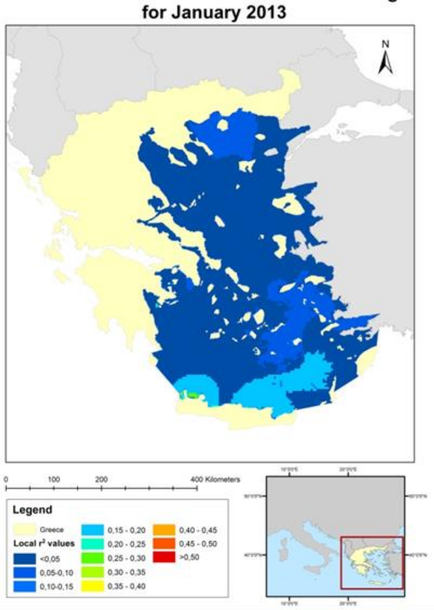

Local r^2 values for ^{137}Cs and MODIS SST4night for February 2013

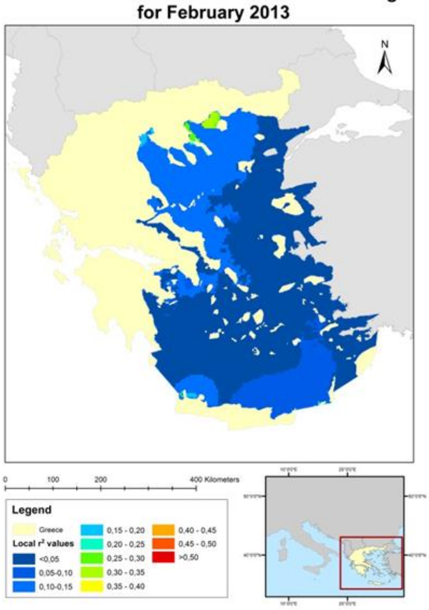

Local r^2 values for ^{137}Cs and MODIS SST4night for April 2013

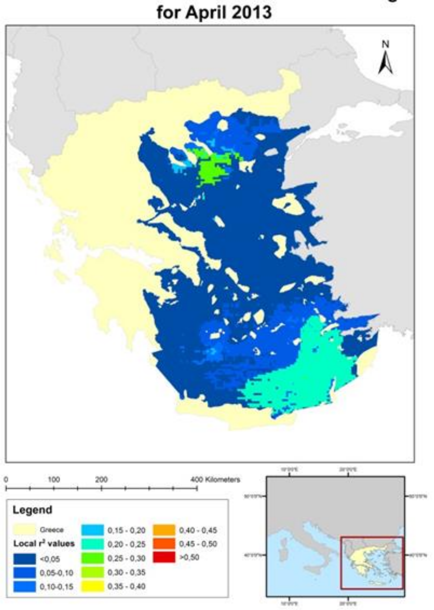

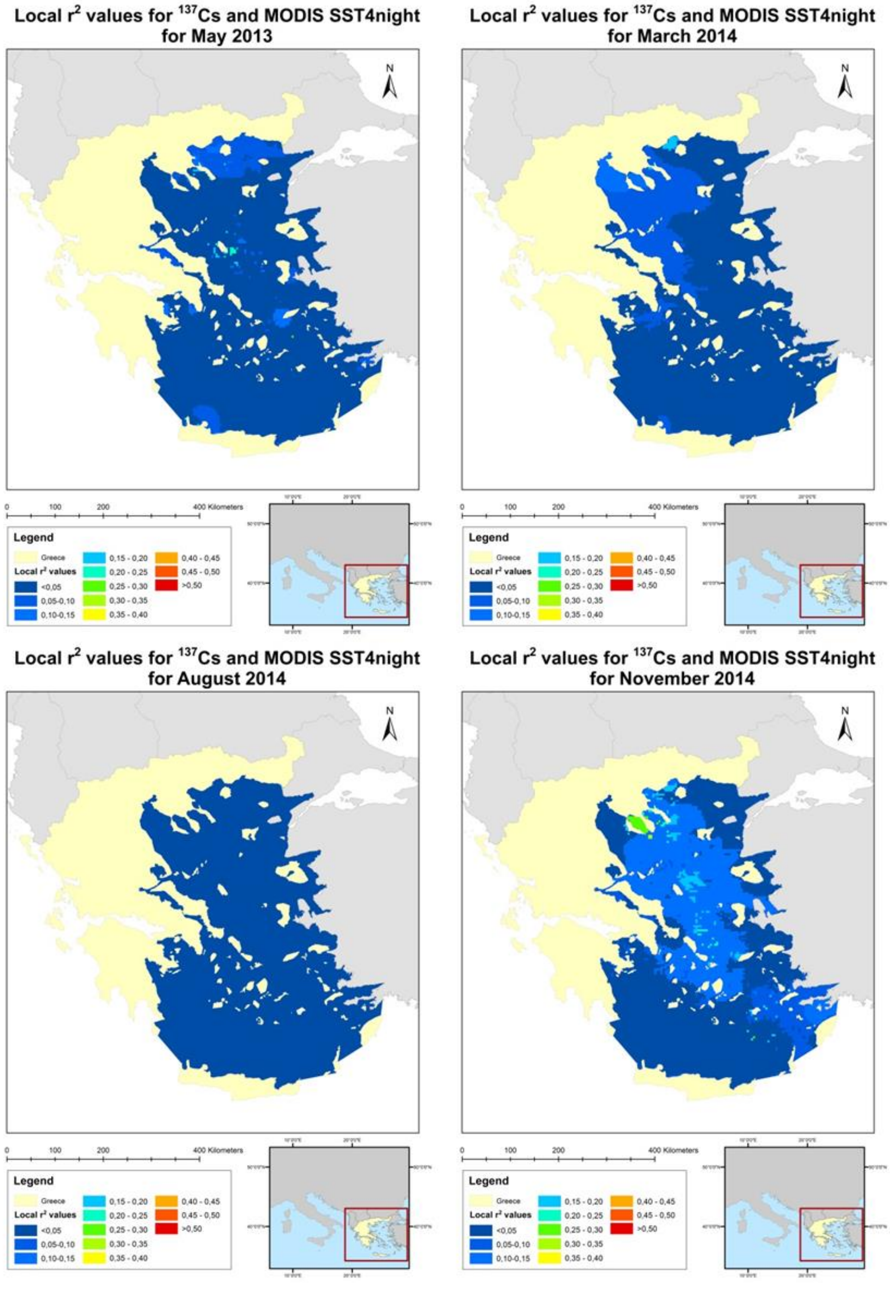

Local r² values for ¹³⁷Cs and MODIS SST4night for May 2013
Local r² values for ¹³⁷Cs and MODIS SST4night for March 2014
Local r² values for ¹³⁷Cs and MODIS SST4night for August 2014
Local r² values for ¹³⁷Cs and MODIS SST4night for November 2014
N
0 100 200 400 Kilometers
Legend
Greece
Local r² values
<0,05
0,05-0,10
0,10-0,15
0,15 - 0,20
0,20 - 0,25
0,25 - 0,30
0,30 - 0,35
0,35 - 0,40
0,40 - 0,45
0,45 - 0,50
>0,50

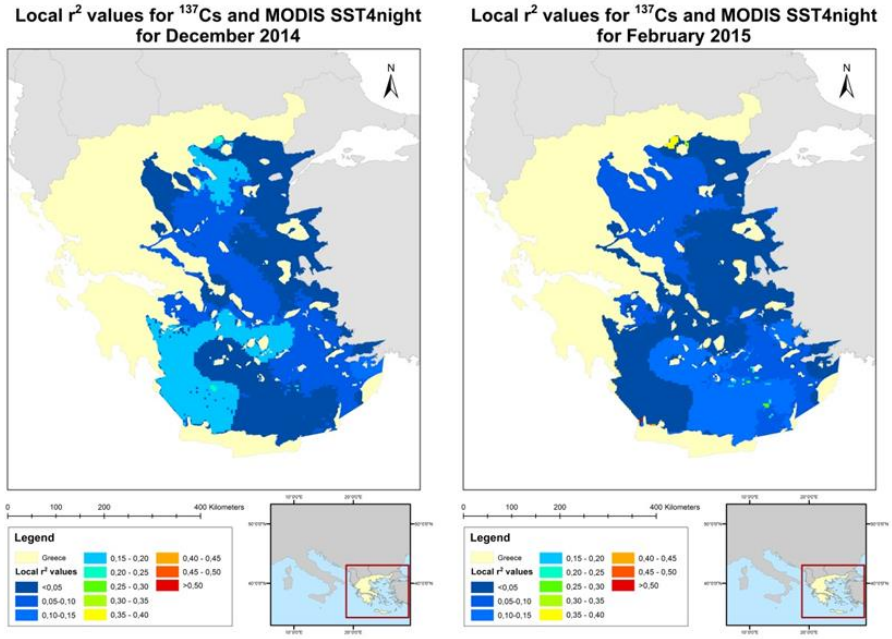

Figure 93. Local r^2 values for ^{137}Cs activity concentrations and MODIS SST4night for the time period March 2012 to February 2015.

The GWR local r^2 results displaying the relation between ^{137}Cs activity concentrations and MODIS SST4night are presented in this part (Figure 93). In the same manner like with MODIS SSTnight, relations are similar in each month with an average r^2 value below 0.3. Nevertheless there are months that their presented r^2 values are above 0.3; those values are present mainly in the coastal part of the North Aegean and in the coastal part of Northwestern Crete. The months that present the highest r^2 values are the month of November 2012 that presents a maximum r^2 value of 0.59 and the month of February 2015 that presents a maximum r^2 value of 0.63 (Mavrokefalou et al., 2016). Both of these values are located in the Northwestern part of Crete Island.

8.2.1.1.3. SSTMORNING

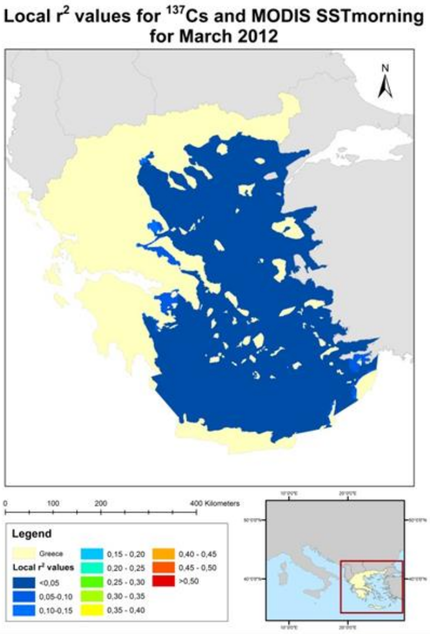

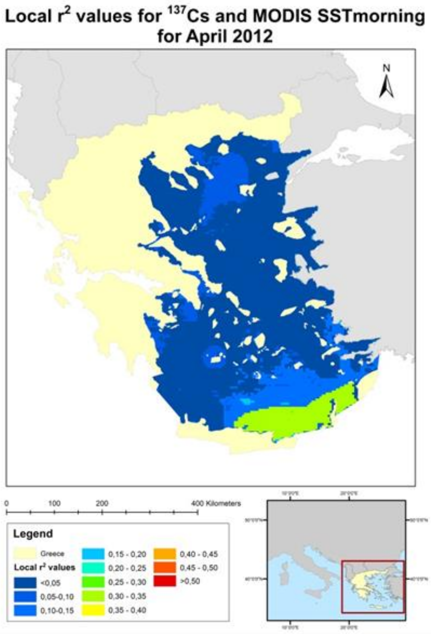

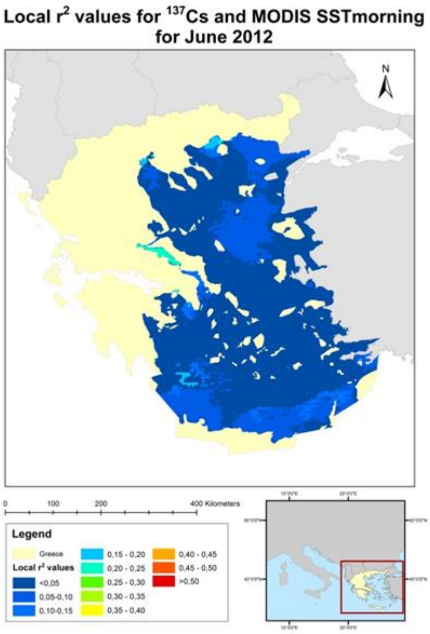

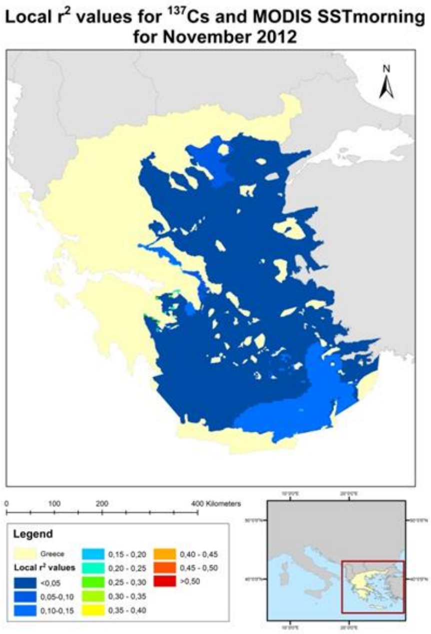

Local r² values for ^{137}Cs and MODIS SSTmorning for December 2012

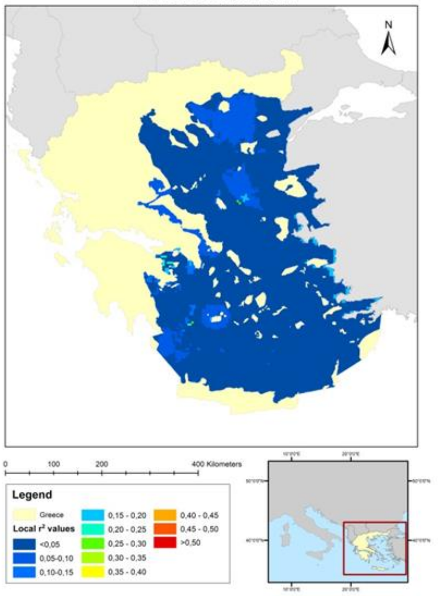

Local r² values for ^{137}Cs and MODIS SSTmorning for January 2013

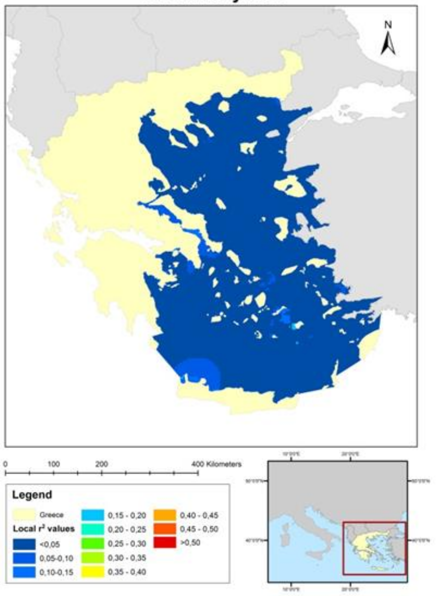

Local r² values for ^{137}Cs and MODIS SSTmorning for February 2013

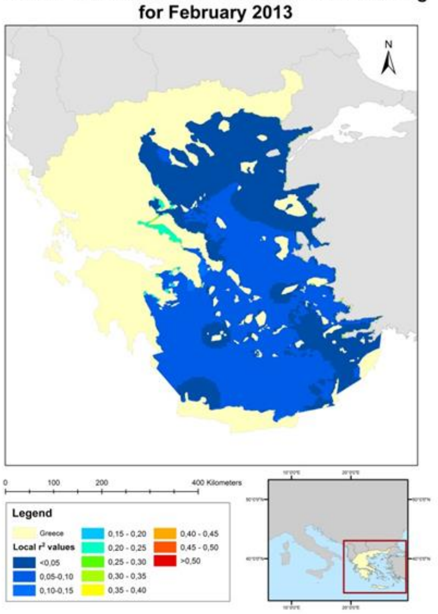

Local r² values for ^{137}Cs and MODIS SSTmorning for April 2013

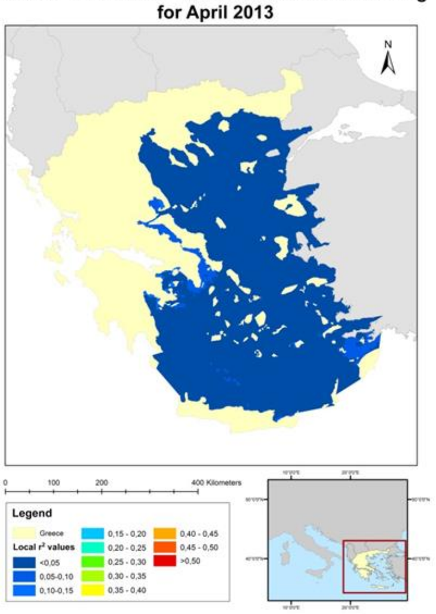

Local r^2 values for ^{137}Cs and MODIS SSTmorning for May 2013

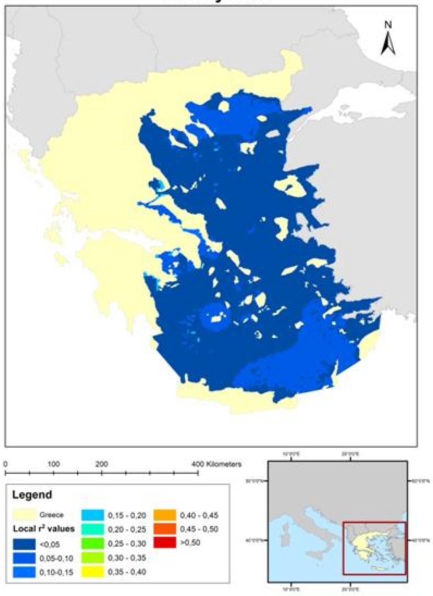

Local r^2 values for ^{137}Cs and MODIS SSTmorning for March 2014

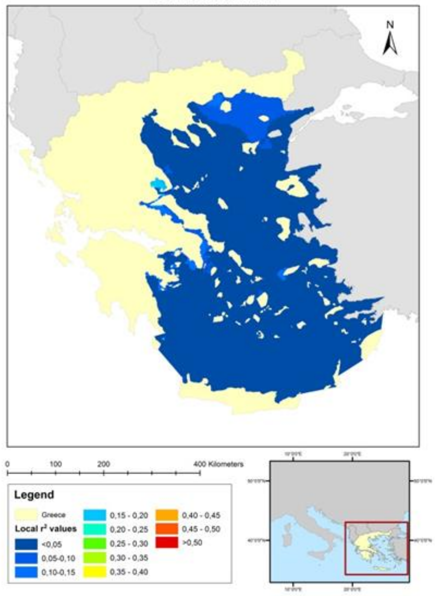

Local r^2 values for ^{137}Cs and MODIS SSTmorning for August 2014

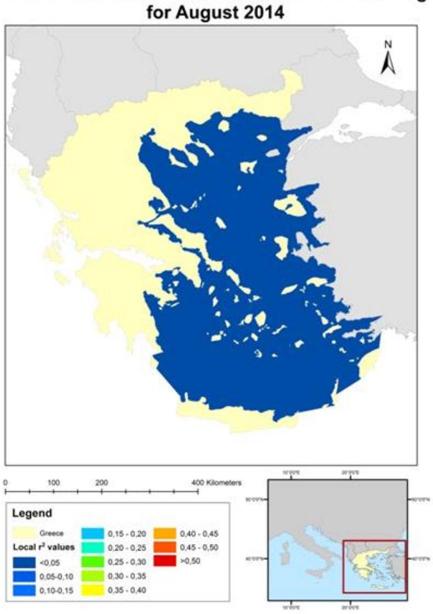

Local r^2 values for ^{137}Cs and MODIS SSTmorning for November 2014

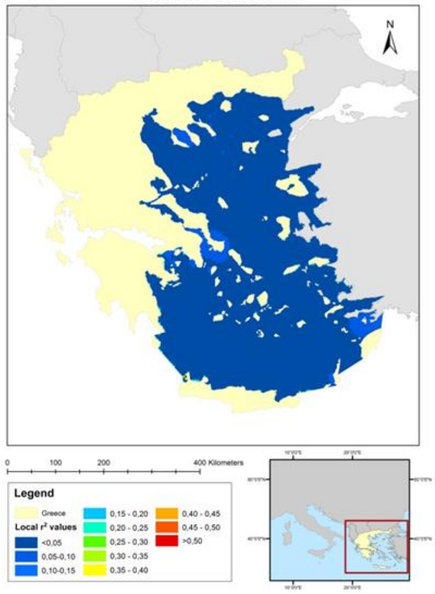

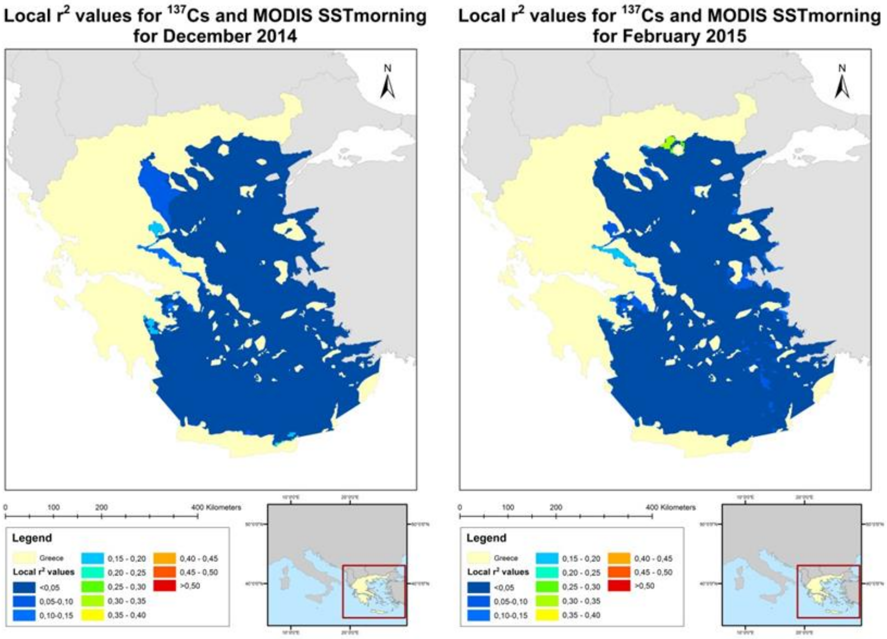

Figure 94. Local r^2 values for ^{137}Cs activity concentrations and MODIS SSTmorning for the time period March 2012 to February 2015.

In this part the GWR local r^2 results for ^{137}Cs activity concentrations and MODIS SSTmorning are shown (Figure 94). By observing the results it seems that the relations are similar in each month. Unlike the MODIS SSTnight and SST4night, when using MODIS SSTmorning, the models are not sufficiently describing the ^{137}Cs activity concentrations in the Aegean Sea, presenting r^2 values below 0.3. Like the models using the other MODIS SST parameters there is no significant r^2 value difference between months. The month presenting the highest r^2 value is the month of November 2014 with a maximum r^2 of 0.45.

8.2.1.1.4. CHLOR_A

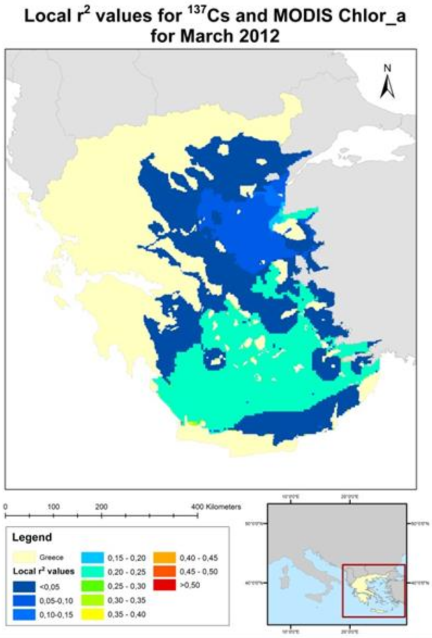

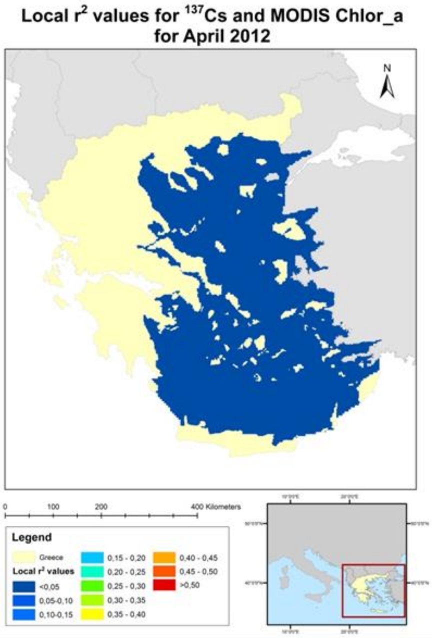

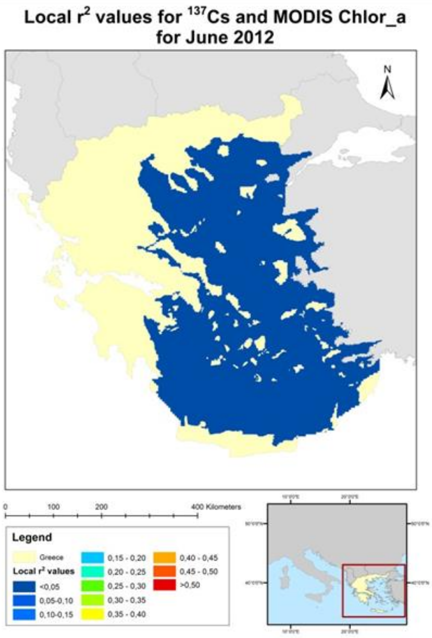

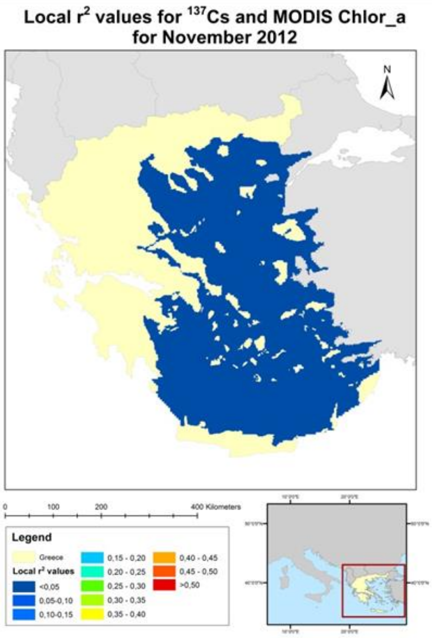

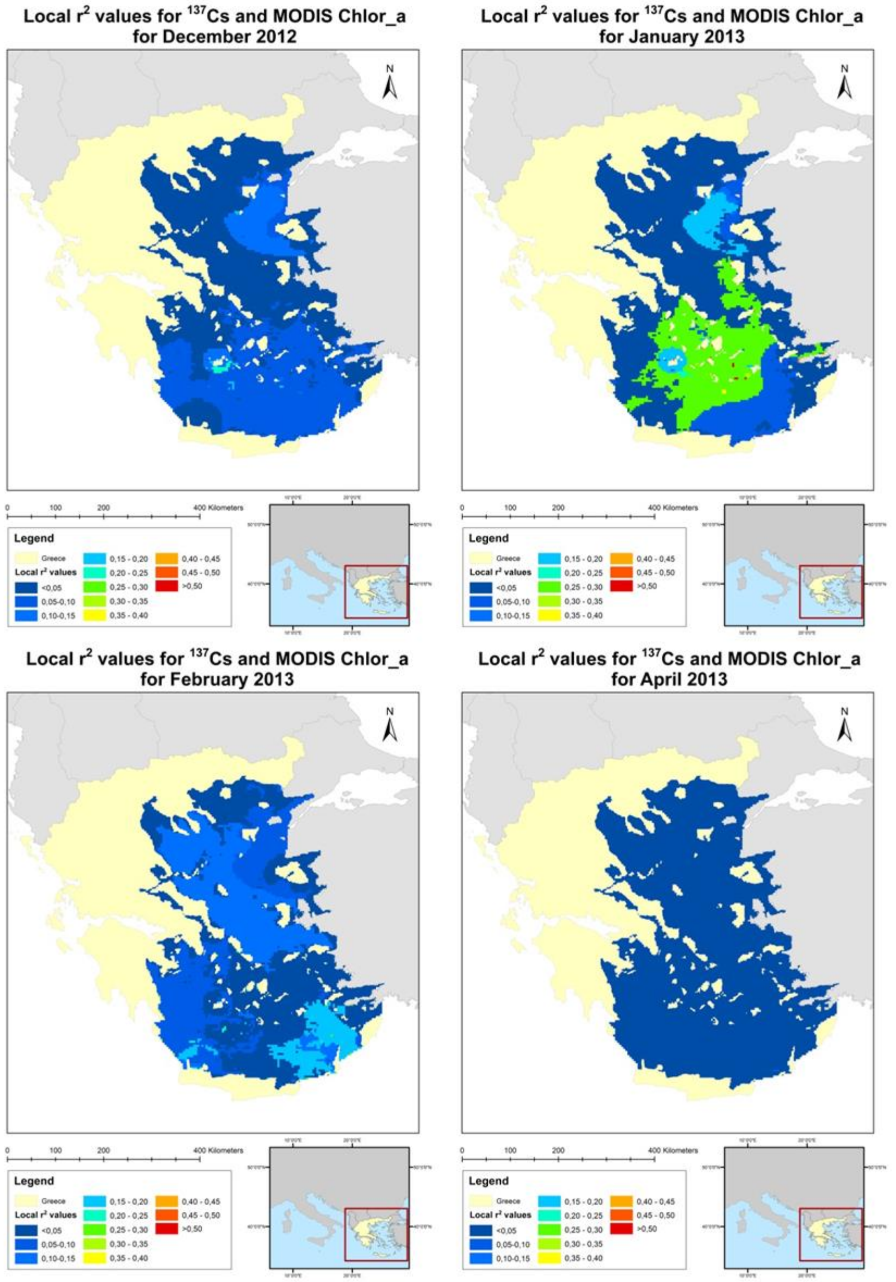
Local r^2 values for ^{137}Cs and MODIS Chlor_a for December 2012
N
0 100 200 400 Kilometers
Legend
Greece
Local r^2 values
<0,05
0,05-0,10
0,10-0,15
0,15 - 0,20
0,20 - 0,25
0,25 - 0,30
0,30 - 0,35
0,35 - 0,40
0,40 - 0,45
0,45 - 0,50
>0,50
Local r^2 values for ^{137}Cs and MODIS Chlor_a for January 2013
N
0 100 200 400 Kilometers
Legend
Greece
Local r^2 values
<0,05
0,05-0,10
0,10-0,15
0,15 - 0,20
0,20 - 0,25
0,25 - 0,30
0,30 - 0,35
0,35 - 0,40
0,40 - 0,45
0,45 - 0,50
>0,50
Local r^2 values for ^{137}Cs and MODIS Chlor_a for February 2013
N
0 100 200 400 Kilometers
Legend
Greece
Local r^2 values
<0,05
0,05-0,10
0,10-0,15
0,15 - 0,20
0,20 - 0,25
0,25 - 0,30
0,30 - 0,35
0,35 - 0,40
0,40 - 0,45
0,45 - 0,50
>0,50
Local r^2 values for ^{137}Cs and MODIS Chlor_a for April 2013
N
0 100 200 400 Kilometers
Legend
Greece
Local r^2 values
<0,05
0,05-0,10
0,10-0,15
0,15 - 0,20
0,20 - 0,25
0,25 - 0,30
0,30 - 0,35
0,35 - 0,40
0,40 - 0,45
0,45 - 0,50
>0,50

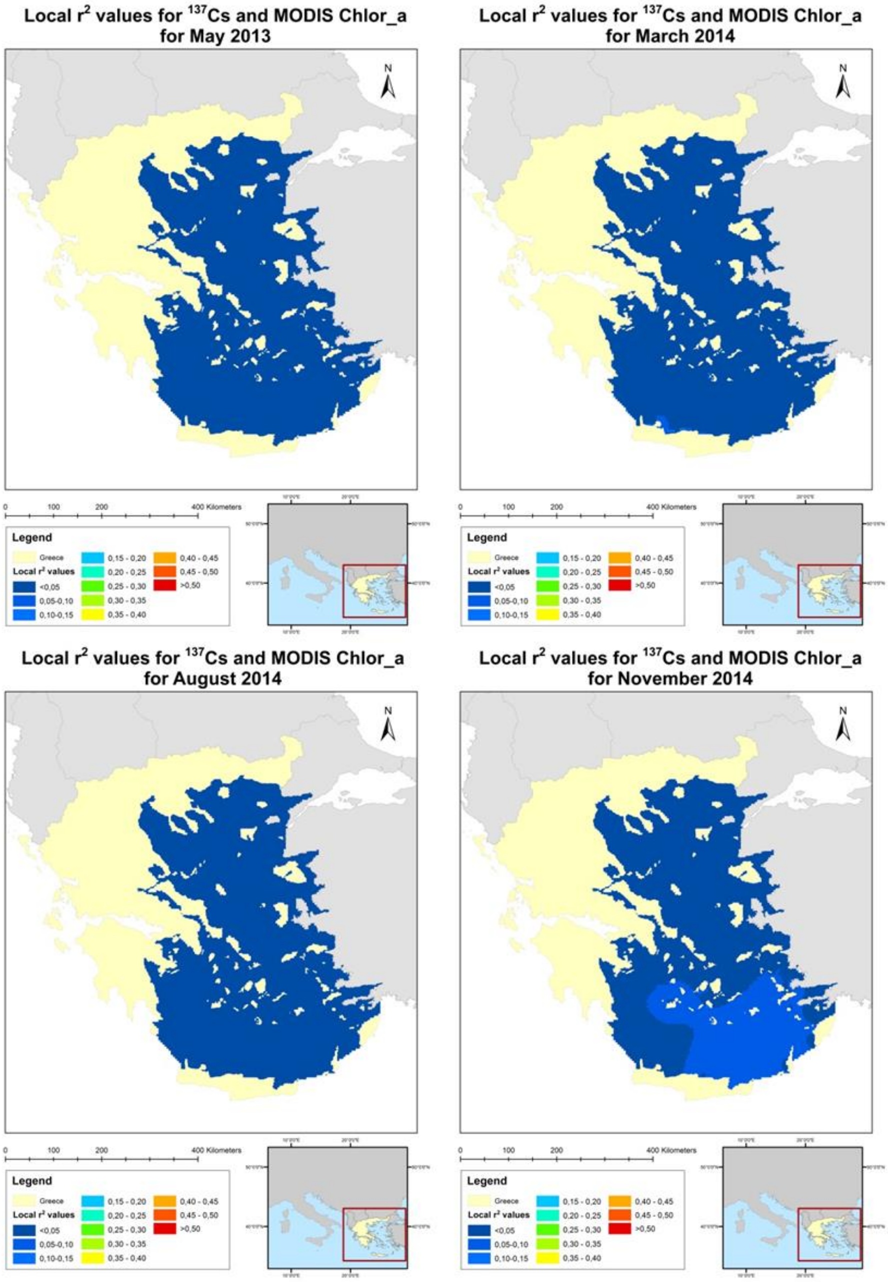

Local r² values for 137Cs and MODIS Chlor_a for May 2013
Local r² values for 137Cs and MODIS Chlor_a for March 2014
Local r² values for 137Cs and MODIS Chlor_a for August 2014
Local r² values for 137Cs and MODIS Chlor_a for November 2014
0 100 200 400 Kilometers
Legend
Greece
Local r² values
<0,05
0,05-0,10
0,10-0,15
0,15 - 0,20
0,20 - 0,25
0,25 - 0,30
0,30 - 0,35
0,35 - 0,40
0,40 - 0,45
0,45 - 0,50
>0,50

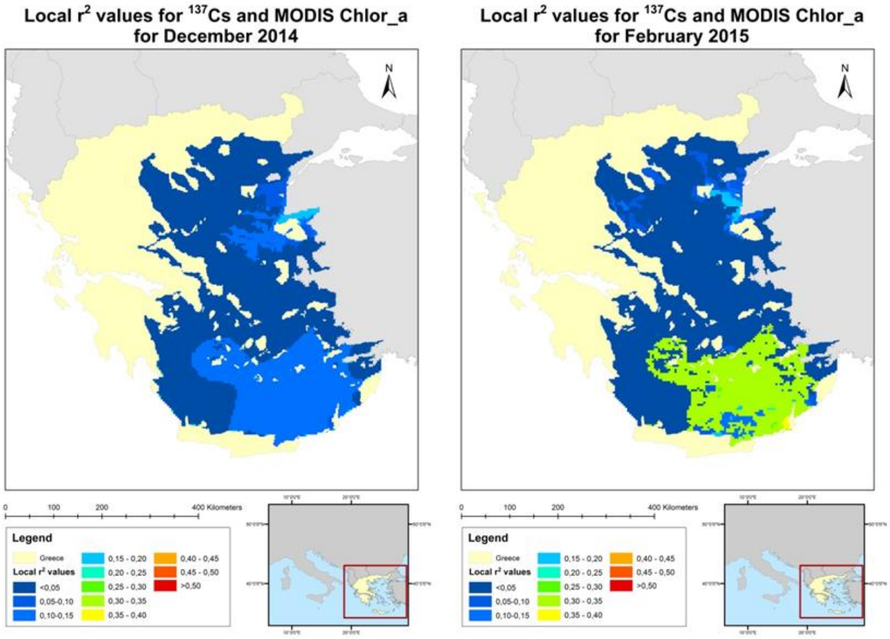

Figure 95. Local r^2 values for ^{137}Cs activity concentrations and MODIS Chlor_a for the time period March 2012 to February 2015.

The GWR local r^2 results that exhibit the spatial linear relations of ^{137}Cs activity concentration and MODIS Chlor_a are shown in this segment (Figure 95). By observing the results, it is obvious that the linear model that uses Chlor_a does not sufficiently describe the values of ^{137}Cs activity concentrations in the Aegean Sea. Higher values are present in Central and South Aegean Sea; with the maximum r^2 value of 0.59 present at the month of January 2013.

8.2.1.1.5. PIC

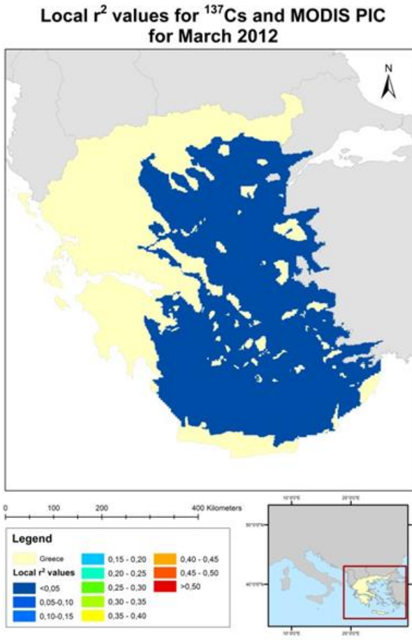

Local r² values for 137Cs and MODIS PIC for March 2012
N
0 100 200 400 Kilometers
Legend
Greece
Local r² values
<0,05
0,05-0,10
0,10-0,15
0,15 - 0,20
0,20 - 0,25
0,25 - 0,30
0,30 - 0,35
0,35 - 0,40
0,40 - 0,45
0,45 - 0,50
>0,50

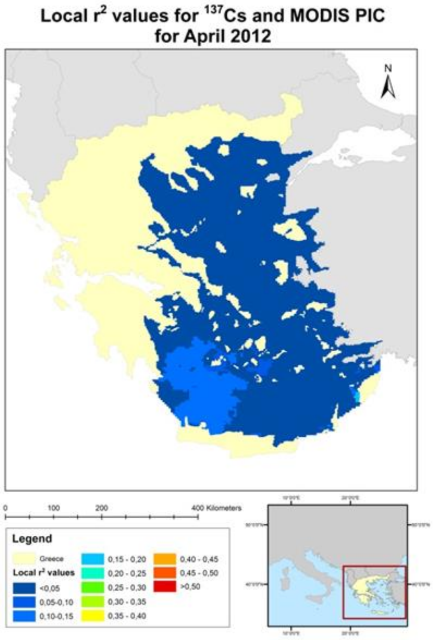

Local r² values for 137Cs and MODIS PIC for April 2012
N
0 100 200 400 Kilometers
Legend
Greece
Local r² values
<0,05
0,05-0,10
0,10-0,15
0,15 - 0,20
0,20 - 0,25
0,25 - 0,30
0,30 - 0,35
0,35 - 0,40
0,40 - 0,45
0,45 - 0,50
>0,50

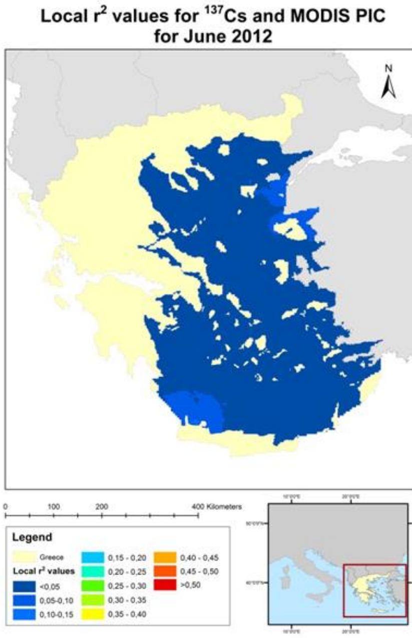

Local r² values for 137Cs and MODIS PIC for June 2012
N
0 100 200 400 Kilometers
Legend
Greece
Local r² values
<0,05
0,05-0,10
0,10-0,15
0,15 - 0,20
0,20 - 0,25
0,25 - 0,30
0,30 - 0,35
0,35 - 0,40
0,40 - 0,45
0,45 - 0,50
>0,50

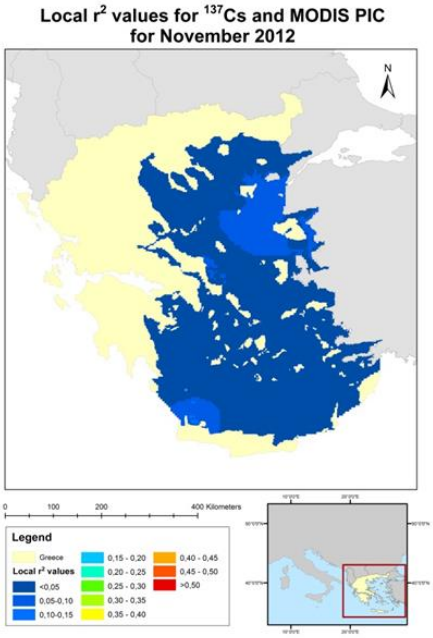

Local r² values for 137Cs and MODIS PIC for November 2012
N
0 100 200 400 Kilometers
Legend
Greece
Local r² values
<0,05
0,05-0,10
0,10-0,15
0,15 - 0,20
0,20 - 0,25
0,25 - 0,30
0,30 - 0,35
0,35 - 0,40
0,40 - 0,45
0,45 - 0,50
>0,50

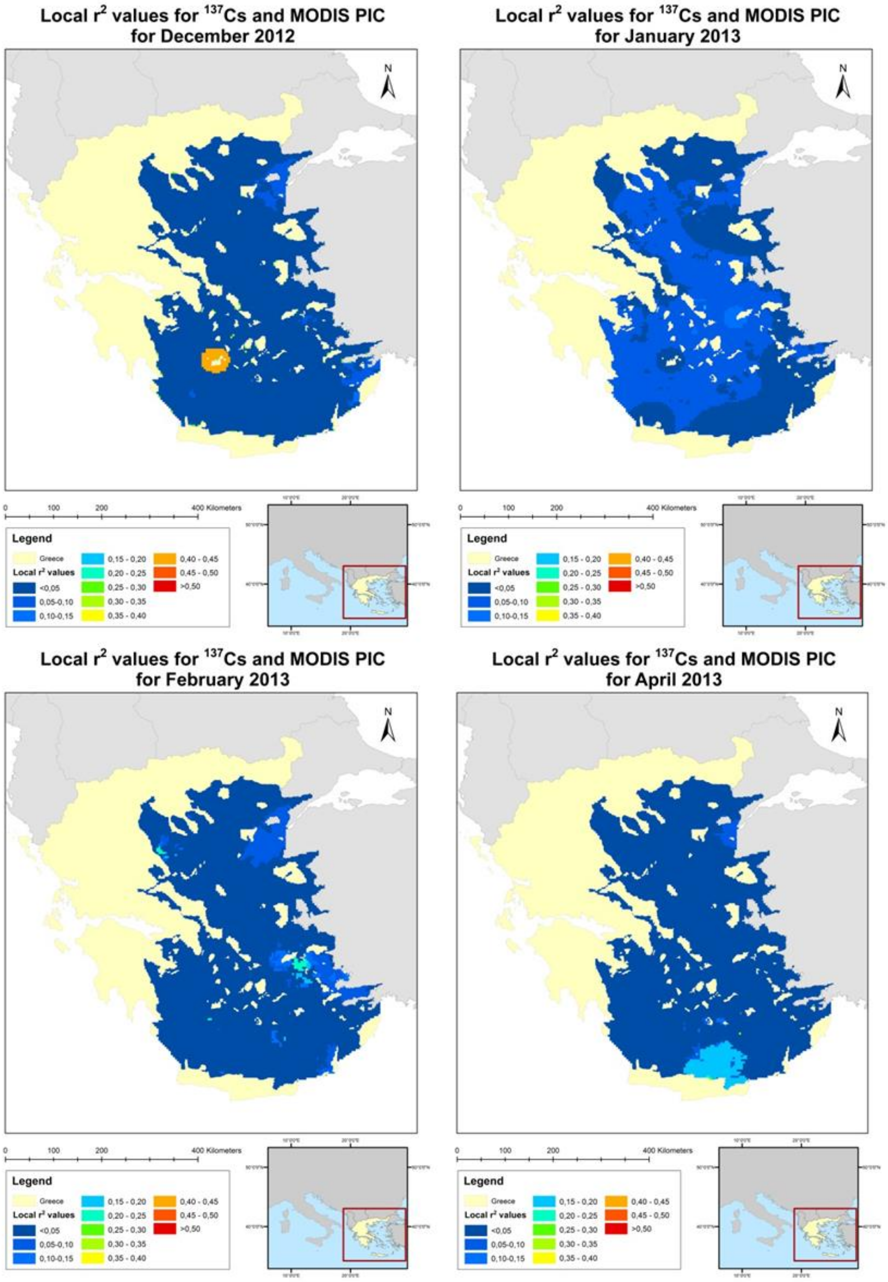
Local r² values for ¹³⁷Cs and MODIS PIC for December 2012
Local r² values for ¹³⁷Cs and MODIS PIC for January 2013
Local r² values for ¹³⁷Cs and MODIS PIC for February 2013
Local r² values for ¹³⁷Cs and MODIS PIC for April 2013
N
0 100 200 400 Kilometers
Legend
Greece
Local r² values
<0,05
0,05-0,10
0,10-0,15
0,15 - 0,20
0,20 - 0,25
0,25 - 0,30
0,30 - 0,35
0,35 - 0,40
0,40 - 0,45
0,45 - 0,50
>0,50

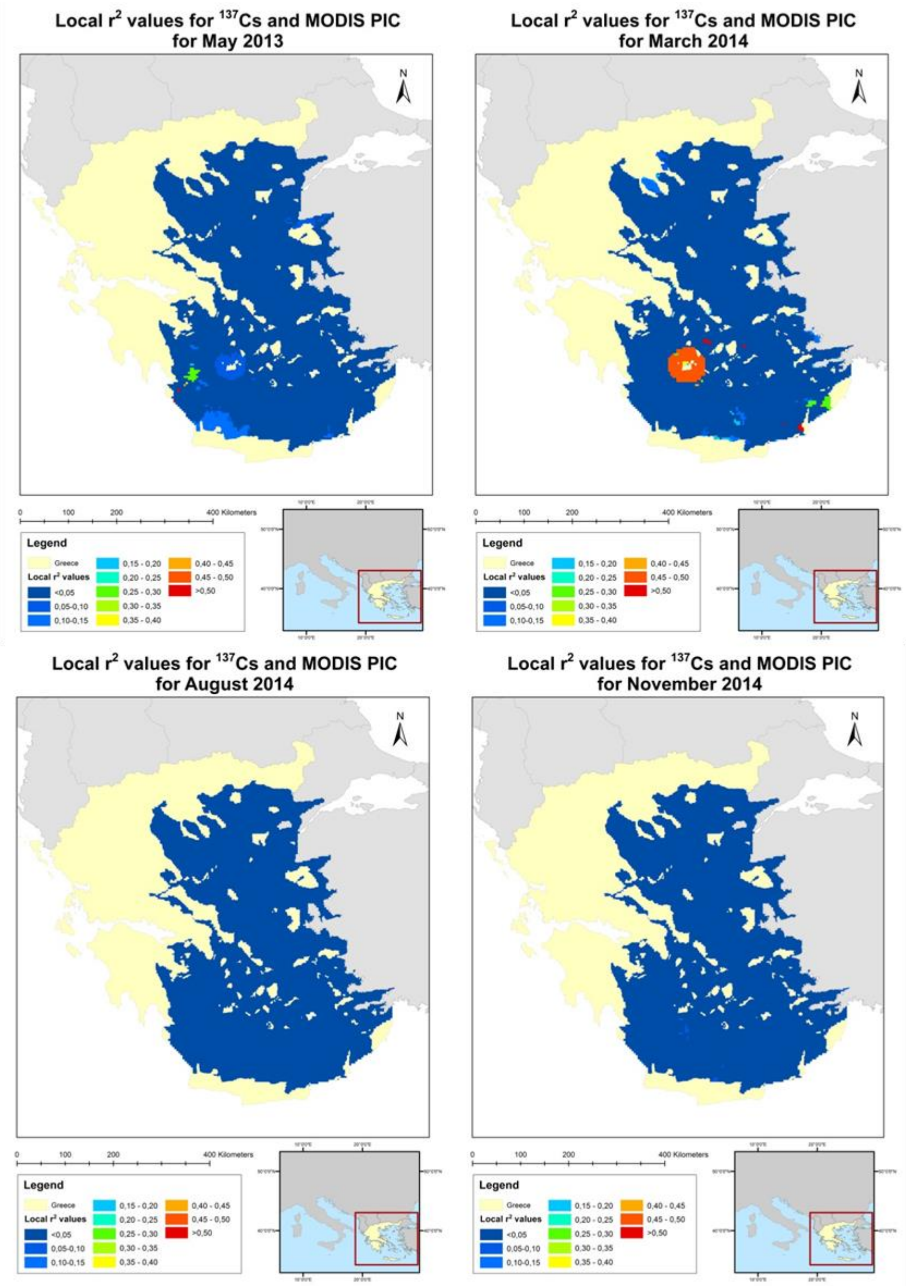
Local r² values for ¹³⁷Cs and MODIS PIC for May 2013
Local r² values for ¹³⁷Cs and MODIS PIC for March 2014
Local r² values for ¹³⁷Cs and MODIS PIC for August 2014
Local r² values for ¹³⁷Cs and MODIS PIC for November 2014
N
0 100 200 400 Kilometers
Legend
Greece
Local r² values
<0,05
0,05-0,10
0,10-0,15
0,15 - 0,20
0,20 - 0,25
0,25 - 0,30
0,30 - 0,35
0,35 - 0,40
0,40 - 0,45
0,45 - 0,50
>0,50

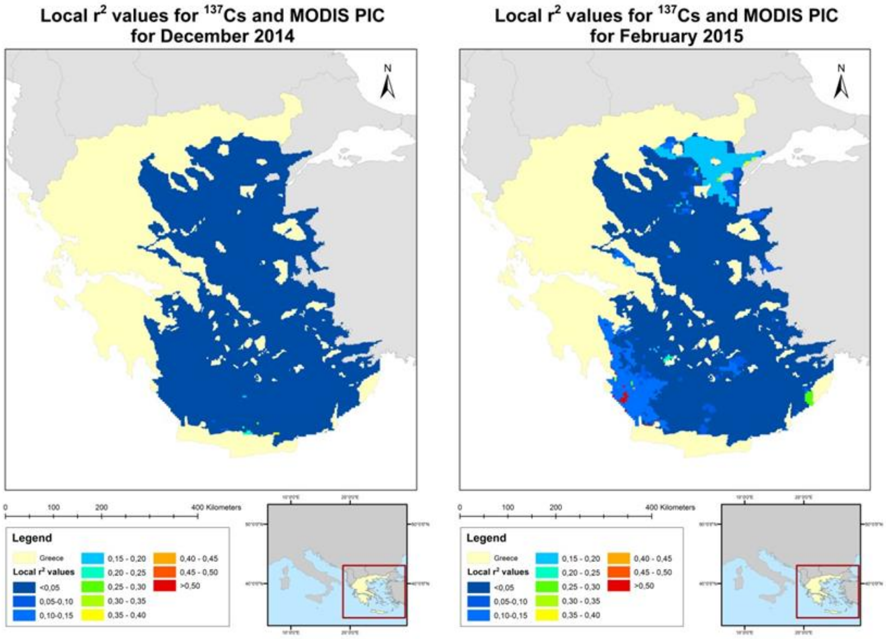

Figure 96. Local r^2 values for ^{137}Cs activity concentrations and MODIS PIC for the time period March 2012 to February 2015.

In this part the GWR local r^2 results that show the linear spatial relation between ^{137}Cs activity concentrations and MODIS PIC are being displayed (Figure 96). Results show that models using MODIS PIC present better results than models using other MODIS parameters. Results look promising with best r^2 values are present mainly in South Aegean Sea, for the months of May 2013, March 2014 and February 2015. The month of May 2013 presents a maximum r^2 value of 0.55; the month of March 2014 presents a maximum r^2 value of 0.88 and the month of February 2015 presents a maximum r^2 value of 0.81.

8.2.1.1.6. POC

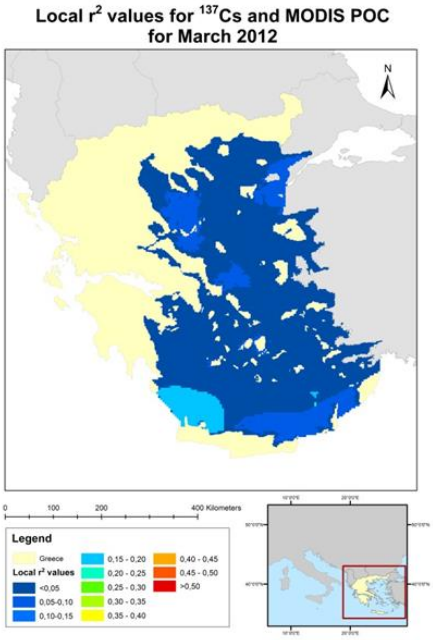
Local r^2 values for ^{137}Cs and MODIS POC
for March 2012
N
0 100 200 400 Kilometers
Legend
Greece
Local r^2 values
<0,05
0,05-0,10
0,10-0,15
0,15 - 0,20
0,20 - 0,25
0,25 - 0,30
0,30 - 0,35
0,35 - 0,40
0,40 - 0,45
0,45 - 0,50
>0,50

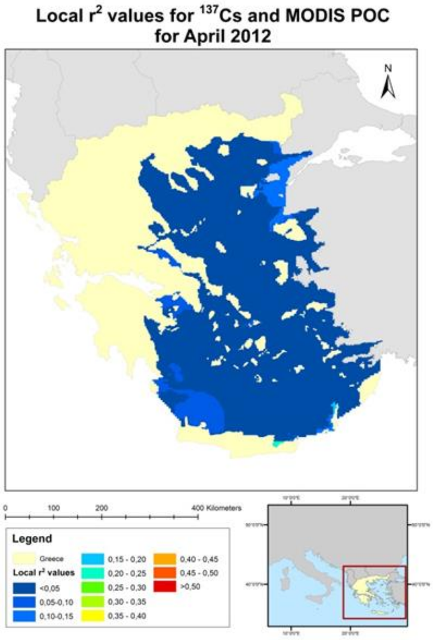
Local r^2 values for ^{137}Cs and MODIS POC
for April 2012
N
0 100 200 400 Kilometers
Legend
Greece
Local r^2 values
<0,05
0,05-0,10
0,10-0,15
0,15 - 0,20
0,20 - 0,25
0,25 - 0,30
0,30 - 0,35
0,35 - 0,40
0,40 - 0,45
0,45 - 0,50
>0,50

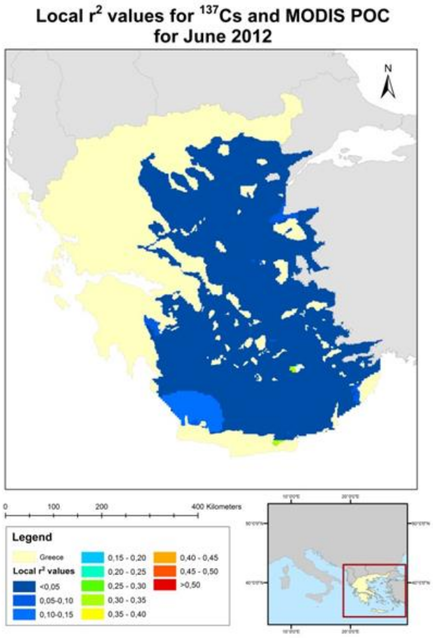
Local r^2 values for ^{137}Cs and MODIS POC
for June 2012
N
0 100 200 400 Kilometers
Legend
Greece
Local r^2 values
<0,05
0,05-0,10
0,10-0,15
0,15 - 0,20
0,20 - 0,25
0,25 - 0,30
0,30 - 0,35
0,35 - 0,40
0,40 - 0,45
0,45 - 0,50
>0,50

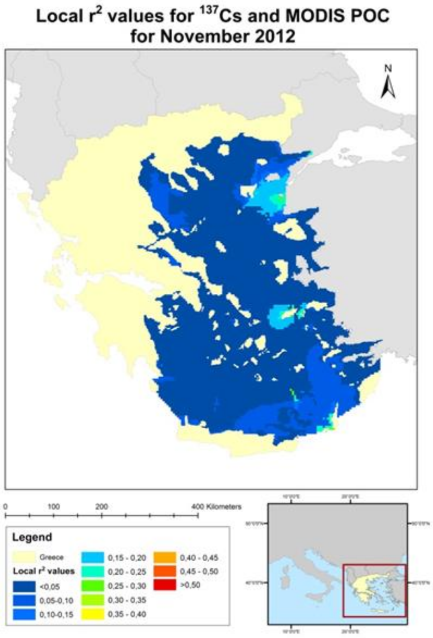
Local r^2 values for ^{137}Cs and MODIS POC
for November 2012
N
0 100 200 400 Kilometers
Legend
Greece
Local r^2 values
<0,05
0,05-0,10
0,10-0,15
0,15 - 0,20
0,20 - 0,25
0,25 - 0,30
0,30 - 0,35
0,35 - 0,40
0,40 - 0,45
0,45 - 0,50
>0,50

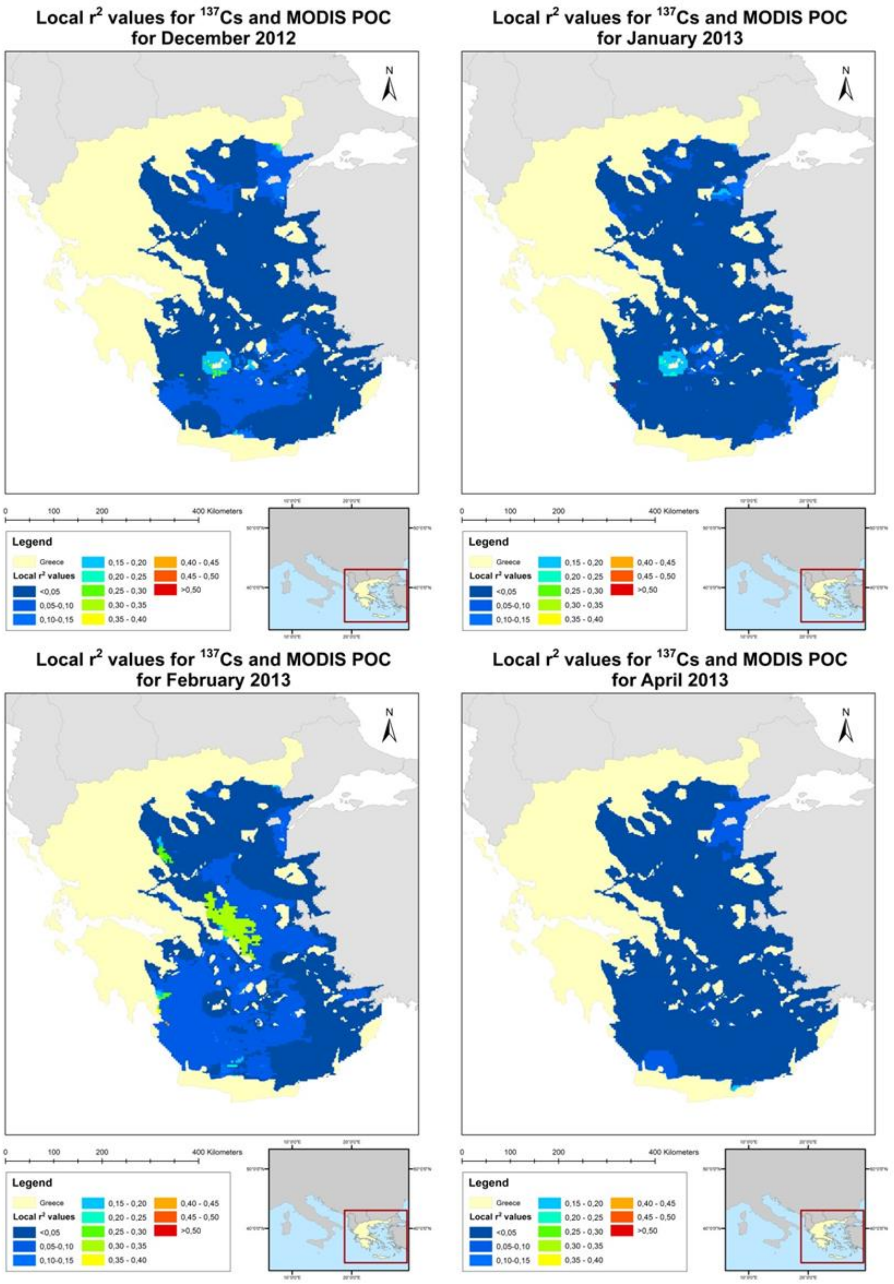
Local r^2 values for ^{137}Cs and MODIS POC for December 2012
N
0 100 200 400 Kilometers
Legend
Greece
Local r^2 values
<0,05
0,05-0,10
0,10-0,15
0,15 - 0,20
0,20 - 0,25
0,25 - 0,30
0,30 - 0,35
0,35 - 0,40
0,40 - 0,45
0,45 - 0,50
>0,50
Local r^2 values for ^{137}Cs and MODIS POC for January 2013
N
0 100 200 400 Kilometers
Legend
Greece
Local r^2 values
<0,05
0,05-0,10
0,10-0,15
0,15 - 0,20
0,20 - 0,25
0,25 - 0,30
0,30 - 0,35
0,35 - 0,40
0,40 - 0,45
0,45 - 0,50
>0,50
Local r^2 values for ^{137}Cs and MODIS POC for February 2013
N
0 100 200 400 Kilometers
Legend
Greece
Local r^2 values
<0,05
0,05-0,10
0,10-0,15
0,15 - 0,20
0,20 - 0,25
0,25 - 0,30
0,30 - 0,35
0,35 - 0,40
0,40 - 0,45
0,45 - 0,50
>0,50
Local r^2 values for ^{137}Cs and MODIS POC for April 2013
N
0 100 200 400 Kilometers
Legend
Greece
Local r^2 values
<0,05
0,05-0,10
0,10-0,15
0,15 - 0,20
0,20 - 0,25
0,25 - 0,30
0,30 - 0,35
0,35 - 0,40
0,40 - 0,45
0,45 - 0,50
>0,50

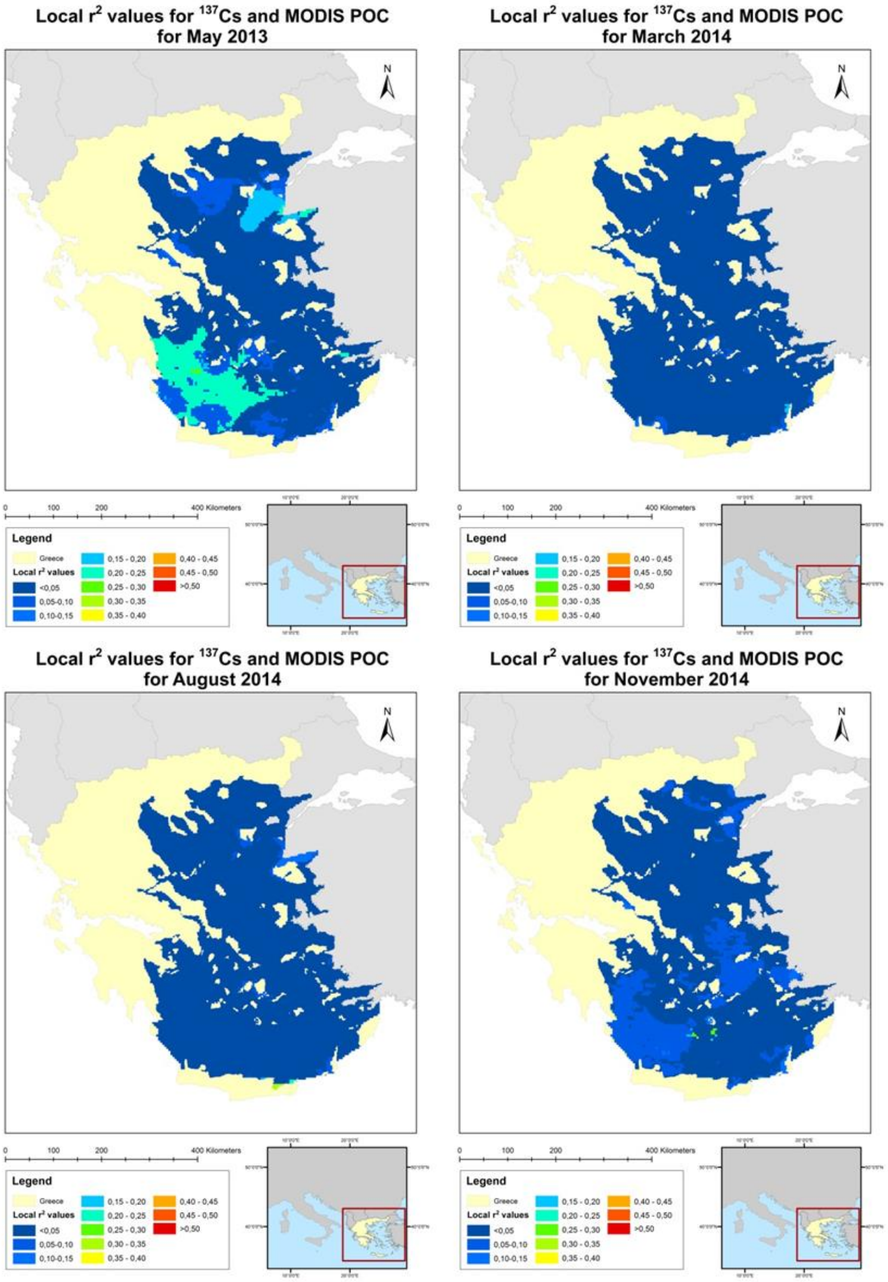
Local r^2 values for ^{137}Cs and MODIS POC for May 2013
Local r^2 values for ^{137}Cs and MODIS POC for March 2014
Local r^2 values for ^{137}Cs and MODIS POC for August 2014
Local r^2 values for ^{137}Cs and MODIS POC for November 2014
N
0 100 200 400 Kilometers
Legend
Greece
Local r^2 values
<0,05
0,05-0,10
0,10-0,15
0,15 - 0,20
0,20 - 0,25
0,25 - 0,30
0,30 - 0,35
0,35 - 0,40
0,40 - 0,45
0,45 - 0,50
>0,50

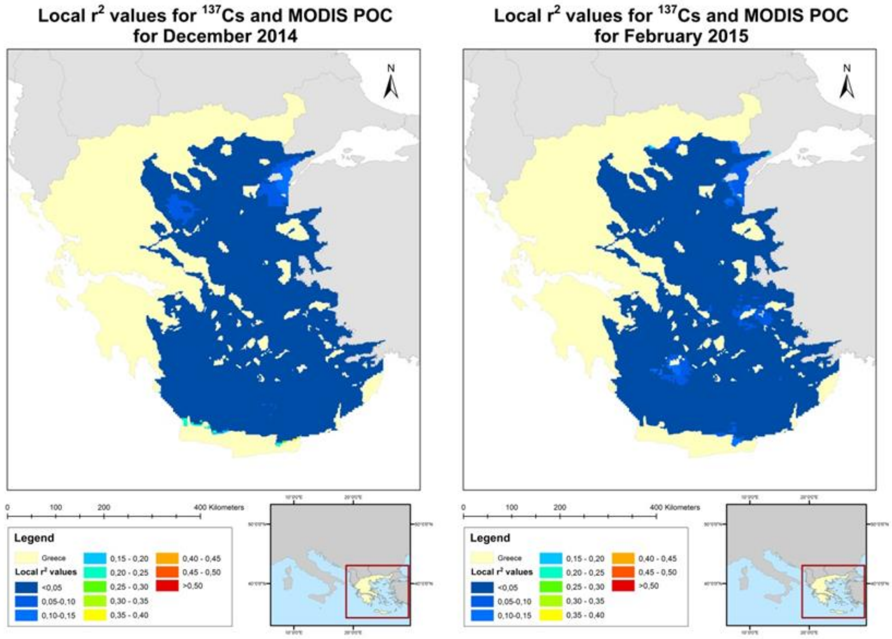

Figure 97. Local r^2 values for ^{137}Cs activity concentrations and MODIS POC for the time period March 2012 to February 2015.

The results of the GWR local r^2, which display the linear relations between ^{137}Cs activity concentrations and MODIS POC are shown in this part (Figure 97). Unlike the models using MODIS PIC, the models using MODIS POC do not sufficiently explain the ^{137}Cs activity concentrations in the Aegean Sea, with most r^2 values being below 0.35. The r^2 values do not change significantly between months, with most of them being similar. The maximum r^2 value of 0.67 is present at the month of January 2013.

8.2.1.1.7. iPAR

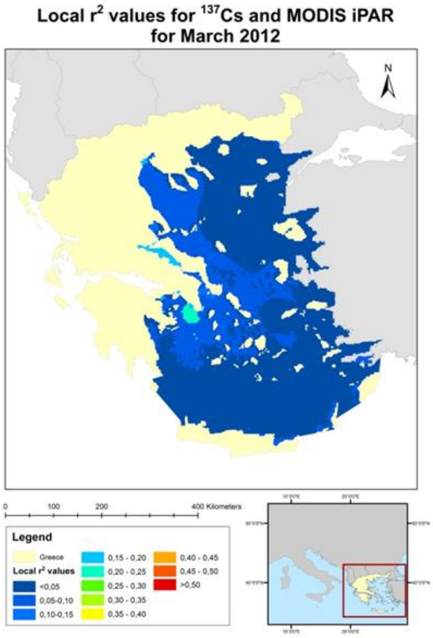
Local r^2 values for ^{137}Cs and MODIS iPAR
for March 2012
N
0 100 200 400 Kilometers
Legend
Greece
Local r^2 values
<0,05
0,05-0,10
0,10-0,15
0,15 - 0,20
0,20 - 0,25
0,25 - 0,30
0,30 - 0,35
0,35 - 0,40
0,40 - 0,45
0,45 - 0,50
>0,50

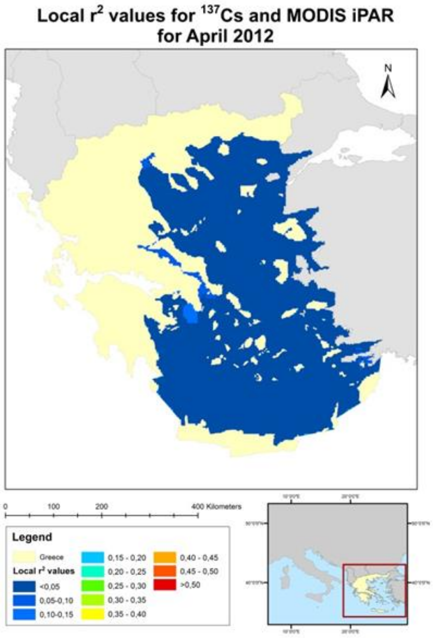
Local r^2 values for ^{137}Cs and MODIS iPAR
for April 2012
N
0 100 200 400 Kilometers
Legend
Greece
Local r^2 values
<0,05
0,05-0,10
0,10-0,15
0,15 - 0,20
0,20 - 0,25
0,25 - 0,30
0,30 - 0,35
0,35 - 0,40
0,40 - 0,45
0,45 - 0,50
>0,50

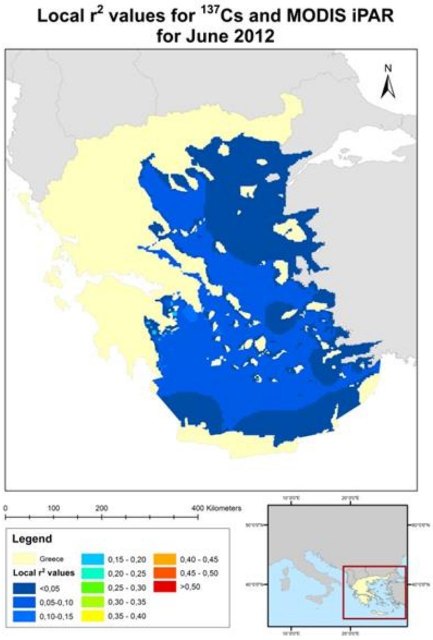
Local r^2 values for ^{137}Cs and MODIS iPAR
for June 2012
N
0 100 200 400 Kilometers
Legend
Greece
Local r^2 values
<0,05
0,05-0,10
0,10-0,15
0,15 - 0,20
0,20 - 0,25
0,25 - 0,30
0,30 - 0,35
0,35 - 0,40
0,40 - 0,45
0,45 - 0,50
>0,50

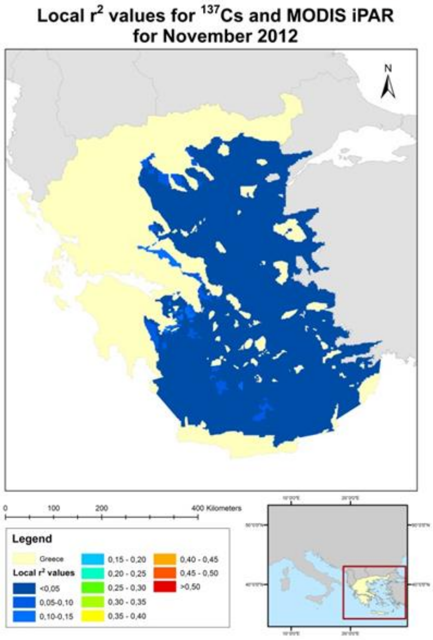
Local r^2 values for ^{137}Cs and MODIS iPAR
for November 2012
N
0 100 200 400 Kilometers
Legend
Greece
Local r^2 values
<0,05
0,05-0,10
0,10-0,15
0,15 - 0,20
0,20 - 0,25
0,25 - 0,30
0,30 - 0,35
0,35 - 0,40
0,40 - 0,45
0,45 - 0,50
>0,50

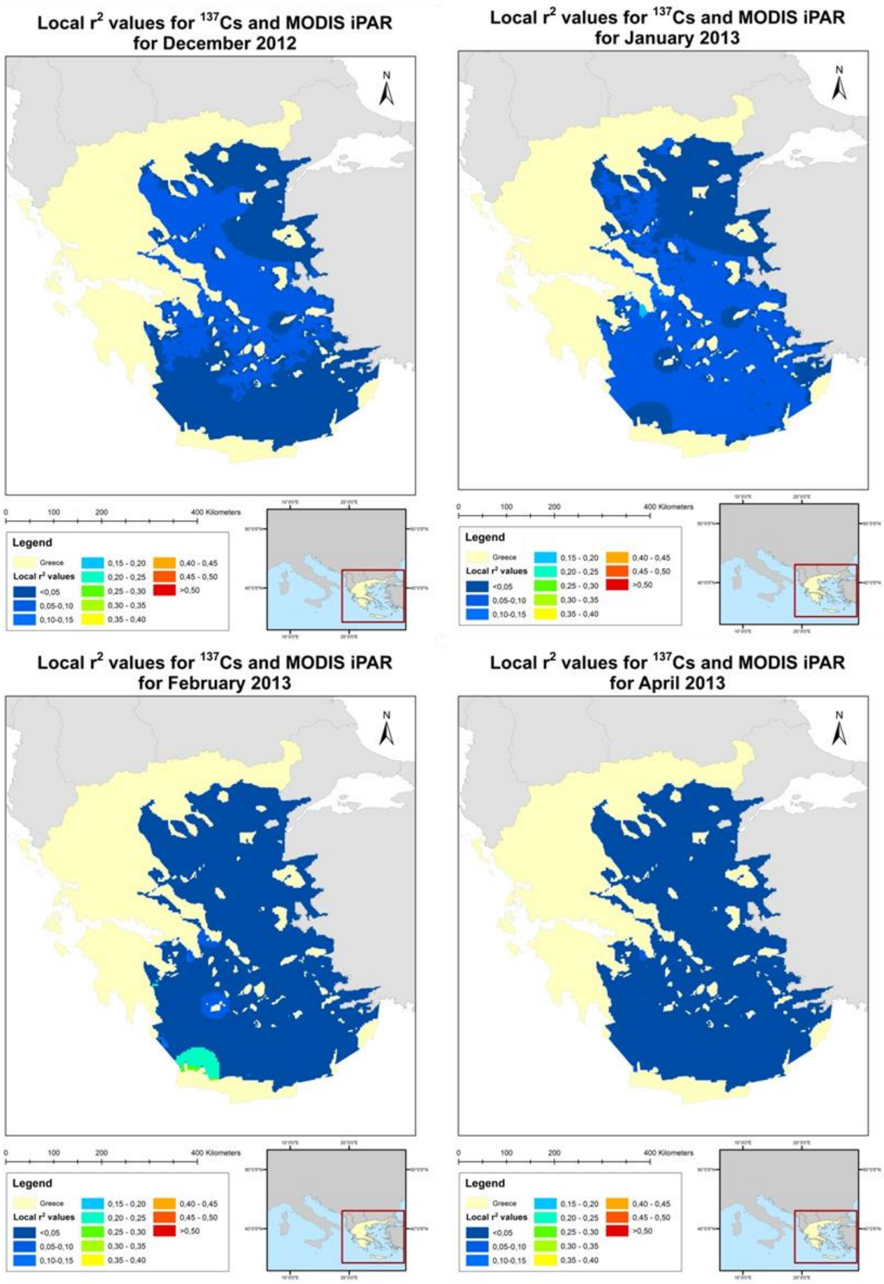

Local r2 values for 137Cs and MODIS iPAR for December 2012
Local r2 values for 137Cs and MODIS iPAR for January 2013
Local r2 values for 137Cs and MODIS iPAR for February 2013
Local r2 values for 137Cs and MODIS iPAR for April 2013
0 100 200 400 Kilometers
Legend
Greece
Local r2 values
<0,05
0,05-0,10
0,10-0,15
0,15 - 0,20
0,20 - 0,25
0,25 - 0,30
0,30 - 0,35
0,35 - 0,40
0,40 - 0,45
0,45 - 0,50
>0,50

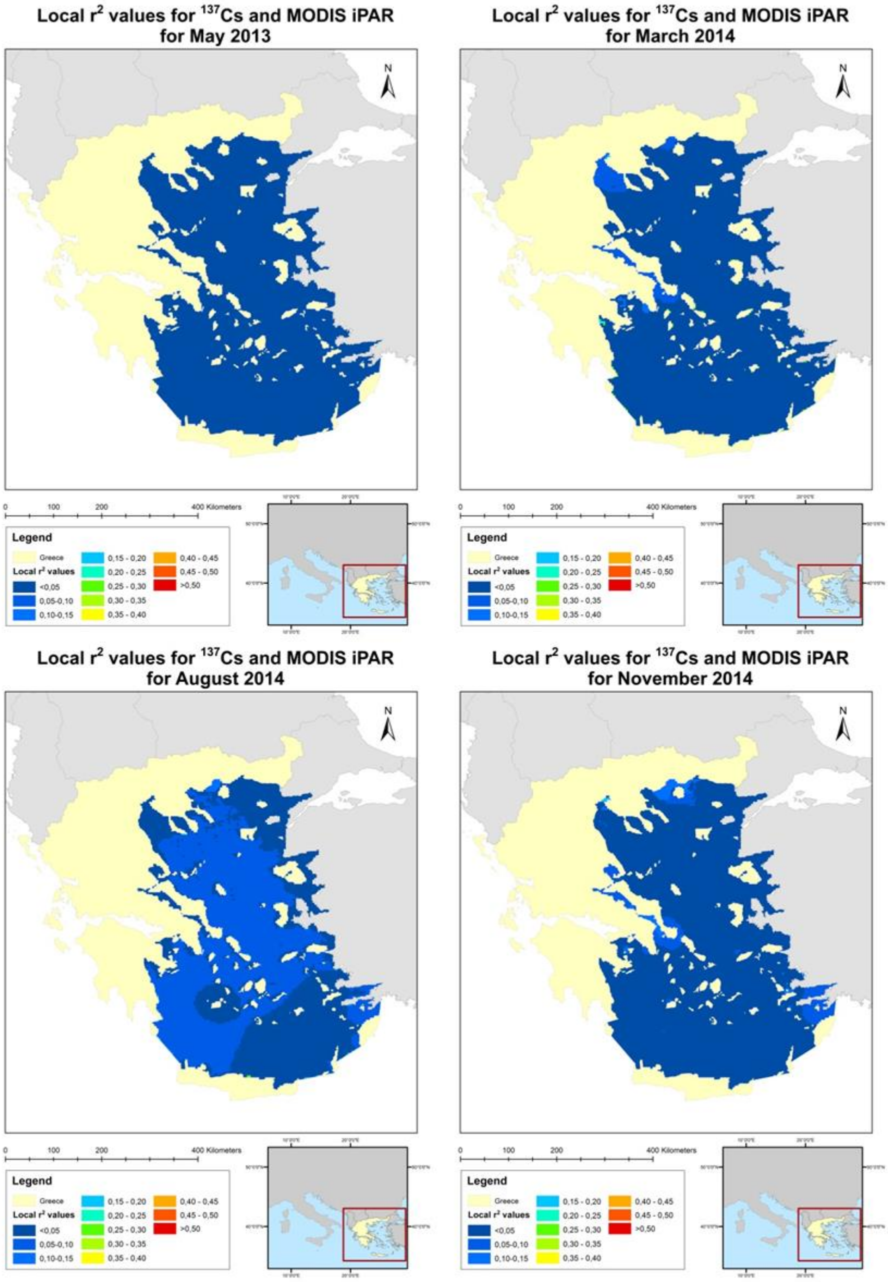
Local r2 values for 137Cs and MODIS iPAR
for May 2013
N
0
100
200
400 Kilometers
Legend
Greece
Local r2 values
<0,05
0,05-0,10
0,10-0,15
0,15 - 0,20
0,20 - 0,25
0,25 - 0,30
0,30 - 0,35
0,35 - 0,40
0,40 - 0,45
0,45 - 0,50
>0,50
Local r2 values for 137Cs and MODIS iPAR
for March 2014
N
0
100
200
400 Kilometers
Legend
Greece
Local r2 values
<0,05
0,05-0,10
0,10-0,15
0,15 - 0,20
0,20 - 0,25
0,25 - 0,30
0,30 - 0,35
0,35 - 0,40
0,40 - 0,45
0,45 - 0,50
>0,50
Local r2 values for 137Cs and MODIS iPAR
for August 2014
N
0
100
200
400 Kilometers
Legend
Greece
Local r2 values
<0,05
0,05-0,10
0,10-0,15
0,15 - 0,20
0,20 - 0,25
0,25 - 0,30
0,30 - 0,35
0,35 - 0,40
0,40 - 0,45
0,45 - 0,50
>0,50
Local r2 values for 137Cs and MODIS iPAR
for November 2014
N
0
100
200
400 Kilometers
Legend
Greece
Local r2 values
<0,05
0,05-0,10
0,10-0,15
0,15 - 0,20
0,20 - 0,25
0,25 - 0,30
0,30 - 0,35
0,35 - 0,40
0,40 - 0,45
0,45 - 0,50
>0,50

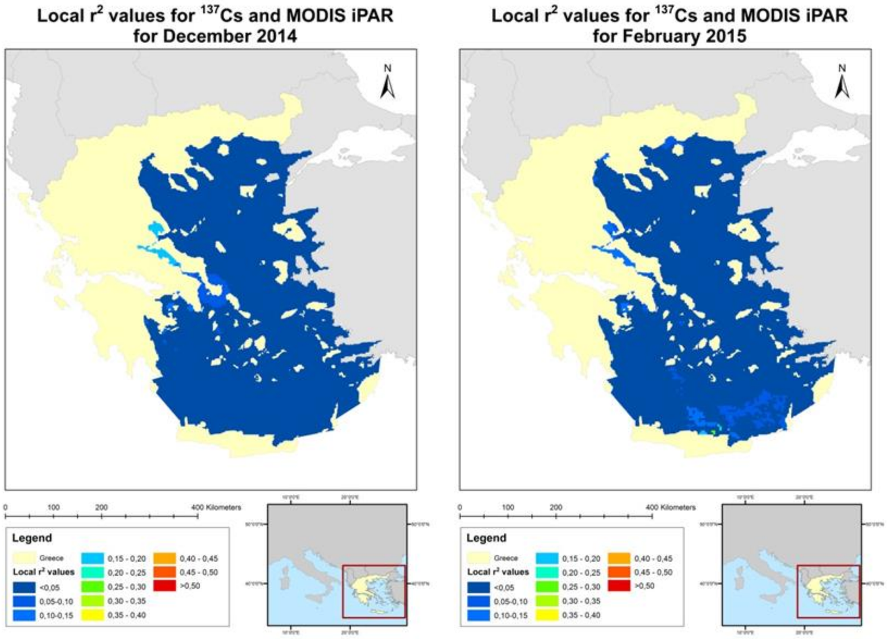

Figure 98. Local r^2 values for ^{137}Cs activity concentrations and MODIS iPAR for the time period March 2012 to February 2015.

In this section the GWR local r^2 results that depict the linear relations between ^{137}Cs activity concentrations and MODIS iPAR are being exhibited (Figure 98). By observing the results, it is obvious that the models using MODIS iPAR are not able to sufficiently describe the values of ^{137}Cs activity concentrations in the Aegean Sea. All the months present similar results, with all r^2 values being below 0.4.

8.2.1.1.8. PAR

Local r^2 values for ^{137}Cs and MODIS PAR for March 2012

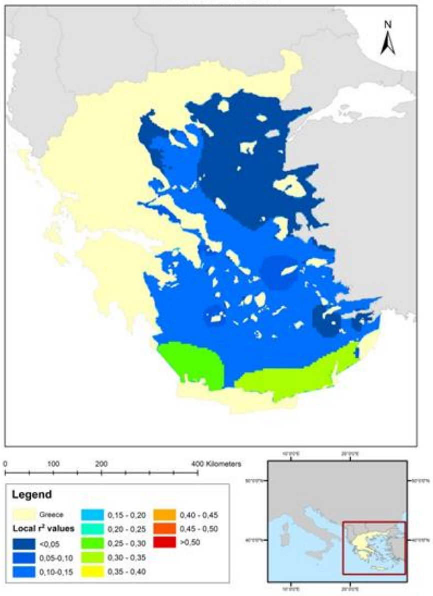

Local r^2 values for ^{137}Cs and MODIS PAR for April 2012

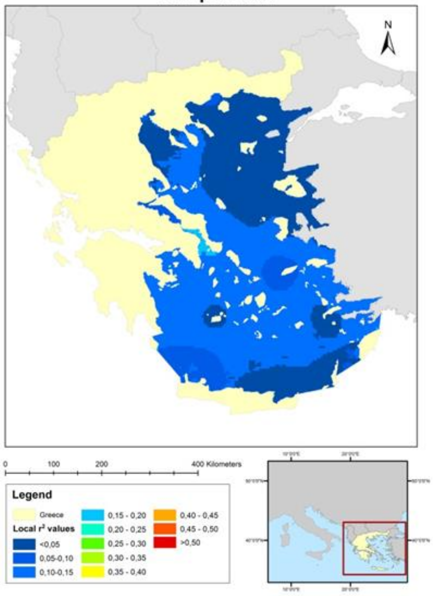

Local r^2 values for ^{137}Cs and MODIS PAR for June 2012

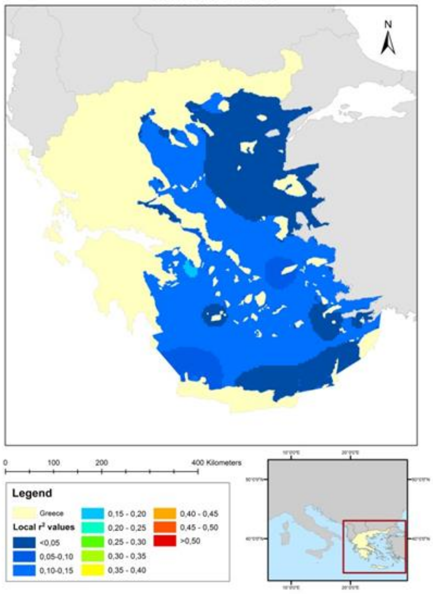

Local r^2 values for ^{137}Cs and MODIS PAR for November 2012

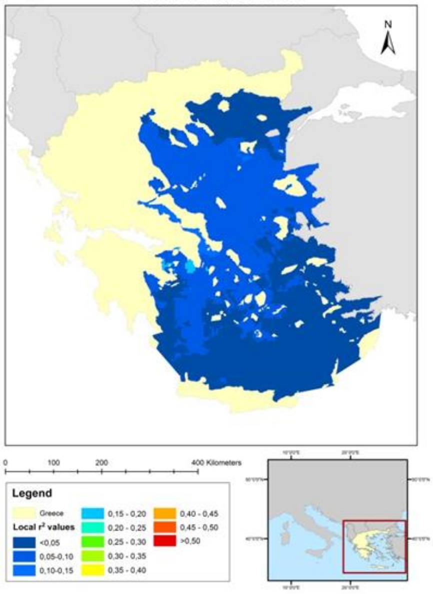

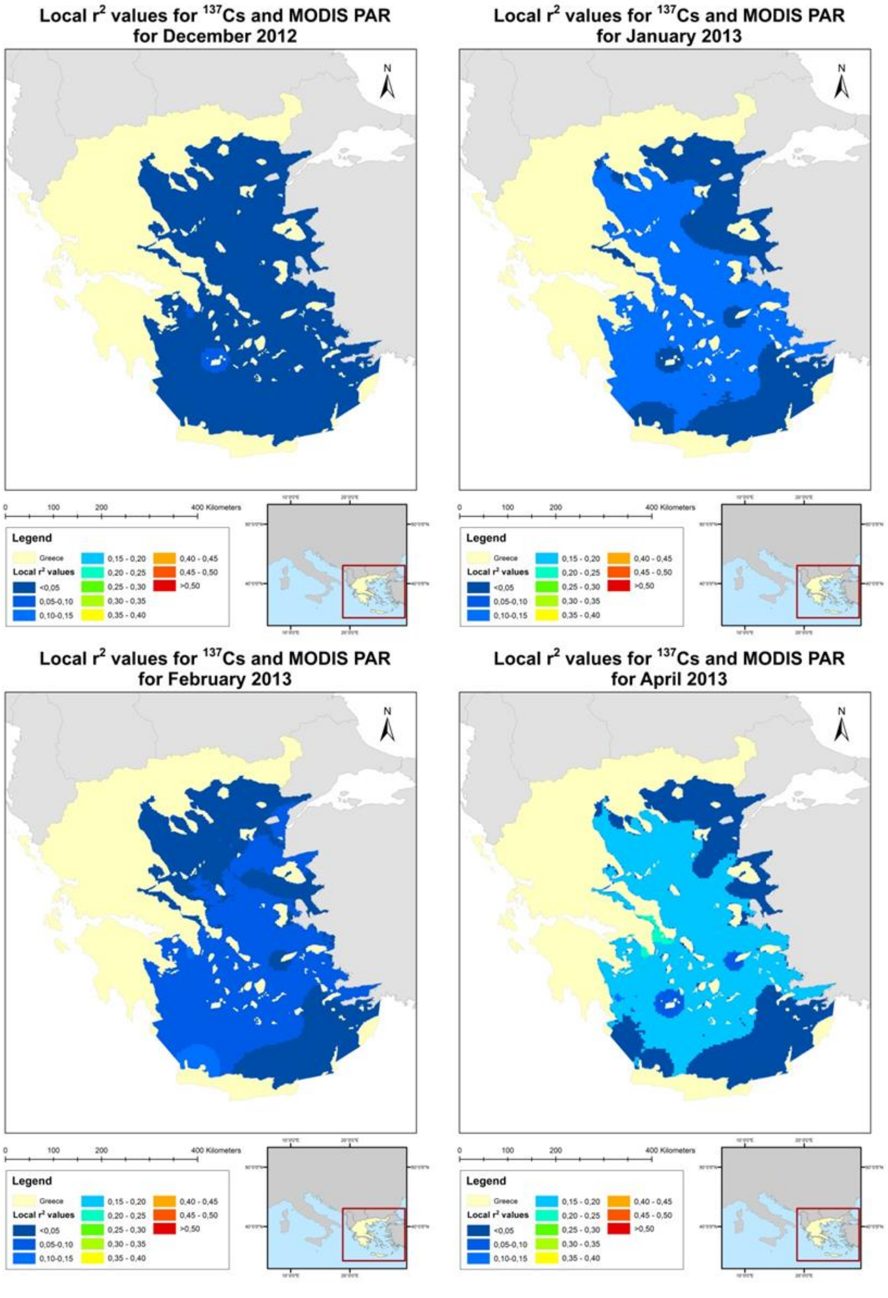
Local r^2 values for ^{137}Cs and MODIS PAR for December 2012
Local r^2 values for ^{137}Cs and MODIS PAR for January 2013
Local r^2 values for ^{137}Cs and MODIS PAR for February 2013
Local r^2 values for ^{137}Cs and MODIS PAR for April 2013
N
0 100 200 400 Kilometers
Legend
Greece
Local r^2 values
<0,05
0,05-0,10
0,10-0,15
0,15 - 0,20
0,20 - 0,25
0,25 - 0,30
0,30 - 0,35
0,35 - 0,40
0,40 - 0,45
0,45 - 0,50
>0,50

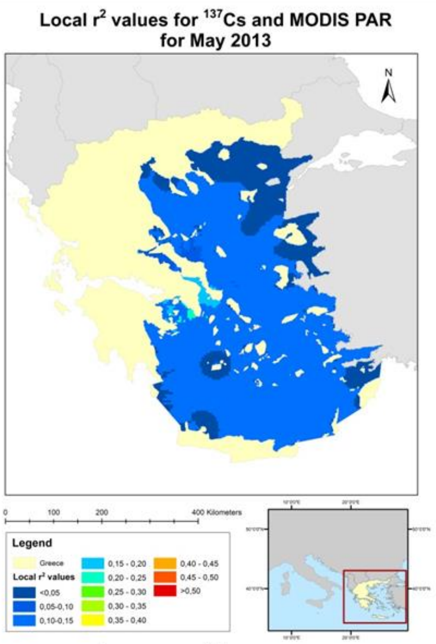
Local r2 values for 137Cs and MODIS PAR
for May 2013
N
0
100
200
400 Kilometers
Legend
Greece
Local r2 values
<0,05
0,05-0,10
0,10-0,15
0,15 - 0,20
0,20 - 0,25
0,25 - 0,30
0,30 - 0,35
0,35 - 0,40
0,40 - 0,45
0,45 - 0,50
>0,50

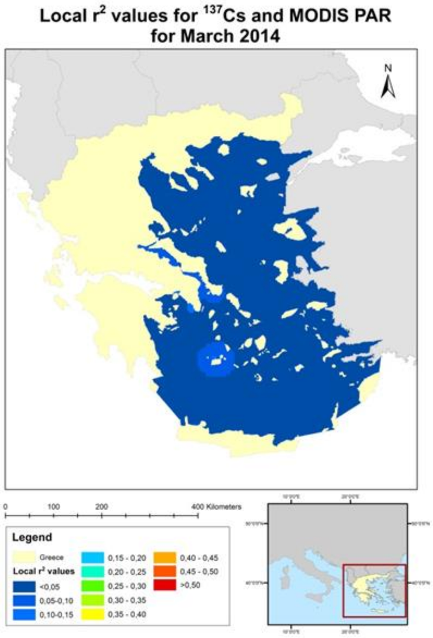
Local r2 values for 137Cs and MODIS PAR
for March 2014
N
0
100
200
400 Kilometers
Legend
Greece
Local r2 values
<0,05
0,05-0,10
0,10-0,15
0,15 - 0,20
0,20 - 0,25
0,25 - 0,30
0,30 - 0,35
0,35 - 0,40
0,40 - 0,45
0,45 - 0,50
>0,50

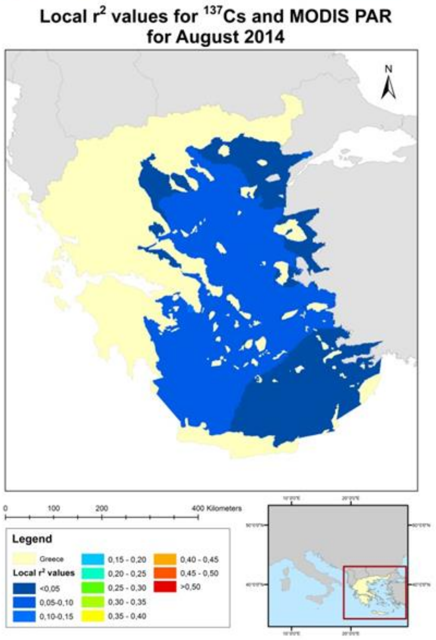
Local r2 values for 137Cs and MODIS PAR
for August 2014
N
0
100
200
400 Kilometers
Legend
Greece
Local r2 values
<0,05
0,05-0,10
0,10-0,15
0,15 - 0,20
0,20 - 0,25
0,25 - 0,30
0,30 - 0,35
0,35 - 0,40
0,40 - 0,45
0,45 - 0,50
>0,50

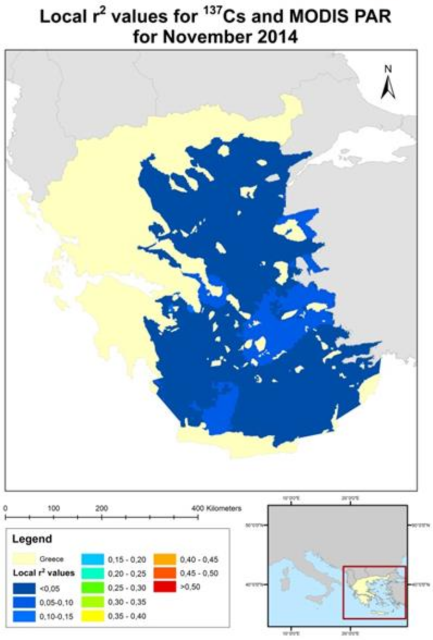
Local r2 values for 137Cs and MODIS PAR
for November 2014
N
0
100
200
400 Kilometers
Legend
Greece
Local r2 values
<0,05
0,05-0,10
0,10-0,15
0,15 - 0,20
0,20 - 0,25
0,25 - 0,30
0,30 - 0,35
0,35 - 0,40
0,40 - 0,45
0,45 - 0,50
>0,50

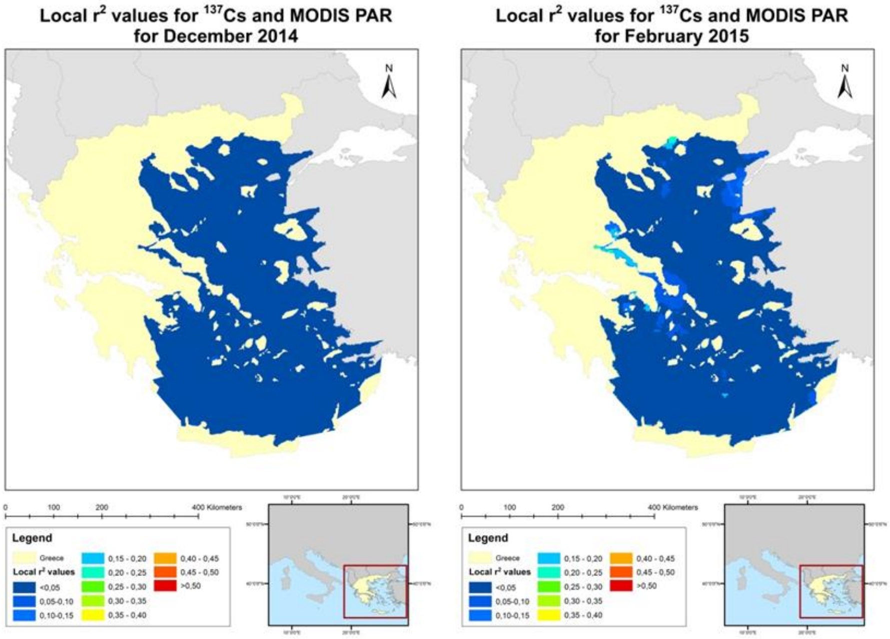

Figure 99. Local r^2 values for ^{137}Cs activity concentrations and MODIS PAR for the time period March 2012 to February 2015.

The results of GWR local r^2 that shows the spatial linear relations between ^{137}Cs activity concentrations and MODIS PAR are being presented in this part (Figure 99). Unlike the models using MODIS iPAR, the models using MODIS PAR present quite better results; however they are not adequately describing the ^{137}Cs activity concentrations in the Aegean Sea. The results between months are quite similar, except for the month of February 2015 that presents the maximum r^2 value of 0.77; the rest of the months present r^2 values under 0.4.

8.2.1.2. PREDICTED ^{137}CS ACTIVITY CONCENTRATIONS

8.2.1.2.1. SSTNIGHT

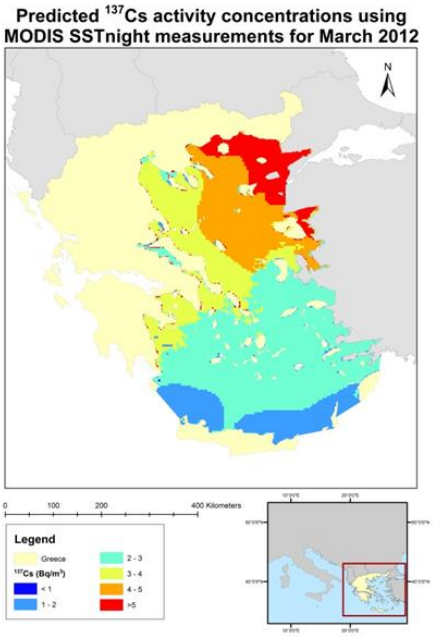

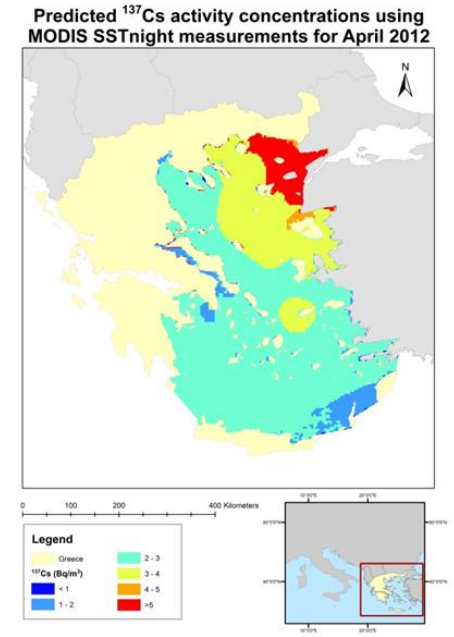

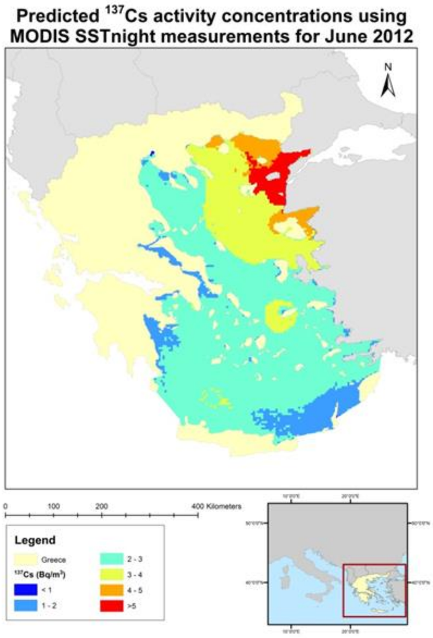

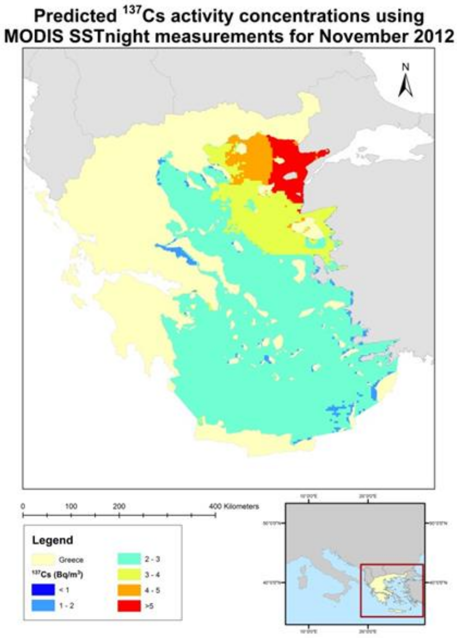

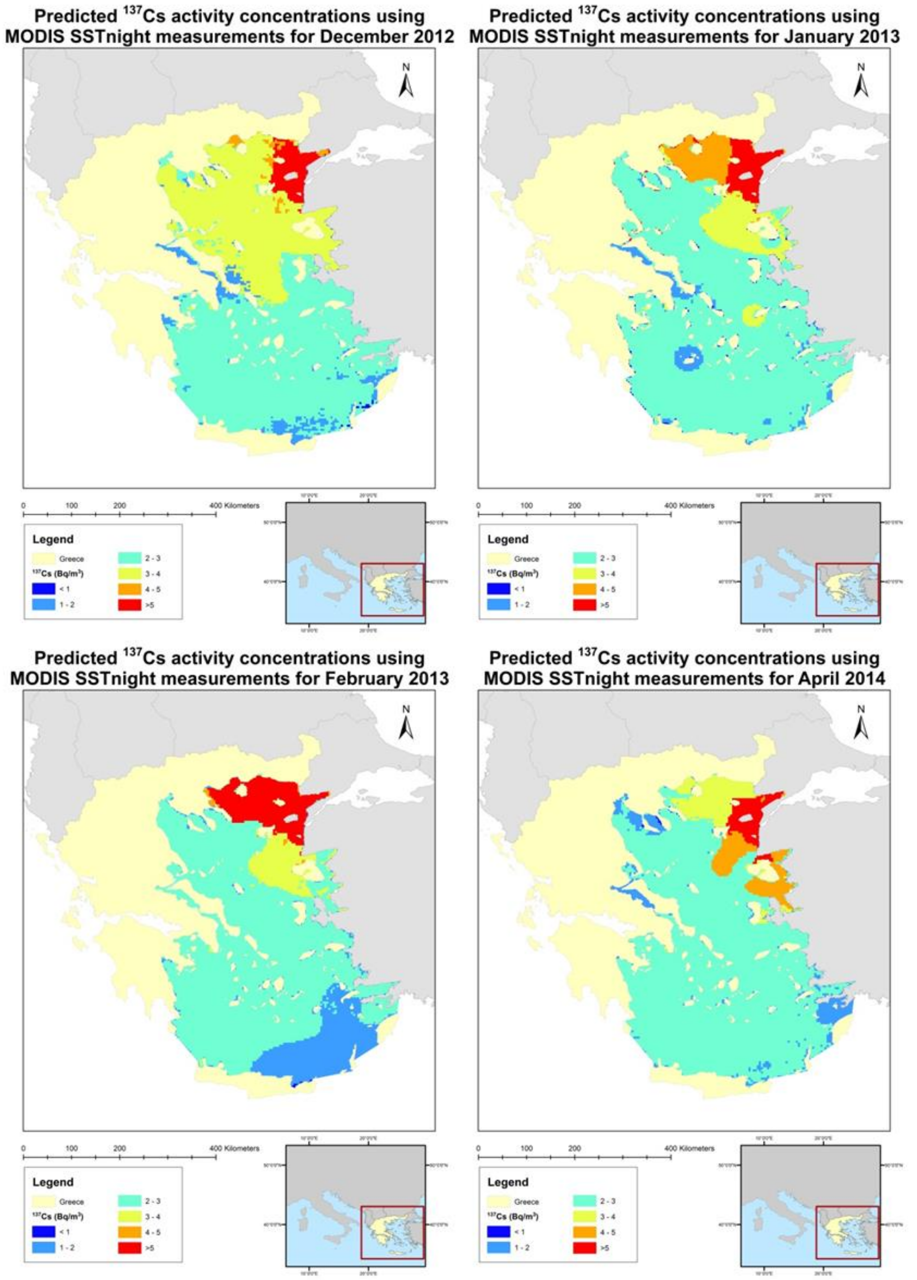
Predicted 137Cs activity concentrations using MODIS SSTnight measurements for December 2012
Predicted 137Cs activity concentrations using MODIS SSTnight measurements for January 2013
Predicted 137Cs activity concentrations using MODIS SSTnight measurements for February 2013
Predicted 137Cs activity concentrations using MODIS SSTnight measurements for April 2014
N
0 100 200 400 Kilometers
Legend
Greece
137Cs (Bq/m3)
< 1
1 - 2
2 - 3
3 - 4
4 - 5
>5

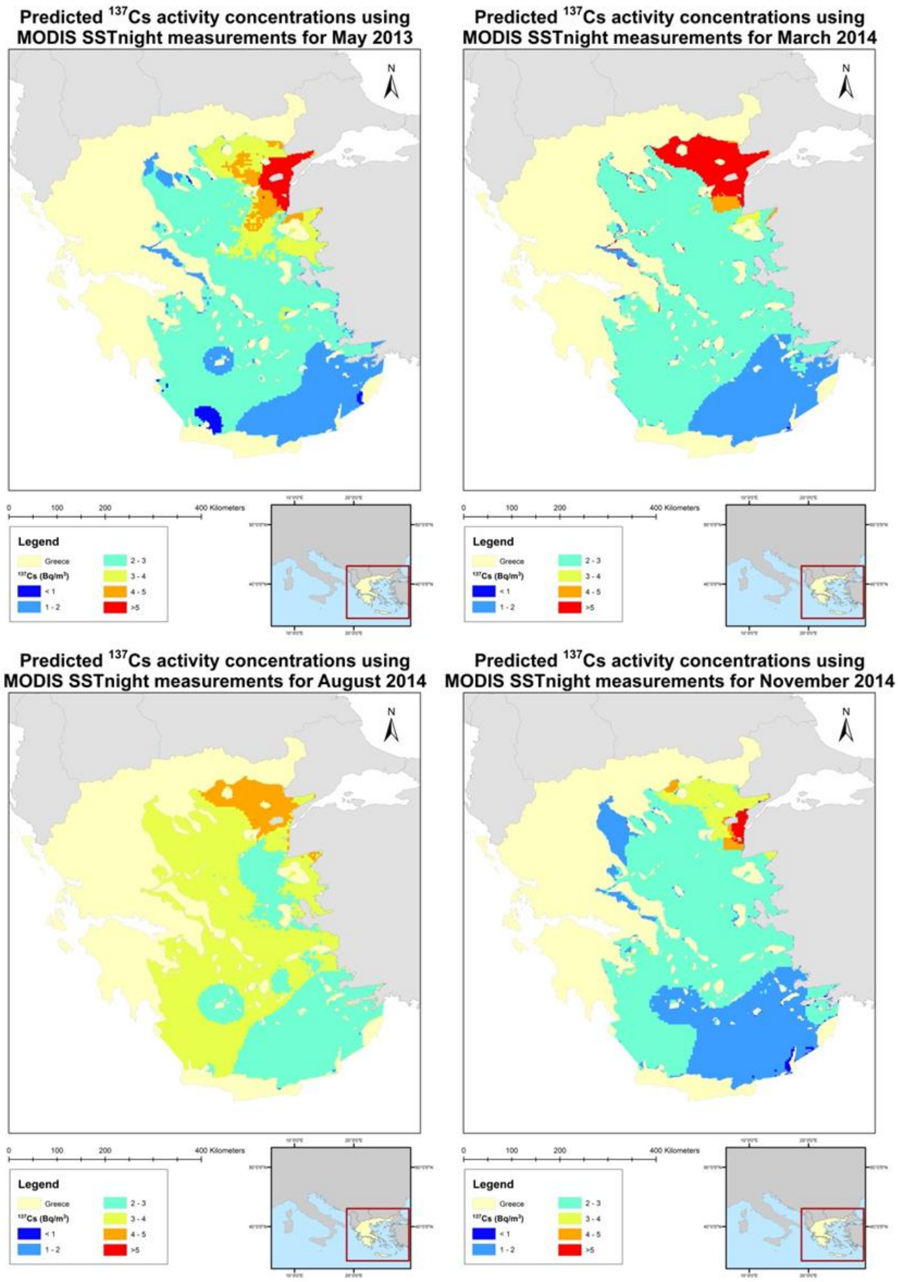
Predicted 137Cs activity concentrations using MODIS SSTnight measurements for May 2013
Predicted 137Cs activity concentrations using MODIS SSTnight measurements for March 2014
Predicted 137Cs activity concentrations using MODIS SSTnight measurements for August 2014
Predicted 137Cs activity concentrations using MODIS SSTnight measurements for November 2014
N
0 100 200 400 Kilometers
Legend
Greece
137Cs (Bq/m3)
< 1
1 - 2
2 - 3
3 - 4
4 - 5
>5

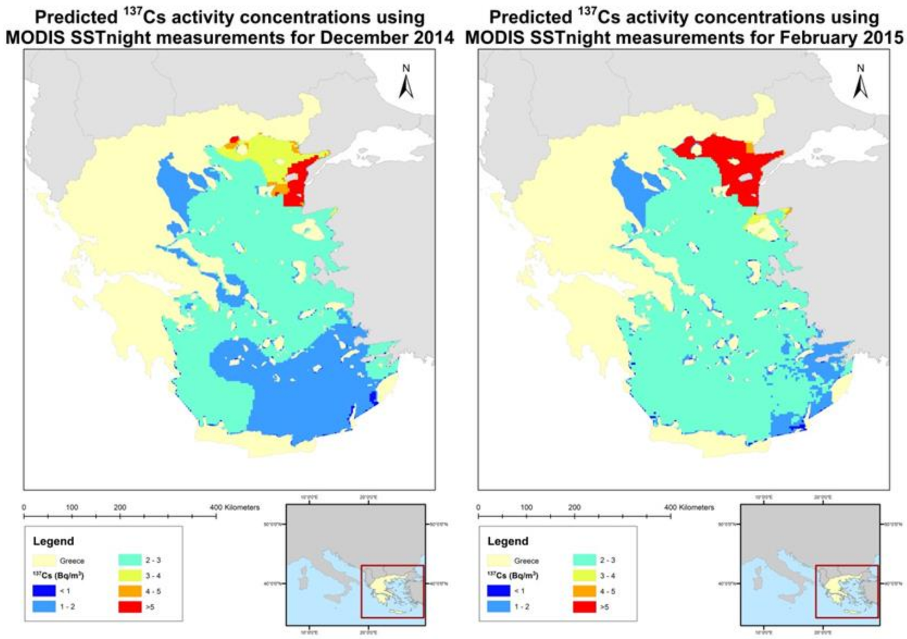

Figure 100. Predicted ^{137}Cs activity concentrations using MODIS SSTnight for the time period March 2012 to February 2015.

In this paragraph the results of GWR predicted ^{137}Cs activity concentrations using MODIS SSTnight are shown (Figure 100). By observing the predicted ^{137}Cs activity concentrations, it can be seen that the model using MODIS SSTnight overestimated the activity concentrations by presenting larger areas that have values over 5 Bq/m^3. Generally the categories of lower concentrations have remained quite the same; however the categories presenting medium concentrations have significantly decreased. The month with the least accurate results is the month of August 2014 and the months with the most accurate results are the months of November 2014 and December 2014.

8.2.1.2.2. SST4NIGHT

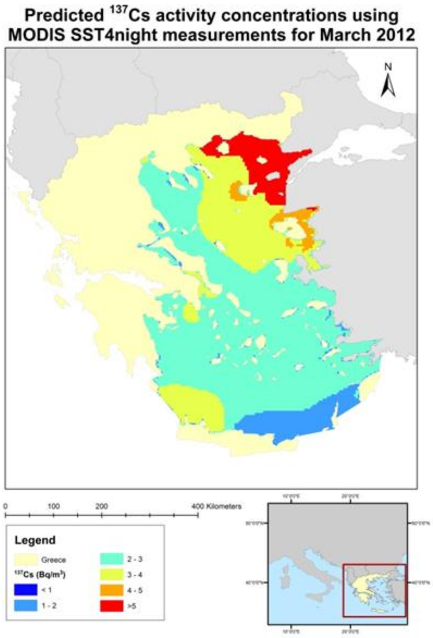

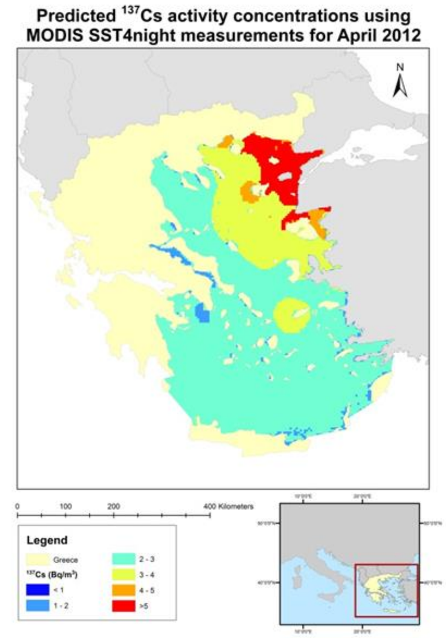

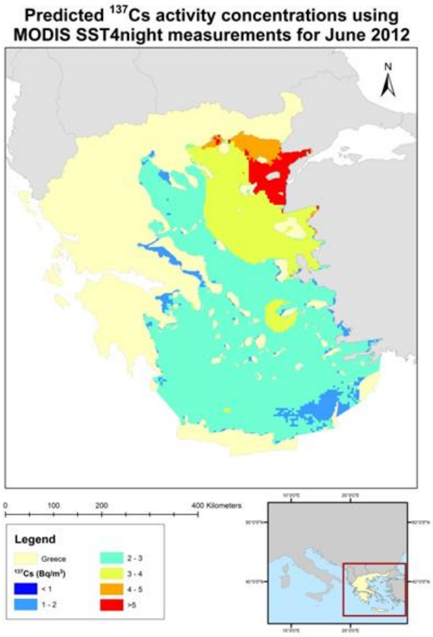

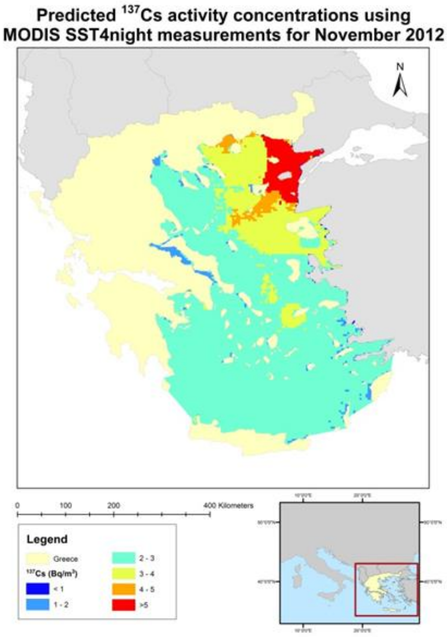

Predicted ^{137}Cs activity concentrations using MODIS SST4night measurements for December 2012

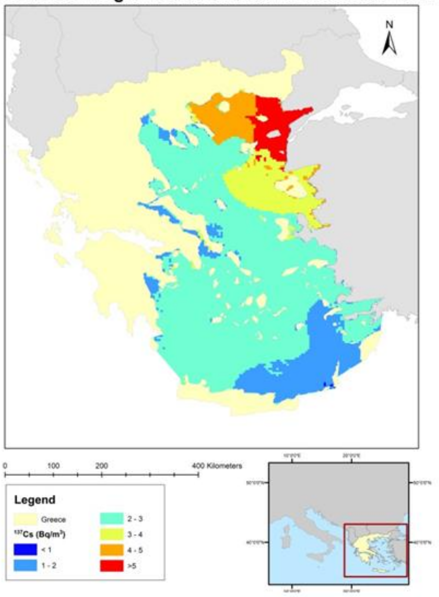

Predicted ^{137}Cs activity concentrations using MODIS SST4night measurements for January 2013

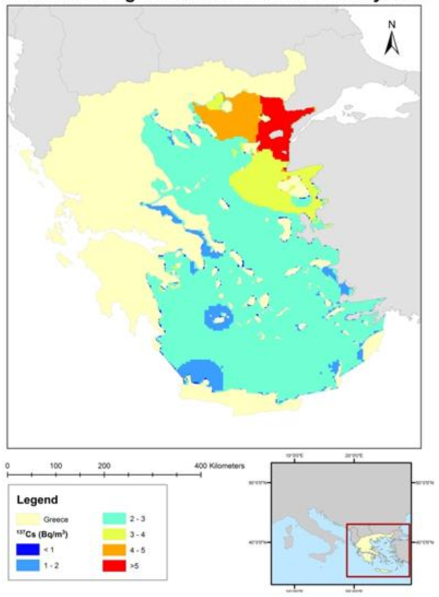

Predicted ^{137}Cs activity concentrations using MODIS SST4night measurements for February 2013

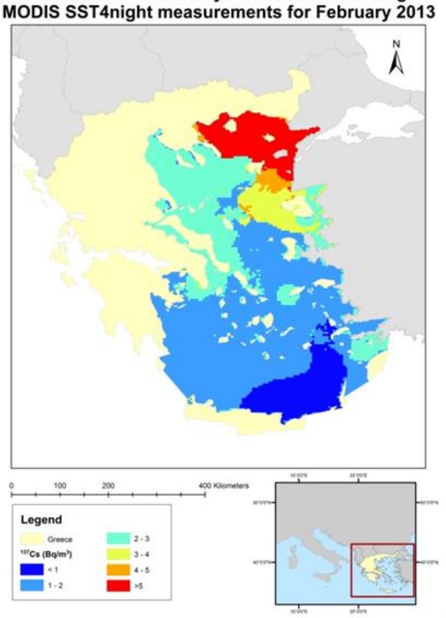

Predicted ^{137}Cs activity concentrations using MODIS SST4night measurements for April 2013

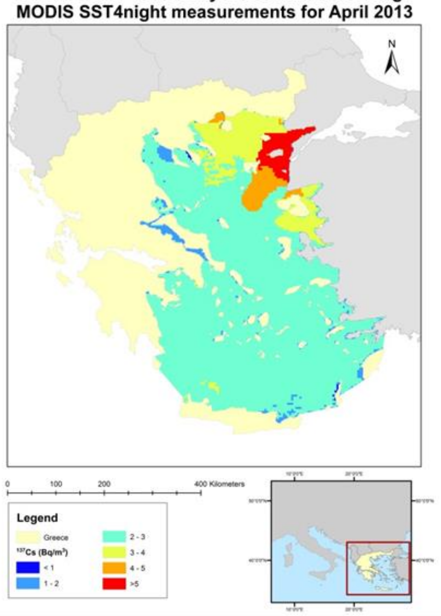

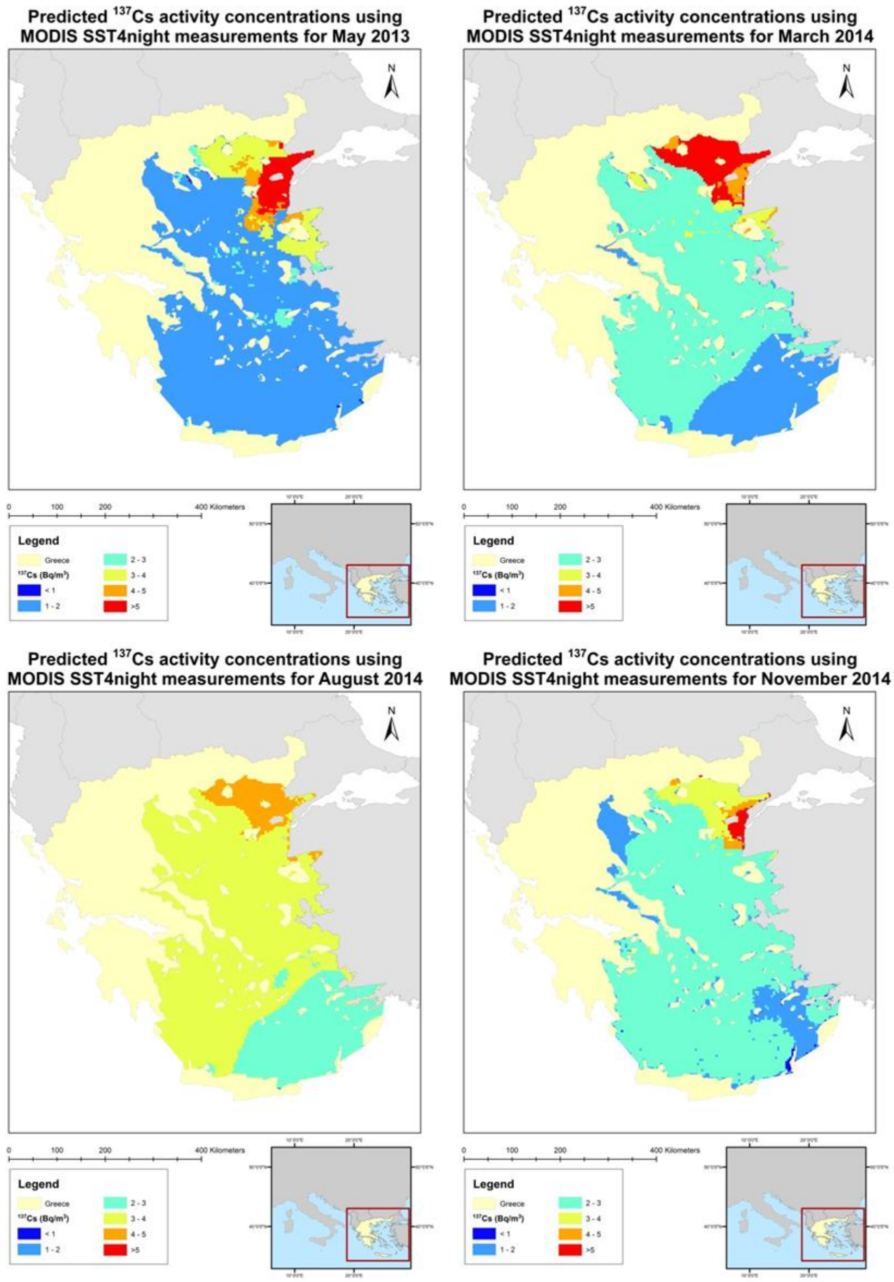
Predicted 137Cs activity concentrations using MODIS SST4night measurements for May 2013
Predicted 137Cs activity concentrations using MODIS SST4night measurements for March 2014
Predicted 137Cs activity concentrations using MODIS SST4night measurements for August 2014
Predicted 137Cs activity concentrations using MODIS SST4night measurements for November 2014
N
0 100 200 400 Kilometers
Legend
Greece
137Cs (Bq/m3)
< 1
1 - 2
2 - 3
3 - 4
4 - 5
>5

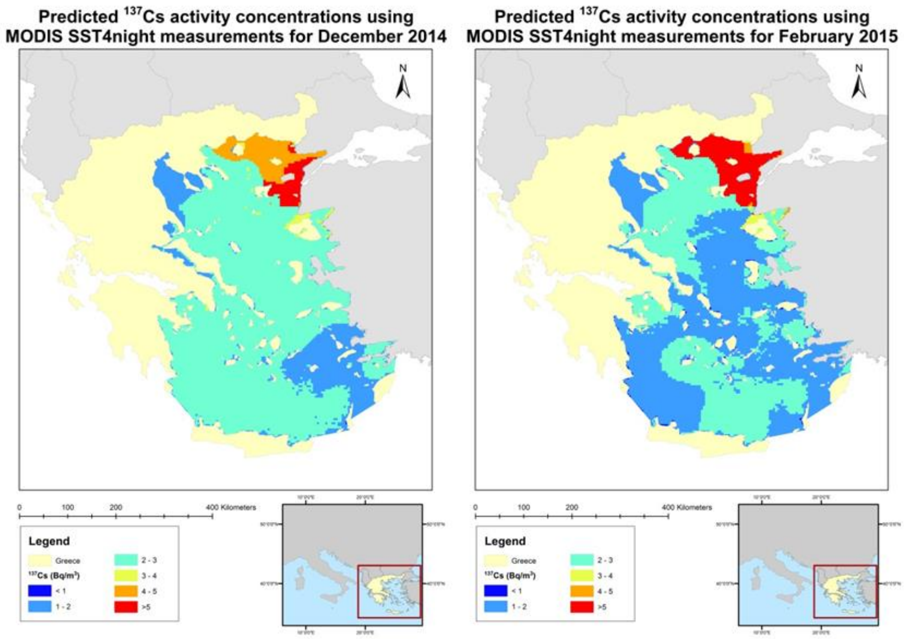

Figure 101. Predicted ^{137}Cs activity concentrations using MODIS SST4night for the time period March 2012 to February 2015.

The results of GWR predicted ^{137}Cs activity concentrations using MODIS SST4night are being exhibited in this part (Figure 101). Like the models using MODIS SSTnight, the models using SST4night also overestimate the values of ^{137}Cs activity concentrations by presenting larger areas over 5 Bq/m^3; however these models also underestimated the values by presenting larger areas below 2 Bq/m^3. The month with the least accurate ^{137}Cs activity concentrations is the month of August 2014, whereas the month with the most accurate ^{137}Cs activity concentrations is the month of March 2012.

8.2.1.2.3. SSTMORNING

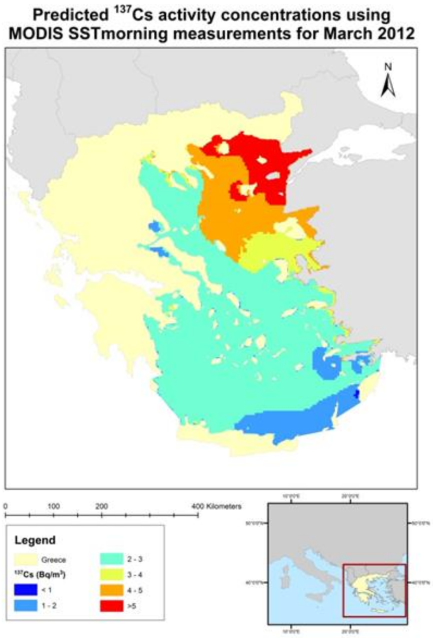

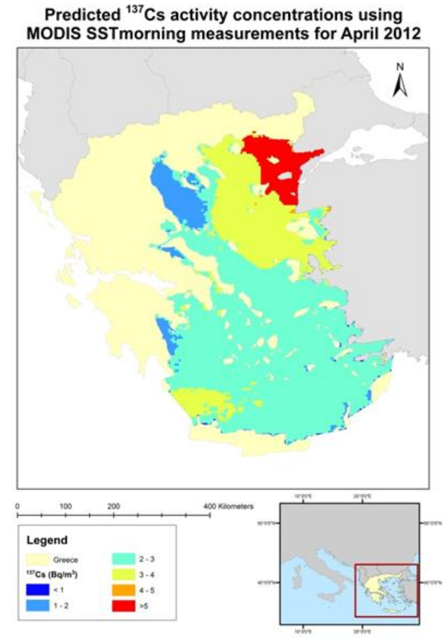

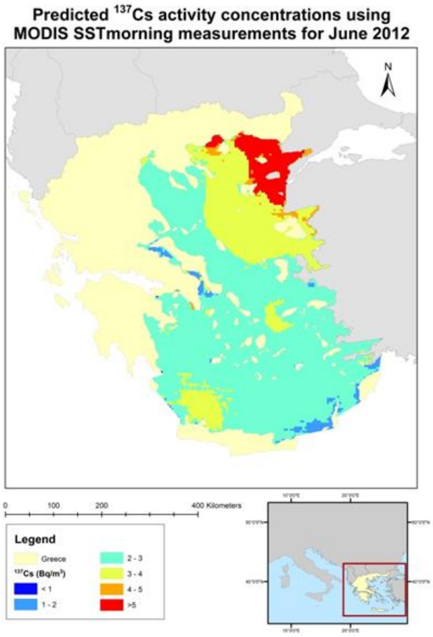

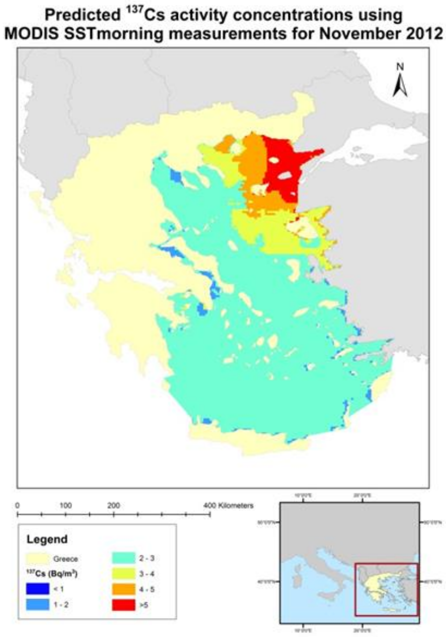

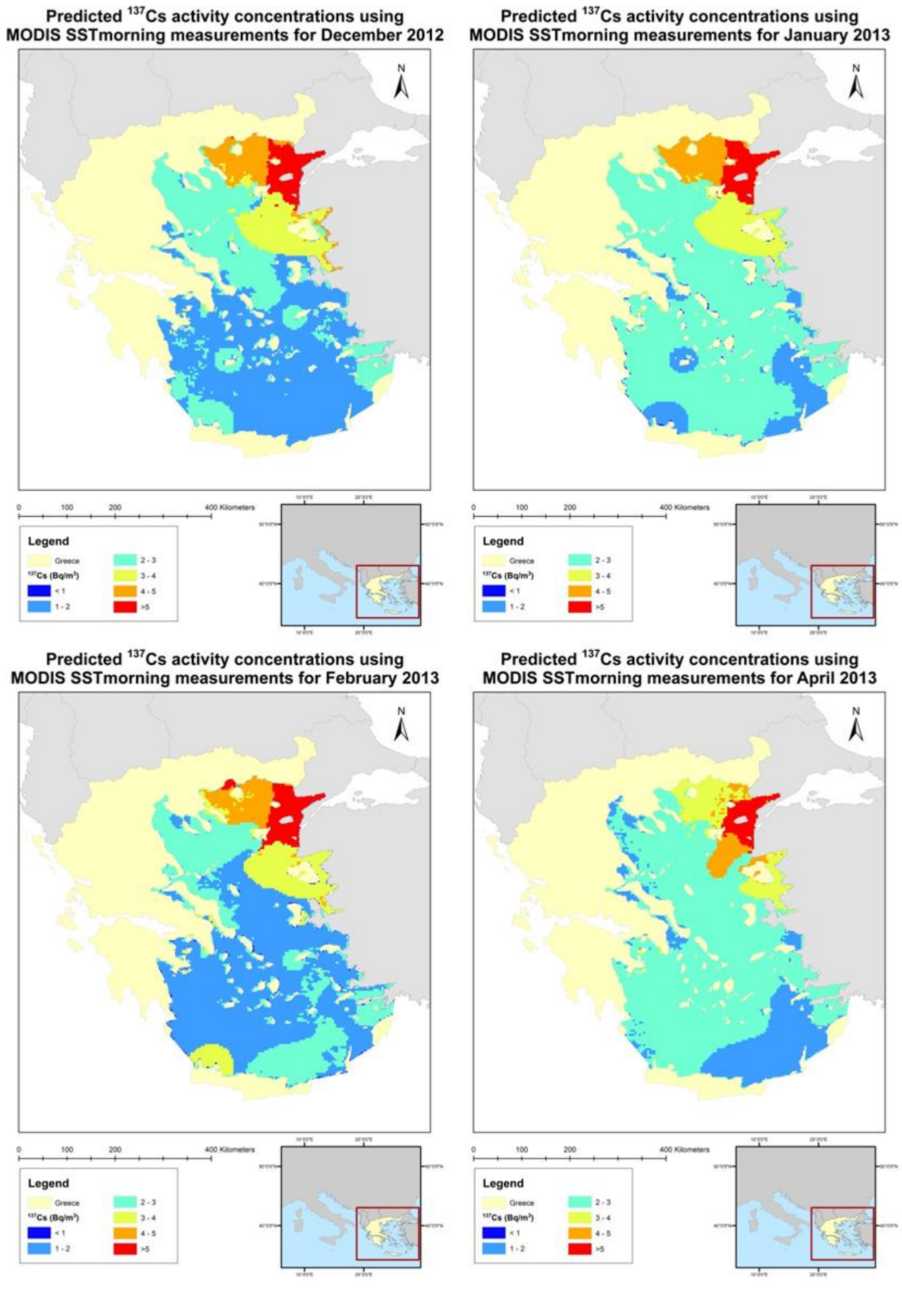
Predicted 137Cs activity concentrations using MODIS SSTmorning measurements for December 2012
Predicted 137Cs activity concentrations using MODIS SSTmorning measurements for January 2013
Predicted 137Cs activity concentrations using MODIS SSTmorning measurements for February 2013
Predicted 137Cs activity concentrations using MODIS SSTmorning measurements for April 2013
N
0 100 200 400 Kilometers
Legend
Greece
137Cs (Bq/m3)
< 1
1 - 2
2 - 3
3 - 4
4 - 5
>5

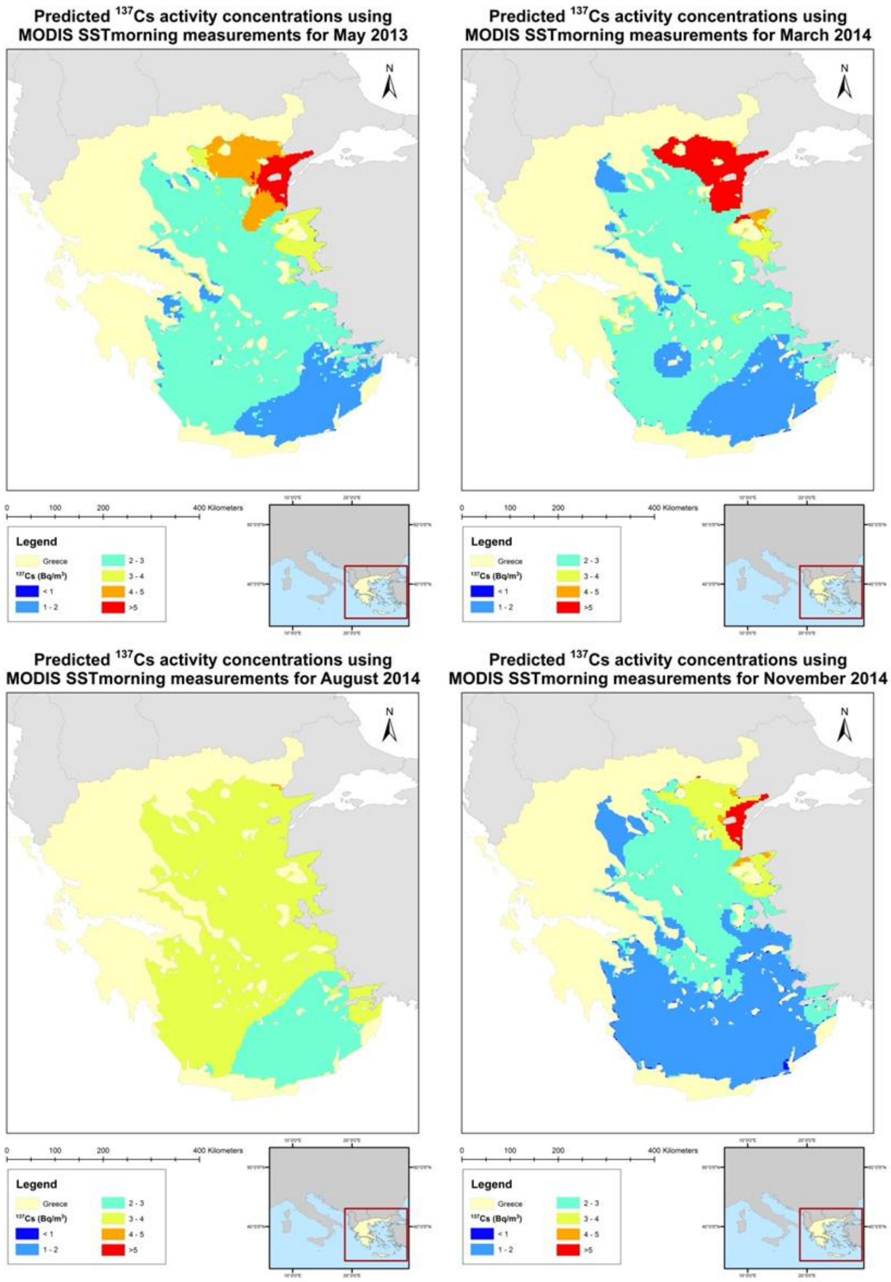
Predicted 137Cs activity concentrations using MODIS SSTmorning measurements for May 2013
Predicted 137Cs activity concentrations using MODIS SSTmorning measurements for March 2014
Predicted 137Cs activity concentrations using MODIS SSTmorning measurements for August 2014
Predicted 137Cs activity concentrations using MODIS SSTmorning measurements for November 2014
N
0 100 200 400 Kilometers
Legend
Greece
137Cs (Bq/m3)
< 1
1 - 2
2 - 3
3 - 4
4 - 5
>5

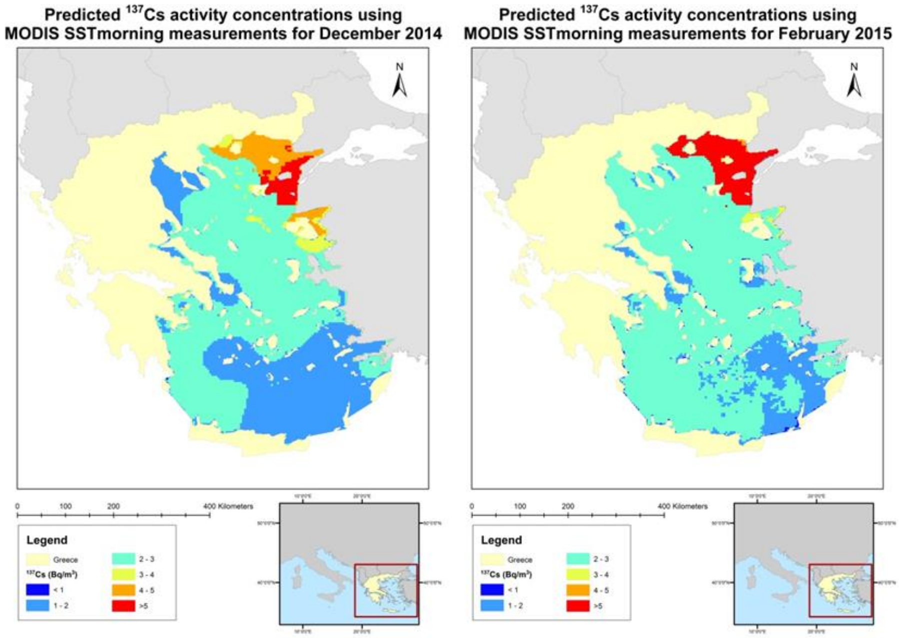

Figure 102. Predicted ^{137}Cs activity concentrations using MODIS SSTmorning for the time period March 2012 to February 2015.

In this paragraph the results of GWR predicted ^{137}Cs activity concentrations using MODIS SSTmorning are displayed (Figure 102). By observing the results, similarities with models using MODIS SSTnight and MODIS SST4night can be seen. These models also overestimated the ^{137}Cs activity concentration values by presenting larger areas over 5 Bq/m^3. Like the models using MODIS SST4night, these models also underestimated activity concentrations by presenting larger areas below 2 Bq/m^3 in several months. The most accurate predicted ^{137}Cs activity concentrations are present for the months of April 2013 and December 2014, whereas the least accurate activity concentrations are present for the month of August 2014.

8.2.1.2.4. CHLOR_A

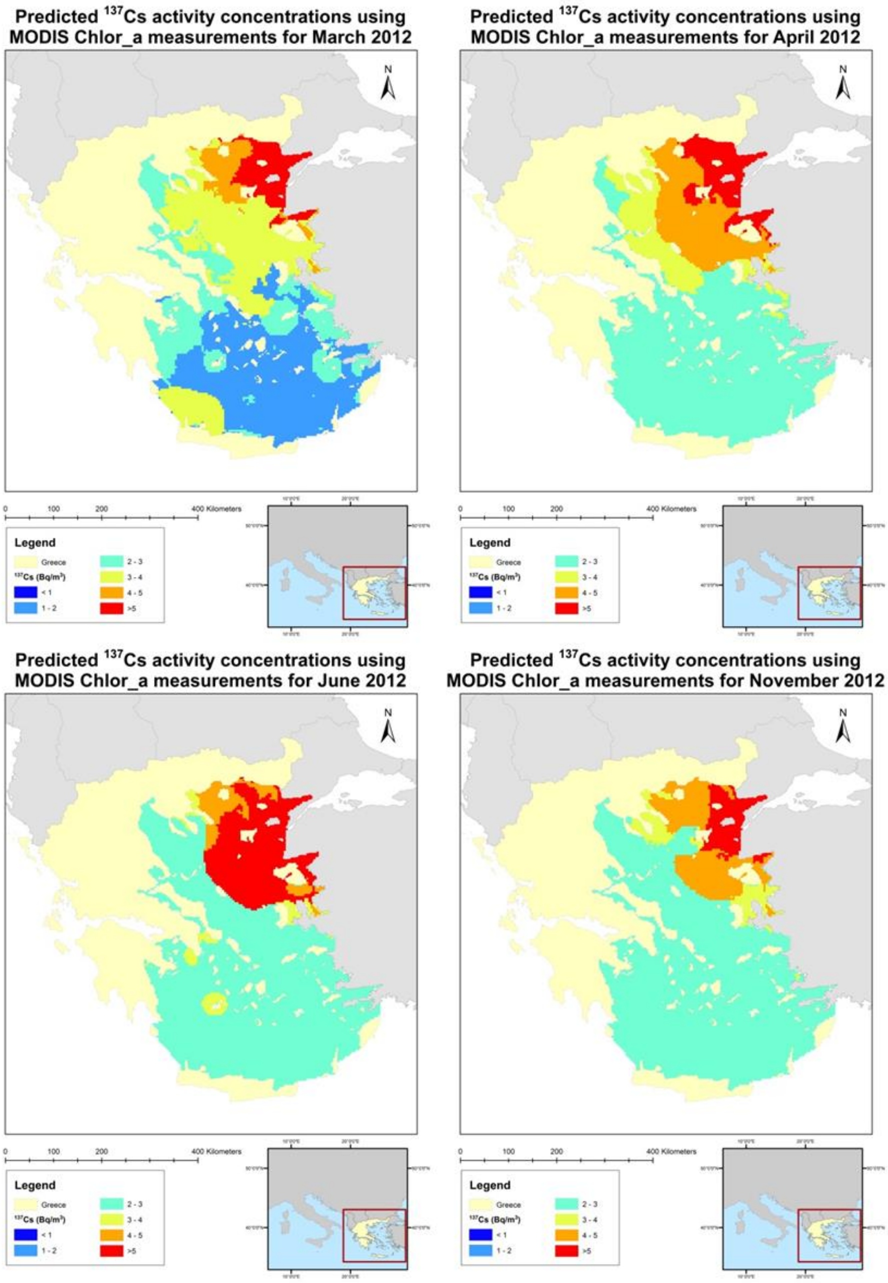

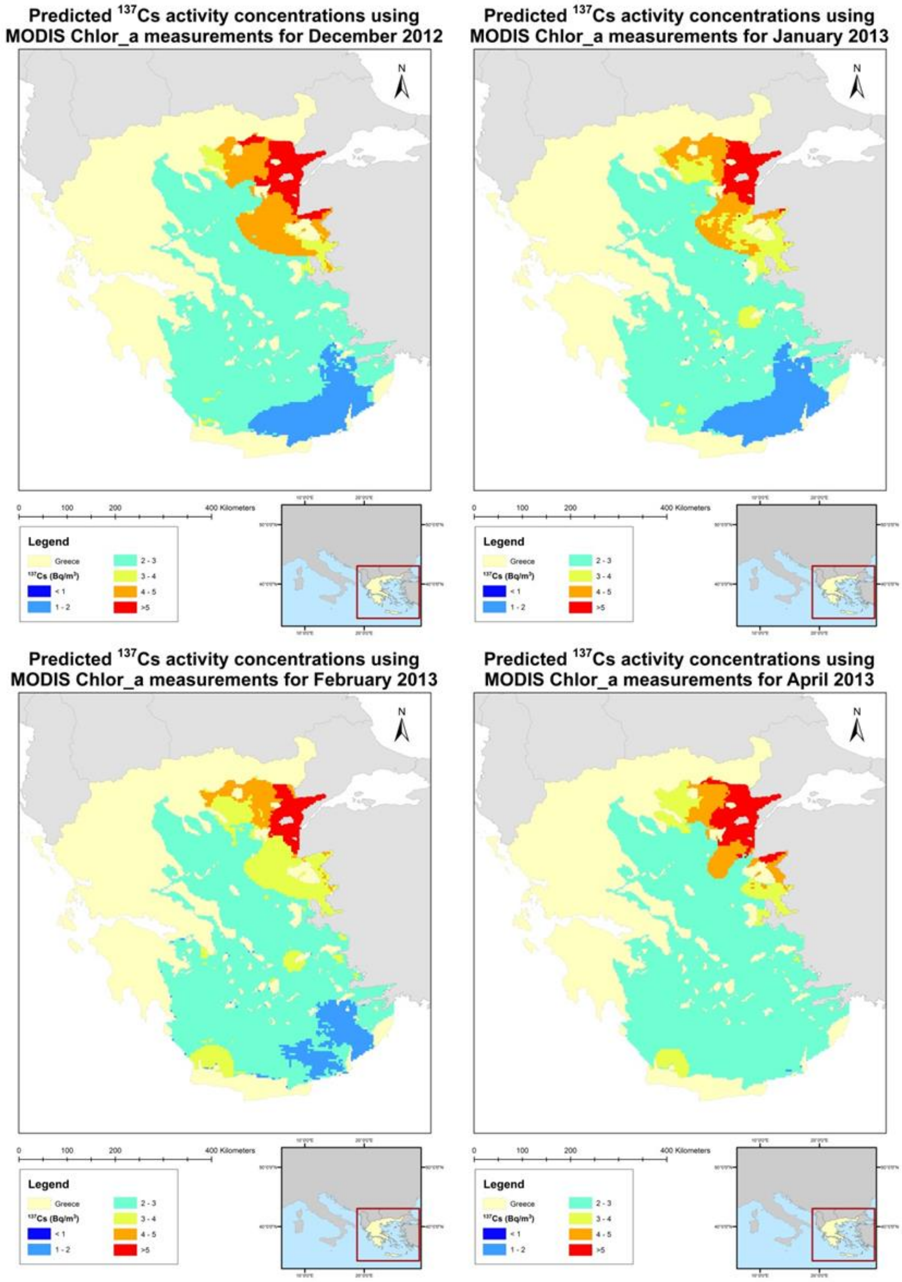

Predicted 137Cs activity concentrations using MODIS Chlor_a measurements for December 2012
0 100 200 400 Kilometers
Legend
Greece
137Cs (Bq/m3)
< 1
1 - 2
2 - 3
3 - 4
4 - 5
>5
Predicted 137Cs activity concentrations using MODIS Chlor_a measurements for January 2013
0 100 200 400 Kilometers
Legend
Greece
137Cs (Bq/m3)
< 1
1 - 2
2 - 3
3 - 4
4 - 5
>5
Predicted 137Cs activity concentrations using MODIS Chlor_a measurements for February 2013
0 100 200 400 Kilometers
Legend
Greece
137Cs (Bq/m3)
< 1
1 - 2
2 - 3
3 - 4
4 - 5
>5
Predicted 137Cs activity concentrations using MODIS Chlor_a measurements for April 2013
0 100 200 400 Kilometers
Legend
Greece
137Cs (Bq/m3)
< 1
1 - 2
2 - 3
3 - 4
4 - 5
>5

Predicted ^{137}Cs activity concentrations using MODIS Chlor_a measurements for May 2013

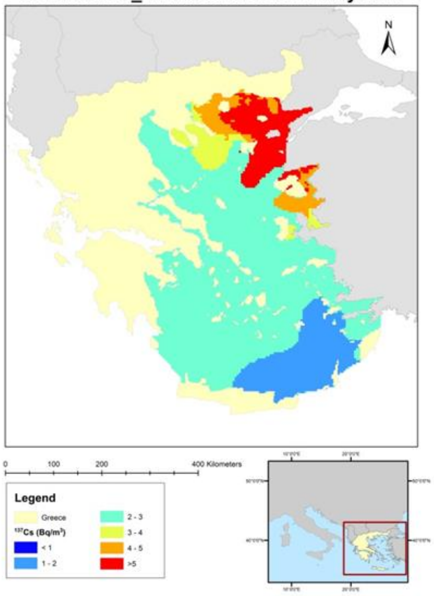

Predicted ^{137}Cs activity concentrations using MODIS Chlor_a measurements for March 2014

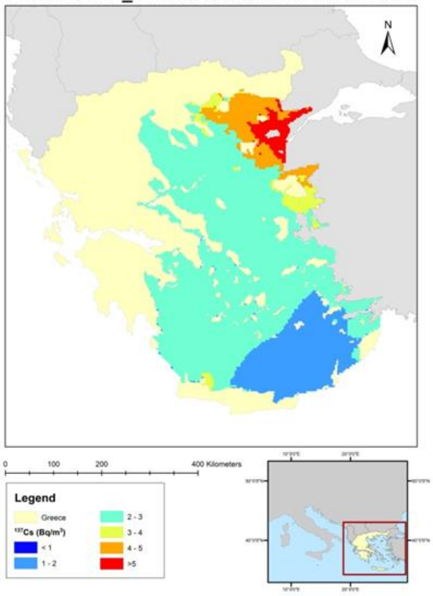

Predicted ^{137}Cs activity concentrations using MODIS Chlor_a measurements for August 2014

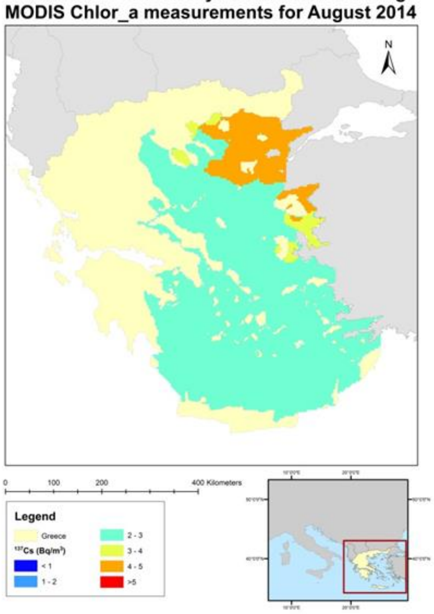

Predicted ^{137}Cs activity concentrations using MODIS Chlor_a measurements for November 2014

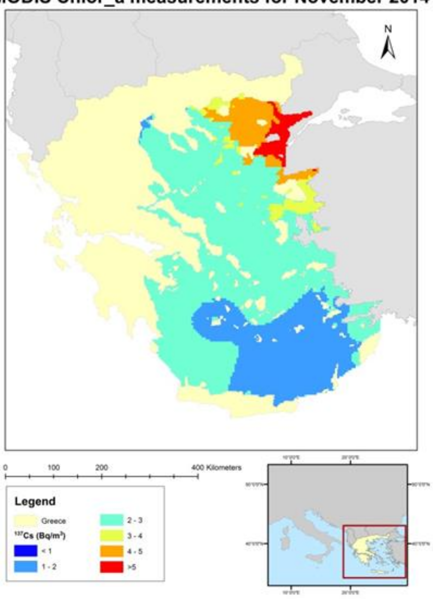

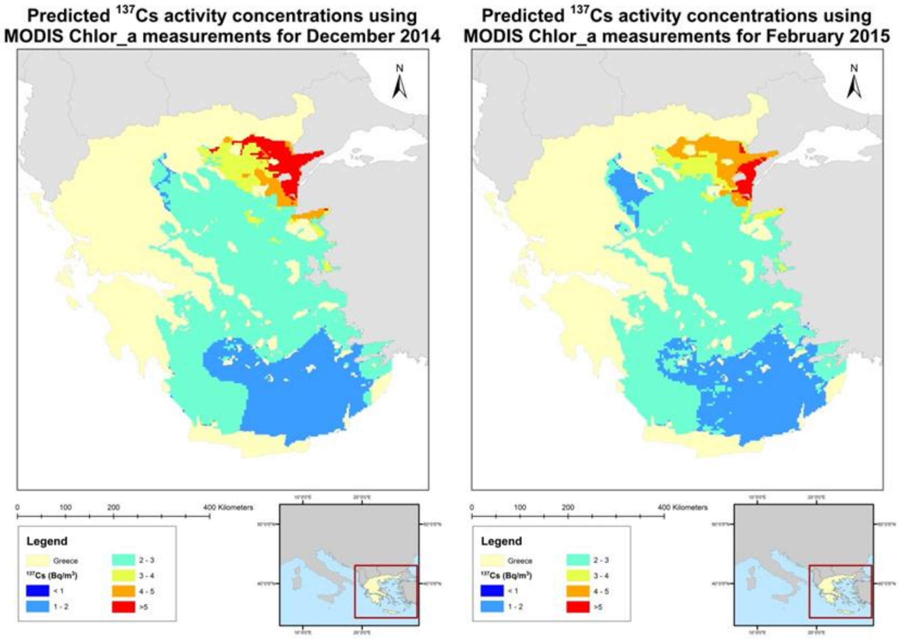

Figure 103. Predicted ^{137}Cs activity concentrations using MODIS Chlor_a for the time period March 2012 to February 2015.

The results of GWR predicted ^{137}Cs activity concentrations using MODIS Chlor_a are shown in this section (Figure 103). Like the models using MODIS SSTnight, MODIS SST4night and MODIS SSTmorning, the models using MODIS Chlor_a are overestimating the 137Cs activity concentration values by presenting larger areas over 5 Bq/m^3. Results also show smaller areas under 2 Bq/m^3, while the rest of the categories remain unchanged. It is obvious that the model using MODIS Chlor_a is not sufficiently predicting the values of ^{137}Cs activity concentrations, with the least accurate being the month of August 2014. The most accurate activity concentrations are present for the month of February 2015.

8.2.1.2.5. PIC

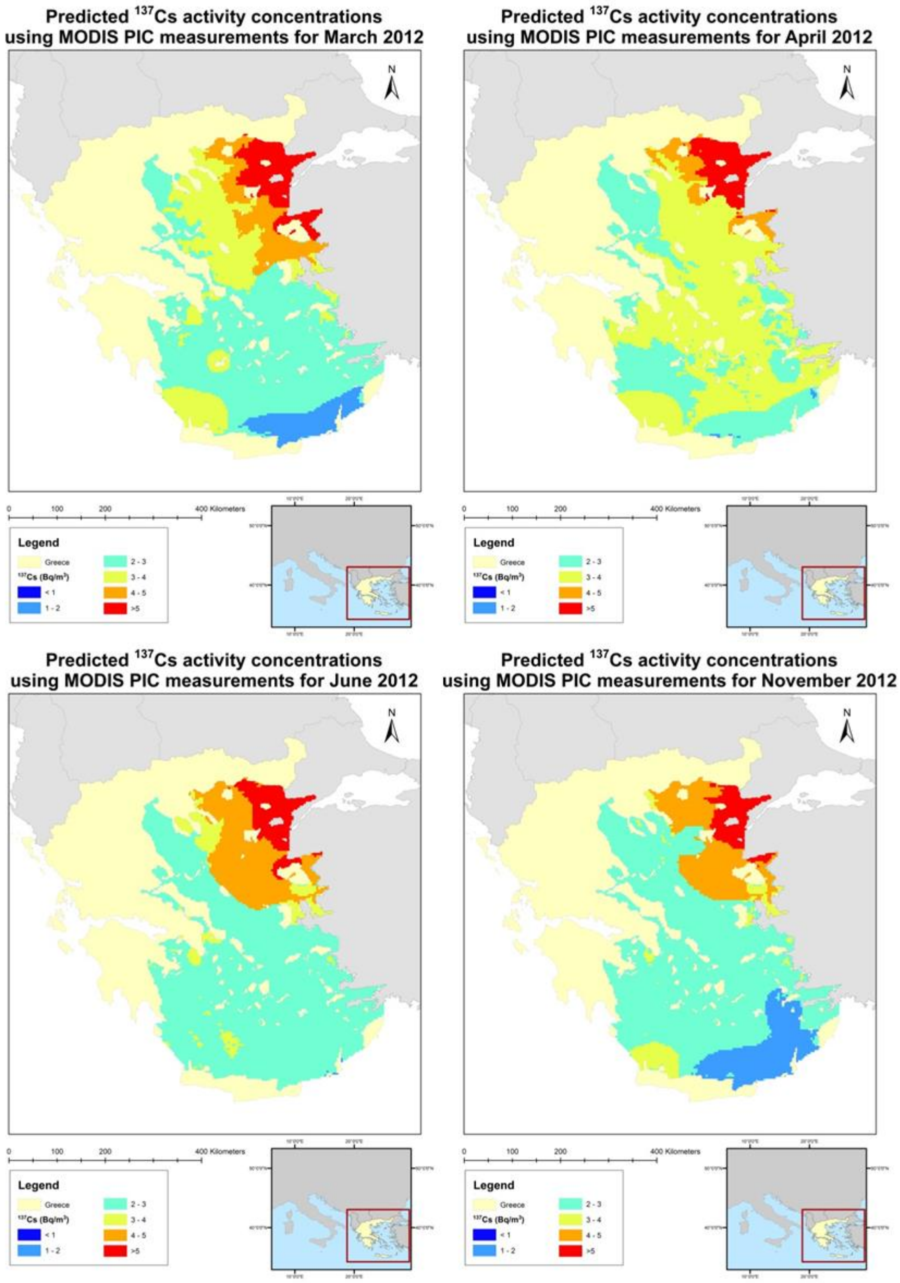
Predicted 137Cs activity concentrations
using MODIS PIC measurements for March 2012
Predicted 137Cs activity concentrations
using MODIS PIC measurements for April 2012
Predicted 137Cs activity concentrations
using MODIS PIC measurements for June 2012
Predicted 137Cs activity concentrations
using MODIS PIC measurements for November 2012
N
0 100 200 400 Kilometers
Legend
Greece
137Cs (Bq/m2)
< 1
1 - 2
2 - 3
3 - 4
4 - 5
>5

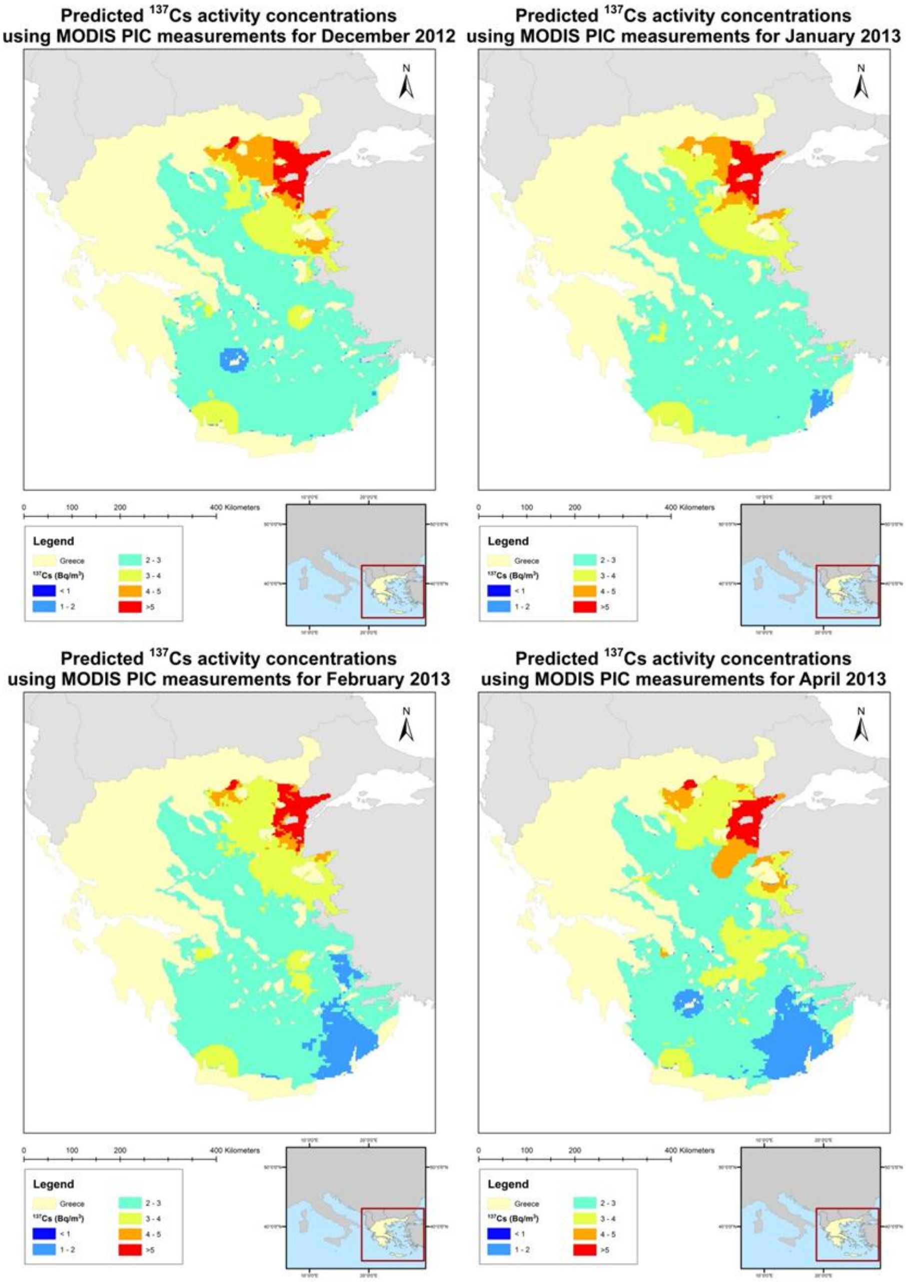
Predicted 137Cs activity concentrations using MODIS PIC measurements for December 2012
Predicted 137Cs activity concentrations using MODIS PIC measurements for January 2013
Predicted 137Cs activity concentrations using MODIS PIC measurements for February 2013
Predicted 137Cs activity concentrations using MODIS PIC measurements for April 2013
N
0 100 200 400 Kilometers
Legend
Greece
137Cs (Bq/m3)
< 1
1 - 2
2 - 3
3 - 4
4 - 5
>5

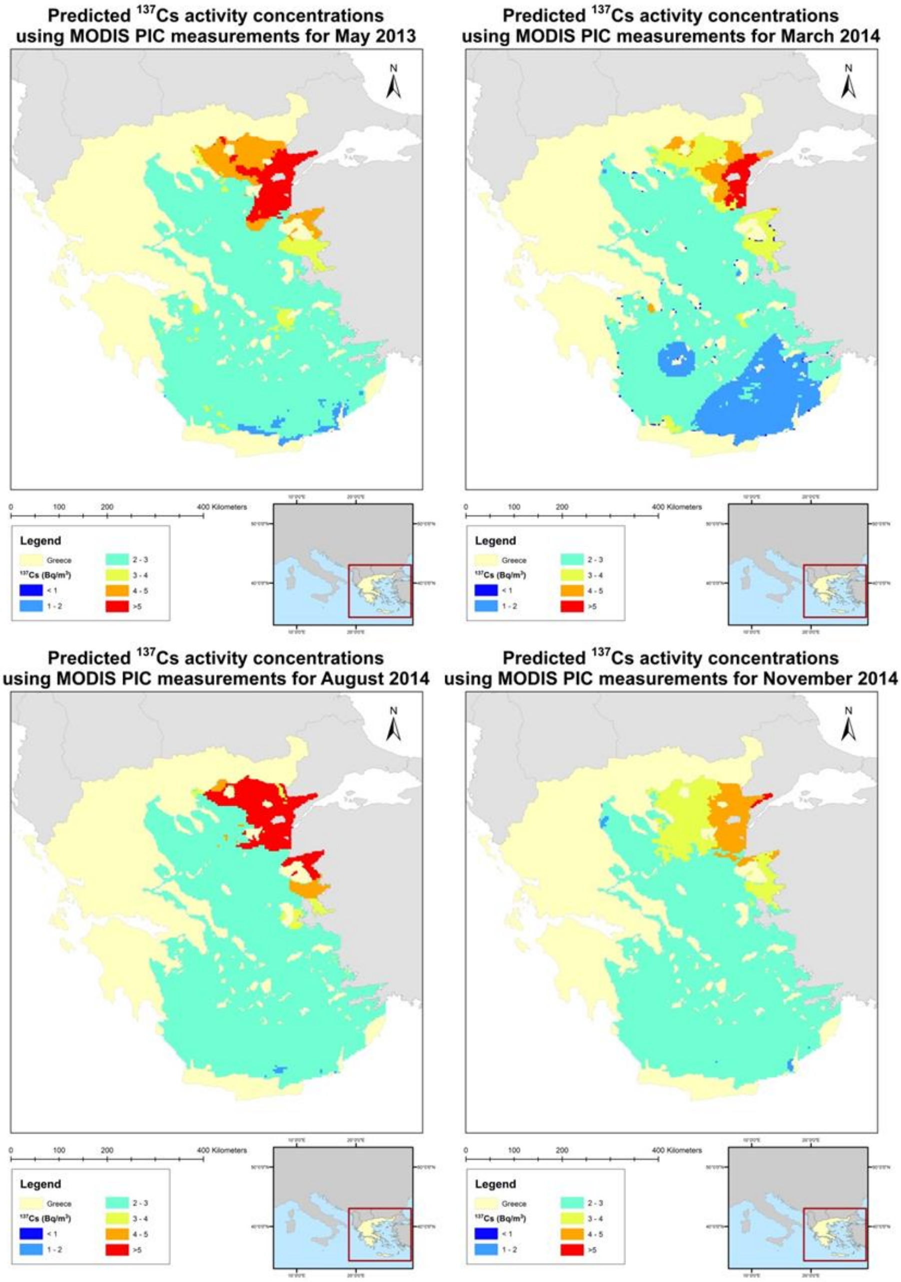
Predicted 137Cs activity concentrations using MODIS PIC measurements for May 2013
N
0 100 200 400 Kilometers
Legend
Greece
137Cs (Bq/m3)
< 1
1 - 2
2 - 3
3 - 4
4 - 5
>5
Predicted 137Cs activity concentrations using MODIS PIC measurements for March 2014
N
0 100 200 400 Kilometers
Legend
Greece
137Cs (Bq/m3)
< 1
1 - 2
2 - 3
3 - 4
4 - 5
>5
Predicted 137Cs activity concentrations using MODIS PIC measurements for August 2014
N
0 100 200 400 Kilometers
Legend
Greece
137Cs (Bq/m3)
< 1
1 - 2
2 - 3
3 - 4
4 - 5
>5
Predicted 137Cs activity concentrations using MODIS PIC measurements for November 2014
N
0 100 200 400 Kilometers
Legend
Greece
137Cs (Bq/m3)
< 1
1 - 2
2 - 3
3 - 4
4 - 5
>5

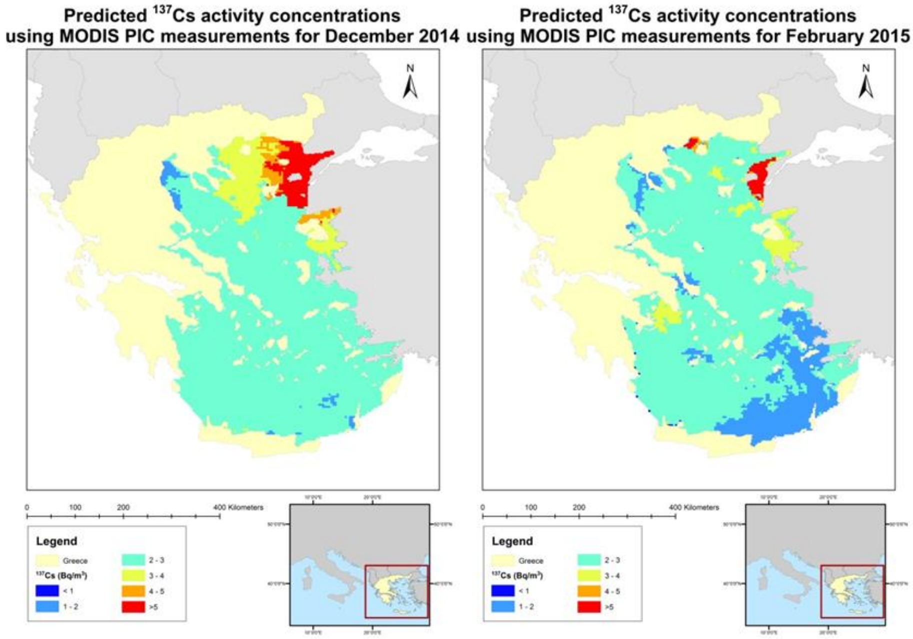

Figure 104. Predicted ^{137}Cs activity concentrations using MODIS PIC for the time period March 2012 to February 2015.

In this section the results of GWR predicted ^{137}Cs activity concentrations using MODIS PIC are being exhibited (Figure 104). By observing the results, it is evident that the models using MODIS PIC to predict the activity values, also overestimates the activity concentration values by presenting larger areas over 5 Bq/m^3. The medium categories also present larger areas than the original ^{137}Cs activity concentrations. The lesser categories have remained almost similar. The months with the least accurate activity concentration values are the months of August 2014 and November 2014. While the months with the most accurate activity concentrations are the months of March 2012, December 2012 and March 2014.

8.2.1.2.6. POC

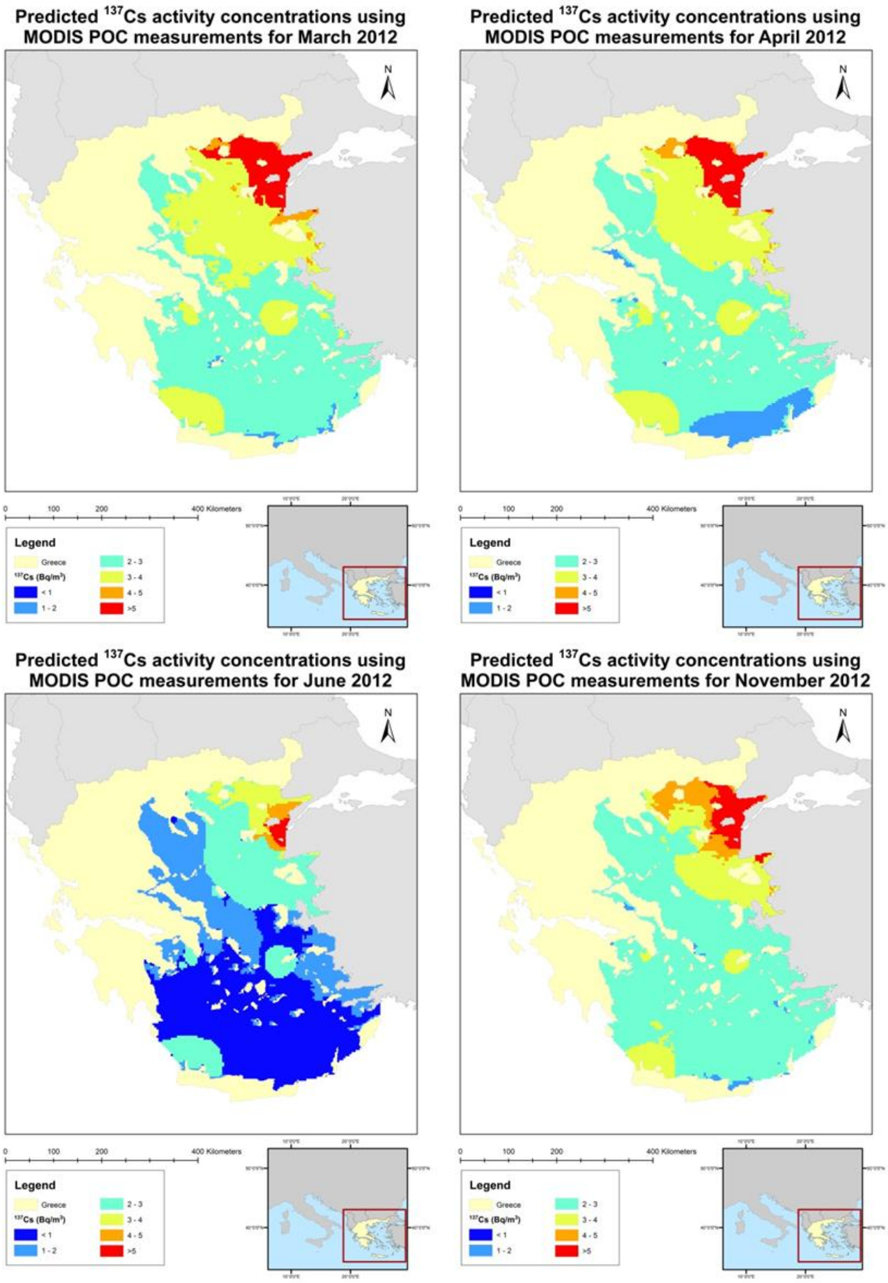
Predicted ^{137}Cs activity concentrations using MODIS POC measurements for March 2012
Predicted ^{137}Cs activity concentrations using MODIS POC measurements for April 2012
Predicted ^{137}Cs activity concentrations using MODIS POC measurements for June 2012
Predicted ^{137}Cs activity concentrations using MODIS POC measurements for November 2012
N
0 100 200 400 Kilometers
Legend
Greece
^{137}Cs (Bq/m^3)
< 1
1 - 2
2 - 3
3 - 4
4 - 5
>5

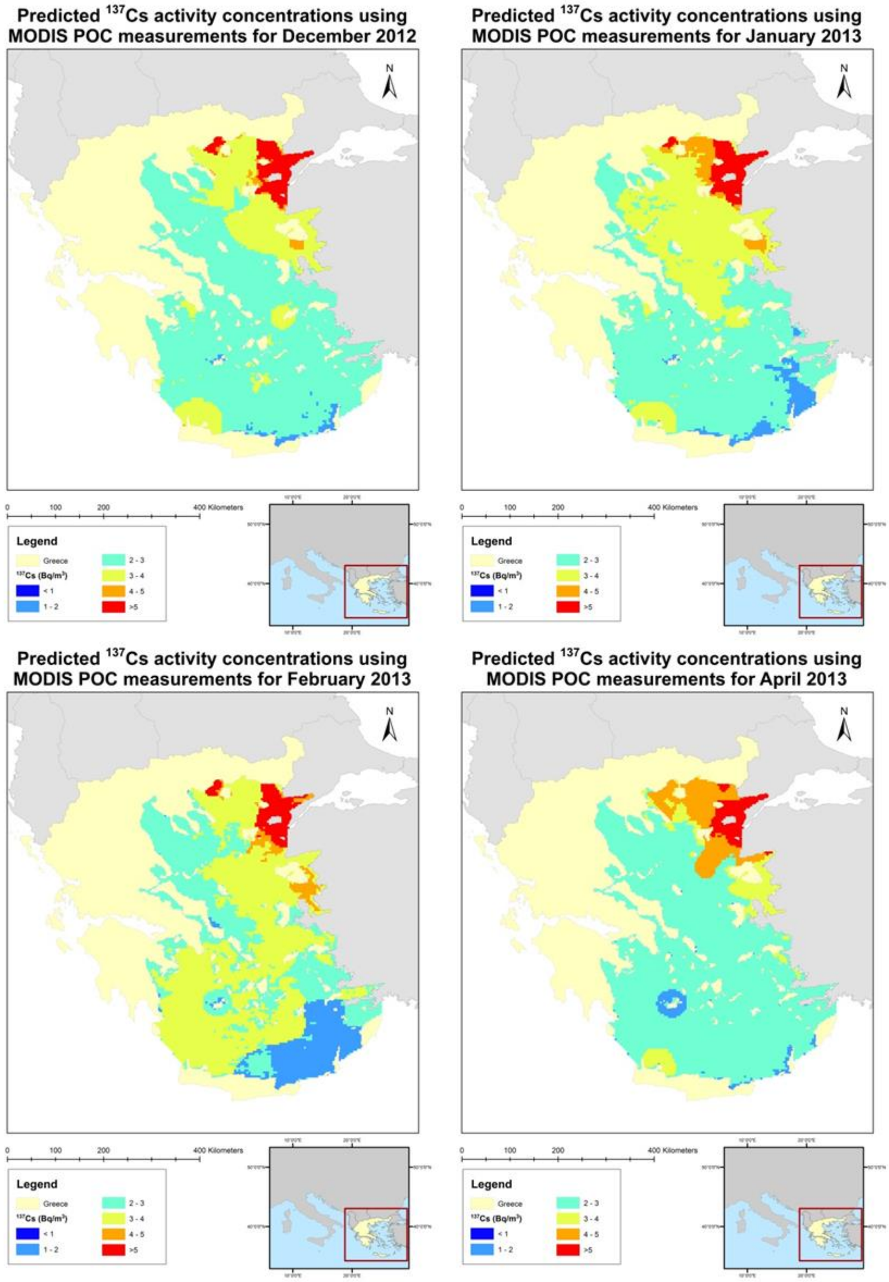
Predicted 137Cs activity concentrations using MODIS POC measurements for December 2012
N
0 100 200 400 Kilometers
Legend
Greece
137Cs (Bq/m3)
< 1
1 - 2
2 - 3
3 - 4
4 - 5
>5
Predicted 137Cs activity concentrations using MODIS POC measurements for January 2013
N
0 100 200 400 Kilometers
Legend
Greece
137Cs (Bq/m3)
< 1
1 - 2
2 - 3
3 - 4
4 - 5
>5
Predicted 137Cs activity concentrations using MODIS POC measurements for February 2013
N
0 100 200 400 Kilometers
Legend
Greece
137Cs (Bq/m3)
< 1
1 - 2
2 - 3
3 - 4
4 - 5
>5
Predicted 137Cs activity concentrations using MODIS POC measurements for April 2013
N
0 100 200 400 Kilometers
Legend
Greece
137Cs (Bq/m3)
< 1
1 - 2
2 - 3
3 - 4
4 - 5
>5

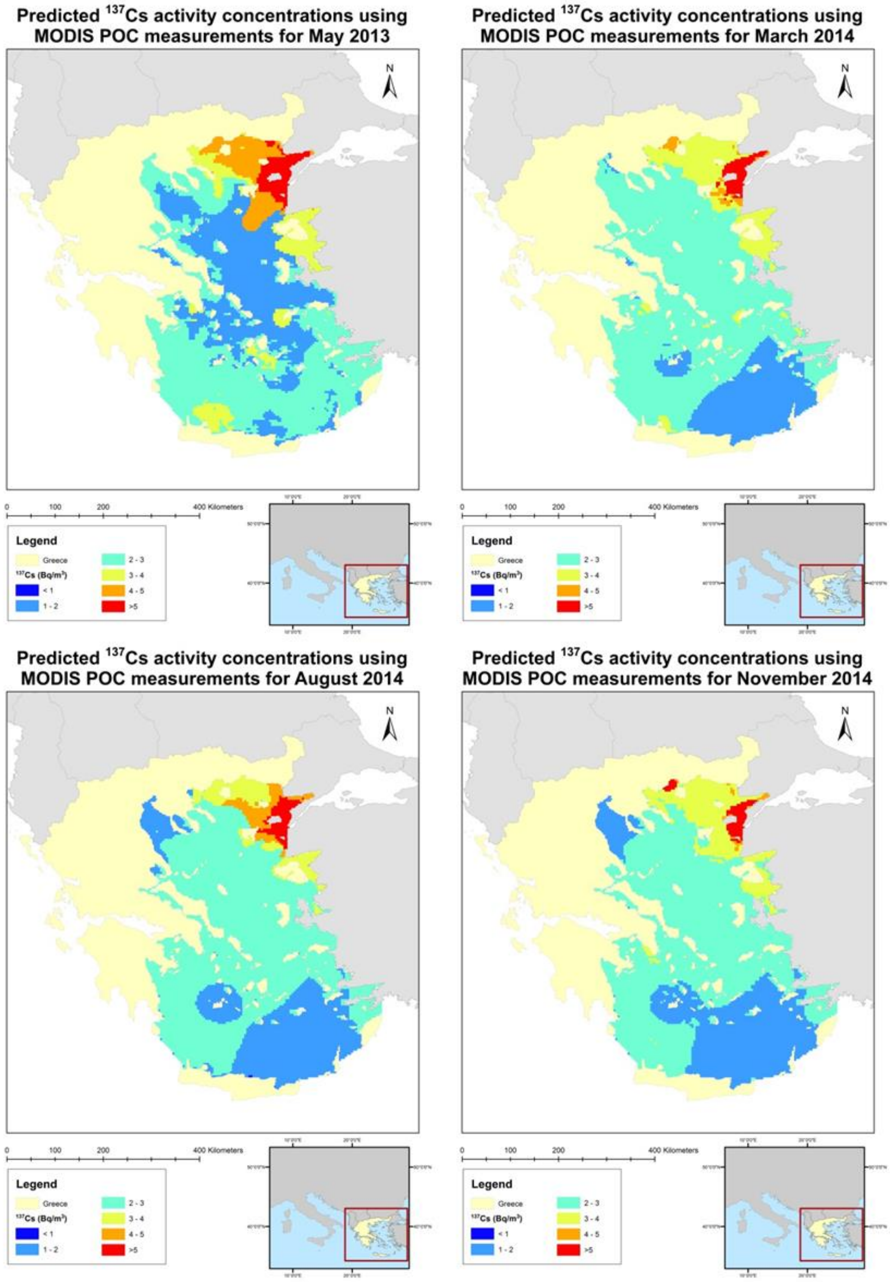
Predicted 137Cs activity concentrations using MODIS POC measurements for May 2013
N
0 100 200 400 Kilometers
Legend
Greece
137Cs (Bq/m3)
< 1
1 - 2
2 - 3
3 - 4
4 - 5
>5
Predicted 137Cs activity concentrations using MODIS POC measurements for March 2014
N
0 100 200 400 Kilometers
Legend
Greece
137Cs (Bq/m3)
< 1
1 - 2
2 - 3
3 - 4
4 - 5
>5
Predicted 137Cs activity concentrations using MODIS POC measurements for August 2014
N
0 100 200 400 Kilometers
Legend
Greece
137Cs (Bq/m3)
< 1
1 - 2
2 - 3
3 - 4
4 - 5
>5
Predicted 137Cs activity concentrations using MODIS POC measurements for November 2014
N
0 100 200 400 Kilometers
Legend
Greece
137Cs (Bq/m3)
< 1
1 - 2
2 - 3
3 - 4
4 - 5
>5

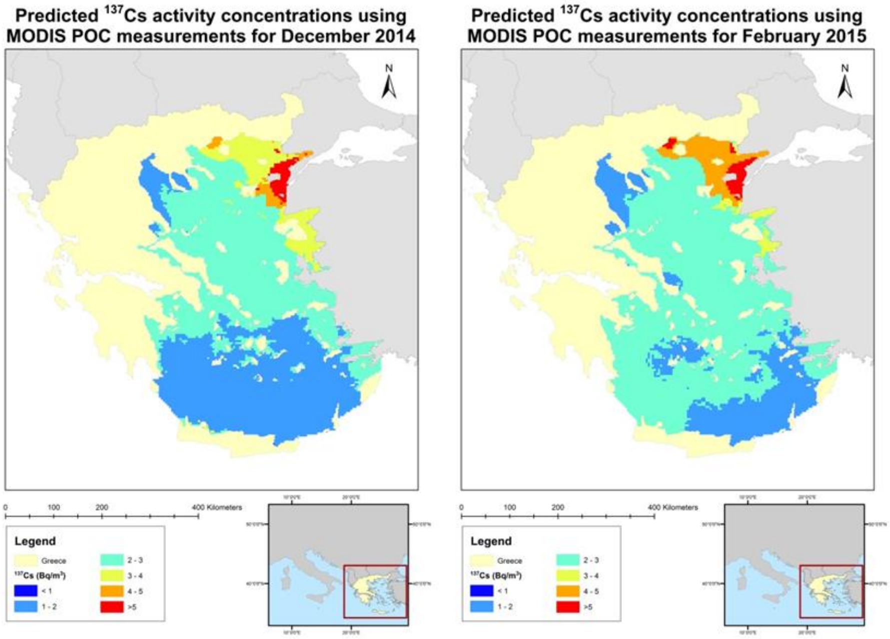

Figure 105. Predicted ^{137}Cs activity concentrations using MODIS POC for the time period March 2012 to February 2015.

The results of GWR predicted ^{137}Cs activity concentrations using MODIS POC are being displayed in this section (Figure 105). Like the models using the other MODIS parameters, the models using MODIS POC also overestimate the activity concentrations values, presenting larger areas over 5 Bq/m^3. In addition the overestimation, the model underestimated the values in several months, presenting larger areas with values under 2 Bq/m^3. The months that present the least accurate results are the months of June 2012 and February 2013. While the months that present the most accurate activity concentrations results are the months of April 2012 and November 2014.

8.2.1.2.7. IPAR

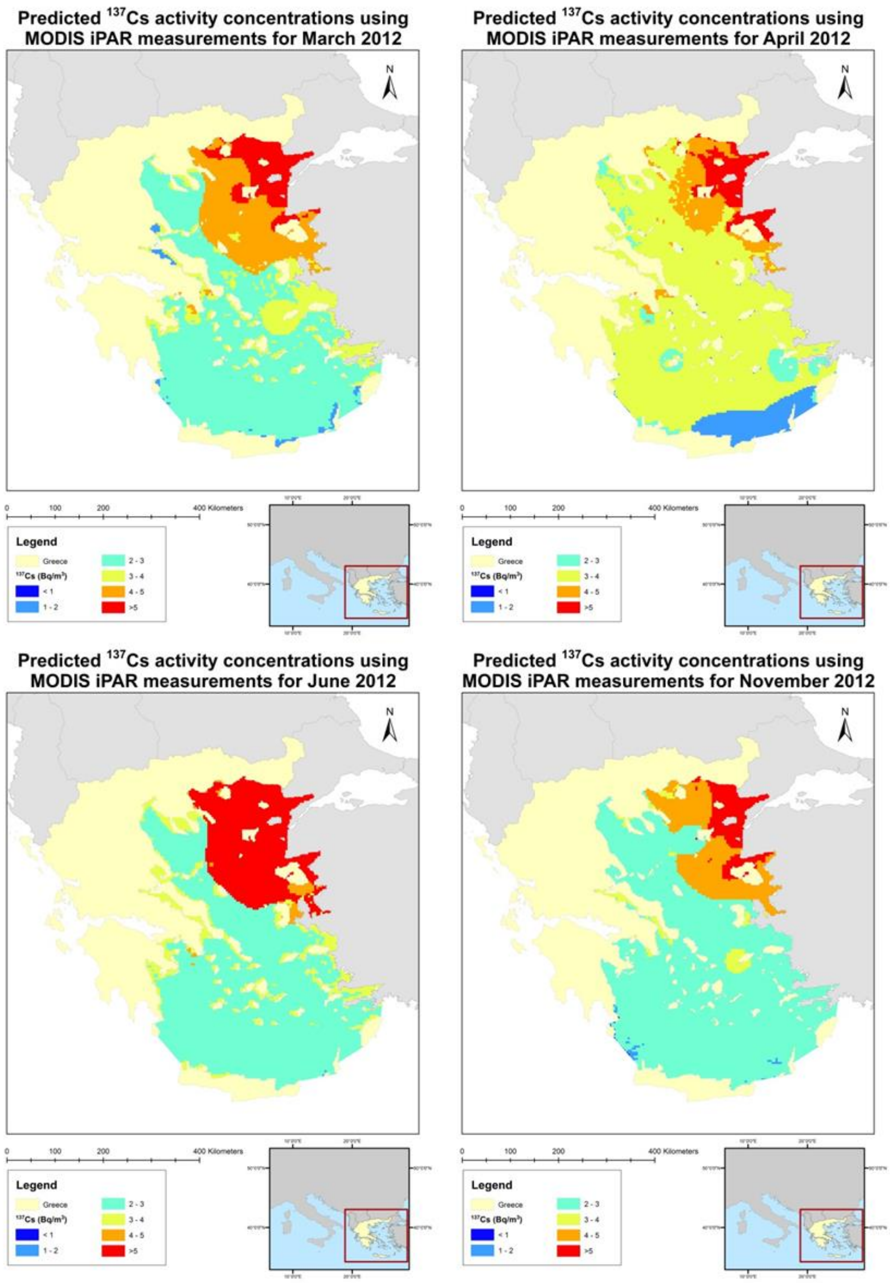

Predicted 137Cs activity concentrations using MODIS iPAR measurements for March 2012
Predicted 137Cs activity concentrations using MODIS iPAR measurements for April 2012
Predicted 137Cs activity concentrations using MODIS iPAR measurements for June 2012
Predicted 137Cs activity concentrations using MODIS iPAR measurements for November 2012
N
0 100 200 400 Kilometers
Legend
Greece
137Cs (Bq/m3)
< 1
1 - 2
2 - 3
3 - 4
4 - 5
>5

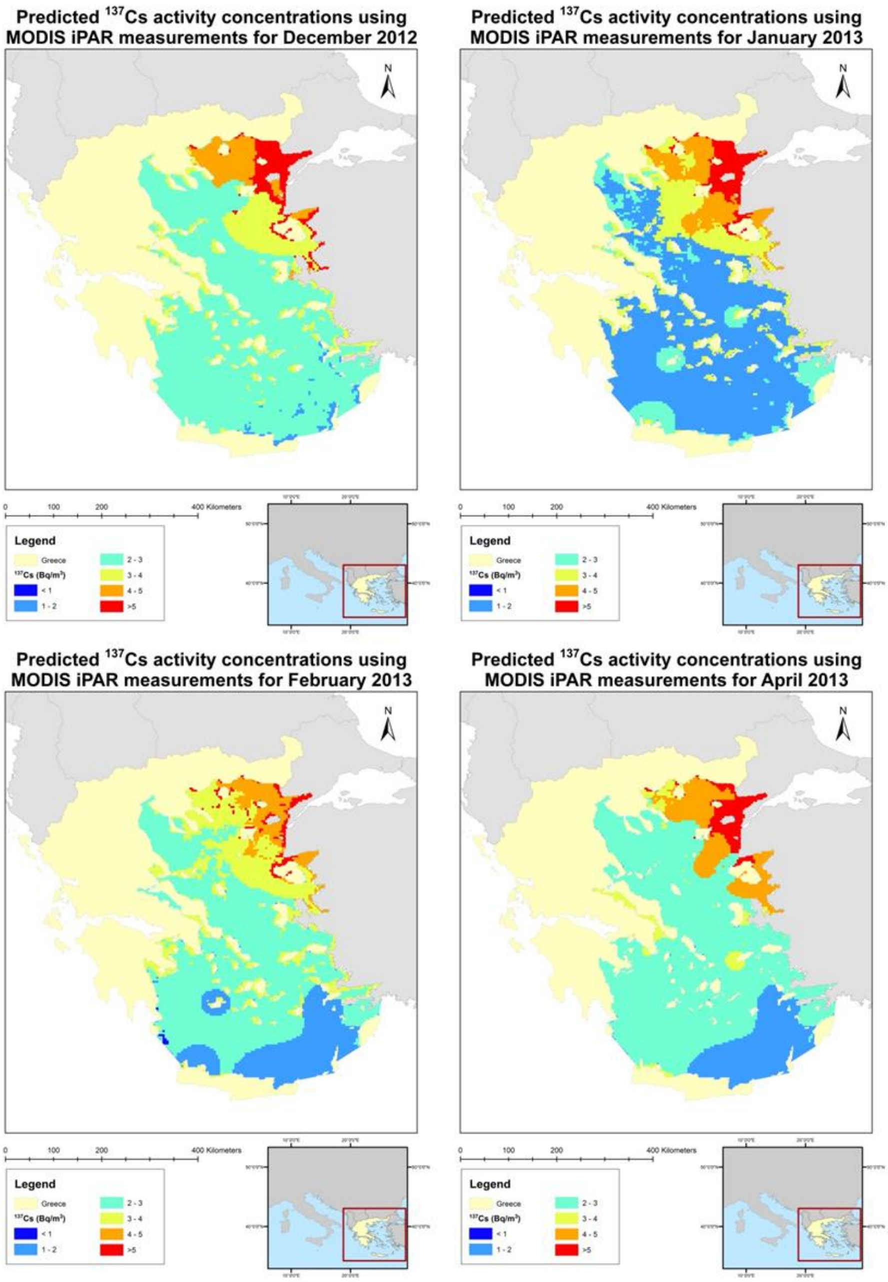
Predicted 137Cs activity concentrations using MODIS iPAR measurements for December 2012
Predicted 137Cs activity concentrations using MODIS iPAR measurements for January 2013
Predicted 137Cs activity concentrations using MODIS iPAR measurements for February 2013
Predicted 137Cs activity concentrations using MODIS iPAR measurements for April 2013
N
0 100 200 400 Kilometers
Legend
Greece
137Cs (Bq/m3)
< 1
1 - 2
2 - 3
3 - 4
4 - 5
>5

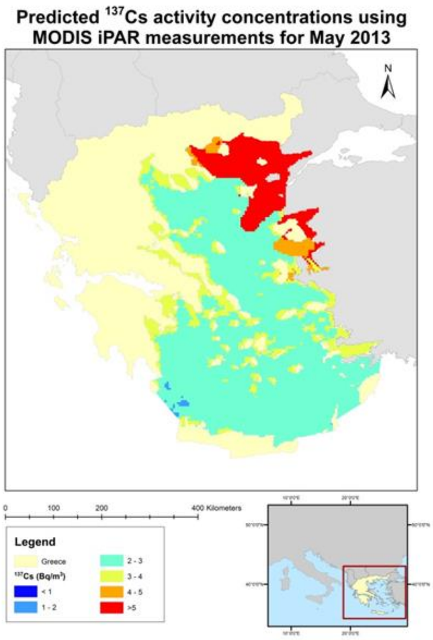
Predicted ^{137}Cs activity concentrations using MODIS iPAR measurements for May 2013
N
0 100 200 400 Kilometers
Legend
Greece
^{137}Cs (Bq/m^3)
< 1
1 - 2
2 - 3
3 - 4
4 - 5
>5

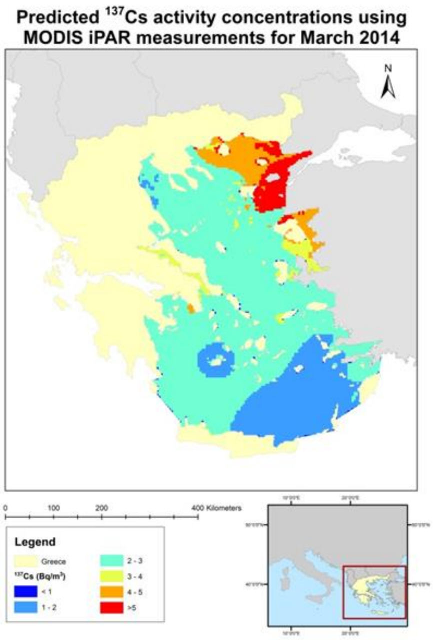
Predicted ^{137}Cs activity concentrations using MODIS iPAR measurements for March 2014
N
0 100 200 400 Kilometers
Legend
Greece
^{137}Cs (Bq/m^3)
< 1
1 - 2
2 - 3
3 - 4
4 - 5
>5

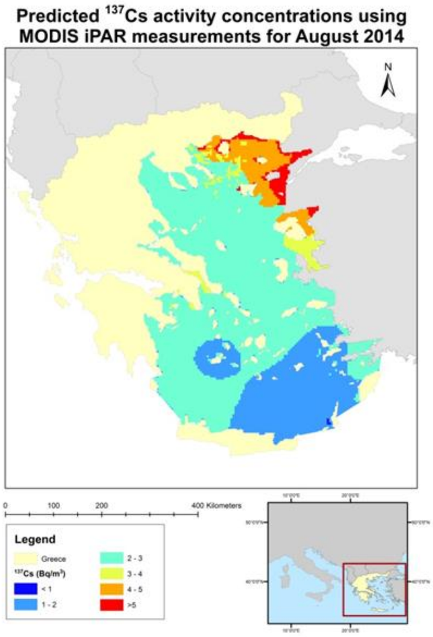
Predicted ^{137}Cs activity concentrations using MODIS iPAR measurements for August 2014
N
0 100 200 400 Kilometers
Legend
Greece
^{137}Cs (Bq/m^3)
< 1
1 - 2
2 - 3
3 - 4
4 - 5
>5

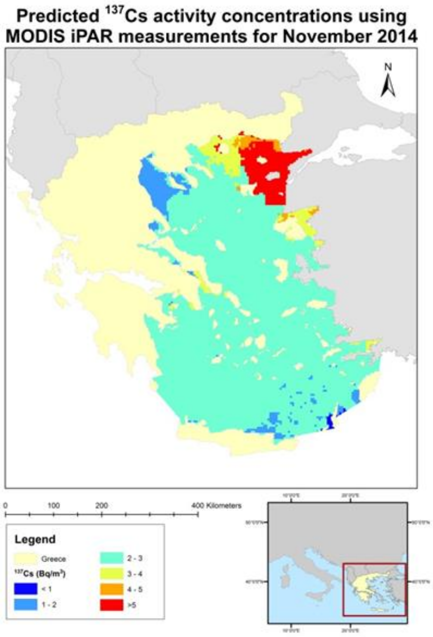
Predicted ^{137}Cs activity concentrations using MODIS iPAR measurements for November 2014
N
0 100 200 400 Kilometers
Legend
Greece
^{137}Cs (Bq/m^3)
< 1
1 - 2
2 - 3
3 - 4
4 - 5
>5

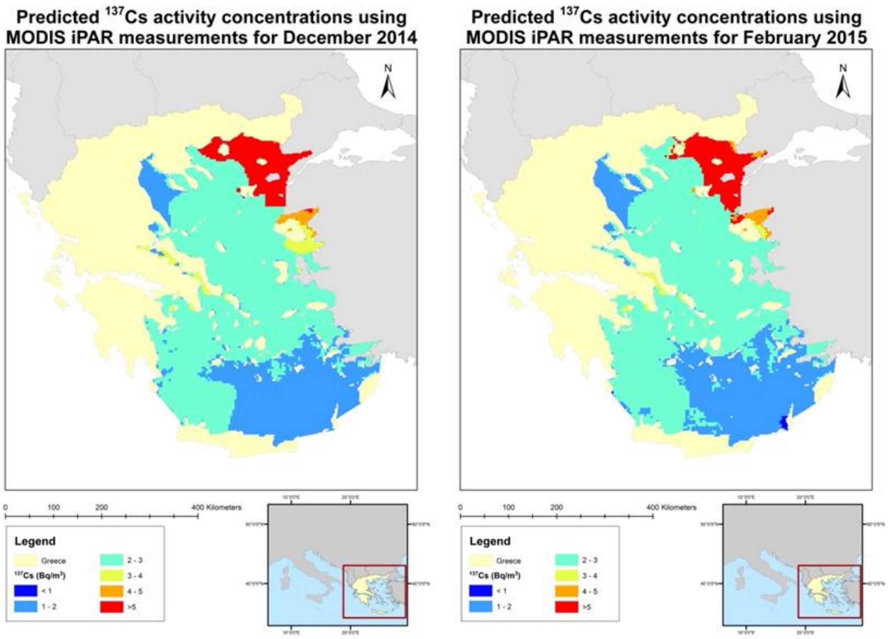

Figure 106. Predicted ^{137}Cs activity concentrations using MODIS iPAR for the time period March 2012 to February 2015.

In this part the results of the GWR predicted activity concentrations using MODIS iPAR are being shown (Figure 106). In the same manner as the models using MODIS SSTnight, MODIS SST4night, MODIS SSTmorning, MODIS Chlor_a, MODIS PIC and MODIS POC, these models also overestimate the concentration values, presenting larger areas over 5 Bq/m^3. Another observation is the underestimation of the ^{137}Cs activity concentration values, presenting larger areas under 2 Bq/m^3. The medium categories have remained quite similar with the original categories (except for the month of April 2012). The months with the least accurate concentration values are the months of April 2012 and January 2013. While the month with the most accurate activity concentrations is the month of February 2013.

8.2.1.2.8. PAR

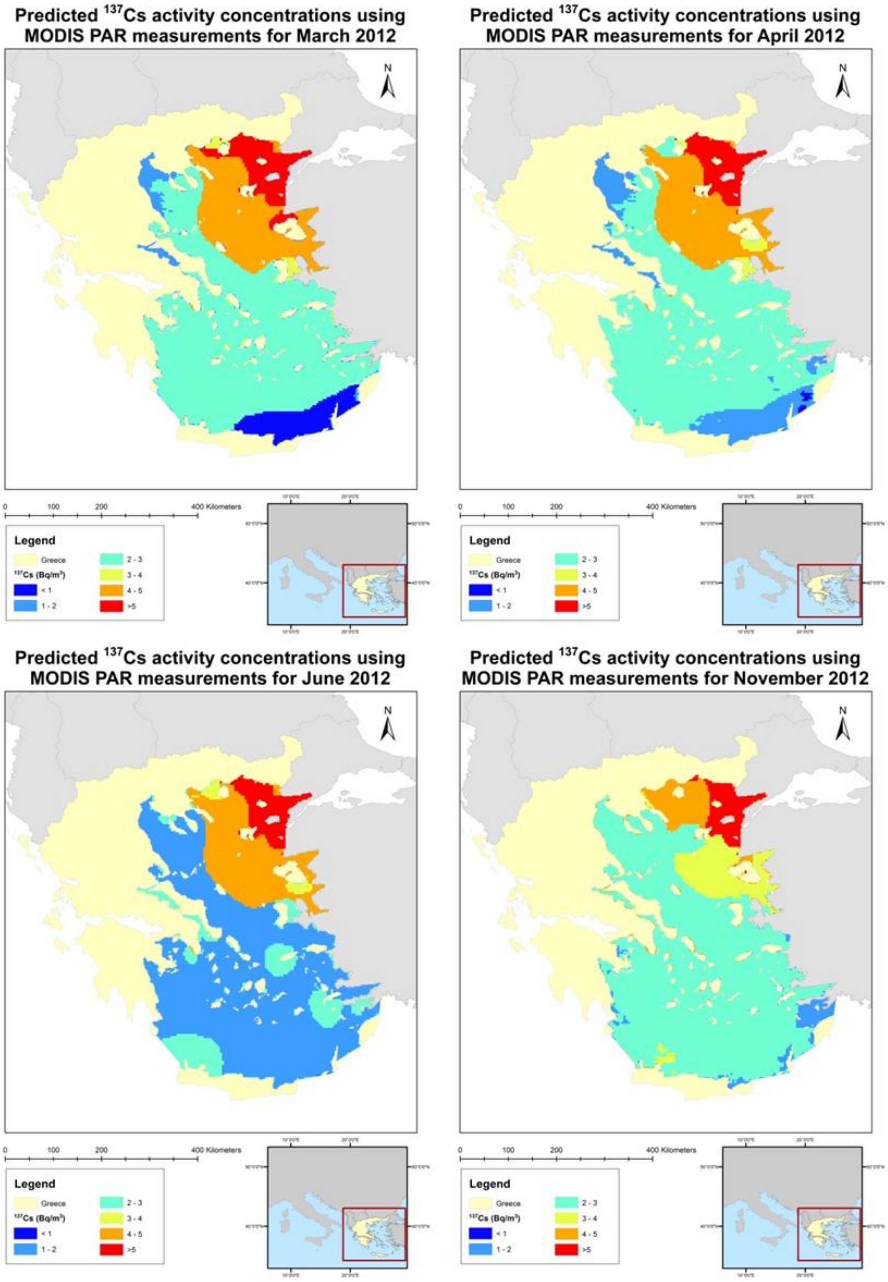
Predicted ^{137}Cs activity concentrations using MODIS PAR measurements for March 2012
Predicted ^{137}Cs activity concentrations using MODIS PAR measurements for April 2012
Predicted ^{137}Cs activity concentrations using MODIS PAR measurements for June 2012
Predicted ^{137}Cs activity concentrations using MODIS PAR measurements for November 2012
N
0 100 200 400 Kilometers
Legend
Greece
^{137}Cs (Bq/m^3)
< 1
1 - 2
2 - 3
3 - 4
4 - 5
>5

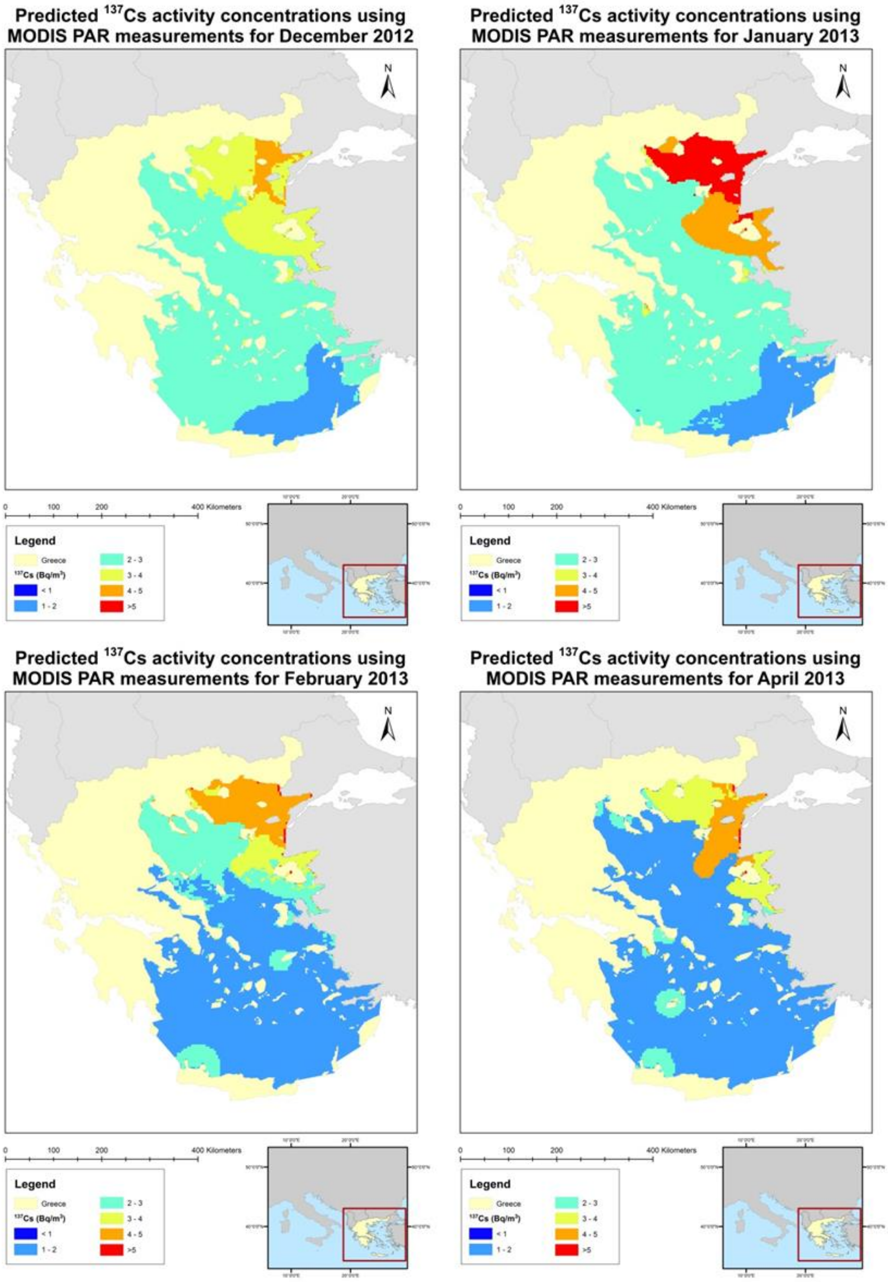
Predicted 137Cs activity concentrations using MODIS PAR measurements for December 2012
Predicted 137Cs activity concentrations using MODIS PAR measurements for January 2013
Predicted 137Cs activity concentrations using MODIS PAR measurements for February 2013
Predicted 137Cs activity concentrations using MODIS PAR measurements for April 2013
N
0 100 200 400 Kilometers
Legend
Greece
137Cs (Bq/m3)
< 1
1 - 2
2 - 3
3 - 4
4 - 5
>5

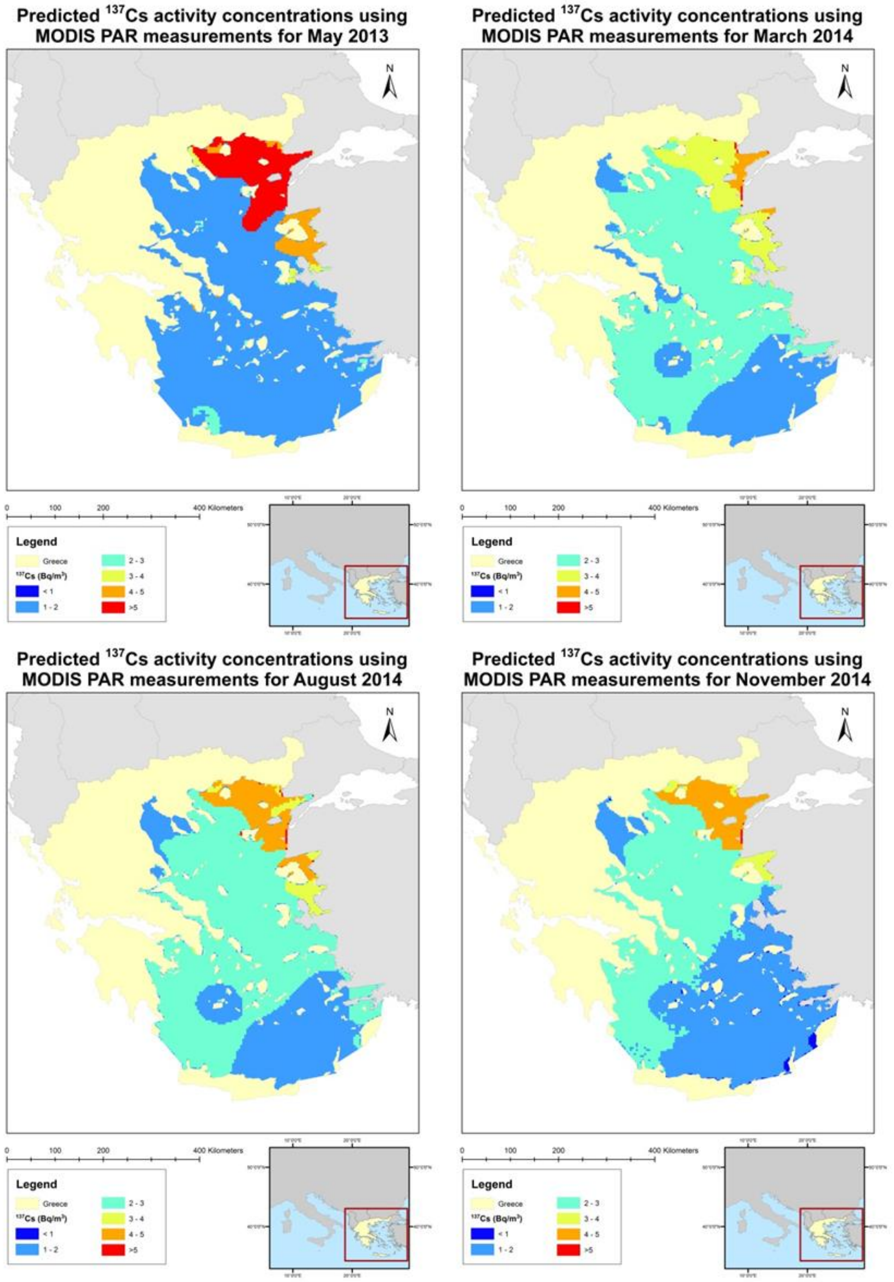
Predicted 137Cs activity concentrations using MODIS PAR measurements for May 2013
Predicted 137Cs activity concentrations using MODIS PAR measurements for March 2014
Predicted 137Cs activity concentrations using MODIS PAR measurements for August 2014
Predicted 137Cs activity concentrations using MODIS PAR measurements for November 2014
N
0 100 200 400 Kilometers
Legend
Greece
137Cs (Bq/m3)
< 1
1 - 2
2 - 3
3 - 4
4 - 5
>5

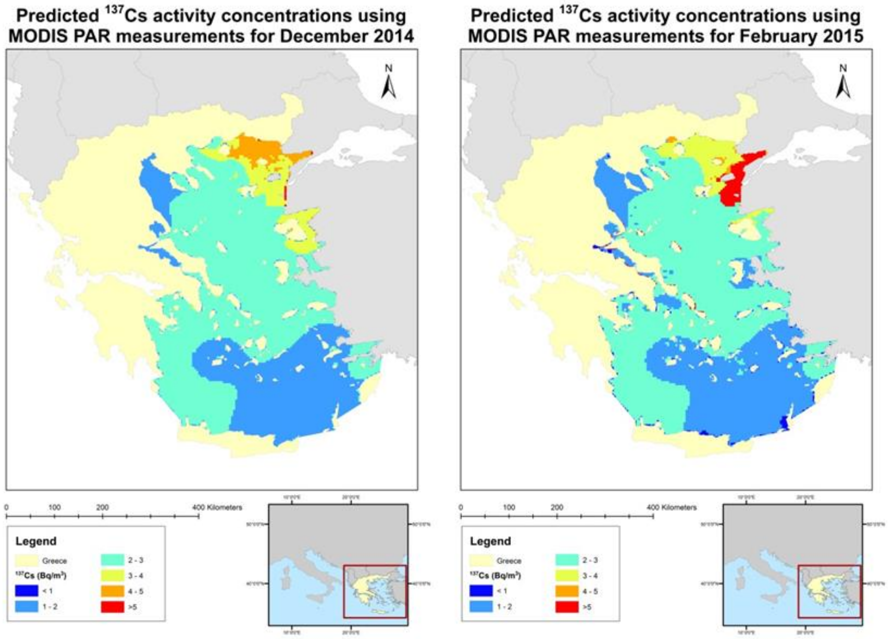

Figure 107. Predicted ^{137}Cs activity concentrations using MODIS PAR for the time period March 2012 to February 2015.

In this section the results of GWR predicted ^{137}Cs activity concentrations using MODIS PAR are being presented (Figure 107). By observing the results, it is evident that there is an overestimation of the values in the same manner as the models using other MODIS parameters. However this model that used MODIS PAR mainly underestimated the activity concentrations, presenting larger areas under 2 Bq/m^3 in comparison to the original values. The months presenting the least accurate values are the months of June 2012, February 2013, April 2013 and May 2013. While the months presenting the most accurate activity concentration values are the months of December 2014 and February 2015.

9. Discussion

In this study, with the use of remote sensing satellite data, in situ marine data and ^{137}Cs activity concentrations, an analysis for the potential relations of ^{137}Cs with satellite and in situ parameters has been performed. The purpose of this study was to investigate the potential relations of ^{137}Cs activity concentration with SMOS data (SST Ascending, SST Descending), MODIS data (SSTnight, SST4night, SSTmorning, Chlor_a, PIC, POC, CDOM index, iPAR, PAR) and POSEIDON data (SST, SSS, Chlor_a). For the area of Souda Bay in Crete, temporal statistical analyses using linear and second degree polynomial regression have been performed. Also map analyses in a GIS using spatial linear regression have been implemented for the Aegean Sea for three years.

9.1. Souda Bay

The first set of results presented, were the Souda Bay relations, using temporal regression, of ^{137}Cs activity concentrations and MODIS satellite parameters for the time period of March 2011 to February 2015. Temporal regression was performed in two ways; linear and second degree polynomial regression, while including and excluding errors. This is done in order to observe the influence of ^{137}Cs activity errors on the regression results. These results show that the polynomial regression models seem to describe better the relations of ^{137}Cs activity concentration and MODIS ocean parameters. The parameters presenting the best r^2 values are MODIS SSTnight (r^2= 0.53), MODIS SST4night (r^2= 0.64), MODIS PIC (r^2= 0.56) and MODIS CDOM (r^2 = 0.69) (Table 5). The relations of ^{137}Cs with Sea Surface Temperature may probably be due to sea water density, where when the temperature rises, due to evaporation, the density is higher; thus, resulting to a higher ^{137}Cs activity concentration. The relations of ^{137}Cs with PIC and CDOM are currently under investigation, but the relations may be due to the particular form of ^{137}Cs, which constitutes the 23% of the distribution form in aquatic environments (Polikarpov, 1966). Moreover it was observed that the relations with SST were better in point 1, mainly due to the close proximity of this point to the Souda Bay sea water sampling station. In addition inside the Souda Bay (point 1) ^{137}Cs activity concentrations showed better relations with SST, whereas outside the Souda Bay (point 5) ^{137}Cs concentrations showed better relations with

PIC; this is also currently under investigation and it is probably because the particulate matter in the Bay is higher than outside, which results to co-precipitation on ^{137}Cs. Concerning the relations of ^{137}Cs with MODIS SSTnight, SST4night and SSTmorning, ^{137}Cs with MODIS SSTmorning do not show any significant relations; this may be due to the fluctuations of the temperature during the day and the stability of the temperature during the night. The models using POC and Chlor_a did not show any significant relations with ^{137}Cs activity concentrations. Furthermore, iPAR and PAR present a low correlation in all MODIS Souda Bay points, which may be explained by the relation of energy flux and temperature, where the greater the energy flux, the higher the temperature rises. It is also important to be noted, that the ^{137}Cs activity concentration errors, affect the results of the regressions performed. It is observed that most r^2 values are higher when the activity errors are included. However in some cases the r^2 values are higher when the activity errors are not included. This is also under investigation.

	Table of r^2 values per point and per parameter for the Souda Bay area describing the second degree polynomial relation of ^{137}Cs and MODIS parameters																	
	SSTnight		SST4night		SSTmorning		Chlor_a		PIC		POC		CDOM		iPAR		PAR	
	Incl. Errors	Excl. Errors	Incl. Errors	Excl. Errors	Incl. Errors	Excl. Errors	Incl. Errors	Excl. Errors	Incl. Errors	Excl. Errors	Incl. Errors	Excl. Errors	Incl. Errors	Excl. Errors	Incl. Errors	Excl. Errors	Incl. Errors	Excl. Errors
Point 1	0.38	**0.53**	0.41	**0.64**	0.32	0.08	0.05	0.03	0.26	0.07	0.14	0.01	-	-	0.16	0.31	0.14	**0.47**
Point 2	0.24	0.02	0.06	0.02	0.24	0.04	0.03	0.03	0.15	0.13	0.04	0.04	**0.69**	0.16	0.22	0.26	0.11	0.43
Point 3	0.05	0.03	0.08	0.08	0.17	0.03	0.05	0.05	0.12	0.20	0.07	0.06	0.39	0.12	0.09	0.32	0.10	**0.47**
Point 4	0.02	0.04	0.04	0.04	0.23	0.08	0.03	0.01	0.21	0.05	0.05	0.01	0.02	0.30	0.18	0.28	0.13	0.41
Point 5	0.27	0.06	0.03	0.05	0.25	0.03	0.03	0.03	0.44	**0.56**	0.05	0.06	0.23	0.16	0.14	0.30	0.15	0.39

Table 5. Table of r^2 values per point and per parameter for the Souda Bay area describing the second degree polynomial relation of ^{137}Cs and MODIS parameters.

The second set of results presented, were the Souda Bay relations, using temporal regression, of ^{137}Cs activity concentrations and SMOS SST for the time period of March 2011 to February 2015. In the same manner like the MODIS parameter analysis, temporal regression was performed in two ways; linear and second degree polynomial regression, while including and excluding errors. However, unlike with MODIS SST, the models using SMOS SST do not sufficiently describe the relation with ^{137}Cs activity concentrations. This phenomenon is possibly explained by the distance of at least 50km that SMOS points have from the Souda Bay sampling station. The r^2 results are similar for all the 5 SMOS points of study. That probably indicates that the temperature values between points are also similar. In addition, there is a great difference between the SST_Ascending and the SST_Descending r^2 results, with SST_Ascending r^2 values being higher that SST_Descending r^2 values (Table 6). This is maybe due to the different Tbrightness (Tb) values from the different acquisition incident angle values between Ascending and Descending passes.

Table of r^2 values per point and per parameter for the Souda Bay area describing the second degree polynomial relation of ^{137}Cs and SMOS parameters				
	SST_A		SST_D	
	Incl. Errors	Excl. Errors	Incl. Errors	Excl. Errors
Point 26	0.16	0.26	0.19	0.08
Point 27	0.16	0.25	0.19	0.09
Point 32	0.16	0.25	0.19	0.10
Point 36	0.16	0.26	0.18	0.11
Point 38	0.17	0.27	0.18	0.11

Table 6. Table of r^2 values per point and per parameter for the Souda Bay area describing the second degree polynomial relation of ^{137}Cs and SMOS parameters.

The third set of results presented, were the Souda Bay relations, using temporal regression, of ^{137}Cs activity concentrations and POSEIDON marine parameters for the time period of March 2011 to February 2015. In the same manner as the previous Souda Bay analyses, temporal regression was performed in two ways; linear and second degree polynomial regression, while including and excluding errors. Results showed that there are relations between the ^{137}Cs activity concentrations and POSEIDON parameters, even though the E1M3A buoy is quite far from the Souda Bay sampling station. Activity concentration errors seem to effect positively the regression, however the effect of the activity concentration errors on regression results is currently under investigation. The r^2 values for each parameter can be seen in table 7, where the SST relations with ^{137}Cs are possibly explained by density, and the relations of Chlor_a and SSS are currently under investigation.

Table of r^2 values per parameter for the Souda Bay area describing the second degree polynomial relation of ^{137}Cs and POSEIDON parameters						
	SST		Chlor_a		SSS	
	Incl. Errors	Excl. Errors	Incl. Errors	Excl. Errors	Incl. Errors	Excl. Errors
Souda Bay	**0.62**	**0.48**	**0.59**	**0.48**	**1**	**1**

Table 7. Table of r^2 values per parameter for the Souda Bay area describing the second degree polynomial relation of ^{137}Cs and POSEIDON parameters.

9.2. Aegean Sea

The next set of results presented, were the monthly GWR local r^2 maps, of ^{137}Cs activity concentrations and MODIS parameters. As it was aforementioned GWR is a spatial form of linear regression. The maximum r^2 values per month and per parameter are shown in table 8.

The first parameter that was analyzed for potential relations with ^{137}Cs activity concentrations was MODIS SSTnight parameter. The month that presented the best r^2 value was March 2014, with an r^2 value of 0.47, which was located in the coastal area of North Aegean. This relation may be due to the water density. The spatial distribution of the values is characterized by higher r^2 values near the coastlines and lower values in Central Aegean; this dispersion seems to be affected by the location of the sampling stations.

The next parameter that was analyzed for potential relations with ^{137}Cs activity concentrations was MODIS SST4night parameter. The months that presented the best r^2 values are the months of November 2012 and February 2015 with r^2 values of 0.59 and 0.63 respectively; this shows that in the location of these values, the models using SST4night can explain the ^{137}Cs activity concentrations. These locations are on the South Aegean Sea near the Island of Crete. Again the spatial distribution of the r^2 values is affected by the sampling points and presenting higher values near the coast line and lower value in the Center Aegean Sea.

Then the parameter that was analyzed for potential relations with ^{137}Cs activity concentrations was MODIS SSTmorning parameter. Unlike the linear models using MODIS SSTnight and SST4night, the models using SSTmorning do not seem to adequately explain the ^{137}Cs activity concentrations in the Aegean Sea, presenting r^2 values below 0.3. This phenomenon may be due to the temperature fluctuations during the day. The spatial distribution for this parameter does not show any significant variation (spatially and seasonally).

The fourth parameter that was analyzed for potential relations with ^{137}Cs activity concentrations was MODIS Chlor_a parameter. The best r^2 value (r^2= 0.59) observed for January 2013, and located in Central Aegean. The rest of the months showed no significant relations. The relation of ^{137}Cs activity concentrations and MODIS Chlor_a is currently under investigation. The spatial distribution using the Chlor_a parameter, is quite different from the previous ones; with higher values concentrated in Central Aegean, around the Cyclades islands. It seems that the distribution may be influenced by the Chlor_a concentrations distribution in the Aegean Sea, where they are higher in the Northern Aegean and the coastal areas and lower in Central and South Aegean.

The fifth parameter that was analyzed for potential relations with ^{137}Cs activity concentrations was MODIS PIC parameter. The best r^2 values are present in the months of May 2013 (r^2= 0.55), March 2014 (r^2= 0.88) and February 2015(r^2= 0.81), and are located in Central and South Aegean Sea. These relations may be due to the particular form of ^{137}Cs. The spatial distribution is characterized by higher values around Milos Island, probably influenced by the sampling station in that area. As it was mentioned before, the GWR results are influenced by the input datasets.

The sixth parameter that was analyzed for potential relations with ^{137}Cs activity concentrations was MODIS POC parameter. The best r^2 value of 0.67 is present during the month of January 2013and is located south of Peloponnesus; the rest of the r^2 values are below 0.45. The relations between ^{137}Cs activity concentrations and MODIS POC are currently being studied. In the same manner as the distribution by using MODIS PIC, the spatial distribution using the POC parameter seems to be also influenced by the Milos Island sampling station. The current spatial dispersion is also influenced by the Dardanelles sampling station.

The final parameters that were analyzed for potential relations with ^{137}Cs activity concentrations were MODIS iPAR and PAR parameters. Concerning the iPAR parameter, the r^2 values presented, are below 0.40; thus the linear models using MODIS iPAR do not sufficiently explain the ^{137}Cs activity concentrations in the Aegean Sea. This observation about the ^{137}Cs and MODIS iPAR relations is currently being examined. The spatial distribution of the r^2 values is characterized by the concentration of the higher values near the Souda Bay area, while presenting an influence from the iPAR dispersion. Concerning the PAR parameter, the best r^2 value (r^2= 0.77) is present during February 2015 and is located near the Souda Bay. This relation may be probably present due to the relation of energy flux and temperature; the higher the energy flux is, the higher the temperature rises. The spatial distribution of the r^2 values is characterized by the concentration of the higher values in the Southern Aegean Sea. The distribution seems to be influenced by the location of the sampling stations.

Generally the spatial linear regression using GWR seem to adequately describe the ^{137}Cs activity concentrations in the locations where the local r^2 values greater than 0.5. One of the most important observations is that the r^2 spatial dispersion patterns were influenced by the input dataset of measurements due to the limitations of GWR. Another important observation is that that the maximum values are present during the winter and spring period.

Table of maximum r^2 values per month and per parameter for the Aegean Sea								
	SSTnight	SST4night	SSTmorning	Chlor_a	PIC	POC	iPAR	PAR
March 2012	0.33	0.29	0.11	0.46	0.02	0.24	0.24	0.40
April 2012	0.46	0.32	0.31	0.03	0.15	0.22	0.17	0.17
June 2012	0.28	0.27	0.28	0.02	0.14	0.35	0.16	0.19
November 2012	0.16	**0.59**	0.25	0.04	0.16	0.29	0.12	0.18
December 2012	0.26	0.20	0.28	0.23	0.47	0.44	0.06	0.09
January 2013	0.35	0.42	0.18	**0.59**	0.16	**0.67**	0.29	0.14
February 2013	0.35	0.31	0.34	0.33	0.24	0.45	0.27	0.13
April 2013	0.45	0.30	0.14	0.06	0.32	0.17	0.22	0.24
May 2013	0.35	0.28	0.28	0.04	**0.55**	0.25	0.06	0.22
March 2014	0.47	0.19	0.33	0.14	**0.88**	0.17	0.40	0.11
August 2014	0.06	0.006	0.001	0.03	0.03	0.34	0.29	0.15
November 2014	0.30	0.38	0.45	0.15	0.09	0.32	0.21	0.15
December 2014	0.37	0.21	0.22	0.22	0.36	0.36	0.20	0.07
February 2015	0.41	**0.63**	0.32	0.37	**0.81**	0.19	0.26	**0.77**

Table 8. Table of maximum r^2 values per month and per parameter for the Aegean Sea.

The second result of the GWR presented was the monthly GWR maps of predicted ^{137}Cs activity concentrations by using MODIS parameters. These results showed the accuracy of the models used. The maps were examined for their accuracy by comparing then to the actual ^{137}Cs activity concentrations maps from the spatial database.

At first were the ^{137}Cs activity concentrations predictions using SSTnight. The predicted values-concentrations follow the pattern of the actual measurements where the higher concentrations are located in the Dardanelles and North Aegean, while the lower activity concentrations are present in the Southern Aegean. The best accurate predictions were for the months of November 2014 and December 2014, where the most similarities in the concentrations were observed. The prediction models seemed to both overestimate and underestimate the concentration values by presenting larger areas over 5 Bq/m^3 and larger areas below 2 Bq/m^3. In other words, by applying the MODIS data to the GWR, the predicted values of ^{137}Cs show better congruence with the upper and lower part of the value spectrum than the middle ones. The exact same phenomena were observed with models using the rest MODIS parameters. The model estimated concentrations that belong to the extreme categories and significantly reduced the values belonging to the middle concentration categories. The exact same phenomena were observed with the regression models using the rest of the MODIS parameters. Where for the models using SSTnight the most accurate prediction was the months of November 2014 and December 2014, for the models using SST4night the most accurate prediction was the month of March 2012, for the models using SSTmorning the most accurate concentration prediction was for the months of April 2012 and December 2014, for the models using Chlor_a the most accurate prediction was for the month of February 2015, for the models using PIC the most accurate predictions were for the months March 2012, December 2012 and March 2014 (Figure 108), for the models using POC the most accurate predictions were for the months of April 2012 and November 2014, for the models using iPAR the most accurate prediction was for the month of February 2013 and finally for the models using PAR the most accurate predictions were for the months of December 2014 and February 2015.

As it was aforementioned all the predictions followed the pattern of the actual measurements where the ^{137}Cs activity concentrations were higher near the Dardanelles and Northern Aegean Sea and lower in Central and South Aegean. These predictions confirmed that during the winter season there is a greater estimation of the values using MODIS parameters than the summer season. The predictions also confirmed the relations between ^{137}Cs and MODIS parameters for the best estimated months; because for the months and parameters where the estimation is better, the r^2 value is higher.

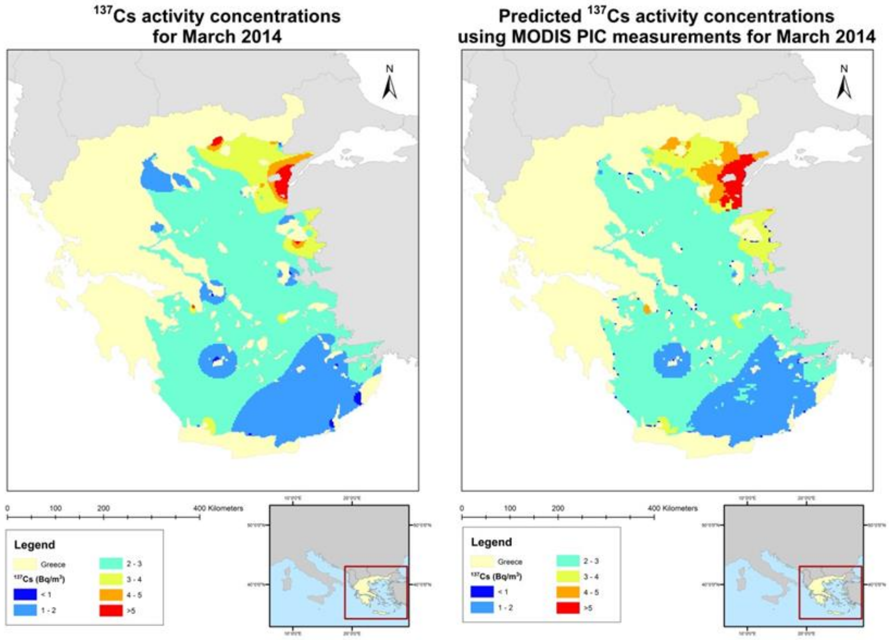

Figure 108. Best estimation of ^{137}Cs activity concentrations (March 2014).

This is an ongoing study and future work will include a more systematic and conjoined with simultaneous satellite passes, sea water sampling from the Aegean Sea and Eastern Mediterranean region. In addition new laboratory analyses will be performed for the new samplings. Equally important are the retrievals of ocean parameters from currently used and other satellite systems. In other words the data of this study are continuously updated, in combination with new measurements in areas that did not participate in the current samplings. Furthermore, a study of the effect of activity errors in regression and a study of the relations found according to the marine characteristics of each area is currently in progress. Also, other types of non-linear regression like logarithmic, exponential, Gaussian and trigonometric are currently under investigation, in order to find the optimal type of regression that best describes the relations of ^{137}Cs with the marine parameters and estimates best the predicted ^{137}Cs activity concentrations. Also analyses by exploring other methods of analysis in combination with GIS will be performed for a point to point comparison between the

^{137}Cs activity concentrations and the marine parameters; these methods will potentially be able to overcome the GIS-GWR limitations encountered in this study. Therefore, a more integrated system based on GIS fed by real time data according to the satellite passes is expected to illustrate the remote radiological image; thus a toolbox including all the necessary parameters is under consideration.

CONCLUSIONS

The results of this study can be concluded as follows:

1. SOUDA BAY

- The second degree polynomial regression models seem to describe better the relation between ^{137}Cs activity concentrations and marine parameters then the linear ones.
- The MODIS parameters that presented the best relations with ^{137}Cs activity concentrations in Souda Bay were SSTnight, SST4night and PIC.
- SMOS SST presented no significant relation with ^{137}Cs activity concentrations due to long distance between SMOS points and Souda Bay sampling station. More focused work has to be done to explore possible further relation.
- SMOS SST_Asceding presented better results than SST_Descending due to the different incident acquisition angle values, which influence the Tbrightness values.
- Even though the POSEIDON buoy was located far from the Souda Bay sampling station, the parameters measured showed significant relations with ^{137}Cs activity concentrations both for linear and polynomial consideration.
- Inside the Souda Bay relations of ^{137}Cs with MODIS SST are better, whereas outside the Souda Bay relations of ^{137}Cs with MODIS PIC are better as the particulate matter in the Gulf is higher than outside, which results to co-precipitation on ^{137}Cs.

2. AEGEAN SEA

- For the Aegean Sea the best correlation results were present when using MODIS SSTnight, MODIS SST4night and MODIS PIC.
- The observed spatial distribution of the r^2 values resulted by GWR in the Aegean Sea is dependent mainly by the ^{137}Cs sampling stations.
- The observed relations in the Aegean Sea were better during the winter season than the summer season.
- The observed predicted ^{137}Cs activity concentrations seem to follow the gradient North to South pattern of the actual measured concentrations, with the higher concentrations to be observed near the Dardanelles and the coastal area of North Aegean and the lower concentrations to be observed in Central and South Aegean.
- By applying the MODIS data to the GWR, the predicted values of ^{137}Cs show better congruence with the upper and lower part of the value spectrum than the middle ones.
- This study is the first documented approach of an innovative consideration of the remote radiological control based on a multidisciplinary research.

BIBLIOGRAPHY AND REFERENCES

Ashraf, M. A., Akib, S., Maah, M. J., Yusoff, I., & Balkhair, K. S. (2014). Cesium-137: Radio-Chemistry, Fate, and Transport, Remedation, and Future Concerns. *Critical Reviews in Environmechnology, 44*(15), pp. 1740-1793.

ATSDR, & Agency for Toxic Substances and Disease Registry. (2004). *Toxicological profile for Cesium.* Atlanta, GA: U.S. Department of Health and Human Services, Public Health Service.

Bailly du Bois, P., Laguionie, P., Boust, D., Korsakissok, I., Didier, D., & Fievet, B. (2012). Estimation of marine source term following Fukushima Dai-ichi accident. *Journal of Environmental Radioactivity*(114), pp. 2-9.

Balch, M. W., Gordon, R. H., & Bowler, C. B. (2005). Calcium carbonate measurements in the surface global ocean based on Moderate-Resolution Imaging Spectroradiometer data. *Journal of Geophysical Research*(110), p. C07001.

Brown, B. O., & Minnett, J. P. (1999). *MODIS Infrared Sea Surface Temprerature Algorithm- Algorithm Theoretical Basis Document.* University of Miami.

Brunsdon, C., Fotheringham, S., & Charlton, M. (1998). Geographically Weighted Regression. *Journal of the Royal Statistical Society: Series D (The Statistician)*(47), pp. 431-443.

Canberra Industries. (2010). Spectrum Analysis. United States of America. Retrieved from http://www.canberra.com/literature/fundamental-principles/pdf/Spectrum-Analysis.pdf

Canberra Industries. (2014). Germanium Detectors. United States of America. Retrieved from http://www.canberra.com/products/detectors/pdf/Germanium-Det-SS-C39606.pdf

Carder, L. K., Chen, F. R., Lee, Z., Hawes , S. K., & Cannizzaro, J. P. (2003). MODIS ocean science tean algorithm theoretical basis document. *Algorithm Theoretical Basis Documents*(19), pp. 7-18.

Charlton, M., & Fotheringham, S. A. (2009). Geographically Weighted Regression: White Paper.

Childs, C. (2004). Interpolating surfaces in ArcGIS Spatial Analyst. *Arc User*(July-September 2004), pp. 32-35.

Choppin, G., & Baisden, P. (1978). *Radiochemistry.* Tallahasee, FL: Florida State University, American Chemical Society.

Devell, L., & Johansson, K. (1994). *Specific Features of Cesium Chemistry and Physics Affecting Reactor Accident Source Term Predictions.* Swetish Nuclear Power Inspectorate (SKI) report 94:29.

ESA. (2016). *ESA BEAM Earth observation Toolbox and Development Platform*. Retrieved 2014, from http://www.brockmann-consult.de: http://www.brockmann-consult.de/cms/web/beam/welcome

ESA, European Space Agency. (2000-2014). *ESA eduspace*. Retrieved 2014, from ESA eduspace: http://www.esa.int/SPECIALS/Eduspace_EN/SEMF9R3Z2OF_0.html

ESA, European Space Agency. (2011). *SMOS ESA*. Retrieved 2014, from SMOS ESA: http://www.esa.int/Our_Activities/Observing_the_Earth/SMOS

Evangeliou, N., & Florou, H. (2012). The dispersion of ^{137}Cs in a shallow Mediterranean embayment (Saronikos Gulf- Elefsis Bay), estimated inventories and residence times. *Journal of Environmental Radioactivity*(113), pp. 87-97.

Evangeliou, N., Florou, H., Bokoros, P., & Scoullos, M. (2009). Temporal and Spatial distribution of ^{137}Cs in Eastern Mediterranean Sea. Horizontal and vertical dispersion in two regions. *Journal of Environmental Radioactivity*(100), pp. 626-636.

Finston, H. L., & Kinsley, M. T. (1961). *The Radiochemistry of Cesium* (Vols. 3035 Nuclear science series, National Academy of Sciences-National Research Council (U.S.) Commitee on Nuclear Science). National Academies.

Florou, H. (1992). *Dispersion and Behaviour of Long Lived Radionuclides in Marine Ecosystems.* Ph.D. thesis, University of Athens, Department of Zoology.

Florou, H. (n.d.). *Environmental Radioactivity - Radioecology.* Athens: Environmental Radioactivity Laboratory, NCSR "D".

Florou, H., & Kritidis, P. (1994). The dispersion of ^{137}Cs in the Aegean Sea. *Radiochimica Acta*(66/67), pp. 415-417.

Florou, H., Kritidis, P., Polikarpov, G. G., Egorov, V., Delfanti, R., & Papucci, C. (2001). Dispersion of Caesium-137 in the Eastern Mediterranean and the Black Sea: The time evolution in relationto the sources and pathways. *North Aegean System Functioning and Inter-Regional Pollution Meeting.* Kavala 28-30/5/2001: National Centre for Marine Research.

Florou, H., Kritidis, P., Vosniakos, F., Polikarpov, G. G., Egorov, V., Delfanti, R., . . . Aladjadjiyan, A. (2002). Dispersion of ^{137}Cs in the Eastern Mediterranean and the Black Sea: the time evolution in relation to the sources and pathways. *Journal of Environmental protection and Ecology, 3*(1), pp. 30-36.

Florou, H., Nicolaou, G., & Evangeliou, N. (2010). The concentration of ^{137}Cs in the surface of the Greek marine environment. *Journal of Environmental Radioactivity*(101), pp. 654-657.

Florou, H., Sykioti, O., Evangeliou, N., Mavrokefalou, G., & Tzempelikou, E. (2014). Remote radiological assessment in the marine environment: SMOS and MODIS observations combined to ^{137}Cs activity concentrations in the Aegean Sea - Greece. *Third International Conference in Radioecology and Environmental Radioactivity.* Barcelona, Spain, 7-12 September 2014.

Folsom, T., & Sreekumaran, C. (1970). Some reference methods for determining radioactive and natural caesium for marine studies. *Reference Methods for Marine Radioactive Studies. Technical Report Series. 118*, pp. 129-149. Vienna: IAEA.

Font, J., Boutin, J., Reul, N., Spurgeon, P., Ballabrera - Poy, J., Chuprin, A., . . . Delwart, S. (2013). SMOS first data analysis for sea surface determination. *International journal of Remote Sensing*(34), pp. 3654 - 3670.

Friedlander, G., Kennedy, J. W., Macias, E. S., & Miller, J. M. (1981). *Nuclear and Radiochemistry* (3rd Edition ed.). John Wiley & Sons.

HCMR, Hellenic Centre for Marine Research. (2012). *Poseidon System*. Retrieved 2016, from Poseidon System: Monitoring, Fore casting and Information system for the Greek Seas: http://poseidon.hcmr.gr/

Holt, M., Campbell, R. J., & Nikitin, M. B. (2012). *Fukushima Nuclear Disaster*. Congressional Research Service.

Hopkins, T. S. (1978). Physical processes in the Mediterranean Basins. In B. Kjerfve, *Estuarine Transport Processes* (1st Edition ed., p. 44). South Carolina: University of South Carolina Press.

IAEA, International Atomic Energy Agency. (2016). *IAEA.org*. Retrieved 2016, from http://www-ns.iaea.org/: http://www-ns.iaea.org/tech-areas/emergency/ines.asp

IPSN, & Institut de protection et de surete nucleaire. (2001). *Radioecology*. IPSN booklets.

Kartalis, K., & Feidas, C. (2006). *Principles and Applications of Satellite Remote Sensing*. Athens: Giourdas Publications.

Katsanevakis, S., & Thessalou-Legaki, M. (2009). Spatial distribution, abundance and habitat use of the protected fan mussel Pinna nobilis in Souda Bay, Crete. *Aquatic Biology*(8), pp. 45-54.

Kemeny, J. G. (1979). *The accident at three mile island, The Need for Change: The legacy of TMI*. Wasington, D.C.

Longley, P., Goodchild, M., Maguire, D., & Rhind, D. (2011). *Geographic Information Systems and Science* (3rd edition ed.). John Wiley & Sons, Ltd.

Mavrokefalou, G., Florou, H., Sykioti, O., & Parcharidis, I. (2016). Integration of Earth Observation satellite data and real time measirements in the Greek marine environment to GIS for advances in radiological remote control. *ESA Living Planet Symposium 2016 Prague 9-13 May*. Prague: ESA.

Mecklenburg, S., Drusch, M., Kerr, Y., Font, J., Neira, M. M., Delwart, S., . . . Carpolicchio, R. (2011). *ESA's Soil Moisture and Salinity Mission: mission performance and operations.*

Melin, F., & Vsmtrepotte, V. (2007). *Multi - Year Analysis of Standard Ocean Colour Products for the European Seas.* European Commission Joint Research Centre Institute for Environment and Sustainability.

Mertikas, S. P. (2006). *Remote Sensing and image digital analysis.* Athens: Ion Publications.

NASA. (2016). *OceanColor SeaDAS*. Retrieved 2014, from http://seadas.gsfc.nasa.gov/: http://seadas.gsfc.nasa.gov/

NASA Goddard Flight Center. (last update 2016). *NASA TERRA the EOS Flagship*. Retrieved 2014, from NASA TERRA the EOS Flagship: http://terra.nasa.gov/

NASA Goddard Space Flight Center. (last updated 2016). *NASA Aqua Project Science*. Retrieved 2014, from NASA Aqua Project Science: http://aqua.nasa.gov/

NASA Goddard Space Flight Center. (last updated 2016). *NASA MODIS MODERATE RESOLUTION IMAGING SPECTRORADIOMETER*. Retrieved 2014, from NASA MODIS MODERATE RESOLUTION IMAGING SPECTRORADIOMETER: http://modis.gsfc.nasa.gov/

NASA Goddard Space Flight Center, Ocean Biology Processing Group. (2014). *OceanColorWEB*. Retrieved 2014, from OceanColorWEB: http://oceancolor.gsfc.nasa.gov/cms/

NASA-OceancolorBiology Processing Group. (2010). *Ocean Level-3 Standard Mapped Image Products*. Techical reports: Data User guides. Retrieved from http://oceancolor.gsfc.nasa.gov/DOCS/Ocean_Color_Level-3_SMI_Products.pdf

NEA Committee on Radiation Protection and Public Health. (1995). *Chernobyl Ten years on: Radiological and Health Impact.* OECD Nuclear Energy Agency.

Papucci, C., & Delfanti, R. (1999). ^{137}Caesium distribution in the eastern Mediterranean Sea: recent changes and future trends. *The Science of the Total Environment*(237/238), pp. 67-75.

Patton, D. D. (1999). History Corner: How Cesium-137 Was Discovered by an Undergraduate Student. *Journal of Nuclear Medicine*(40), pp. 18N-31N.

Petihakis, G., Nittis, K., Ballas, D., Kassis, D., & Pagonis , P. (2009). The POSEIDON reference time-series stations of the Eastern Mediterranean Sea. *Mediterranean Marine Science*(18, SPECIAL ISSUE 2013), pp. 5-18.

Polikarpov, G. G. (1966). *Radioecology of aquatic organisms.* New York: Reinhold.

Poulos, E. S., Drakopoulos, P. G., & Collins, M. B. (1997). Seasonal variability in sea surface oceanographic conditions in the Aegean Sea (Eastern Mediterranean): an overview. *Journal of Marine Systems*(13), pp. 225-244.

Reguigui, N. (September 2006). *Gamma Spectrometry: Practical Information.*

Saenko, V. (2011). The Chernobyl Accident and its Consequences. *Clinical Oncology*(23), pp. 234-243.

Skliris, N., Mantziafou, A., Sofianos, S., & Gkanasos, A. (2010). Satellite-derives variability of the Aegean Sea ecohydrodynamics. *Continental Shelf Research, 30*(5), pp. 403-418.

Smith, J., & Bersford, N. A. (2005). *Chernobyl Catastrophe and Consequences.* Chchester, UK: Springer in association with Praxis Publishing.

Sofianos, S., Johns, W., Lascaratos, A., Murray, S., Olson, D., & Theocharis, A. (2002). *Draft Report of the Aegean Sea Workshop.* Report, Rhodes.

Spurgeon, P., Font, J., Boutin, J., Reul, N., Tenerelli, J., Vergely, J.-l., . . . Waldteufel, P. (2010). Ocean Salinity Retrieval Approaches for the SMOS Satellite.

Stramski, D., Raynolds, A. R., & Kaczmarek, S. (2008). Relationships between the surface concentration of particulate organic carbon and optical properties in the eastern South Pacific and eastern Atlantic Oceans. *Biogeosciences*(5), pp. 171-201.

Sykioti, O. (2015). Joint satellite and radioactivity measurements for radiological assessment in the marine environment. *3rd Hellenic Forum on Science, Technology & Innovation: Innovation on Radiation Protection technology.* Athens.

Sykioti, O., Florou, H., Mavrokefalou, G., & Evangeliou, N. (2014). Correlations of salinity temperature and ocean colour variations from SMOS and MODIS satellite data in the Eastern Mediterranean and the Black Sea for creating an inventrory data base as to be compared to conservative radionuclides for remote recording . *10th International Congress of the Hellenic Geographical Society*, *Special Session 3*, pp. 1273-1283. Thessaloniki, Greece, 22-24 October 2014.

Thomson, R. E., & Emery, W. J. (2014). *Data analysis methods in physical oceanography* (3rd edition ed.). Elsevier.

Valaoras, D., Kassis, D., Perivoliotis, L., Pagonis, P., Hondronasios, A., & Nittis, K. (2013). Temperature ans Salinity Variability in the Greek Seas based on POSEIDON stations time series: preliminary results. *10th Hellenic Symposium on Oceanography and Fisheries.*

Van Der Stricht, E., & Kirchmann, R. (2001). *Radioecology: Radioactivity & Ecosystems.* Liege, Belgium: Fortemps.

Walker, S. J. (2004). *Three Mile Island: A Nuclear Crisis in Historical Perspective.* Berkeley: University of California Press.

Werdell, J. P., & Bailey, W. S. (2005). An improved bio-optical dataset for ocean color algorithm development and satellite data product validation. *Remote Sensing of Environment*(98), pp. 122-140.

Wong, M. K., Jokela, T. A., & Noshkin, V. E. (1994). *Radiochemical procedures for analysis of Pu, Am, Cs and Sr in seawater, soil, sediments and biota samples.Technical Report UCRL-ID-116497.* Livermore, CA, USA: Lawrence Livermore National Laboratory.

Wurl, O. (2009). *Practical Guidelines for the Analysis of Seawater.* (O. Wurl, Ed.) United States of America: CRC Press.

Zervakis, V., & Georgopoulos, D. (2001). Hydrology and circulation in the North Aegean (Eastern Mediterranean) throughout 1997-1998. *Mediterranean Marine Science, 3*(1), pp. 5-20.

APPENDIX

1.1. AEGEAN SEA TIMESERIES

1.1.1. SATELLITE DATA

1.1.1.1. SMOS

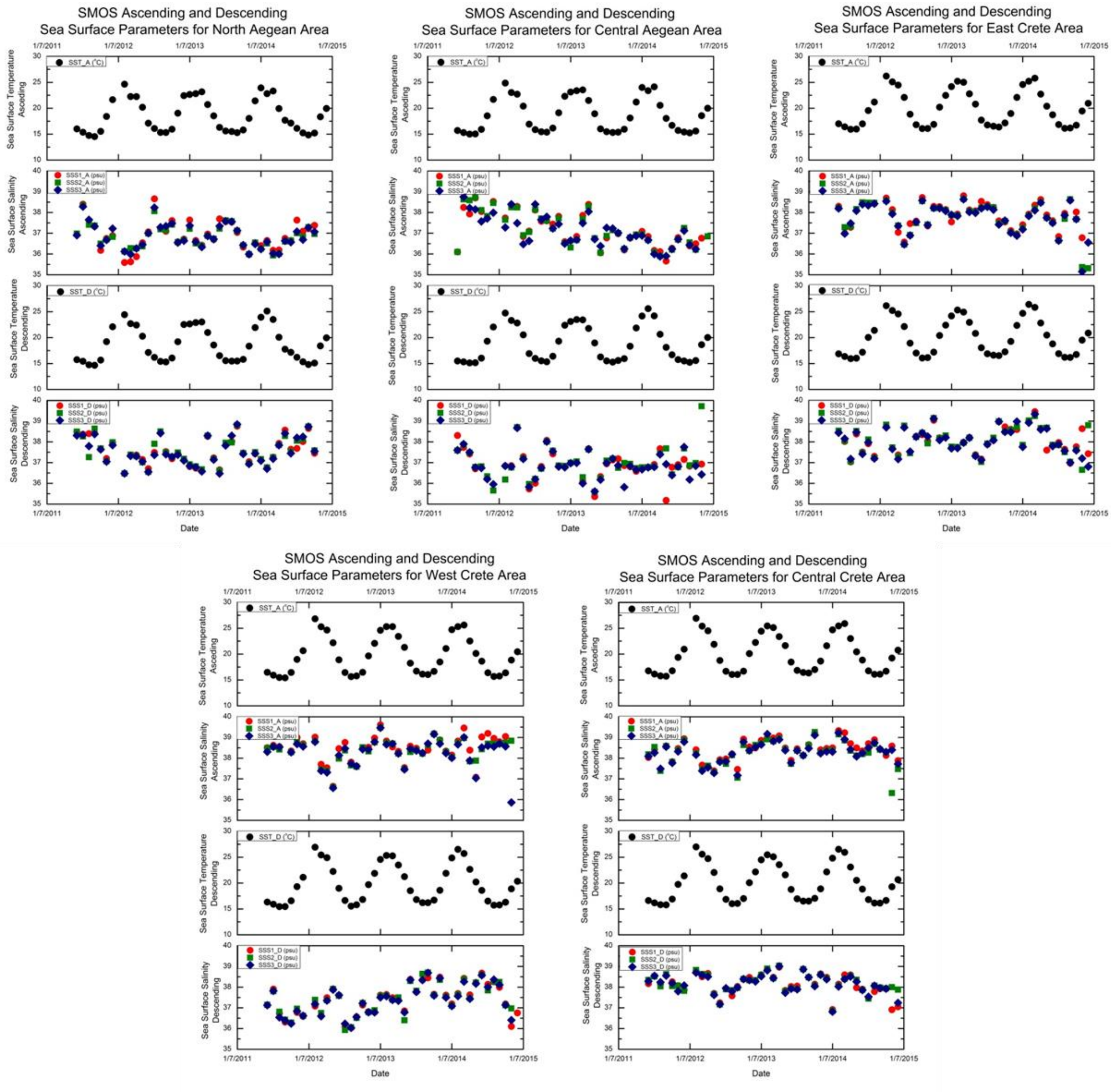

Appendix 1. SMOS data timeseries for the Aegean Sea according to the five main regions.

1.1.1.2. MODIS

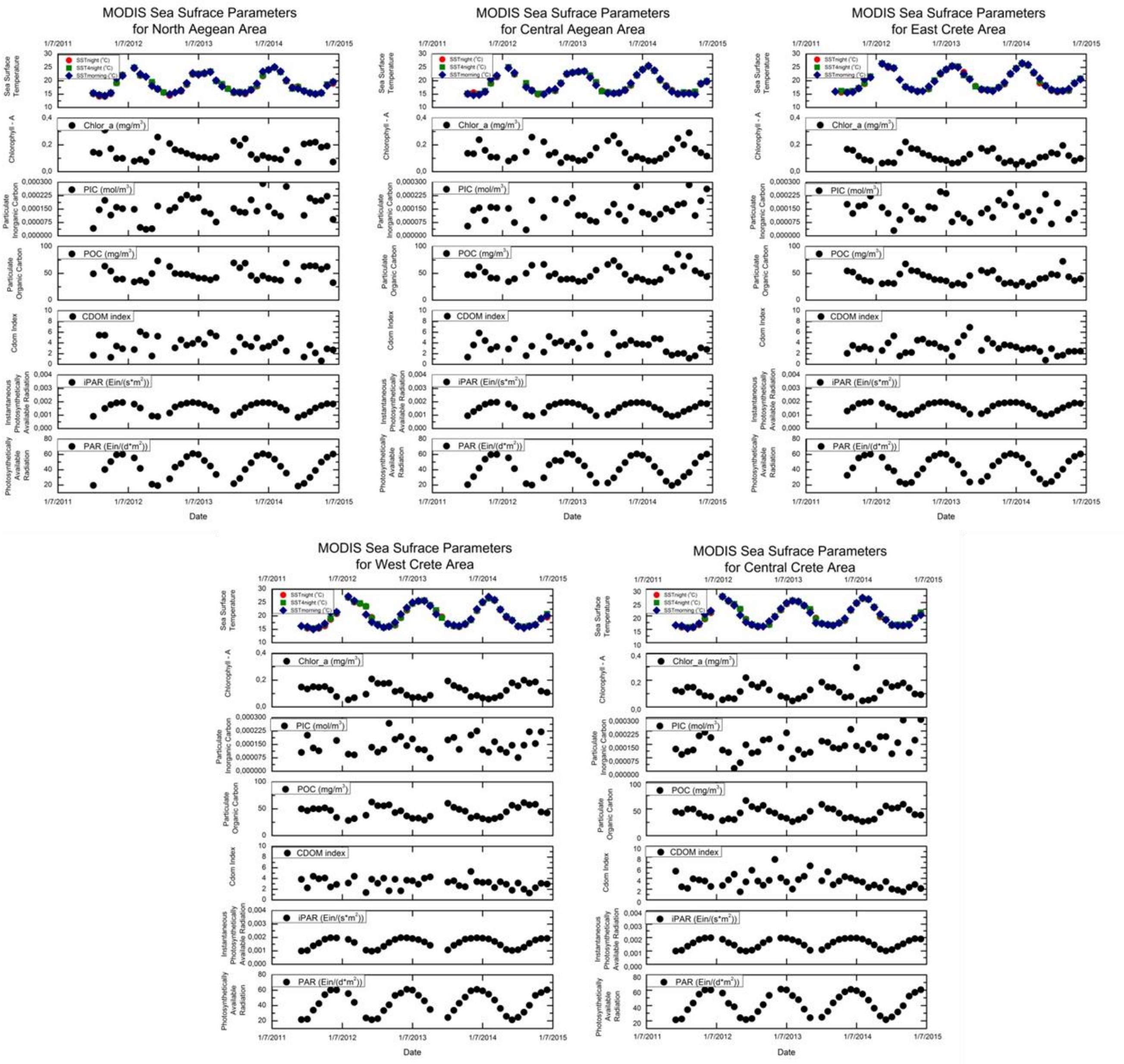

Appendix 2. MODIS data timeseries for the Aegean Sea according to the five main regions.

1.1.2. POSEIDON DATA

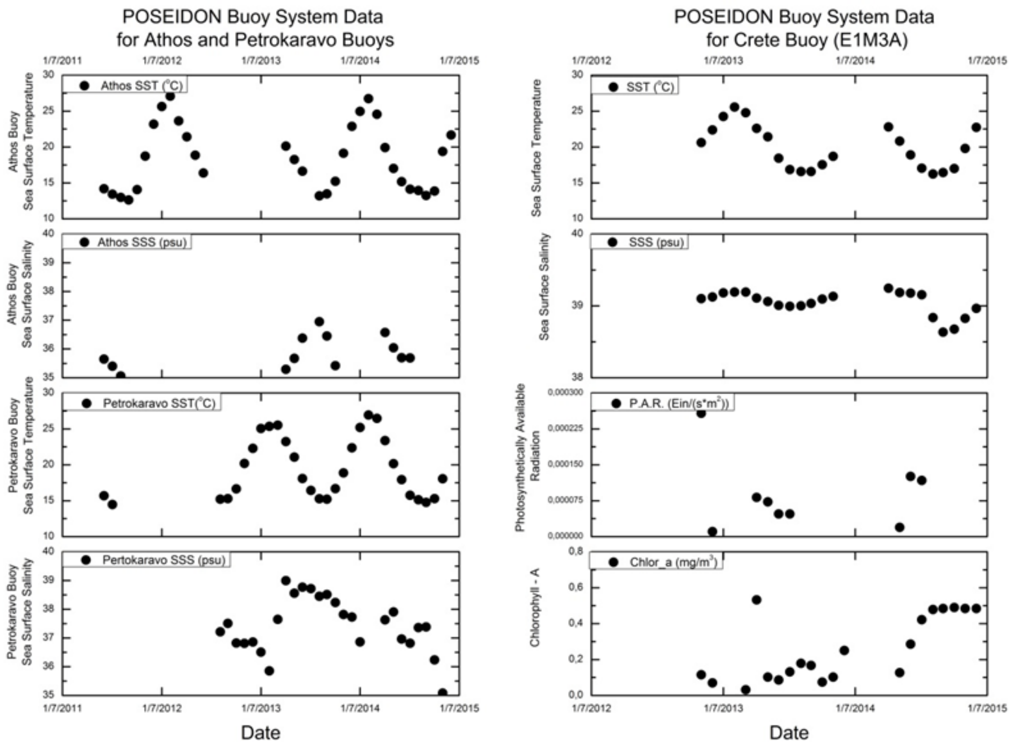

Appendix 3. POSEIDON data timeseries for the 3 buoys in the Aegean Sea.

1.2. Souda Bay Timeseries

1.2.1. SMOS

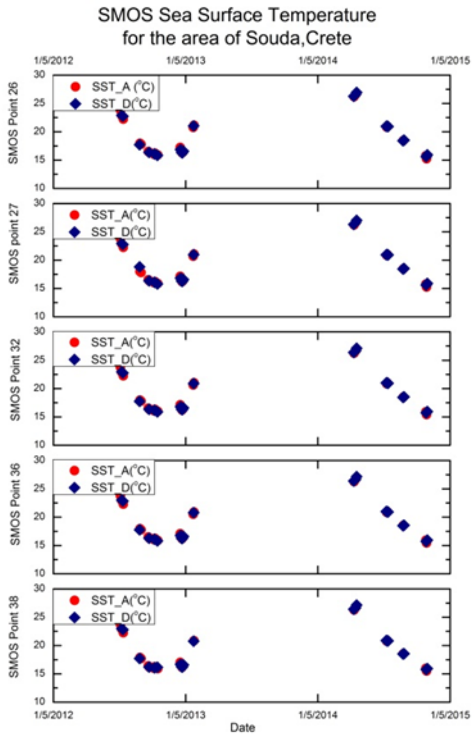

Appendix 4. SMOS data timeseries for the Souda Bay area.

1.2.2. MODIS

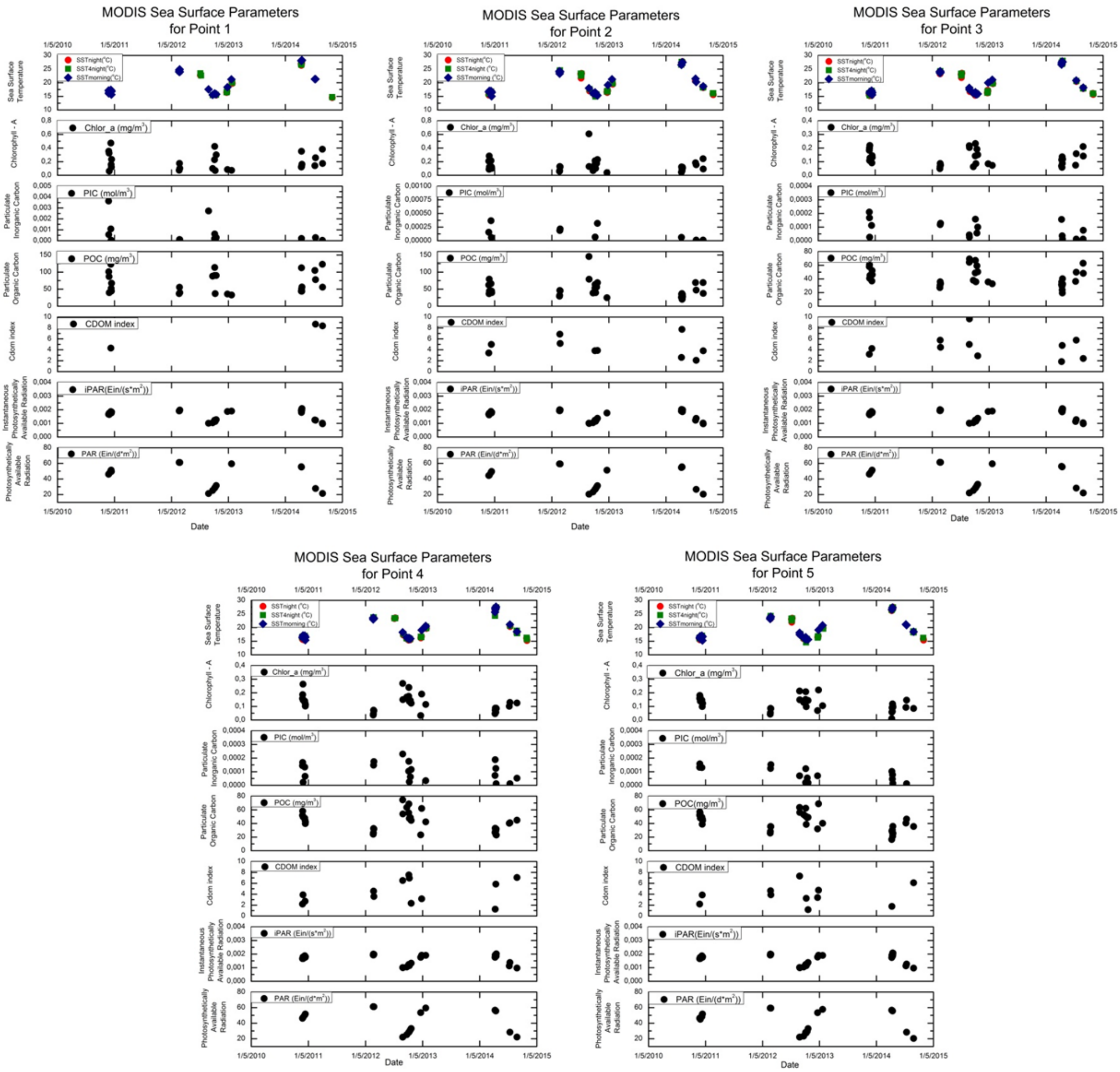

Appendix 5. MODIS data timeseries for the Souda Bay area.

1.2.3. POSEIDON

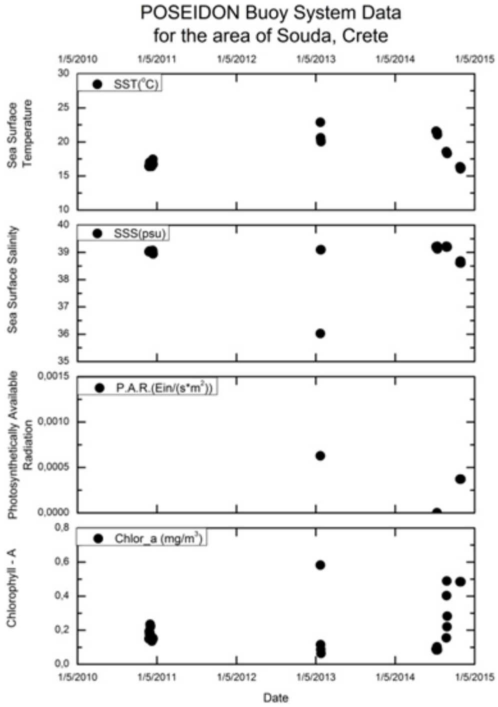

Appendix 6. POSEIDON data timeseries for the Souda Bay area.

1.2.4. ^{137}Cs

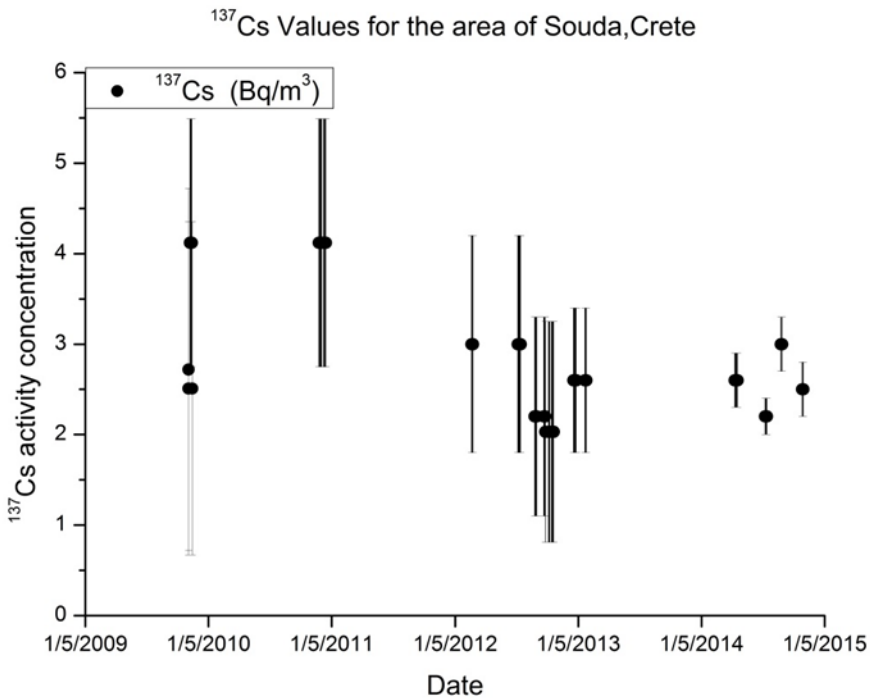

Appendix 7. ^{137}Cs activity concentrations timeseries for the Souda Bay area.

1.3. RELATIONS INVESTIGATION BETWEEN SATELLITE MEASUREMENTS AND POSEIDON DATA

1.3.1.1. SMOS

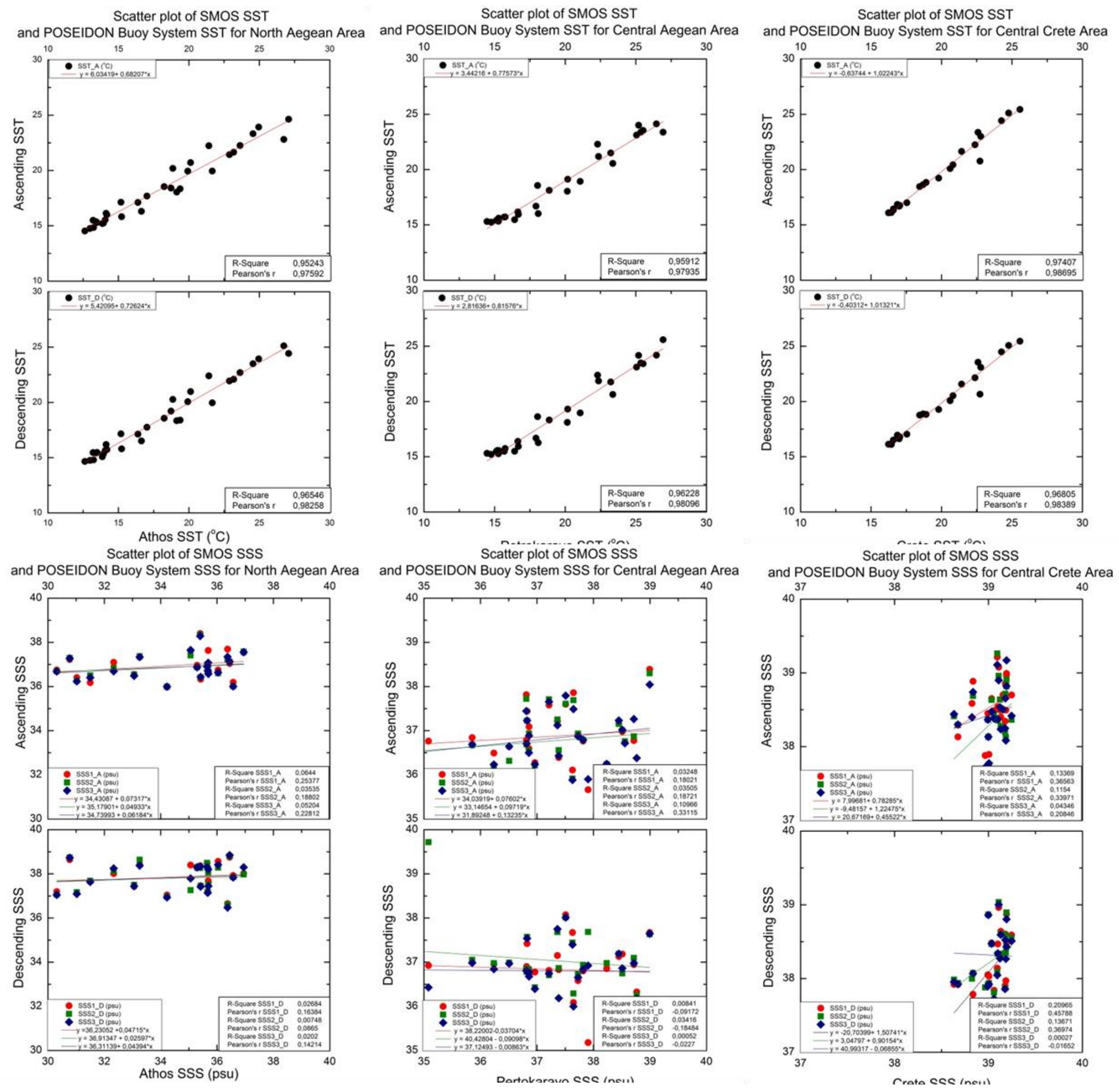

Appendix 8. SMOS and POSEIDON scatter plots depicting their linear relation.

1.3.1.2. MODIS

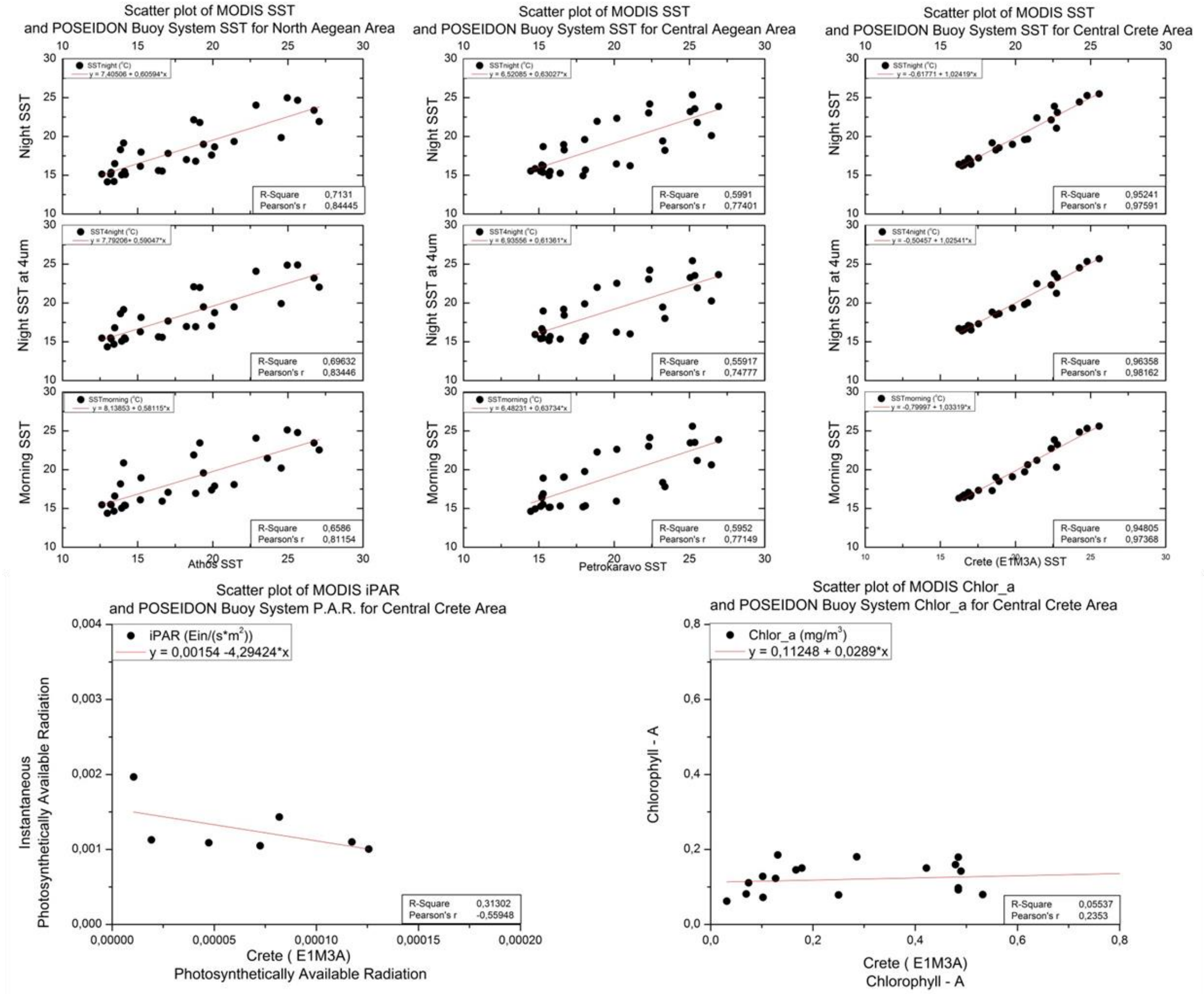

Appendix 9. MODIS and POSEIDON scatter plots depicting their linear relation.

1.4. Spatial Database maps

1.4.1.1. ^{137}Cs Activity Concentrations

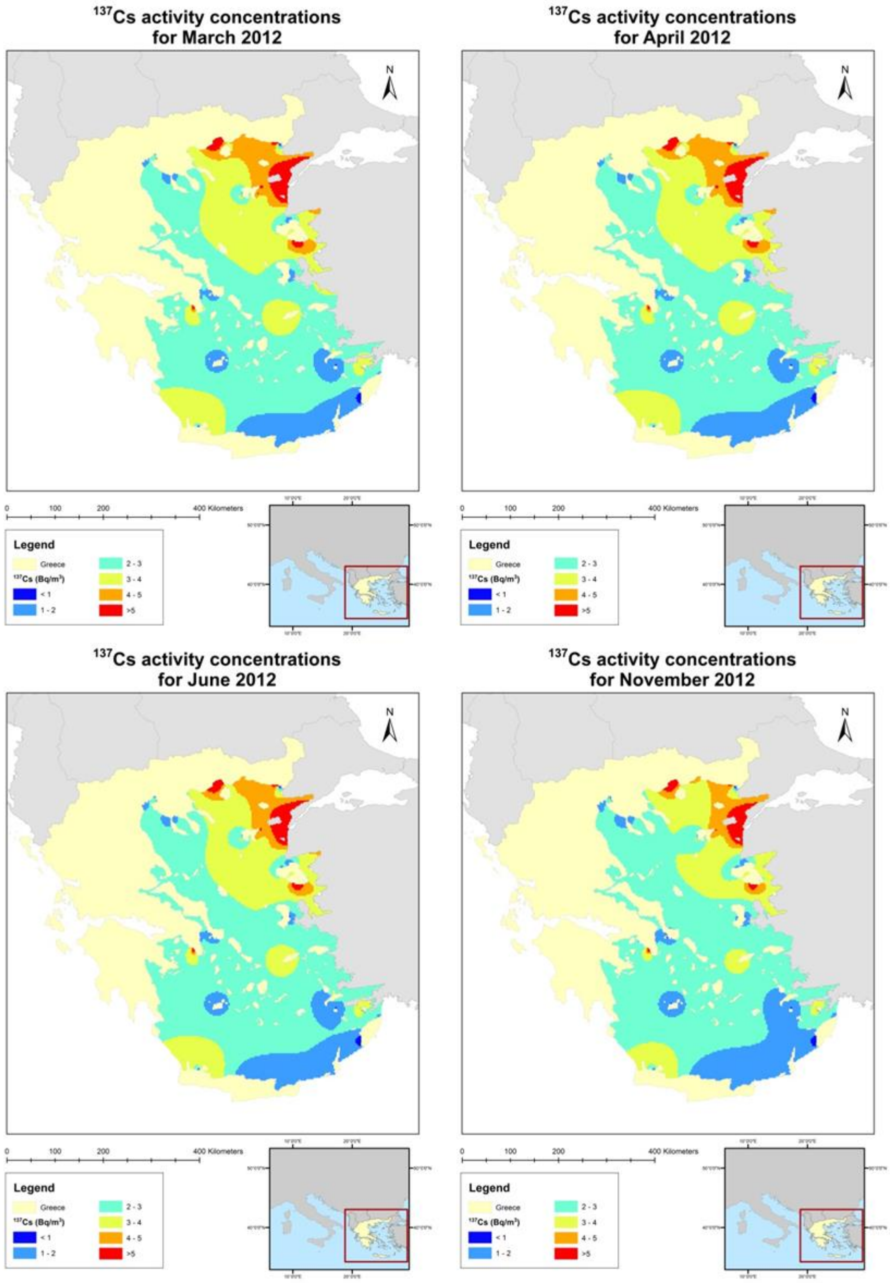

^{137}Cs activity concentrations for December 2012

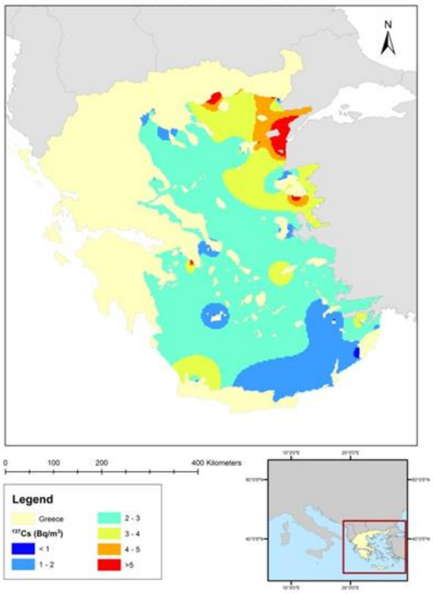

^{137}Cs activity concentrations for January 2013

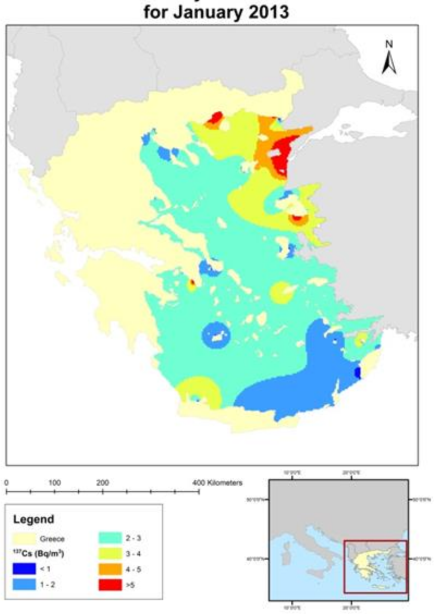

^{137}Cs activity concentrations for February 2013

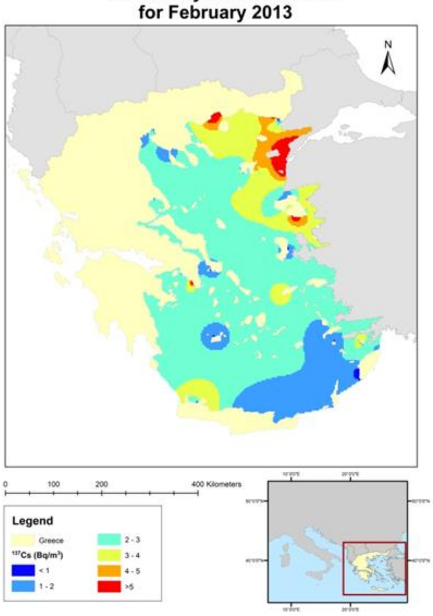

^{137}Cs activity concentrations for April 2013

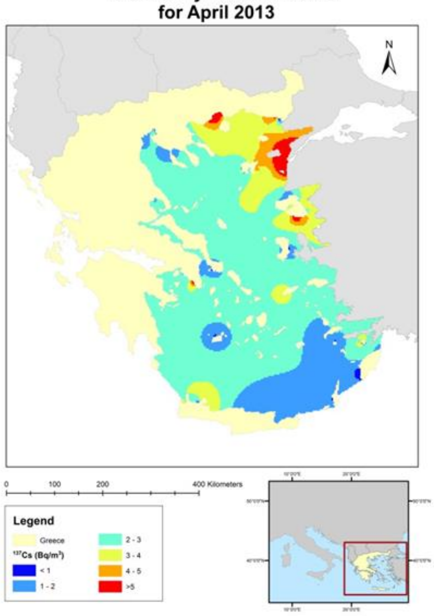

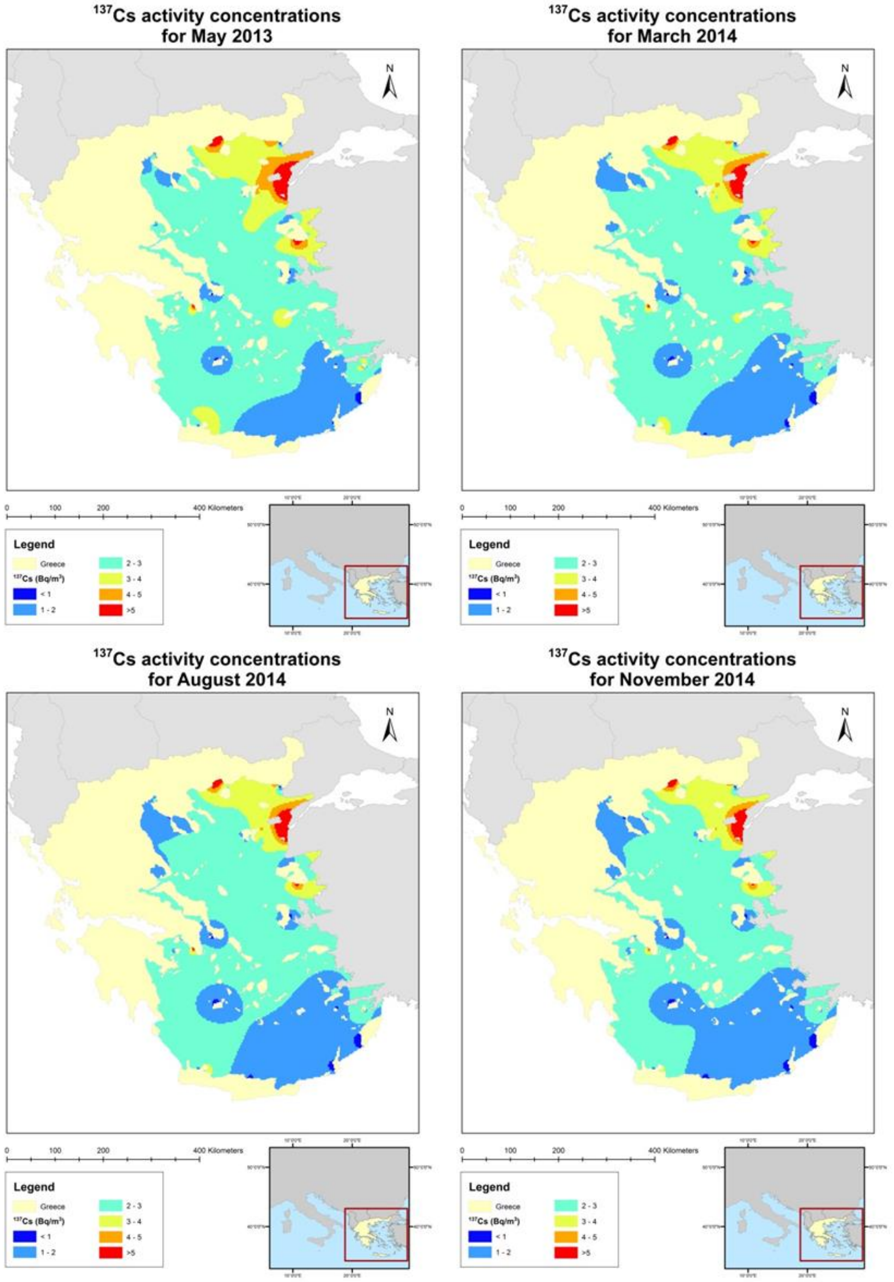

137Cs activity concentrations
for May 2013
N
0 100 200 400 Kilometers
Legend
Greece
137Cs (Bq/m3)
< 1
1 - 2
2 - 3
3 - 4
4 - 5
>5
137Cs activity concentrations
for March 2014
N
0 100 200 400 Kilometers
Legend
Greece
137Cs (Bq/m3)
< 1
1 - 2
2 - 3
3 - 4
4 - 5
>5
137Cs activity concentrations
for August 2014
N
0 100 200 400 Kilometers
Legend
Greece
137Cs (Bq/m3)
< 1
1 - 2
2 - 3
3 - 4
4 - 5
>5
137Cs activity concentrations
for November 2014
N
0 100 200 400 Kilometers
Legend
Greece
137Cs (Bq/m3)
< 1
1 - 2
2 - 3
3 - 4
4 - 5
>5

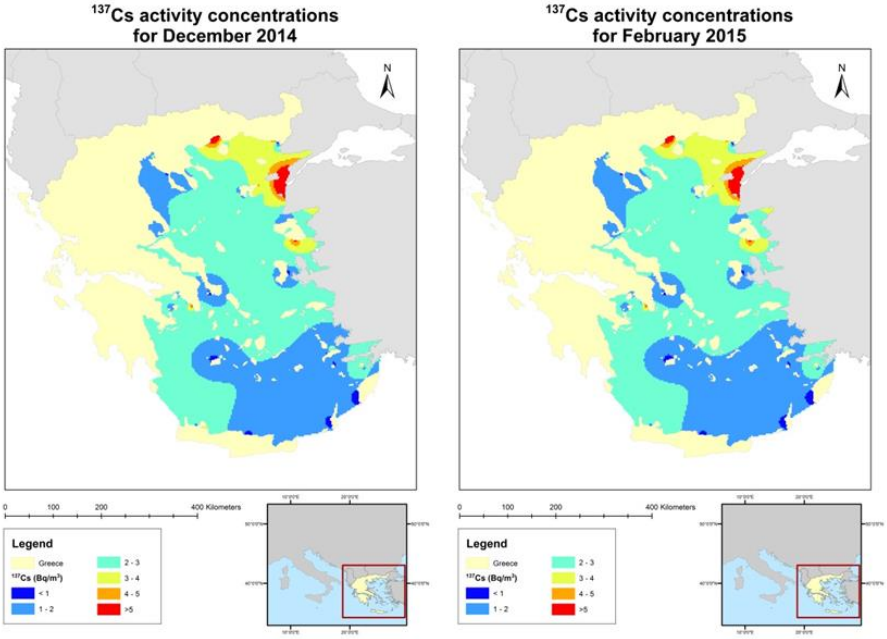

Appendix 10. ^{137}Cs activity concentrations for the time period March 2012 to February 2015.

1.4.1.2. SSTNIGHT

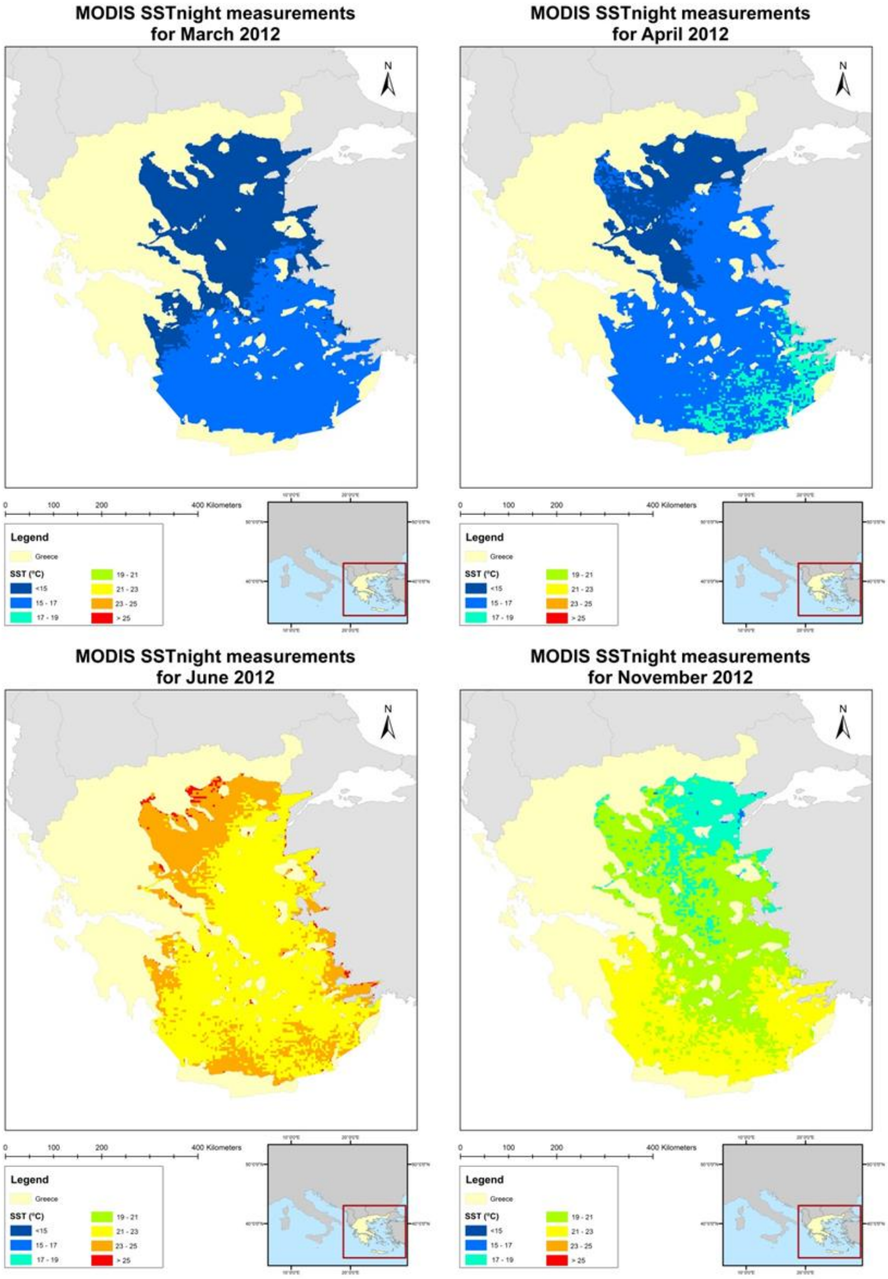

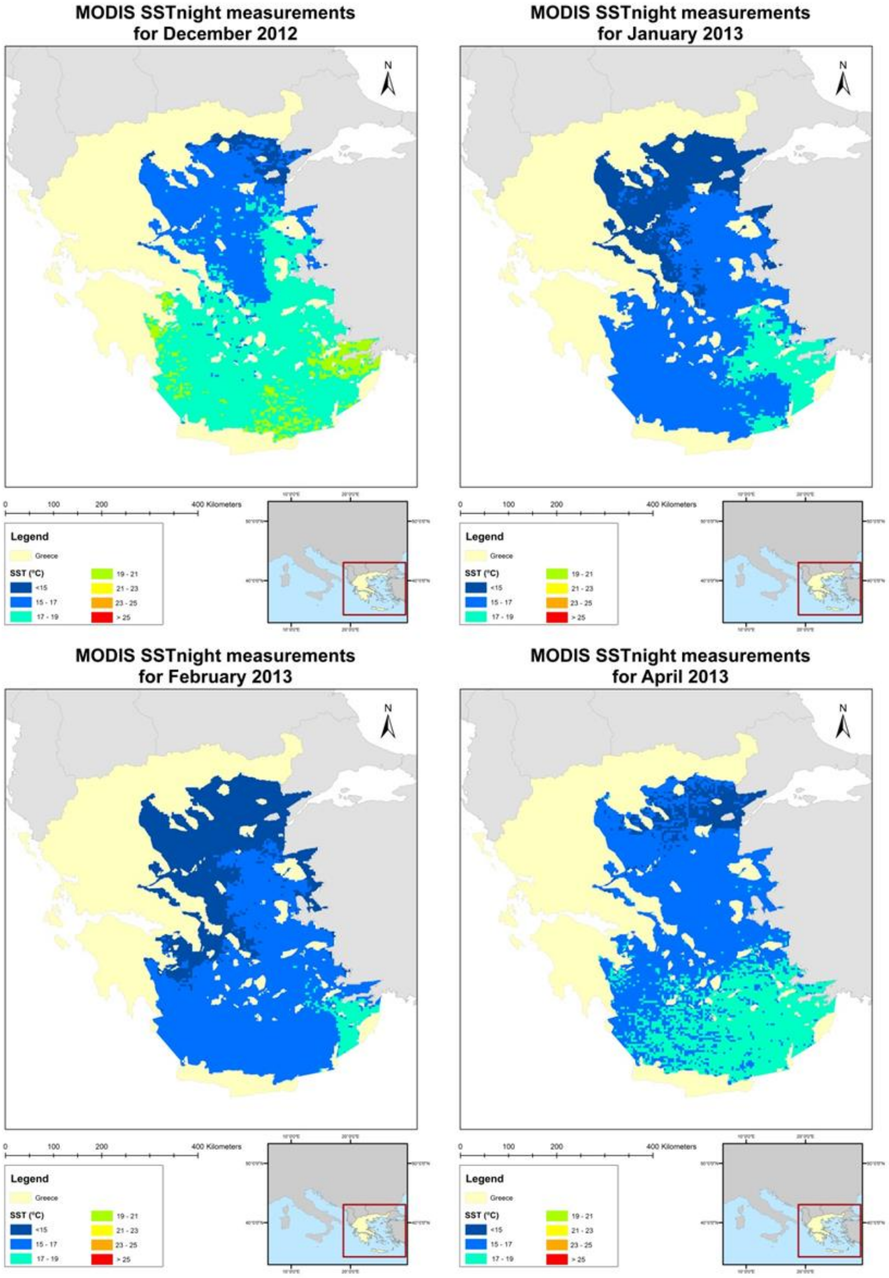
MODIS SSTnight measurements for December 2012
MODIS SSTnight measurements for January 2013
MODIS SSTnight measurements for February 2013
MODIS SSTnight measurements for April 2013
N
0 100 200 400 Kilometers
Legend
Greece
SST (°C)
<15
15 - 17
17 - 19
19 - 21
21 - 23
23 - 25
> 25

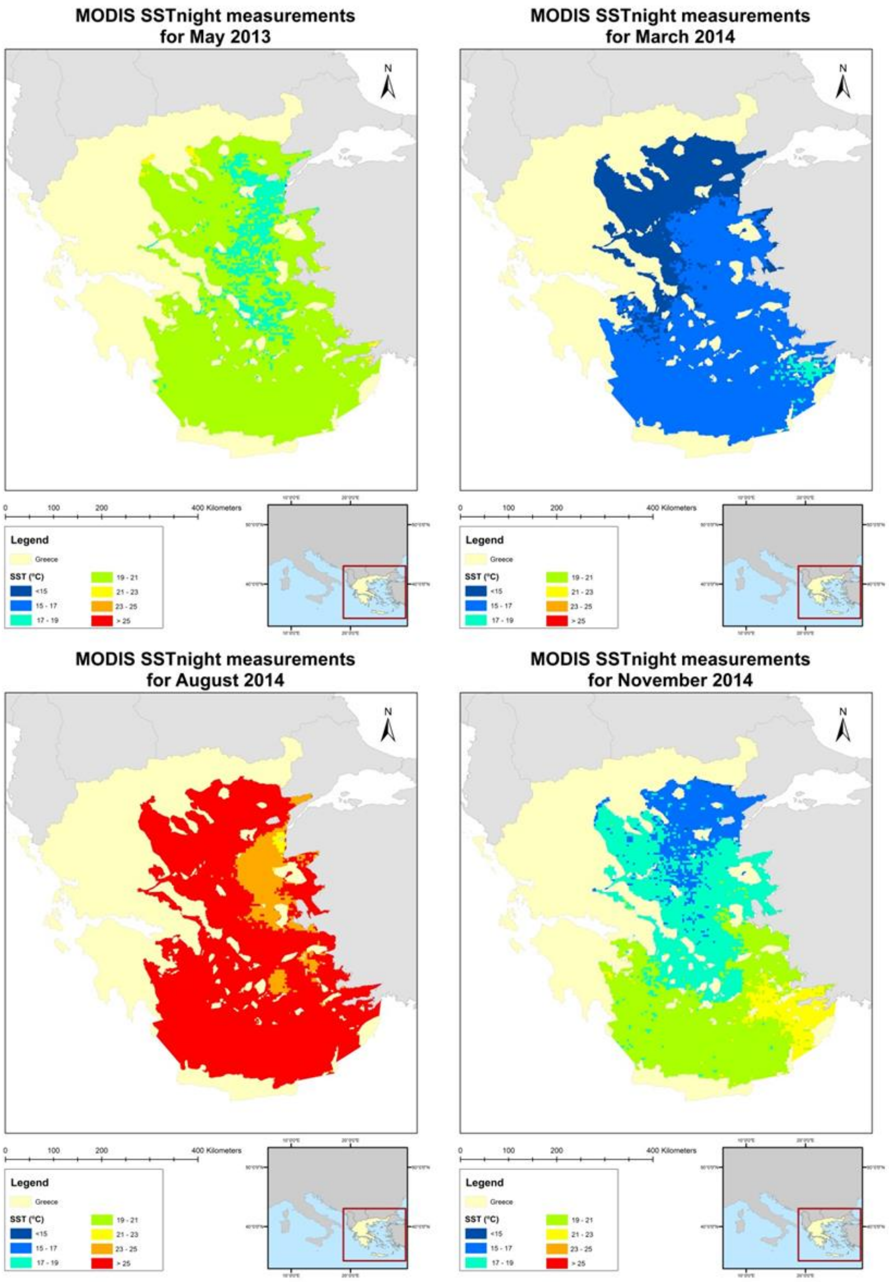
MODIS SSTnight measurements
for May 2013
MODIS SSTnight measurements
for March 2014
MODIS SSTnight measurements
for August 2014
MODIS SSTnight measurements
for November 2014
0
100
200
400 Kilometers
Legend
Greece
SST (°C)
<15
15 - 17
17 - 19
19 - 21
21 - 23
23 - 25
> 25

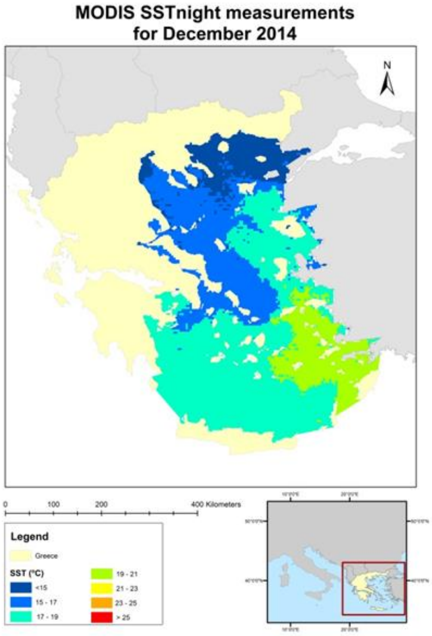

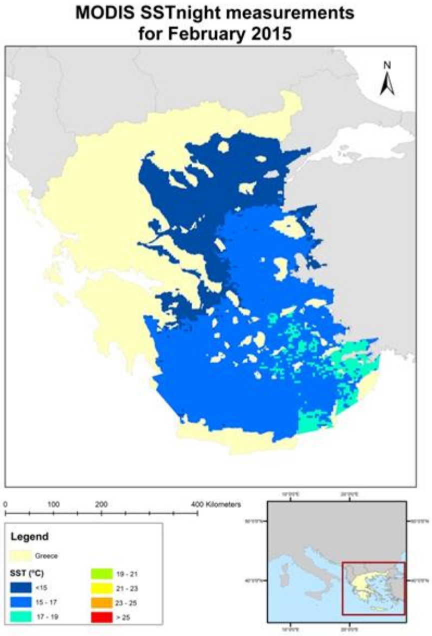

Appendix 11. MODIS SSTnight measurements for the time period March 2012 to February 2015.

1.4.1.3. SST4NIGHT

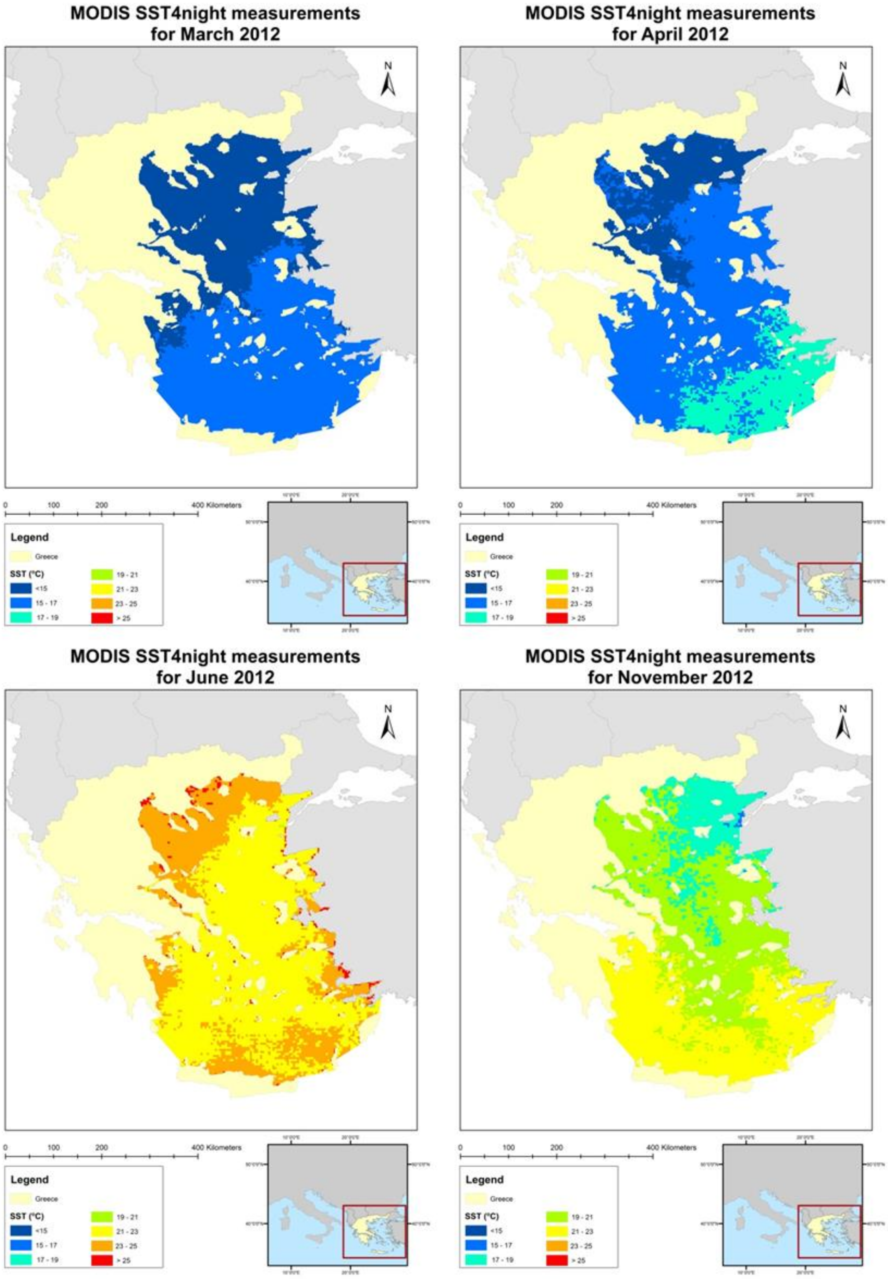

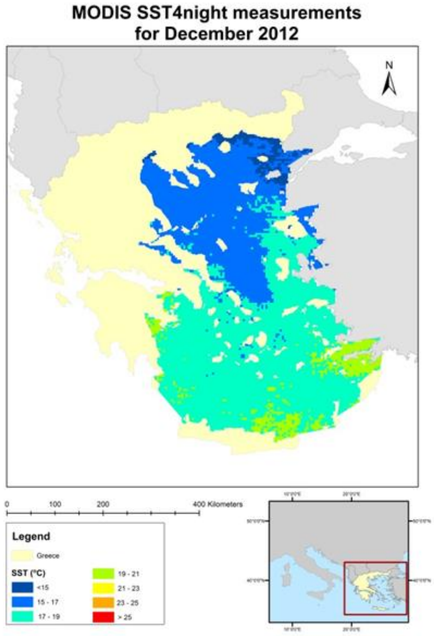
MODIS SST4night measurements
for December 2012
N
0
100
200
400 Kilometers
Legend
Greece
SST (°C)
<15
15 - 17
17 - 19
19 - 21
21 - 23
23 - 25
> 25

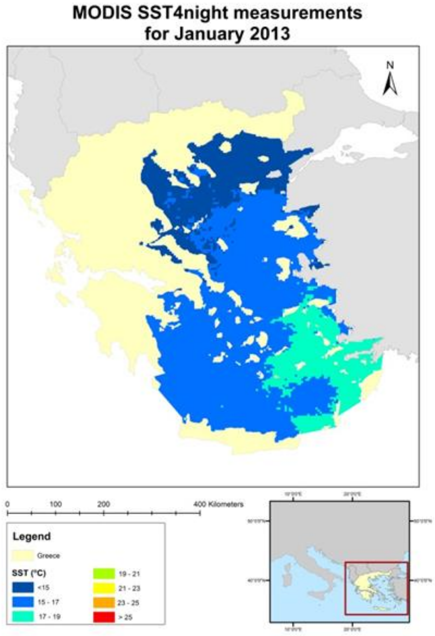
MODIS SST4night measurements
for January 2013
N
0
100
200
400 Kilometers
Legend
Greece
SST (°C)
<15
15 - 17
17 - 19
19 - 21
21 - 23
23 - 25
> 25

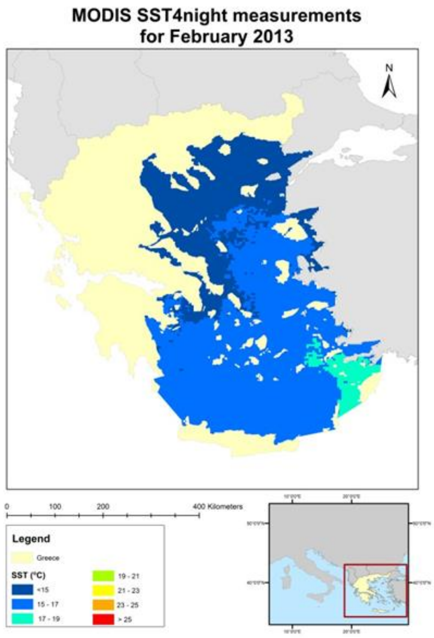
MODIS SST4night measurements
for February 2013
N
0
100
200
400 Kilometers
Legend
Greece
SST (°C)
<15
15 - 17
17 - 19
19 - 21
21 - 23
23 - 25
> 25

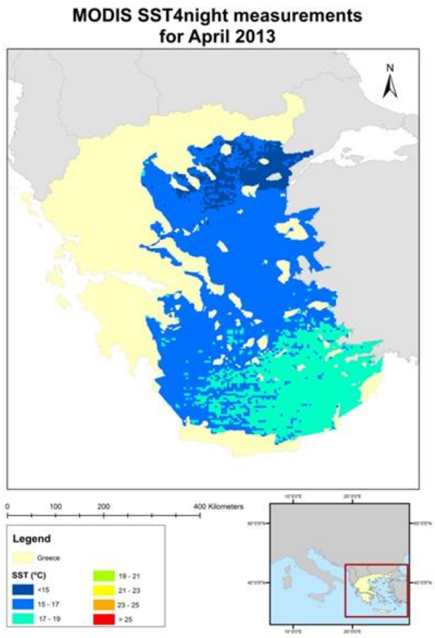
MODIS SST4night measurements
for April 2013
N
0
100
200
400 Kilometers
Legend
Greece
SST (°C)
<15
15 - 17
17 - 19
19 - 21
21 - 23
23 - 25
> 25

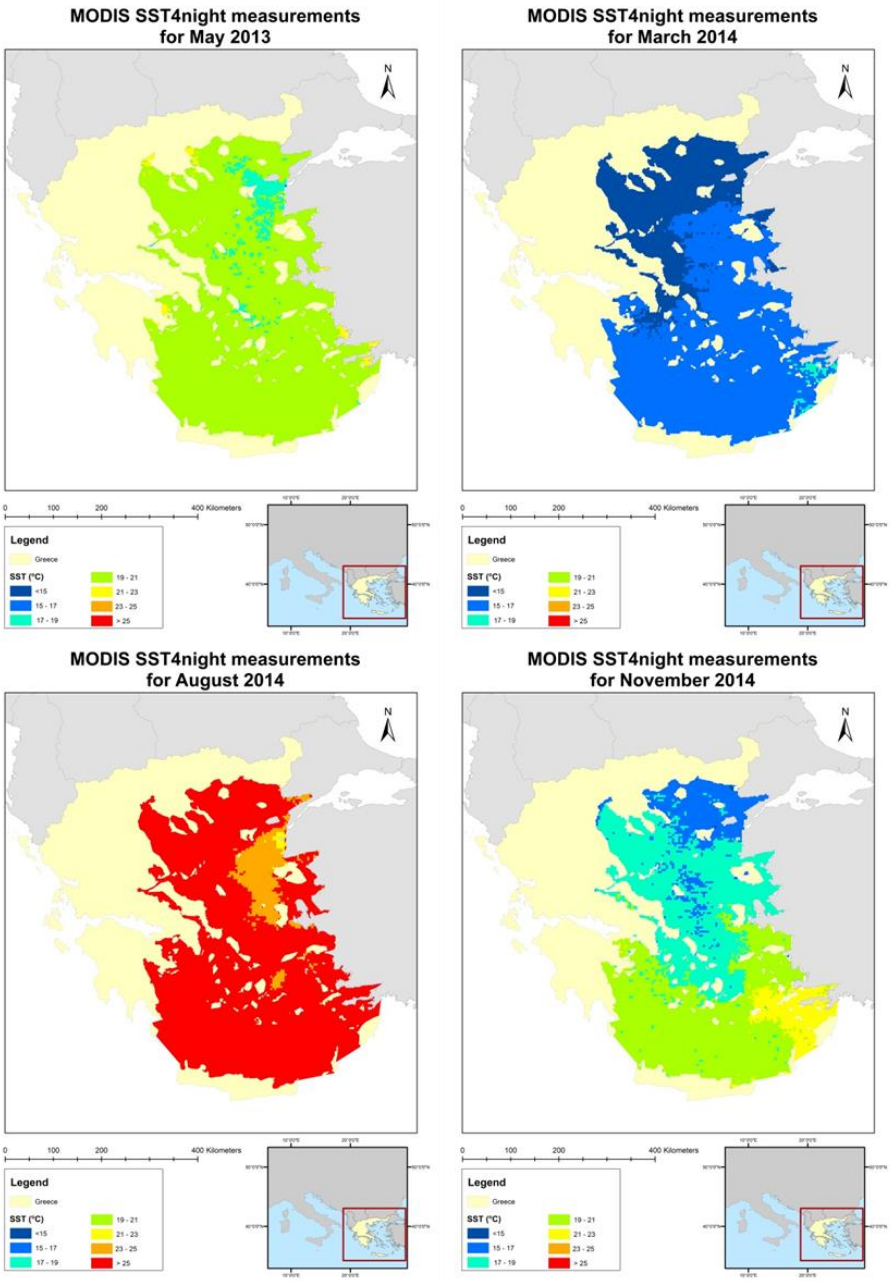
MODIS SST4night measurements for May 2013
MODIS SST4night measurements for March 2014
MODIS SST4night measurements for August 2014
MODIS SST4night measurements for November 2014
0 100 200 400 Kilometers
Legend
Greece
SST (°C)
<15
15 - 17
17 - 19
19 - 21
21 - 23
23 - 25
> 25

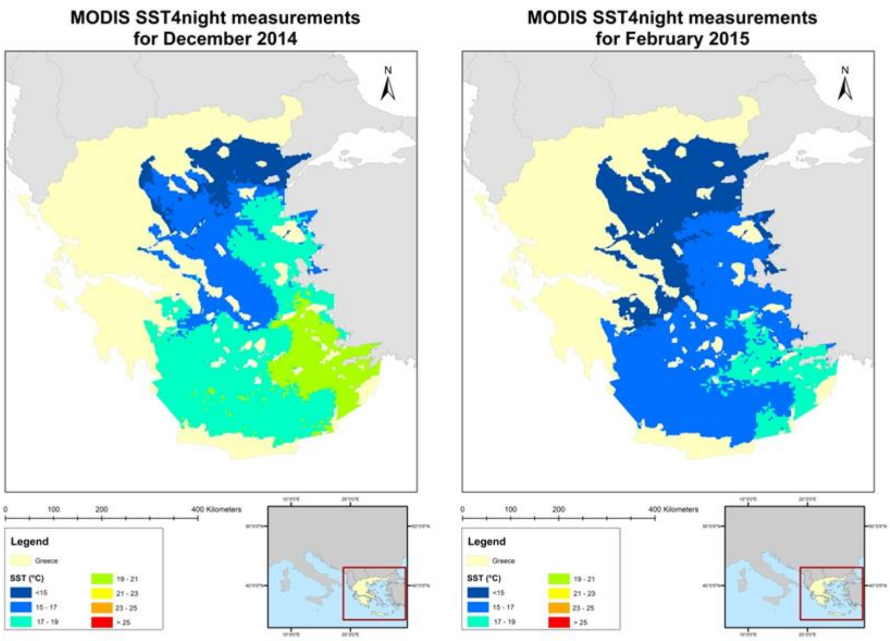

Appendix 12. MODIS SST4night measurements for the time period March 2012 to February 2015.

1.4.1.4. SSTMORNING

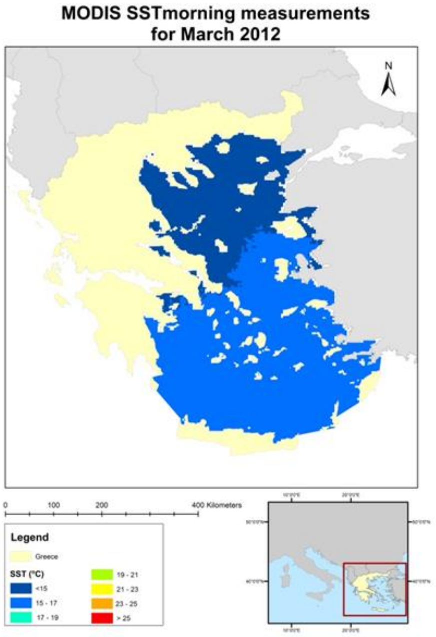

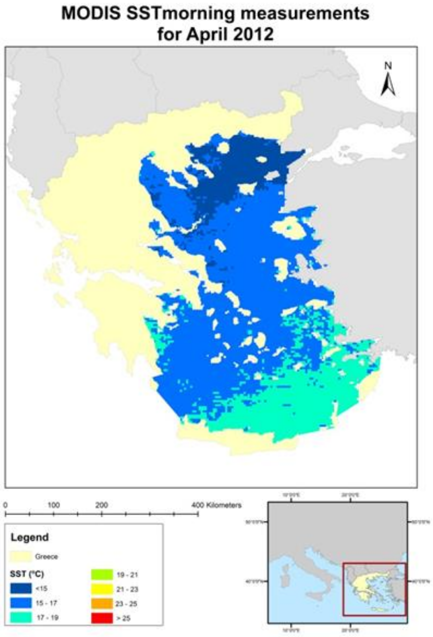

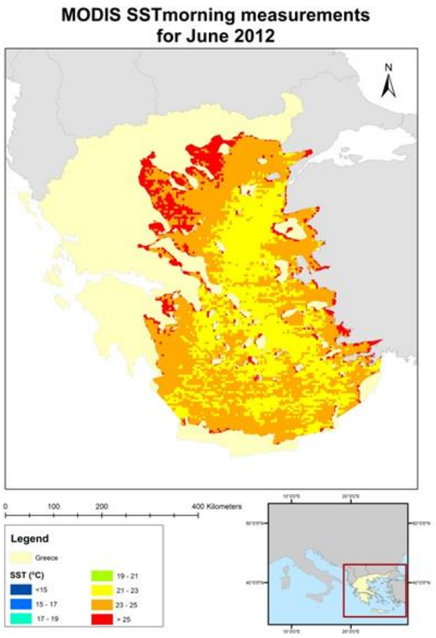

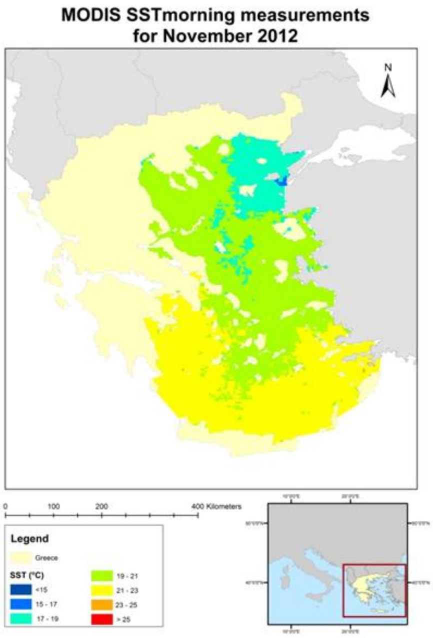

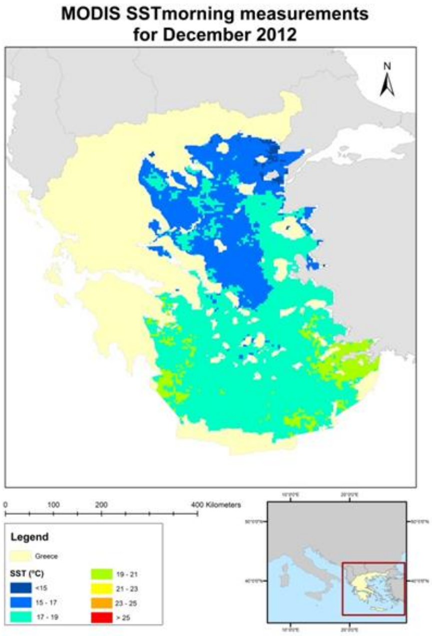
MODIS SSTmorning measurements
for December 2012
N
0 100 200 400 Kilometers
Legend
Greece
SST (°C)
<15
15 - 17
17 - 19
19 - 21
21 - 23
23 - 25
> 25

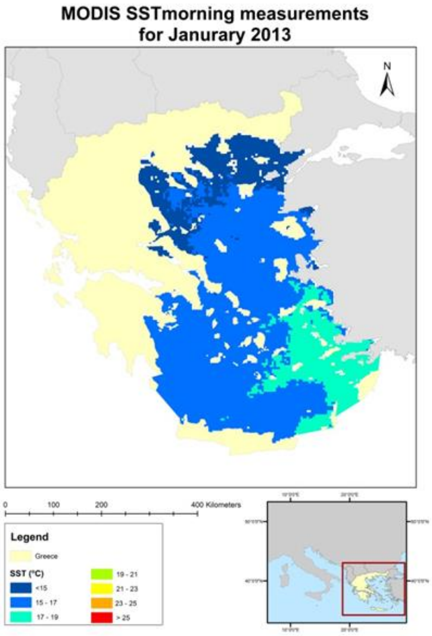
MODIS SSTmorning measurements
for Janurary 2013
N
0 100 200 400 Kilometers
Legend
Greece
SST (°C)
<15
15 - 17
17 - 19
19 - 21
21 - 23
23 - 25
> 25

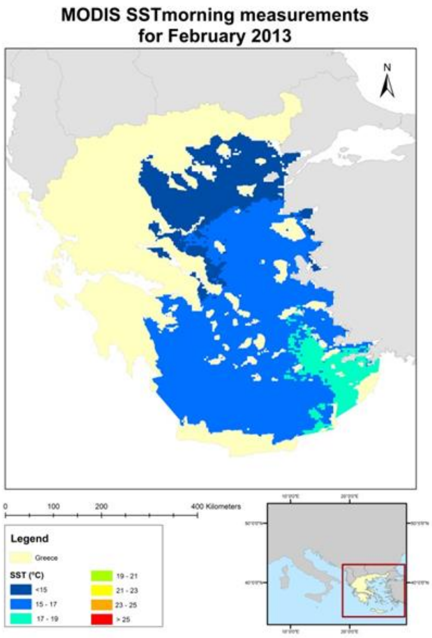
MODIS SSTmorning measurements
for February 2013
N
0 100 200 400 Kilometers
Legend
Greece
SST (°C)
<15
15 - 17
17 - 19
19 - 21
21 - 23
23 - 25
> 25

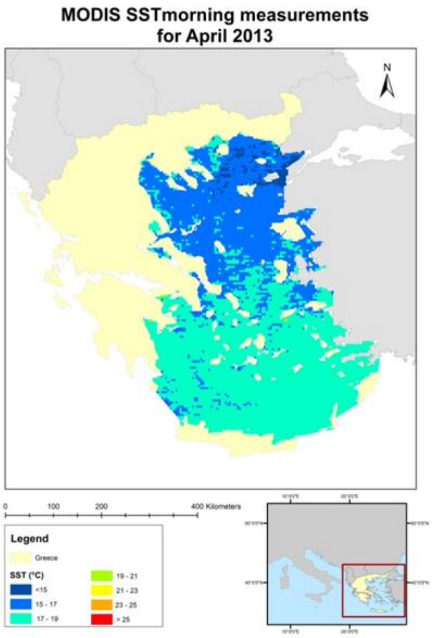
MODIS SSTmorning measurements
for April 2013
N
0 100 200 400 Kilometers
Legend
Greece
SST (°C)
<15
15 - 17
17 - 19
19 - 21
21 - 23
23 - 25
> 25

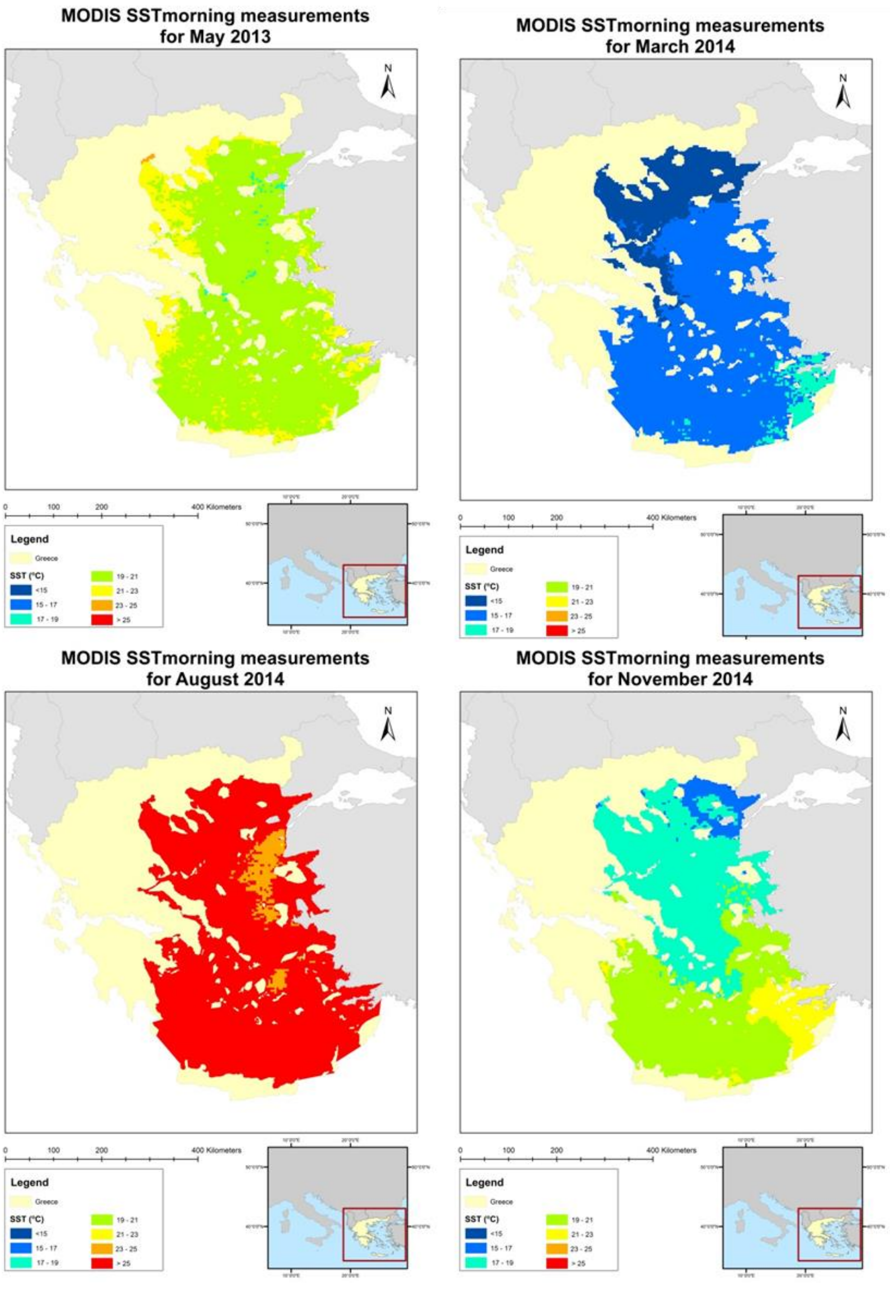
MODIS SSTmorning measurements for May 2013
MODIS SSTmorning measurements for March 2014
MODIS SSTmorning measurements for August 2014
MODIS SSTmorning measurements for November 2014
N
0
100
200
400 Kilometers
Legend
Greece
SST (°C)
<15
15 - 17
17 - 19
19 - 21
21 - 23
23 - 25
> 25

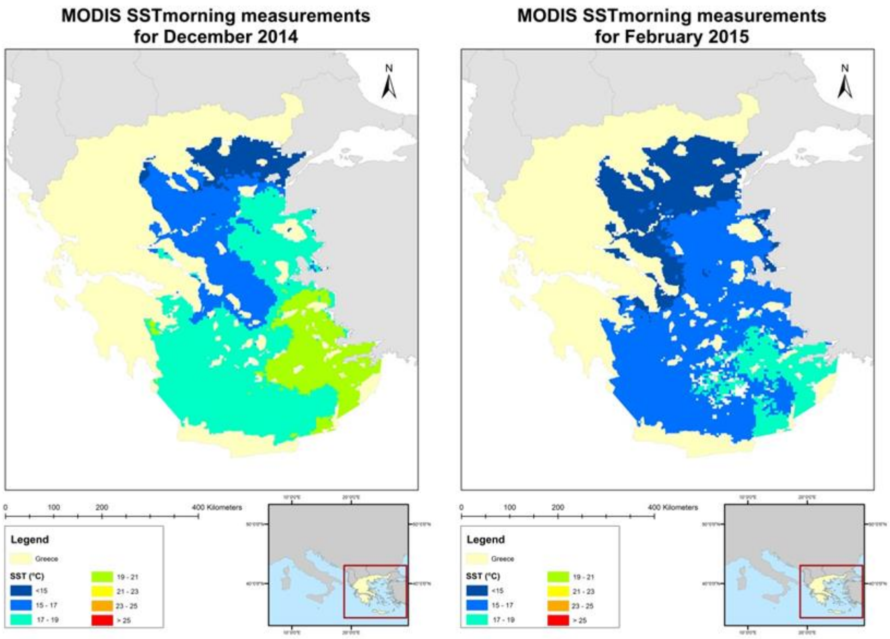

Appendix 13. MODIS SSTmorning measurements for the time period March 2012 to February 2015.

1.4.1.5. CHLOR_A

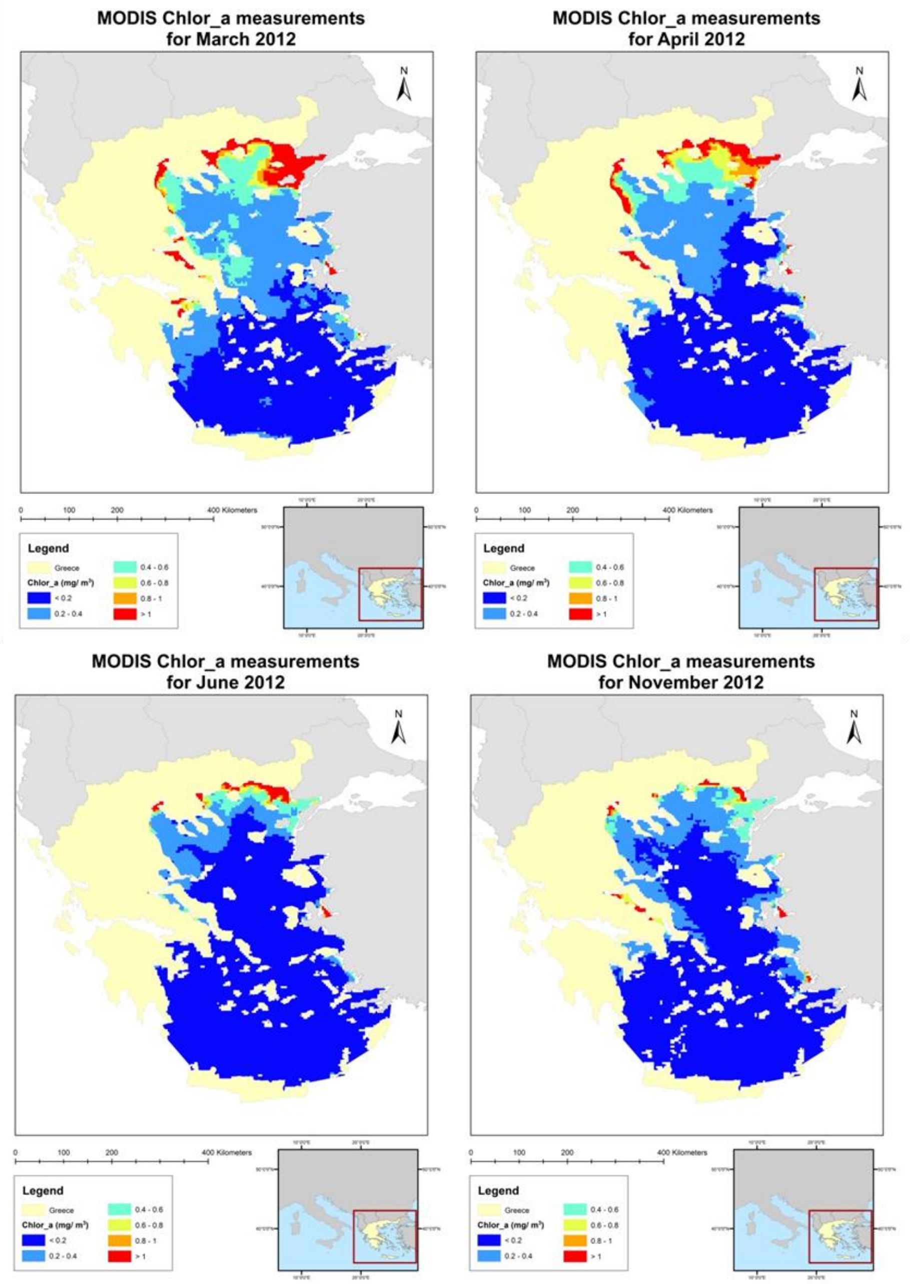
MODIS Chlor_a measurements for March 2012
N
0 100 200 400 Kilometers
Legend
Greece
Chlor_a (mg/ m^3)
< 0.2
0.2 - 0.4
0.4 - 0.6
0.6 - 0.8
0.8 - 1
> 1
MODIS Chlor_a measurements for April 2012
N
0 100 200 400 Kilometers
Legend
Greece
Chlor_a (mg/ m^3)
< 0.2
0.2 - 0.4
0.4 - 0.6
0.6 - 0.8
0.8 - 1
> 1
MODIS Chlor_a measurements for June 2012
N
0 100 200 400 Kilometers
Legend
Greece
Chlor_a (mg/ m^3)
< 0.2
0.2 - 0.4
0.4 - 0.6
0.6 - 0.8
0.8 - 1
> 1
MODIS Chlor_a measurements for November 2012
N
0 100 200 400 Kilometers
Legend
Greece
Chlor_a (mg/ m^3)
< 0.2
0.2 - 0.4
0.4 - 0.6
0.6 - 0.8
0.8 - 1
> 1

MODIS Chlor_a measurements
for December 2012

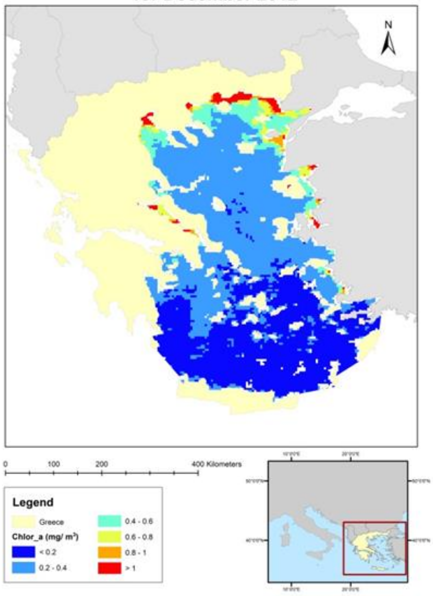

MODIS Chlor_a measurements
for January 2013

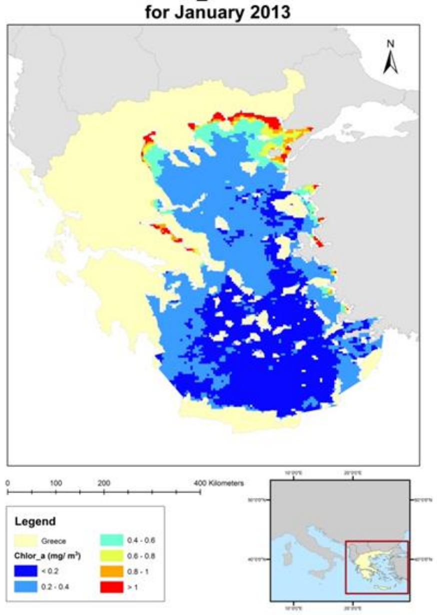

MODIS Chlor_a measurements
for February 2013

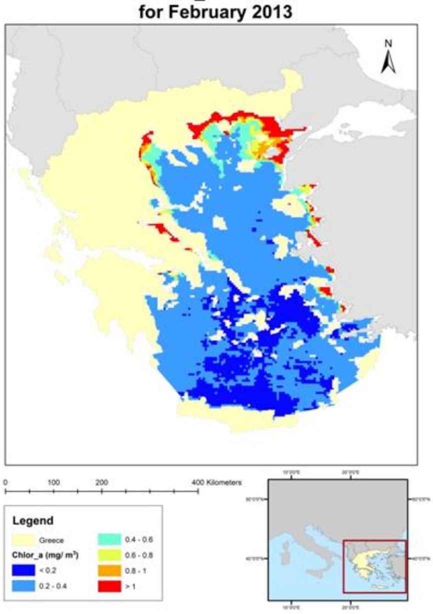

MODIS Chlor_a measurements
for April 2013

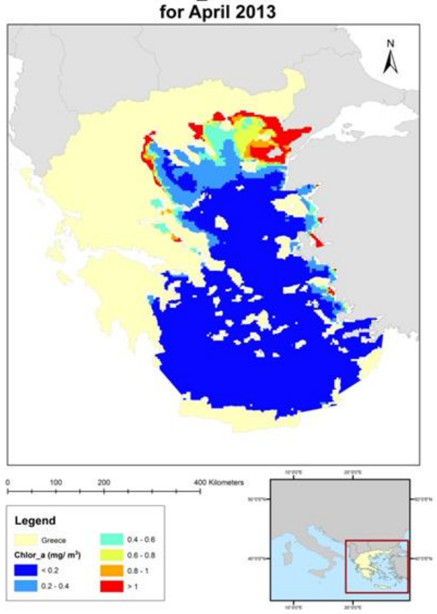

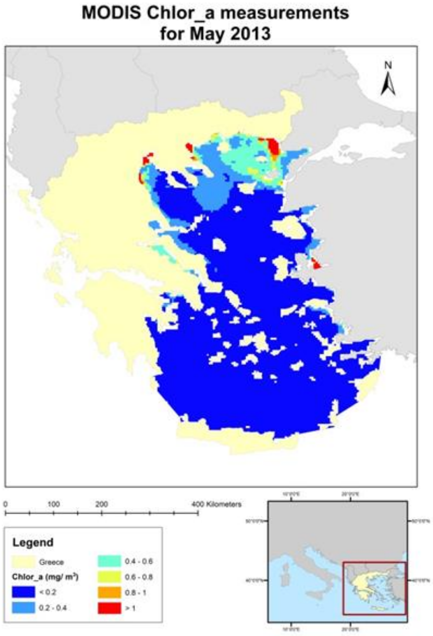
MODIS Chlor_a measurements
for May 2013
N
0 100 200 400 Kilometers
Legend
Greece
Chlor_a (mg/ m3)
< 0.2
0.2 - 0.4
0.4 - 0.6
0.6 - 0.8
0.8 - 1
> 1

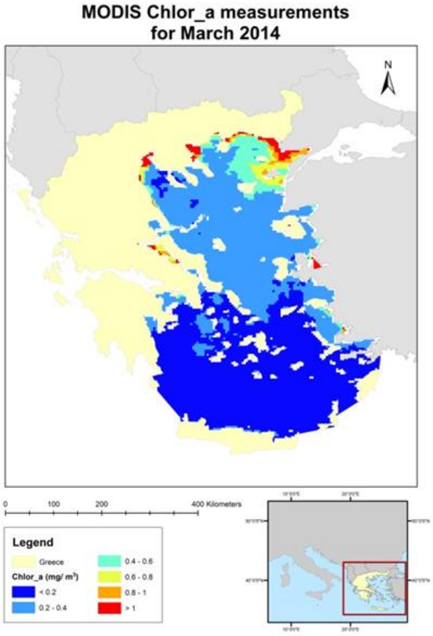
MODIS Chlor_a measurements
for March 2014
N
0 100 200 400 Kilometers
Legend
Greece
Chlor_a (mg/ m3)
< 0.2
0.2 - 0.4
0.4 - 0.6
0.6 - 0.8
0.8 - 1
> 1

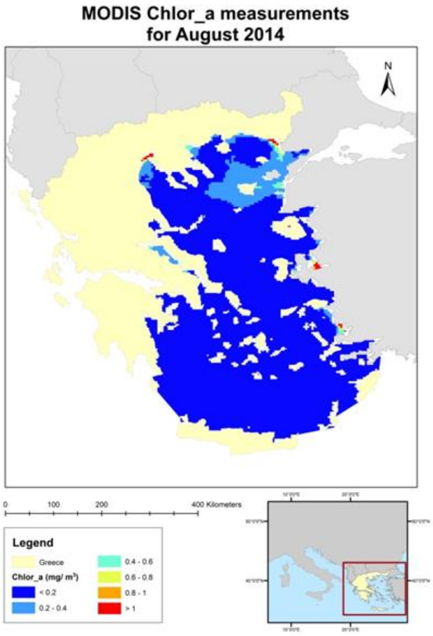
MODIS Chlor_a measurements
for August 2014
N
0 100 200 400 Kilometers
Legend
Greece
Chlor_a (mg/ m3)
< 0.2
0.2 - 0.4
0.4 - 0.6
0.6 - 0.8
0.8 - 1
> 1

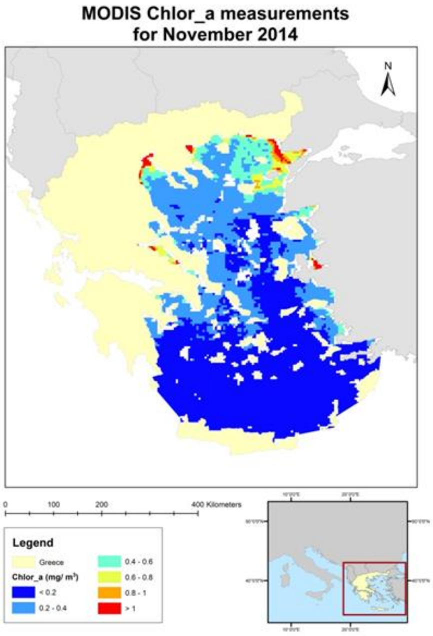
MODIS Chlor_a measurements
for November 2014
N
0 100 200 400 Kilometers
Legend
Greece
Chlor_a (mg/ m3)
< 0.2
0.2 - 0.4
0.4 - 0.6
0.6 - 0.8
0.8 - 1
> 1

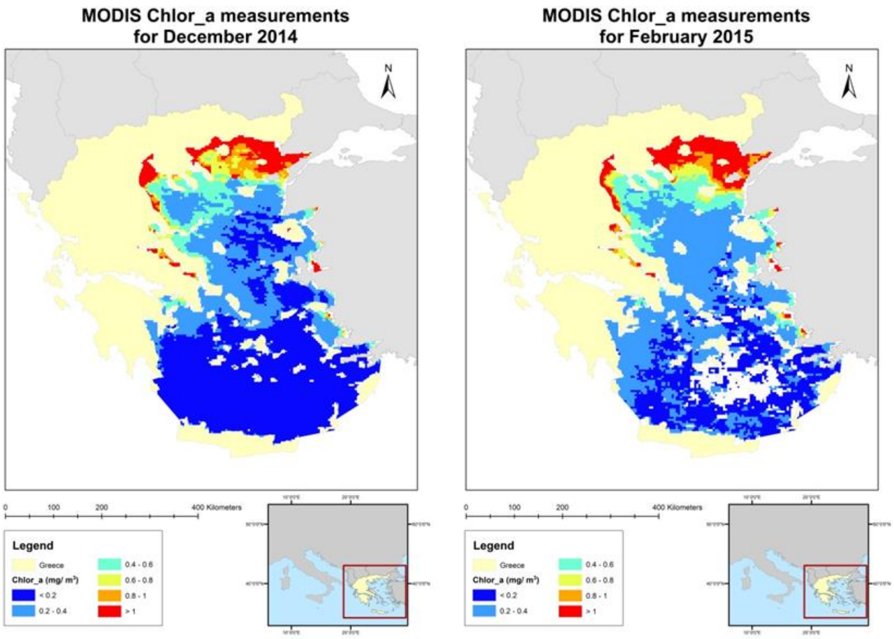

Appendix 14. MODIS Chlor_a measurements for the time period March 2012 to February 2015.

1.4.1.6. PIC

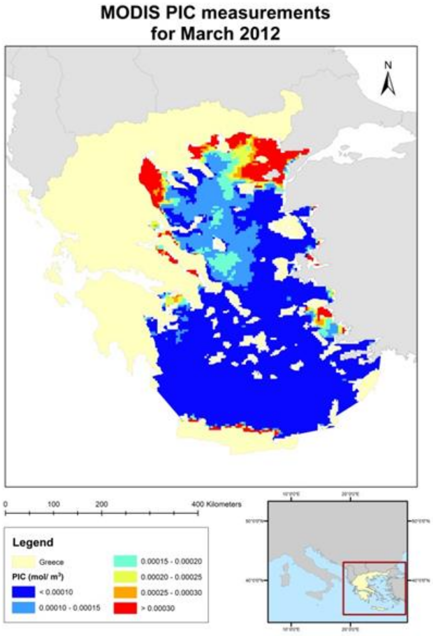
MODIS PIC measurements
for March 2012
Legend
Greece
PIC (mol/ m³)
< 0.00010
0.00010 - 0.00015
0.00015 - 0.00020
0.00020 - 0.00025
0.00025 - 0.00030
> 0.00030
400 Kilometers

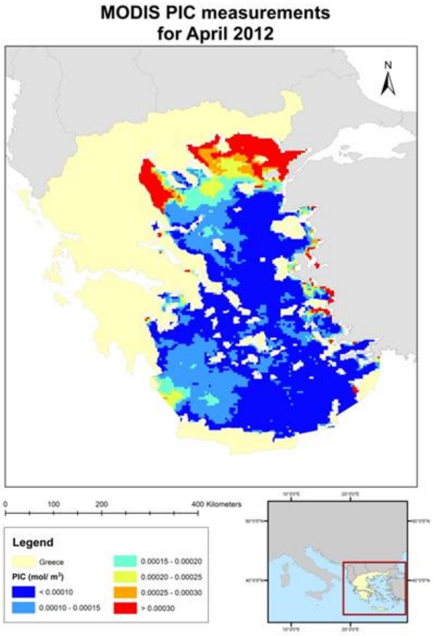
MODIS PIC measurements
for April 2012
Legend
Greece
PIC (mol/ m³)
< 0.00010
0.00010 - 0.00015
0.00015 - 0.00020
0.00020 - 0.00025
0.00025 - 0.00030
> 0.00030
400 Kilometers

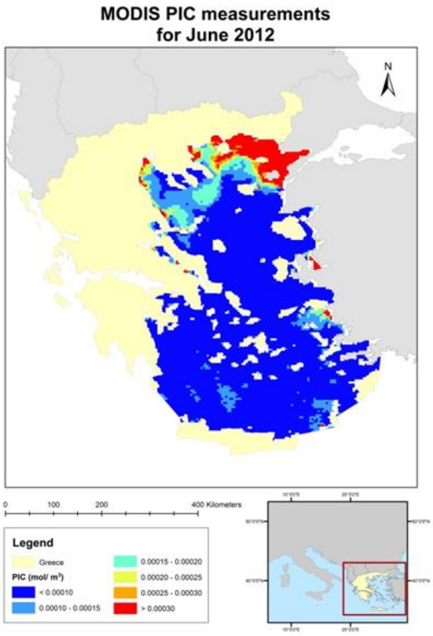
MODIS PIC measurements
for June 2012
Legend
Greece
PIC (mol/ m³)
< 0.00010
0.00010 - 0.00015
0.00015 - 0.00020
0.00020 - 0.00025
0.00025 - 0.00030
> 0.00030
400 Kilometers

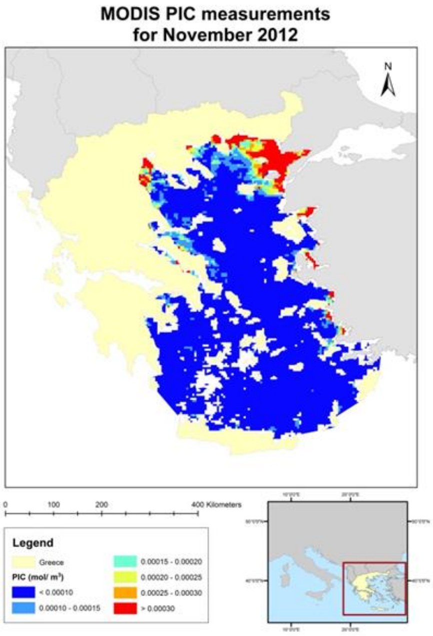
MODIS PIC measurements
for November 2012
Legend
Greece
PIC (mol/ m³)
< 0.00010
0.00010 - 0.00015
0.00015 - 0.00020
0.00020 - 0.00025
0.00025 - 0.00030
> 0.00030
400 Kilometers

MODIS PIC measurements for December 2012

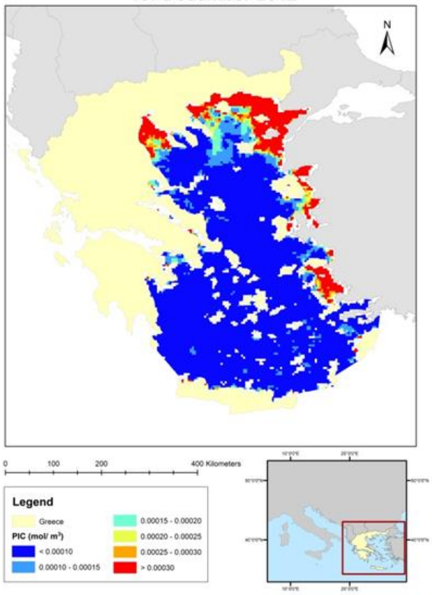

MODIS PIC measurements for January 2013

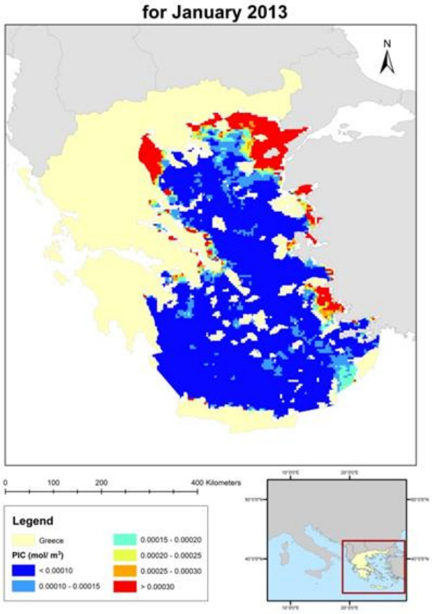

MODIS PIC measurements for February 2013

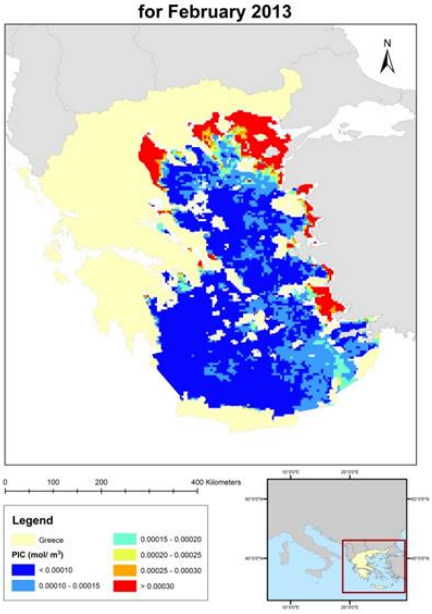

MODIS PIC measurements for April 2013

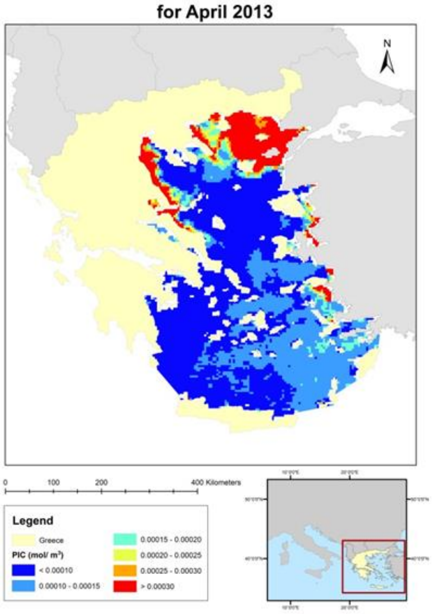

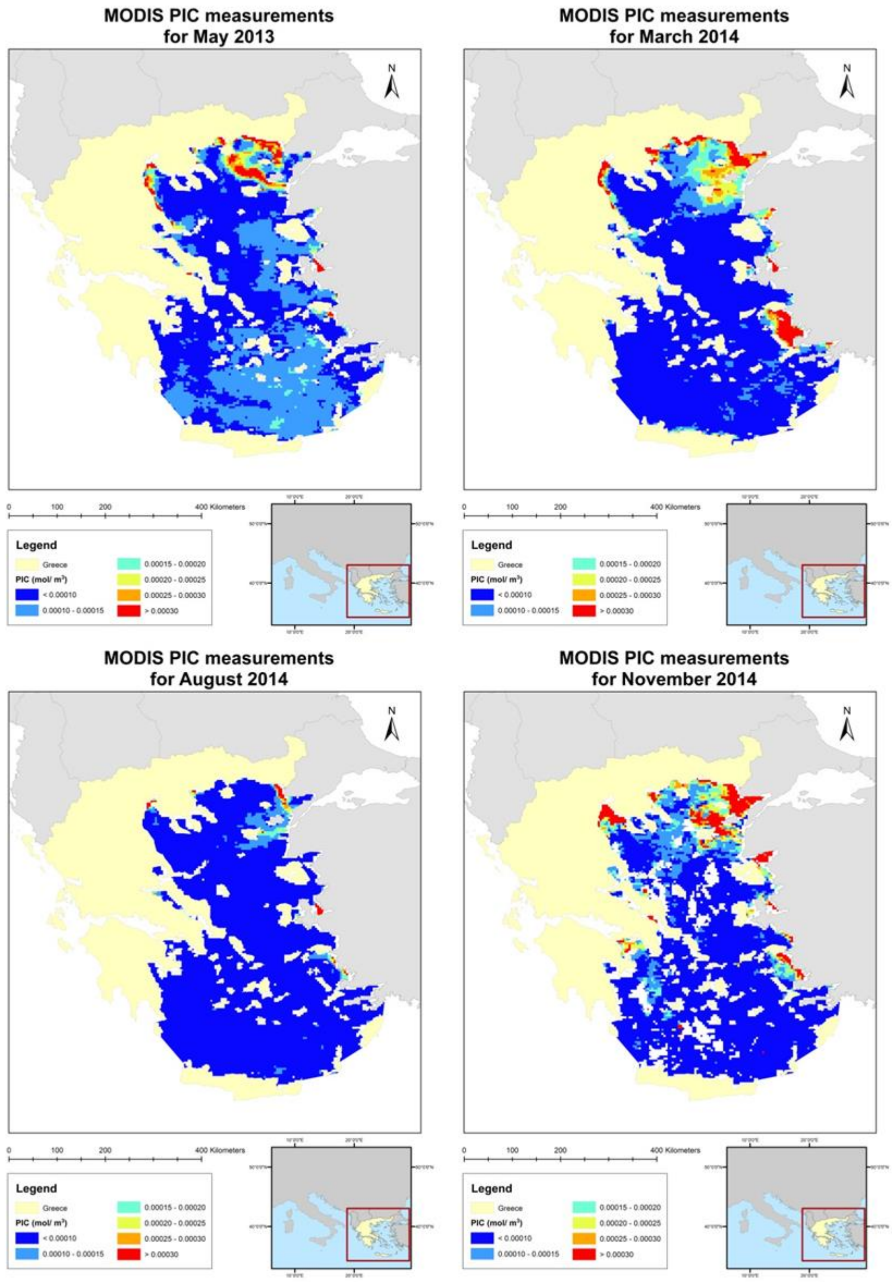
MODIS PIC measurements
for May 2013
MODIS PIC measurements
for March 2014
MODIS PIC measurements
for August 2014
MODIS PIC measurements
for November 2014
N
0 100 200 400 Kilometers
Legend
Greece
PIC (mol/ m3)
< 0.00010
0.00010 - 0.00015
0.00015 - 0.00020
0.00020 - 0.00025
0.00025 - 0.00030
> 0.00030

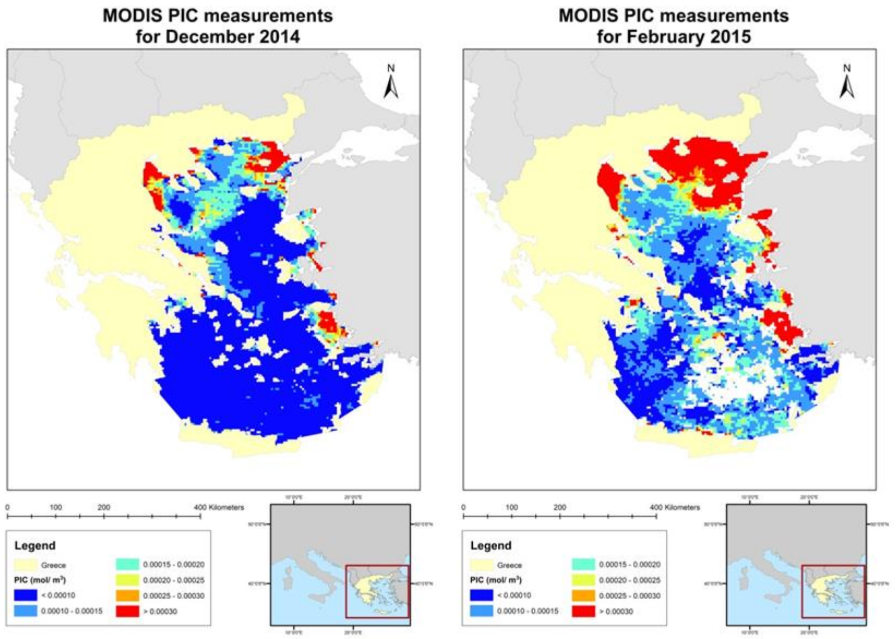

Appendix 15. MODIS PIC measurements for the time period March 2012 to February 2015.

1.4.1.7. POC

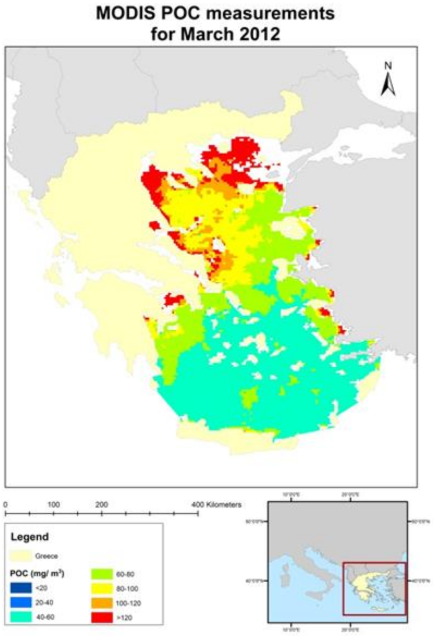
MODIS POC measurements
for March 2012
N
0 100 200 400 Kilometers
Legend
Greece
POC (mg/ m3)
<20
20-40
40-60
60-80
80-100
100-120
>120

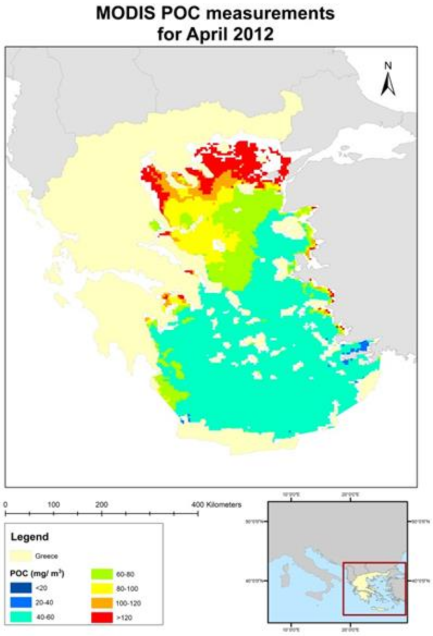
MODIS POC measurements
for April 2012
N
0 100 200 400 Kilometers
Legend
Greece
POC (mg/ m3)
<20
20-40
40-60
60-80
80-100
100-120
>120

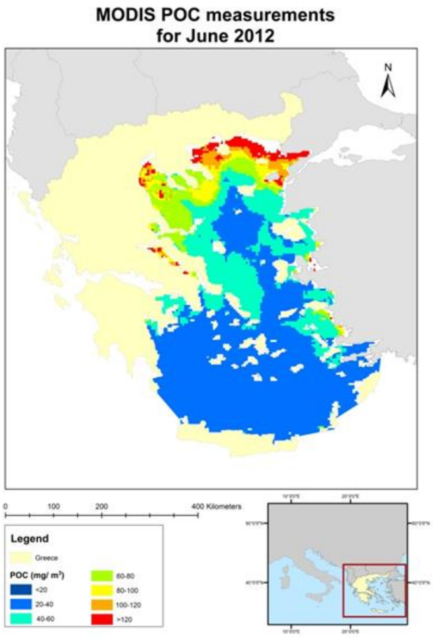
MODIS POC measurements
for June 2012
N
0 100 200 400 Kilometers
Legend
Greece
POC (mg/ m3)
<20
20-40
40-60
60-80
80-100
100-120
>120

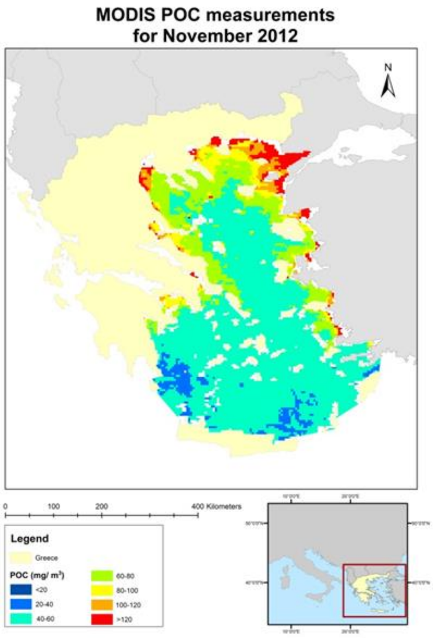
MODIS POC measurements
for November 2012
N
0 100 200 400 Kilometers
Legend
Greece
POC (mg/ m3)
<20
20-40
40-60
60-80
80-100
100-120
>120

MODIS POC measurements for December 2012

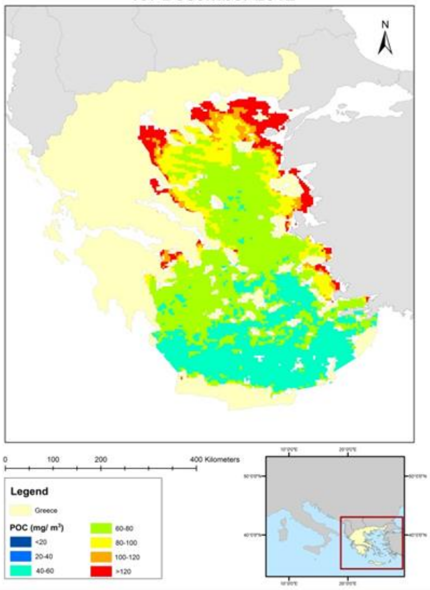

MODIS POC measurements for January 2013

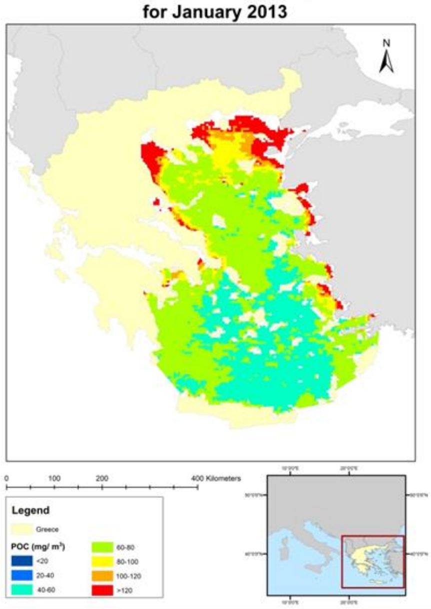

MODIS POC measurements for February 2013

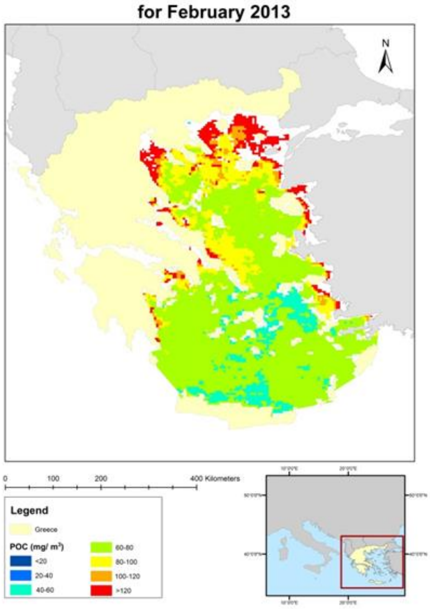

MODIS POC measurements for April 2013

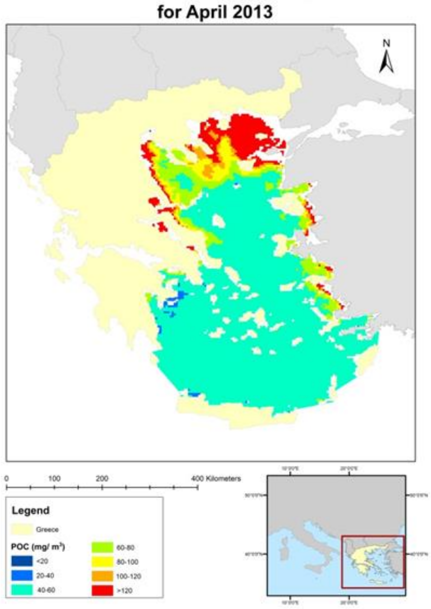

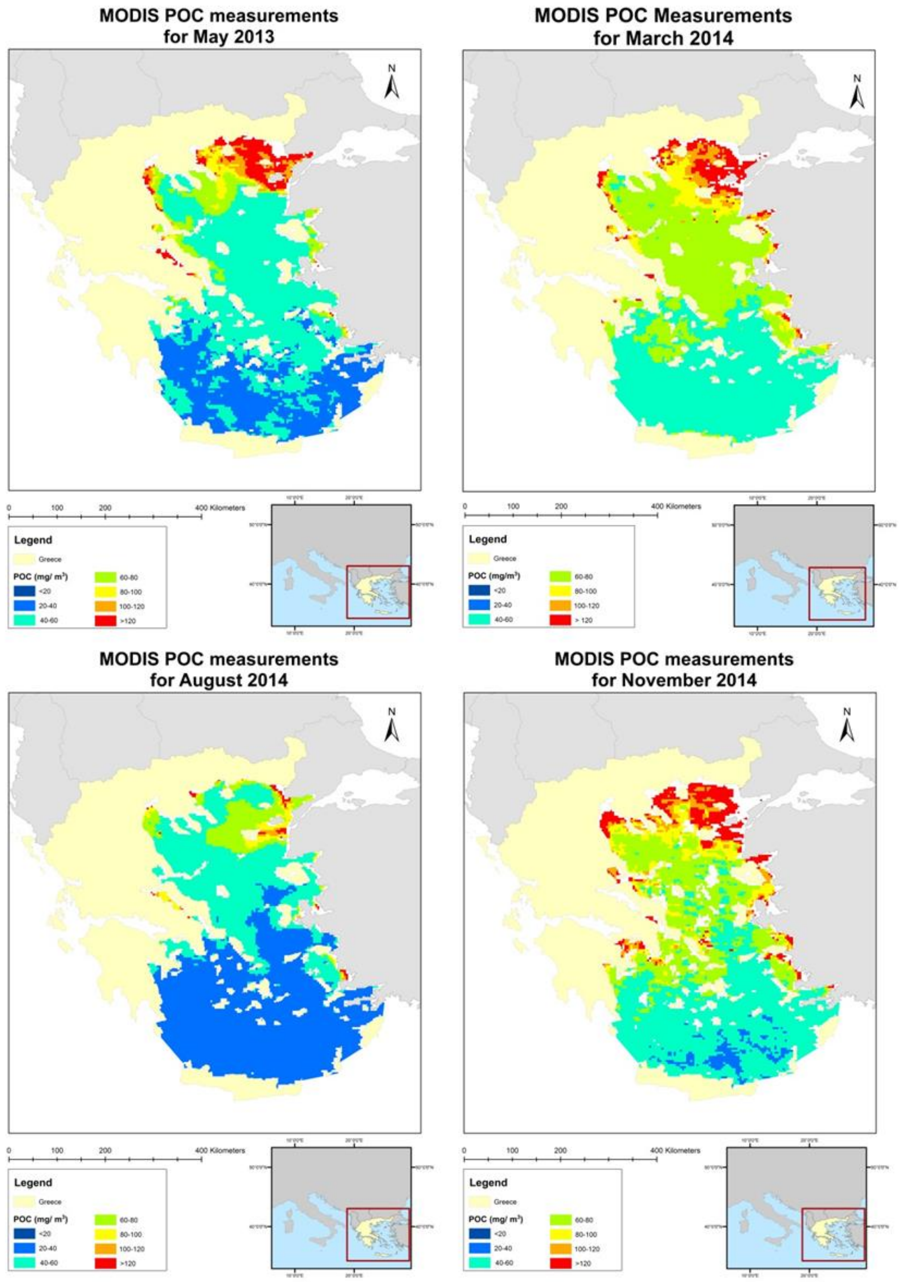
MODIS POC measurements
for May 2013
MODIS POC Measurements
for March 2014
MODIS POC measurements
for August 2014
MODIS POC measurements
for November 2014
N
0
100
200
400 Kilometers
Legend
Greece
POC (mg/ m³)
<20
20-40
40-60
60-80
80-100
100-120
>120

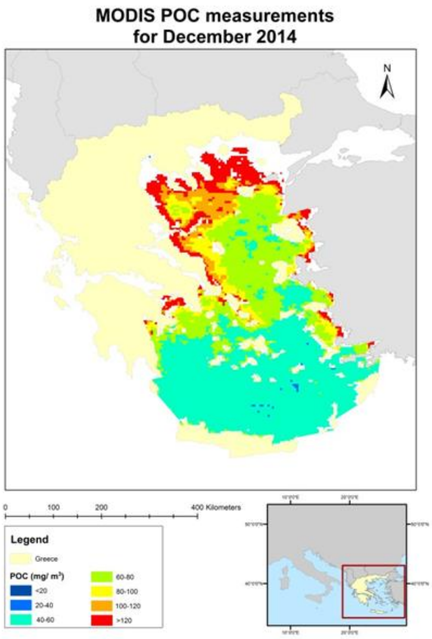

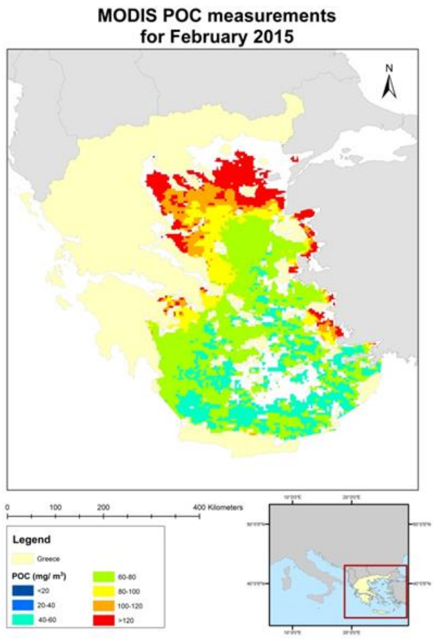

Appendix 16. MODIS POC measurements for the time period March 2012 to February 2015.

1.4.1.8. iPAR

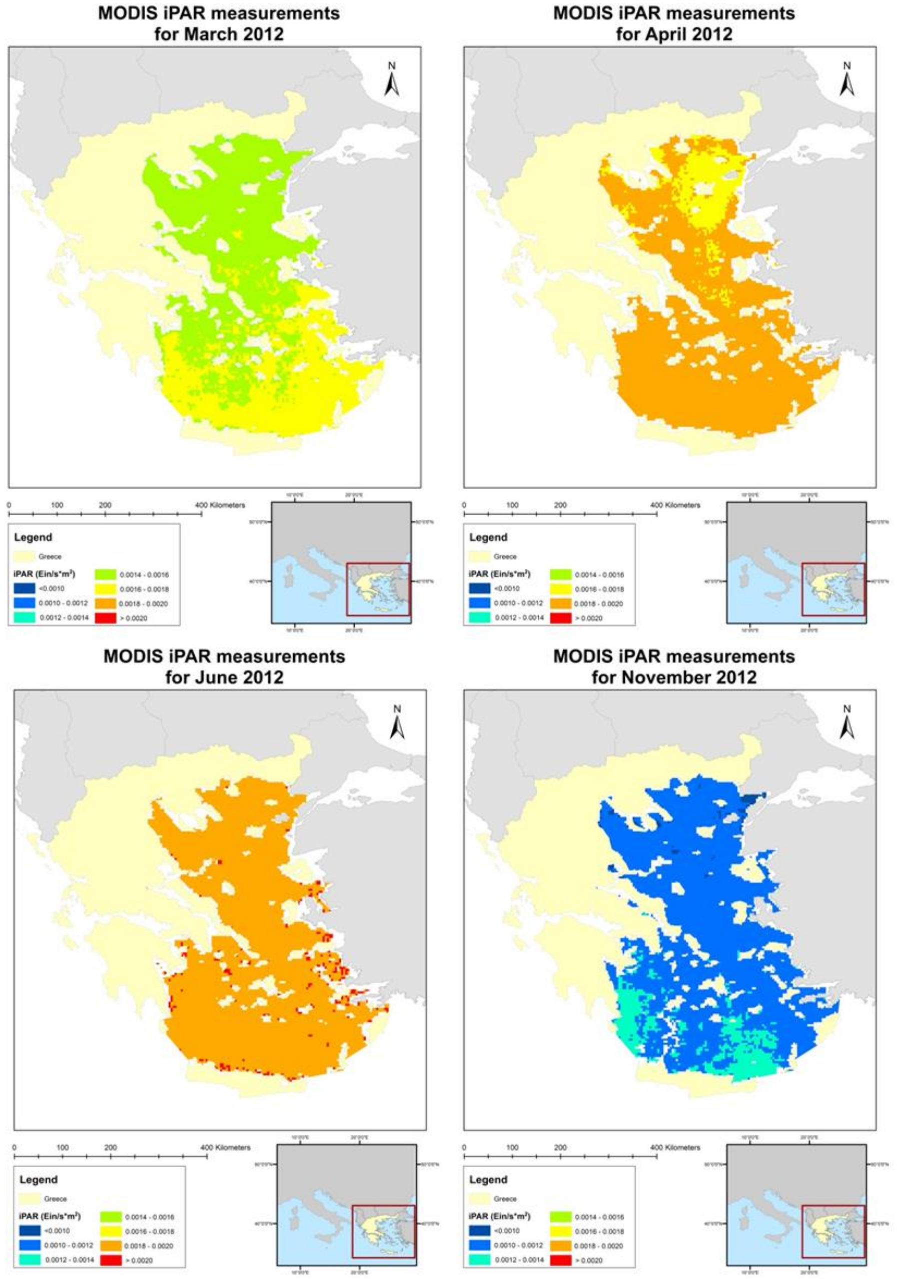
MODIS iPAR measurements
for March 2012
N
0
100
200
400 Kilometers
Legend
Greece
iPAR (Ein/s*m²)
<0.0010
0.0010 - 0.0012
0.0012 - 0.0014
0.0014 - 0.0016
0.0016 - 0.0018
0.0018 - 0.0020
> 0.0020
MODIS iPAR measurements
for April 2012
N
0
100
200
400 Kilometers
Legend
Greece
iPAR (Ein/s*m²)
<0.0010
0.0010 - 0.0012
0.0012 - 0.0014
0.0014 - 0.0016
0.0016 - 0.0018
0.0018 - 0.0020
> 0.0020
MODIS iPAR measurements
for June 2012
N
0
100
200
400 Kilometers
Legend
Greece
iPAR (Ein/s*m²)
<0.0010
0.0010 - 0.0012
0.0012 - 0.0014
0.0014 - 0.0016
0.0016 - 0.0018
0.0018 - 0.0020
> 0.0020
MODIS iPAR measurements
for November 2012
N
0
100
200
400 Kilometers
Legend
Greece
iPAR (Ein/s*m²)
<0.0010
0.0010 - 0.0012
0.0012 - 0.0014
0.0014 - 0.0016
0.0016 - 0.0018
0.0018 - 0.0020
> 0.0020

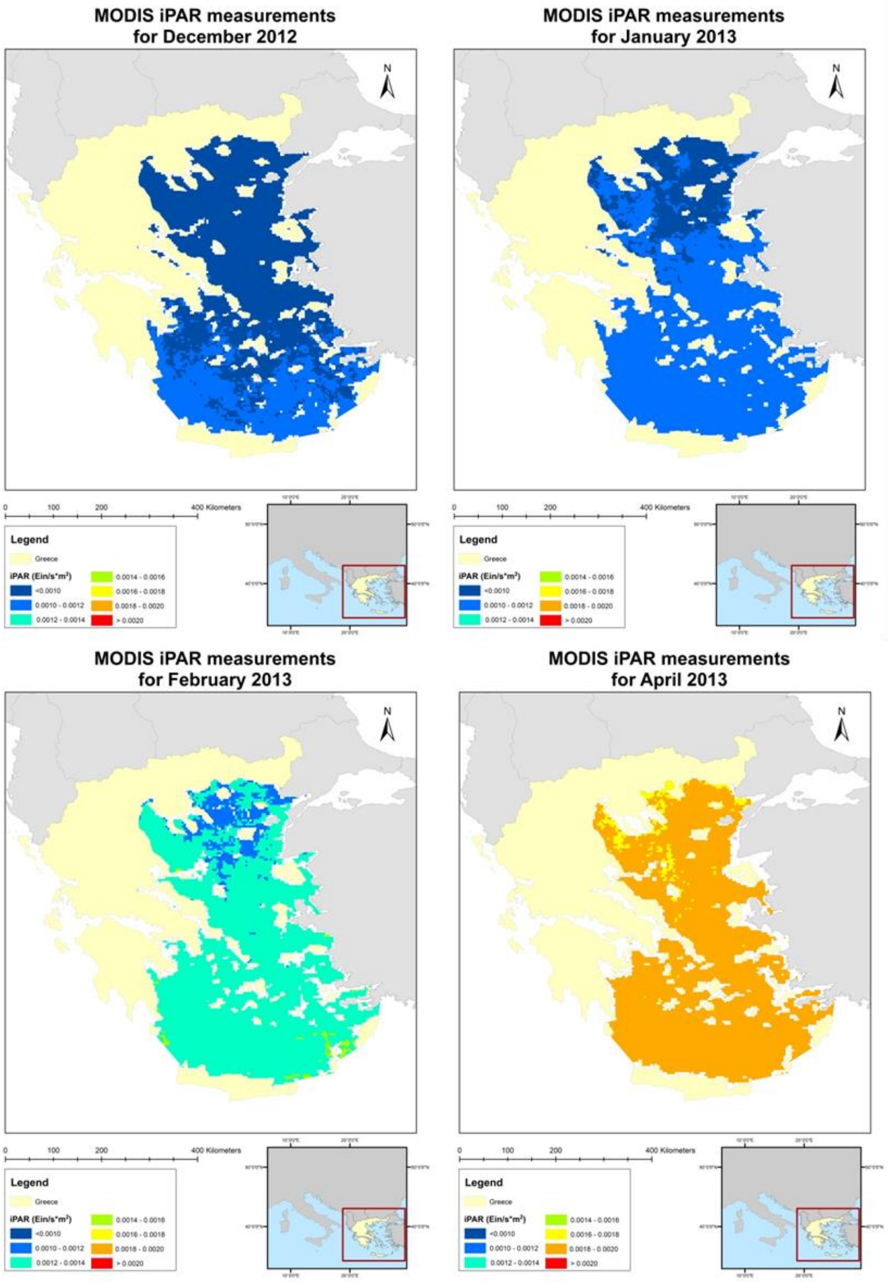
MODIS iPAR measurements
for December 2012
N
0
100
200
400 Kilometers
Legend
Greece
iPAR (Ein/s*m2)
<0.0010
0.0010 - 0.0012
0.0012 - 0.0014
0.0014 - 0.0016
0.0016 - 0.0018
0.0018 - 0.0020
> 0.0020
MODIS iPAR measurements
for January 2013
N
0
100
200
400 Kilometers
Legend
Greece
iPAR (Ein/s*m2)
<0.0010
0.0010 - 0.0012
0.0012 - 0.0014
0.0014 - 0.0016
0.0016 - 0.0018
0.0018 - 0.0020
> 0.0020
MODIS iPAR measurements
for February 2013
N
0
100
200
400 Kilometers
Legend
Greece
iPAR (Ein/s*m2)
<0.0010
0.0010 - 0.0012
0.0012 - 0.0014
0.0014 - 0.0016
0.0016 - 0.0018
0.0018 - 0.0020
> 0.0020
MODIS iPAR measurements
for April 2013
N
0
100
200
400 Kilometers
Legend
Greece
iPAR (Ein/s*m2)
<0.0010
0.0010 - 0.0012
0.0012 - 0.0014
0.0014 - 0.0016
0.0016 - 0.0018
0.0018 - 0.0020
> 0.0020

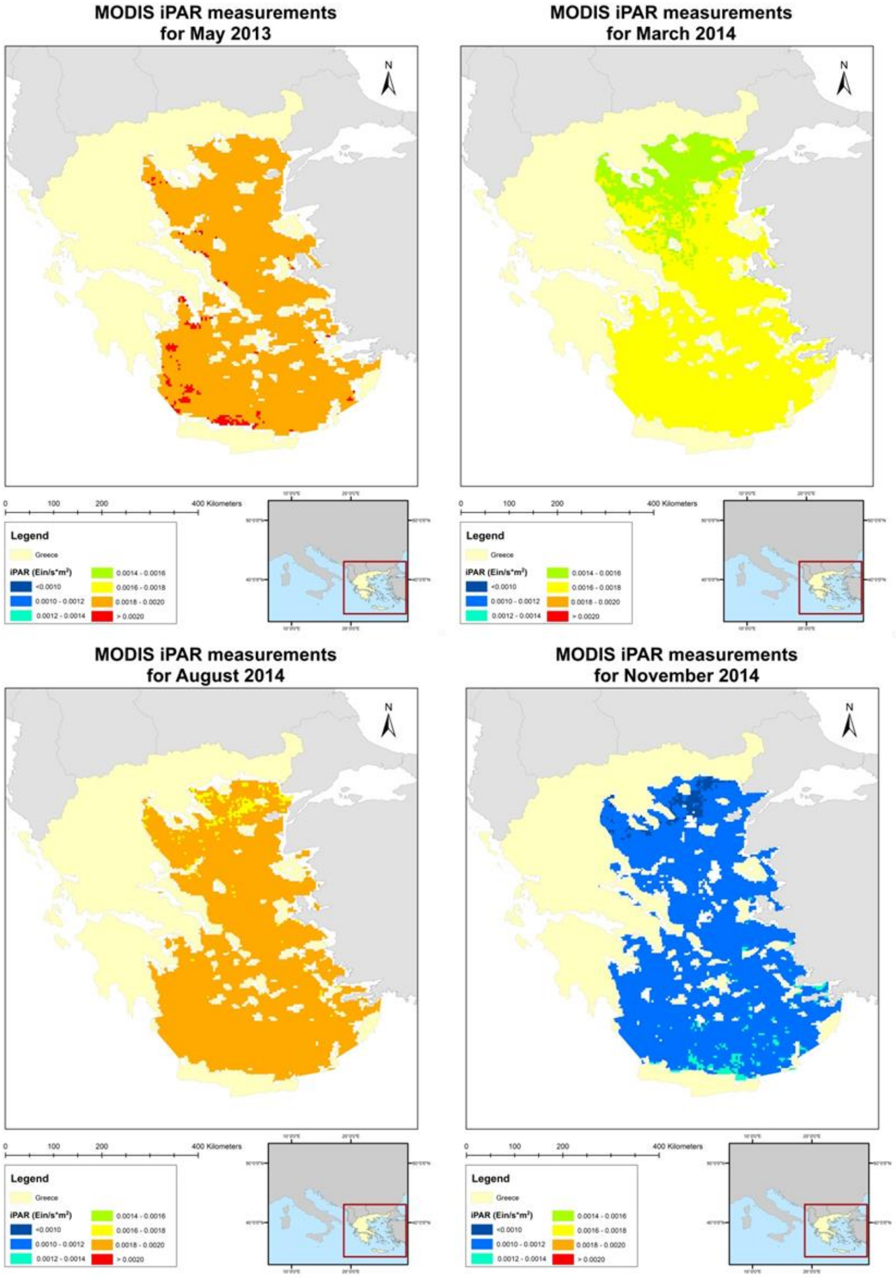

MODIS iPAR measurements for May 2013
MODIS iPAR measurements for March 2014
MODIS iPAR measurements for August 2014
MODIS iPAR measurements for November 2014
N
0 100 200 400 Kilometers
Legend
Greece
iPAR (Ein/s*m2)
<0.0010
0.0010 - 0.0012
0.0012 - 0.0014
0.0014 - 0.0016
0.0016 - 0.0018
0.0018 - 0.0020
> 0.0020

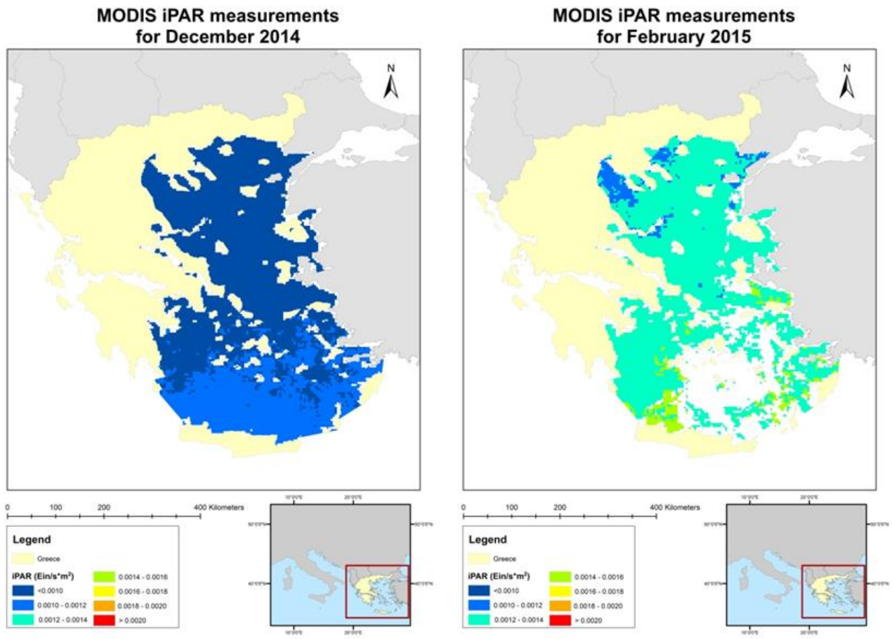

Appendix 17. MODIS iPAR measurements for the time period March 2012 to February 2015.

1.4.1.9. PAR

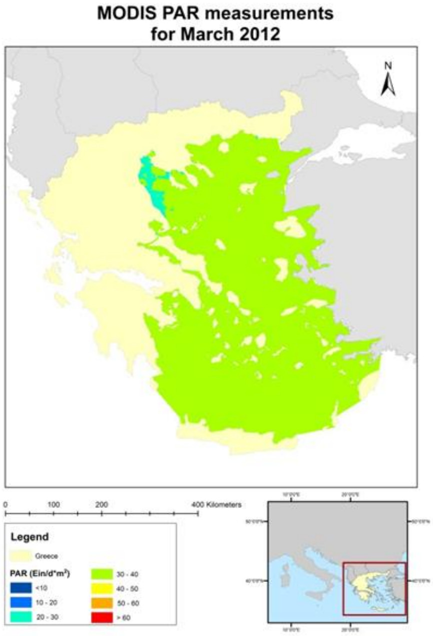
MODIS PAR measurements
for March 2012
N
0
100
200
400 Kilometers
Legend
Greece
PAR (Ein/d*m2)
<10
10 - 20
20 - 30
30 - 40
40 - 50
50 - 60
> 60

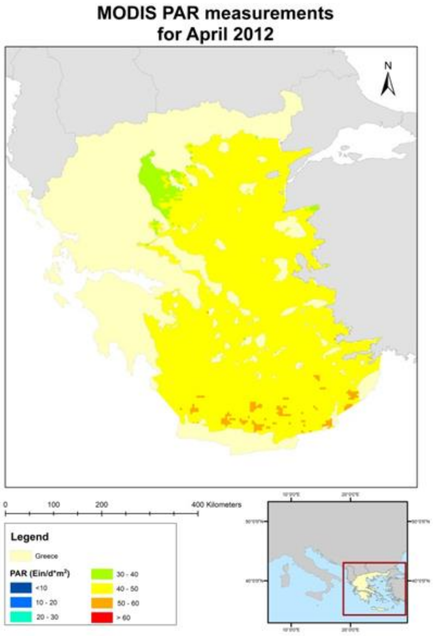
MODIS PAR measurements
for April 2012
N
0
100
200
400 Kilometers
Legend
Greece
PAR (Ein/d*m2)
<10
10 - 20
20 - 30
30 - 40
40 - 50
50 - 60
> 60

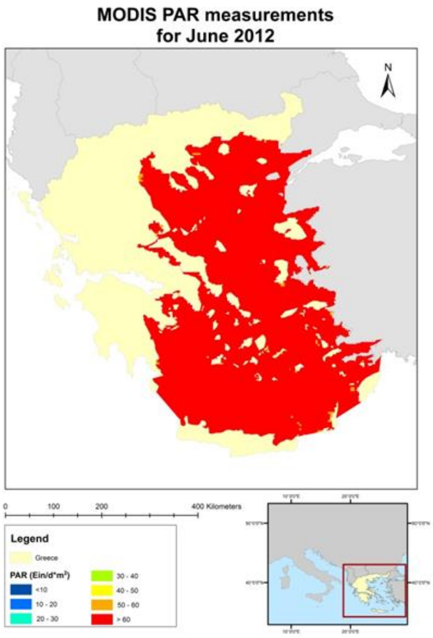
MODIS PAR measurements
for June 2012
N
0
100
200
400 Kilometers
Legend
Greece
PAR (Ein/d*m2)
<10
10 - 20
20 - 30
30 - 40
40 - 50
50 - 60
> 60

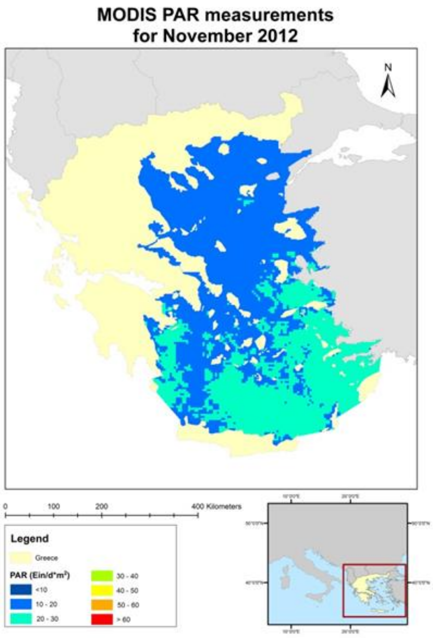
MODIS PAR measurements
for November 2012
N
0
100
200
400 Kilometers
Legend
Greece
PAR (Ein/d*m2)
<10
10 - 20
20 - 30
30 - 40
40 - 50
50 - 60
> 60

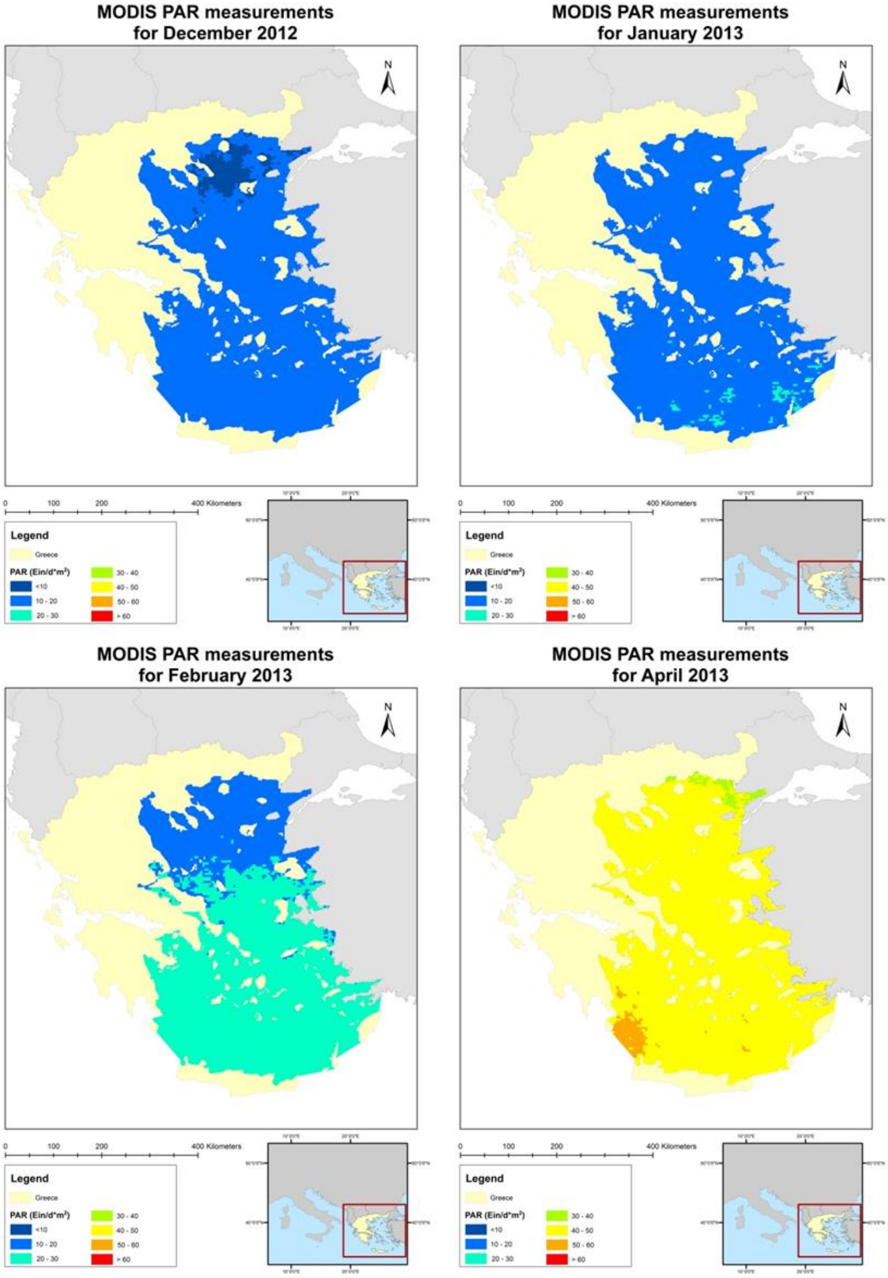
MODIS PAR measurements for December 2012
MODIS PAR measurements for January 2013
MODIS PAR measurements for February 2013
MODIS PAR measurements for April 2013
0 100 200 400 Kilometers
Legend
Greece
PAR (Ein/d*m2)
<10
10 - 20
20 - 30
30 - 40
40 - 50
50 - 60
> 60

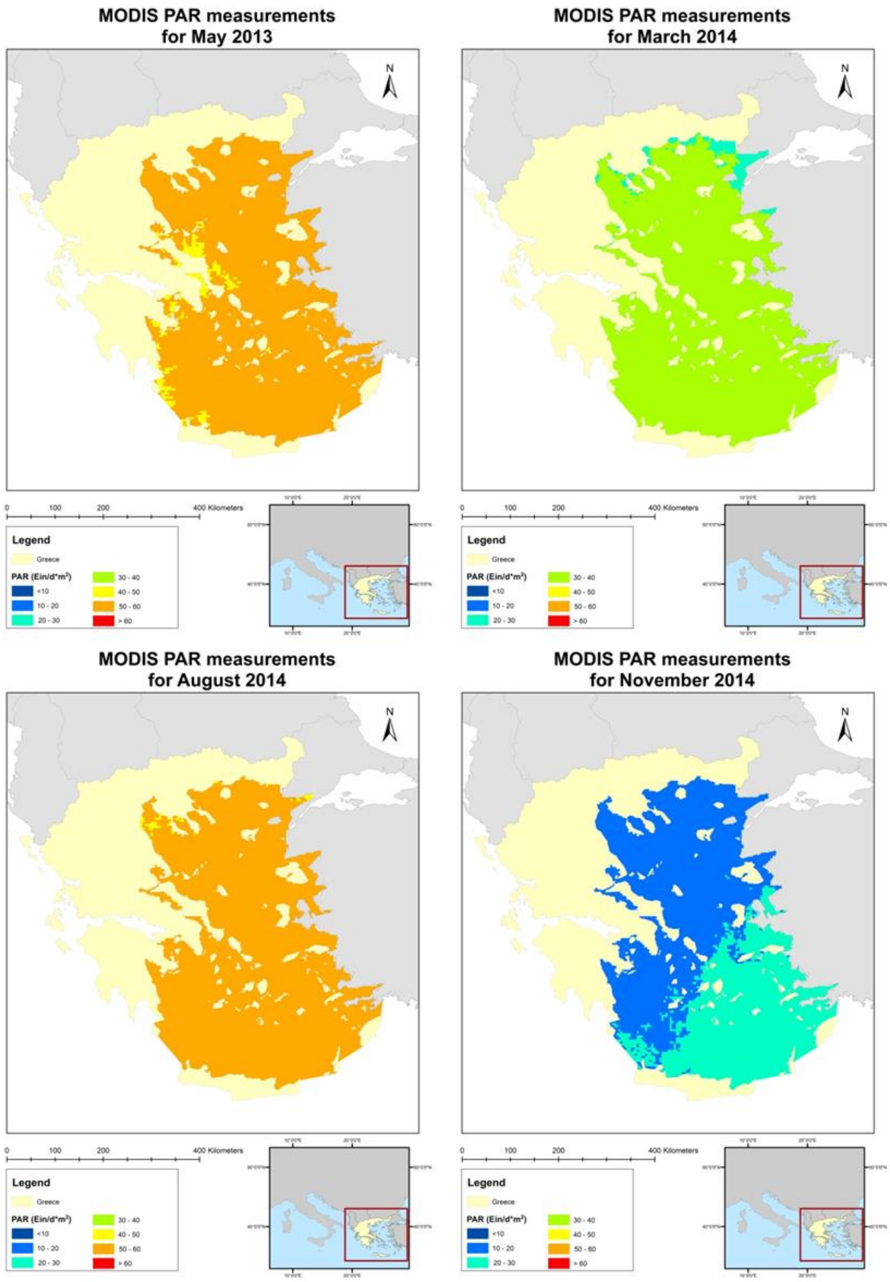
MODIS PAR measurements
for May 2013
MODIS PAR measurements
for March 2014
MODIS PAR measurements
for August 2014
MODIS PAR measurements
for November 2014
N
0 100 200 400 Kilometers
Legend
Greece
PAR (Ein/d*m^2)
<10
10 - 20
20 - 30
30 - 40
40 - 50
50 - 60
> 60

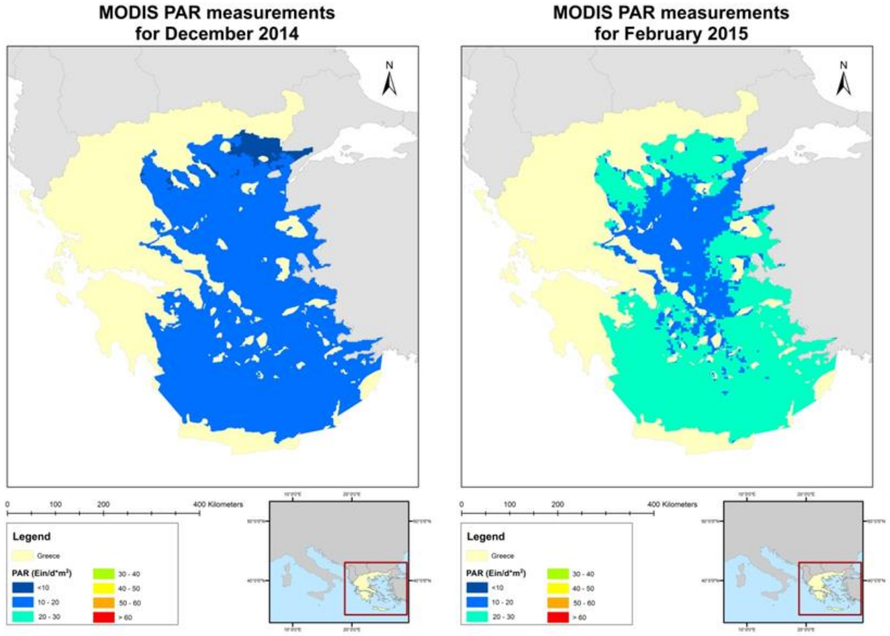

Appendix 18. MODIS PAR measurements for the time period March 2012 to February 2015.

1.4.1.10. SMOS SST_A

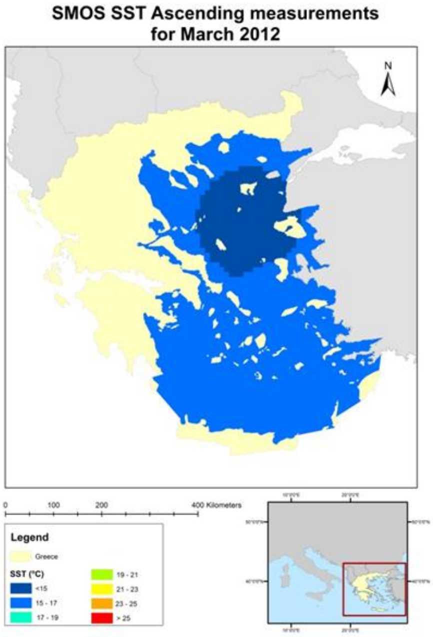

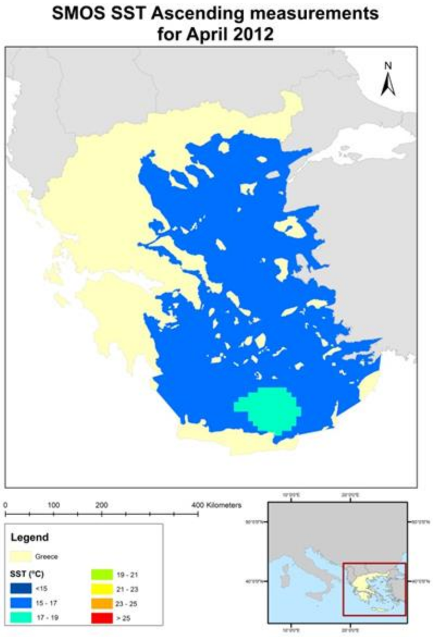

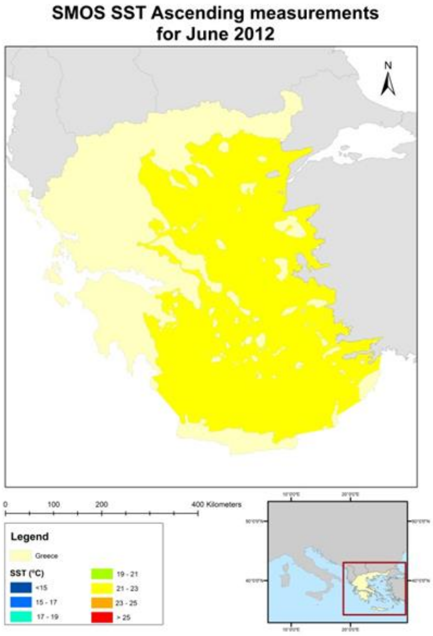

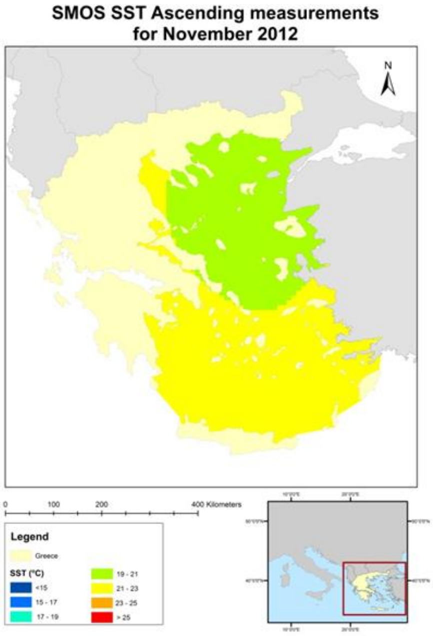

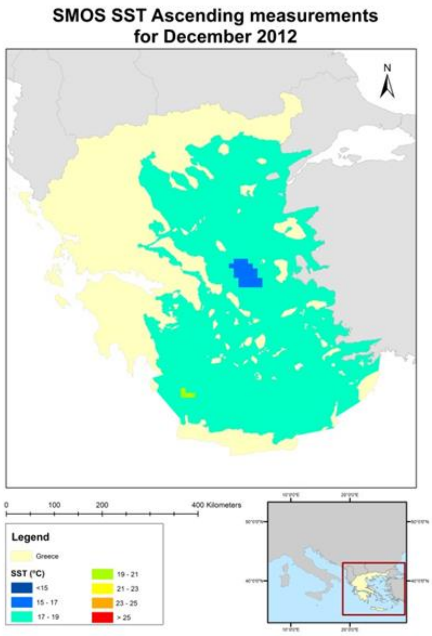
SMOS SST Ascending measurements
for December 2012
N
0 100 200 400 Kilometers
Legend
Greece
SST (°C)
<15
15 - 17
17 - 19
19 - 21
21 - 23
23 - 25
> 25

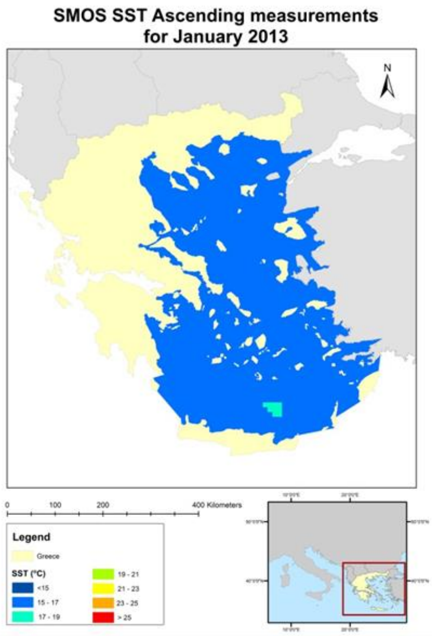
SMOS SST Ascending measurements
for January 2013
N
0 100 200 400 Kilometers
Legend
Greece
SST (°C)
<15
15 - 17
17 - 19
19 - 21
21 - 23
23 - 25
> 25

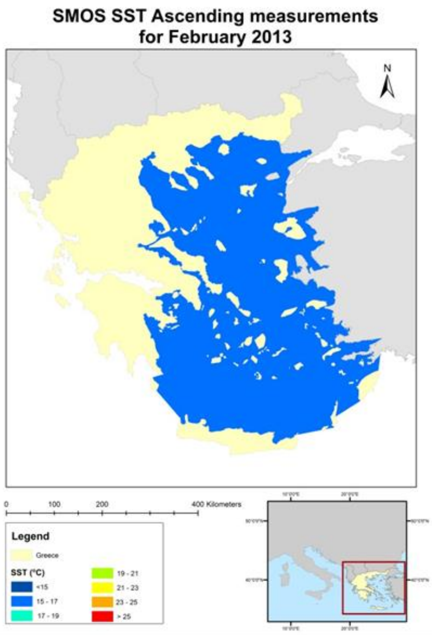
SMOS SST Ascending measurements
for February 2013
N
0 100 200 400 Kilometers
Legend
Greece
SST (°C)
<15
15 - 17
17 - 19
19 - 21
21 - 23
23 - 25
> 25

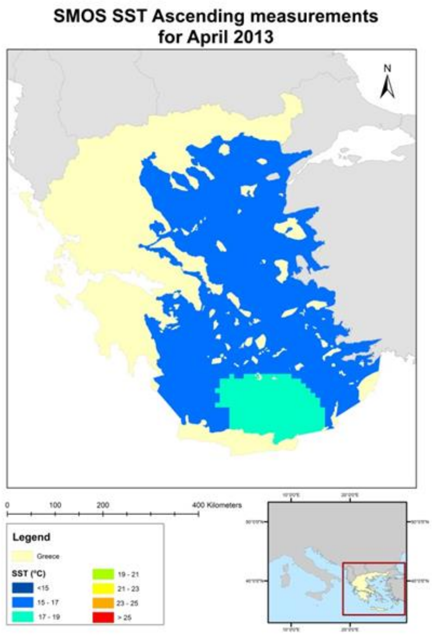
SMOS SST Ascending measurements
for April 2013
N
0 100 200 400 Kilometers
Legend
Greece
SST (°C)
<15
15 - 17
17 - 19
19 - 21
21 - 23
23 - 25
> 25

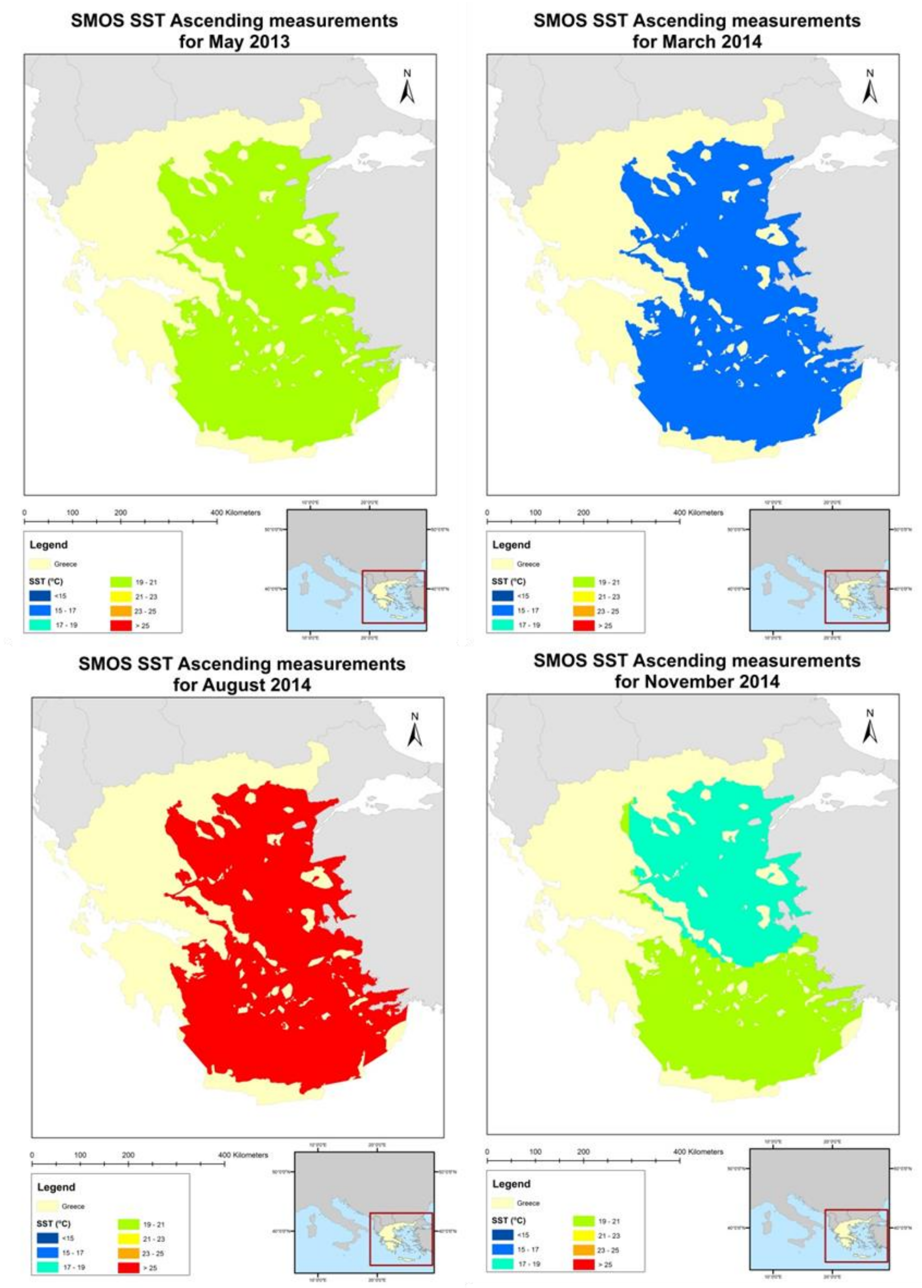
SMOS SST Ascending measurements for May 2013
SMOS SST Ascending measurements for March 2014
SMOS SST Ascending measurements for August 2014
SMOS SST Ascending measurements for November 2014
N
0 100 200 400 Kilometers
Legend
Greece
SST (°C)
<15
15 - 17
17 - 19
19 - 21
21 - 23
23 - 25
> 25

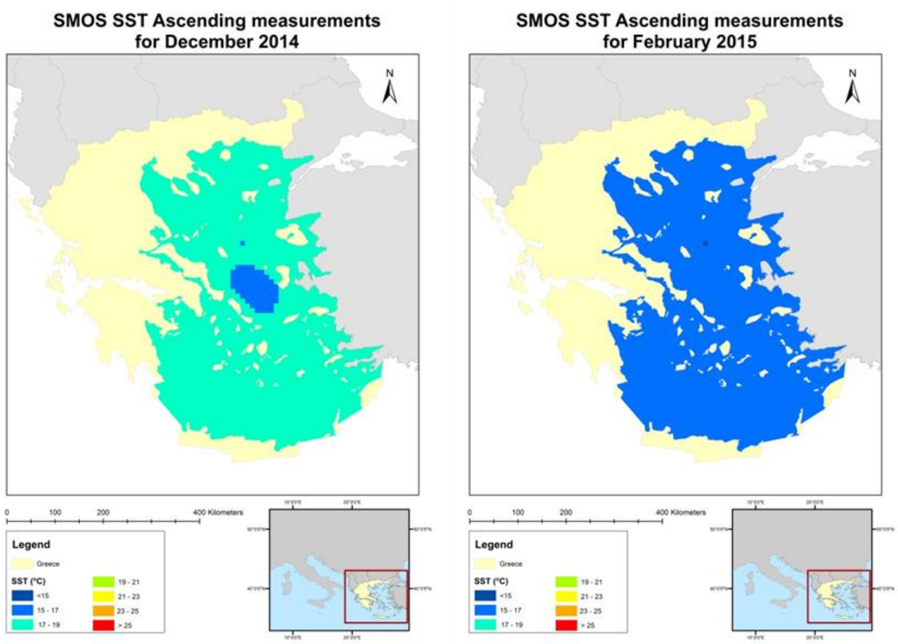

Appendix 19. SMOS SST_Ascending measurements for the time period March 2012 to February 2015.

1.4.1.11. SMOS SST_D

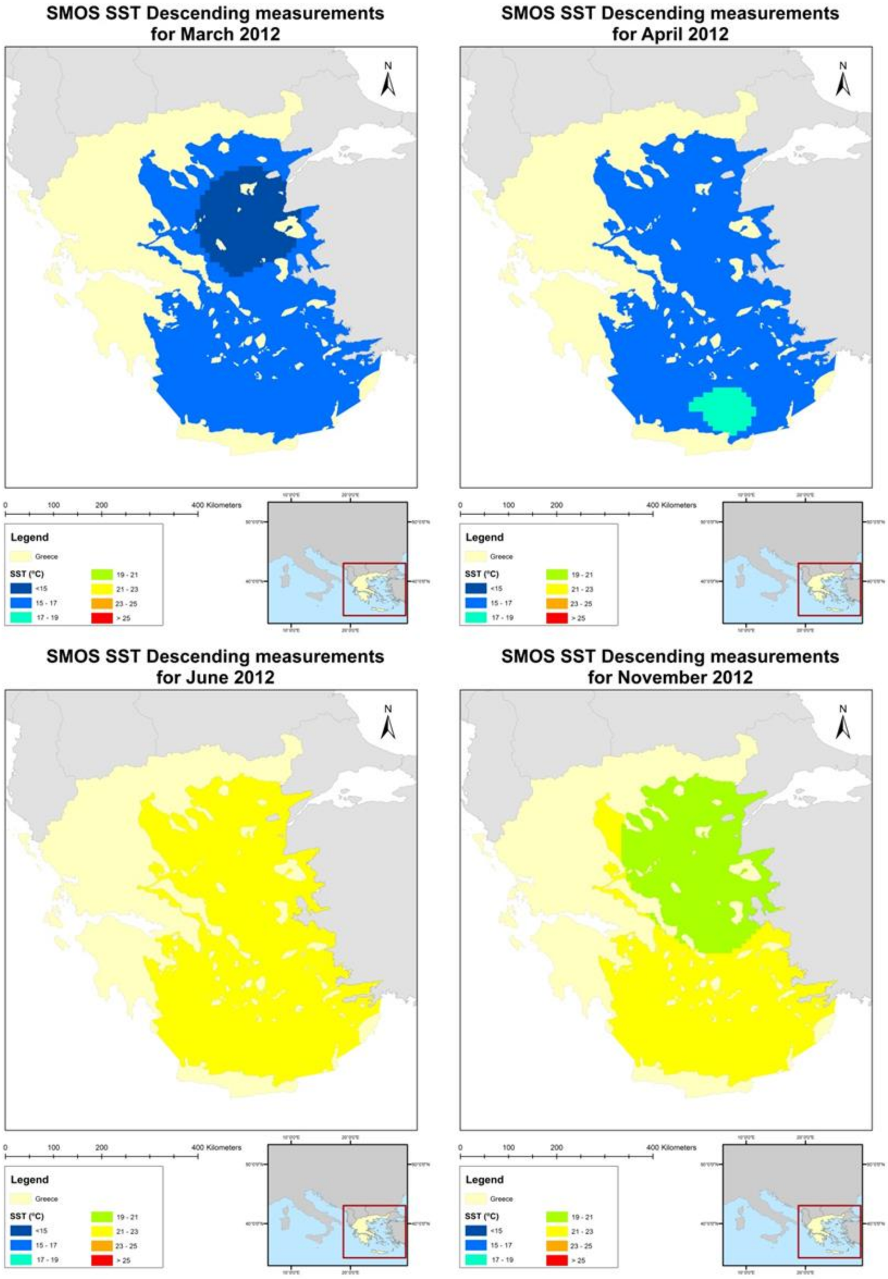

SMOS SST Descending measurements for December 2012

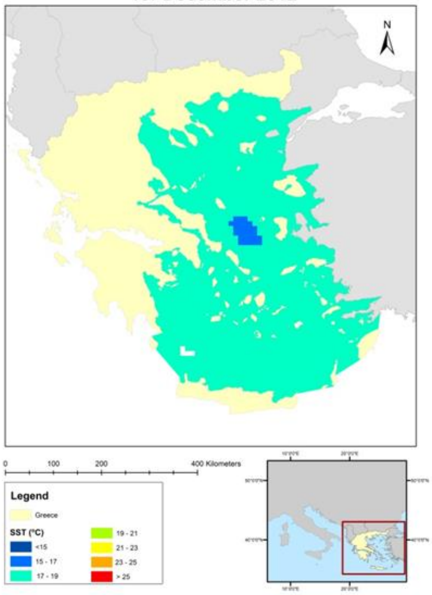

SMOS SST Descending measurements for January 2013

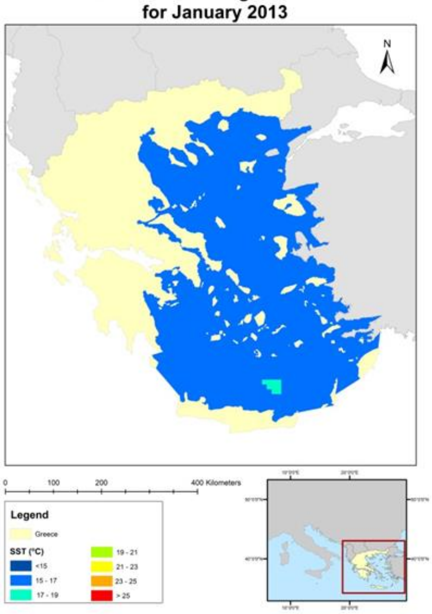

SMOS SST Descending measurements for February 2013

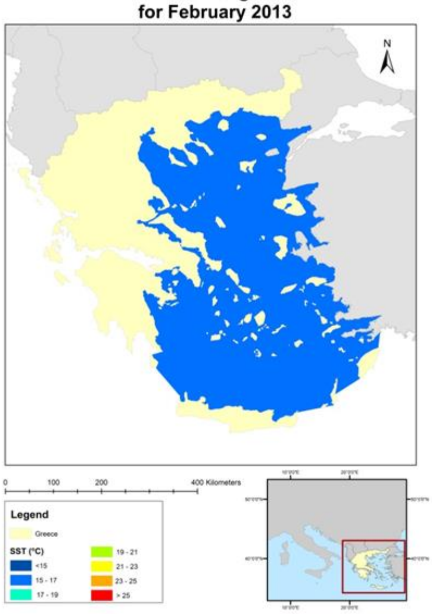

SMOS SST Descending measurements for April 2013

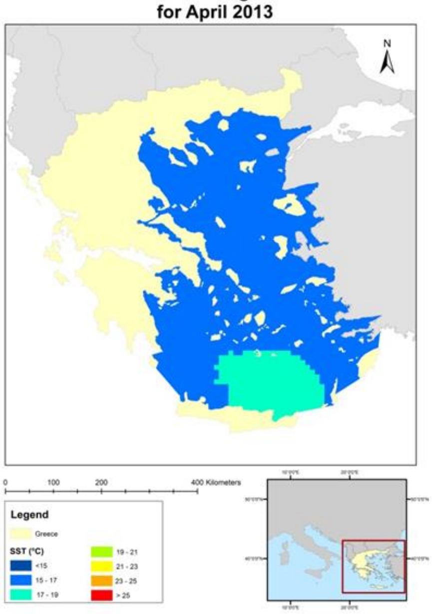

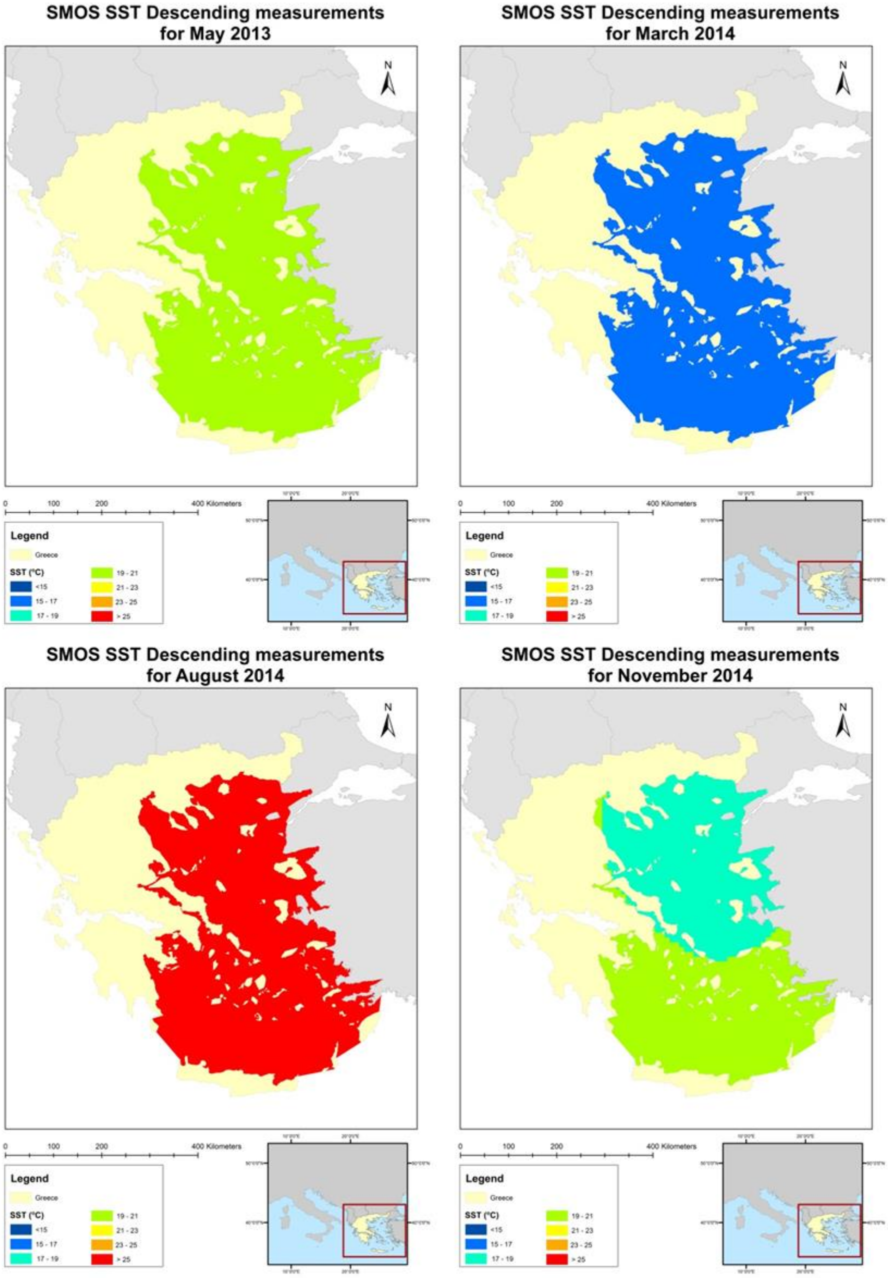
SMOS SST Descending measurements for May 2013
SMOS SST Descending measurements for March 2014
SMOS SST Descending measurements for August 2014
SMOS SST Descending measurements for November 2014
N
0 100 200 400 Kilometers
Legend
Greece
SST (°C)
<15
15 - 17
17 - 19
19 - 21
21 - 23
23 - 25
> 25

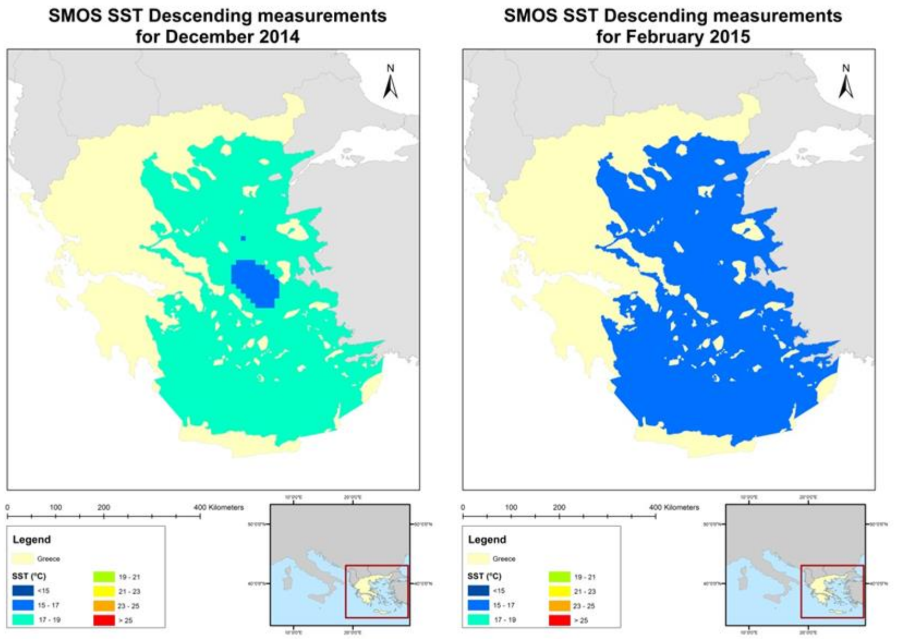

Appendix 20. SMOS SST_Descending measurements for the time period March 2012 to February 2015.